Dissertation

Submitted to the

Combined Faculty of Natural Sciences and Mathematics
of the Ruperto Carola University Heidelberg, Germany

for the degree of

Doctor of Natural Sciences

Presented by

Manuel Reitberger (M.Sc.)

born in Heidelberg, Germany

Oral examination: 30th March 2021

Regulation of ABCB1 expression is a potential therapeutic target in drug resistant pancreatic cancer

Referees: Prof. Dr. Andreas Trumpp

Dr. Richard Harbottle

Abstract

Pancreatic ductal adenocarcinoma (PDAC) is an aggressive and lethal disease with a miserable prognosis. Chemotherapeutic regimens, like FOLFIRINOX or gemcitabine plus nab-paclitaxel remain the standard treatment of care in patients diagnosed with PDAC while only achieving a modest increase in overall survival. Transcriptional subtyping of PDAC discerns tumors into two broad lineages which provides the opportunity to improve patient stratification and treatment, but has not been translated into clinical practice yet. Meanwhile, resistance to chemotherapy continues to be the limiting factor that prevents a patient's cure from cancer and finding improved therapeutic options could overcome resistance of PDAC to current treatment regimens.

With our previously established culturing model for patient-derived PDAC cells, we could investigate the development of resistance to paclitaxel and/or gemcitabine in the different subtypes. We developed a long-term treatment regime that enabled the generation of drug-resistant cells which were analyzed in a multi-omics approach. ATP-binding cassette (ABC) transporter B1 (ABCB1), a membrane-bound glycoprotein that is predominantly expressed in excretory tissue and a common resistance mechanism against paclitaxel in various tumor entities, was found to be overexpressed in all paclitaxel-resistant cells. CRISPR/Cas9-guided knockout and pharmacological inhibition re-sensitized these drug resistant cancer cells to paclitaxel. We found ABCB1 to be heterogeneously expressed in the paclitaxel resistant cell population and expression was lost after prolonged absence of paclitaxel treatment. Short-term drug treatment dynamically increased the proportion of ABCB1-expressing cells in former paclitaxel resistant cell population, re-acquiring paclitaxel-resistance. In of the paclitaxel resistant cell lines, expression of ABCB1 was further enhanced by *de novo* generation of extrachromosomal DNA (ecDNA), carrying the ABCB1 gene. Similar to ABCB1 gene expression, number ecDNA inside paclitaxel resistant cells was dynamically increased upon paclitaxel treatment.

These findings describe a dual mechanism for acquired ABCB1 expression that is dependent on paclitaxel treatment and leads to the induction of ABCB1 expression and amplification of ABCB1-carrying ecDNA.

Zusammenfassung

Das duktale Pankreaskarzinom (PDAC) ist eine aggressive und tödliche Krankheit mit schlechter Prognose für die betroffenen Patienten. Die chemotherapeutische Behandlung mit FOLFIRINOX oder Gemcitabine plus nab-Paclitaxel bleibt die Standardtherapie bei Patienten mit PDAC, wobei diese Behandlungen nur zu einer geringfügigen Steigerung der Überlebensspanne führen. Die transkriptionelle Klassifizierung unterteilt PDAC in zwei große Linien, was die Möglichkeit bietet, die Patientenstratifizierung und -behandlung zu verbessern, jedoch noch nicht in die klinische Praxis umgesetzt wurde. Weiterhin ist die Resistenz gegen Chemotherapie der limitierende Faktor, der die Heilung eines Patienten von Krebs verhindert. Die Suche nach verbesserten therapeutischen Methoden könnte die Resistenz von PDAC gegen aktuelle Behandlungsschemata überwinden. Mit unserem zuvor etablierten Kultivierungsmodell für von Patienten stammende PDAC-Zellen konnten wir die Entwicklung der Resistenz gegen Paclitaxel und/oder Gemcitabin in den verschiedenen Subtypen untersuchen. Wir entwickelten ein Langzeit-Behandlungsregime, das die Generierung von medikamentenresistenten Zellen ermöglichte, die auf transkriptioneller und genomischer Ebene analysiert wurden. Wir konnten zeigen, dass der ATP-bindende Kassetten (ABC)-Transporter B1 (ABCB1), ein membrangebundenes Glykoprotein, das vorwiegend im exkretorischen Gewebe exprimiert wird und ein häufiger Resistenzmechanismus gegen Paclitaxel in verschiedenen Tumorentitäten ist, in allen Paclitaxel-resistenten Zellen überexprimiert ist. CRISPR/Cas9-gesteuerter Knockout und pharmakologische Hemmung re-sensibilisierten diese medikamentenresistenten Krebszellen gegenüber Paclitaxel. Wir fanden heraus, dass ABCB1 in der Paclitaxel-resistenten Zellpopulation heterogen exprimiert wird und die Expression nach längerer Nichtbehandlung mit Paclitaxel verloren ging. Eine kurzzeitige medikamentöse Behandlung erhöhte in dynamischer Weise den Anteil der ABCB1-exprimierenden Zellen in der ehemals Paclitaxel-resistenten Zellpopulation und führte zur Wiederherstellung der Paclitaxel-Resistenz. In einer der Paclitaxel-resistenten Zelllinien wurde die Expression von ABCB1 durch *de novo*-Generierung von extrachromosomaler DNA (ecDNA), die das ABCB1-Gen trägt, weiter verstärkt. Ähnlich wie bei der ABCB1-Genexpression konnte die Anzahl der ecDNA innerhalb der Paclitaxel-resistenten Zellen durch Paclitaxel-Behandlung dynamisch reguliert werden.

Diese Befunde beschreiben einen dualen Mechanismus für die erworbene Expression von ABCB1, der über die Paclitaxel-Behandlung reguliert wird und zur Induktion der ABCB1-Expression und zur Vermehrung der ABCB1-tragenden ecDNA führt.

Declarations

The work presented in this dissertation was performed from June 2016 until December 2020 at the German Cancer Research Center (DKFZ, Heidelberg) and the Heidelberg Institute for Stem Cell Technology and Experimental Medicine (HI-STEM, Heidelberg) under the supervision of Prof. Dr. Andreas Trumpp and Dr. Martin Sprick.

Declarations according to § 8 (3) c), d) and h) of the Doctoral Degree Regulations:

a) I hereby declare that I have written the submitted dissertation myself and, in this process, have used no other sources or materials than those explicitly indicated.
b) I hereby declare that I have not applied to be examined at any other institution, nor have I used the dissertation in this way or any other form at any other institution as an examination paper nor submitted it to any other faculty as dissertation.

I hereby consent to the verification of the dissertation by means of electronic data processing programs against standing scientific standards

List of Content

1 Introduction

1.1 Pancreatic Cancer

Pancreatic cancer is an aggressive and lethal disease with a miserable prognosis[1]. In the Western World, pancreatic cancer has become the fourth leading cause of cancer-related deaths and is predicted to become the second leading cause by 2030[2]. By then, pancreatic cancer-related deaths are expected to reach 63,000, almost doubled compared to 20 years ago (37,000). For 2020, the American Cancer Society estimates 57,600 new pancreatic cancer cases, an increase of 8% compared to 2016 and of those new cases, more than 47,000 patients will be expected to die from pancreatic cancer[1,3].

The 5-year survival rate for pancreatic cancer is ~9%, the lowest survival rate among all cancers[1]. Although pancreatic cancer only makes up 4.8% of all new cancer cases worldwide (No.=459,000), the associated mortality was around 432,000, which would estimate that only 6% of all pancreatic cancer patients survive this disease[4]. In general, pancreatic cancer can be described as a disease of the elderly and 90% of new cases are patients of age 55 or more with a peak incidence rate for ages between 70-90 years [5,6]. In addition, men (13.9 cases per 100,000) are 30% more likely to develop pancreatic cancer than women (10.9 cases per 100,000)[6]. In the United States, African-Americans have not only the highest incidence among all races, they are also at higher risk of initial diagnosis occurring during late/advanced stage tumor progression and are consequently less likely to undergo surgery for the disease[6].

The pancreas inherits two distinct organs in one, being the exocrine pancreas (acinar and ductal cells) and the endocrine pancreas (islet cells)[7]. The exocrine gland, representing 95% of the pancreatic tissue mass, produces a variety of digestive enzymes that are secreted to break down fats, proteins and carbohydrates and to support the assimilation of nutrients into the body. The endocrine compartment is responsible for maintenance of glucose homeostasis through excretion of major peptide hormones like insulin and glucagon[7,8]. Hence, depending on the origin and localization of the pancreatic cancer, the disease can be classified into two tumor types named exocrine and endocrine. Pancreatic ductal adenocarcinoma (PDAC) and its variants originate from the exocrine pancreas and account for 90% of all pancreatic cancers[5]. Pancreatic neuroendocrine tumors (PNETs) were thought to arise from the endocrine islets, however, recent studies suggest that these tumors evolved from pluripotent cells in the ductal epithelium and represent 1-2% of all pancreatic tumors[9-12]. Additional rare pancreatic tumors include colloid carcinomas (2%), solid-pseudopapillary tumors (2%), acinar cell carcinomas

(1%), pancreatoblastomas (0.5%) and further tumor variants, such as signet ring cell, medullary, adenosquamous, hepatoid and undifferentiated carcinomas[13]. Since the pancreatic cancer incidence has increased over the last decades and is mainly rising in the Western world, it is possible that environmental factors could play a key role in defining pancreatic cancer risk factors, several of which have been described to increases the chance of developing pancreatic cancer during the lifetime[14]. As previously outlined, pancreatic cancer is primarily a disease of the elderly and its occurrence remains rare until the age of 30, but accelerates exponentially afterwards until it peaks in the 7th and 8th decades[6]. Epidemiological studies showed that people with blood groups A, B or AB have a higher probability to develop pancreatic cancer compared to people with blood group 0[15]. Chronic pancreatitis is progressive inflammatory disease that involves fibrosis, acinar and islet cell loss, and has been reported to increase the risk of pancreatic cancer by more than 13-fold[5,6]. Another well-established risk factor is diabetes and for both, diabetes mellitus and type-2 diabetes, the chance of developing pancreatic cancer is two-fold higher compared to those without diabetes[16,17]. Furthermore, obesity and elevated body mass index (BMI) were found to increase the risk of pancreatic cancer by up to three-fold[18]. Analysis by several studies revealed that the risk of pancreatic cancer increased by 10% for every 5 BMI units[5]. Cigarette smoking is also considered a leading modifiable risk factor in pancreatic cancer and several studies have demonstrated that heavy smokers have a two-fold to three-fold higher risk of developing pancreatic cancer than non-smokers[19,20]. Approximately 10% of all pancreatic cancers diagnosed in patients have a hereditary component[21]. Starting from one relative, the risk of developing pancreatic cancer is already amplified by 80%[22]. The risk of familial pancreatic cancer ranges from three-fold to up to 57-fold with three affected first-degree relatives[23]. Several germline mutations have been linked to familial pancreatic cancer, including genes like *ATM*, *BRCA1/2*, *CDKN2A*, *FANCC*, *FANCG*, *PALB2*, *MLH1*, *PRSS1*, *STK11*, with varying degrees of increased risk for pancreatic cancer[14,24,25].

1.2 Pancreatic ductal adenocarcinoma

PDAC is composed of a solid, highly sclerotic mass with insufficiently delineated edges forming a white poorly-defined mass[26,27]. It also displays a highly dispersed and infiltrative type of growth, accompanied by an extensive stromal reaction termed desmoplastic reaction, poor vascularization and, thus, is enclosed by a hypoxic and harsh microenvironment[28,29]. The majority of PDAC is located in the head of the pancreas (65%) while the rest are found in the pancreas body (15%) and tail (15%)[5,26].

Using molecular pathology and detailed analyses of the genome by several studies, a model of PDAC progression evolved that explains the stepwise progression from premalignant pancreatic lesions in the epithelium of the duct to an invasive malignancy[30]. These premalignant mucinous lesions can be divided into histologically distinct microscopic and macroscopic precursors[30]. Microscopic precursor lesions (< 5 mm in diameter) include the most common precursor lesions, being pancreatic intraepithelial neoplasia (PanIN), and the atypical flat lesions (AFL)[31]. AFL are tiny tubular lesions, located in the acinar compartment and feature a ductal phenotype, hence, they might originate from acinar-ductal metaplasia[31]. AFL were mostly found in patients with familial predisposition for PDAC[32]. PanINs are composed of columnar to cuboidal cells with varying levels of mucin and, depending on the degree of dysplasia, are subclassified as low-grade PanIN or high-grade PanIN[27,33-35]. PanINs are often found in close proximity to infiltrating adenocarcinomas and harbor many of the same genetic alterations as found in infiltrating pancreatic cancer[36,37]. Activating mutation in *KRAS* and telomere shortening are the earliest occurring genetic aberrations to be found in low-grade PanIN[38]. More than 90% of low-grade PanIN carry mutations in the *KRAS* gene locus and telomere shortening may contribute to chromosomal instability and finally chromosomal abnormalities[39,40]. Mutations in *CDKN2A*, *SMAD4* and *TP53* occur later and can be found in high-grad PanINs, as well as in 50-80% of invasive PDAC[13,41,42]. Interestingly, the rate of activating *KRAS* mutation increases in relation to the grade of PanIN[30,43]. Mucinous cystic neoplasms (MCN) and Intraductal papillary mucinous neoplasms (IPMN) belong to the macroscopic (> 1 cm in diameter) precursor lesions of PDAC[26,44]. IPMNs are mucin-producing epithelial neoplasms that are classified according to their site of origin and histomorphology profile[45-47]. Main-duct type IPMN are usually classified as intestinal-type IPMN, while branch-duct type IPMN are mostly gastric-type IPMN[45-47]. This distinction is of great importance as the risk of malignancy is significantly higher in main-duct type IPMN compared to branch-duct type IPMN[48,49]. Similarly, to PanIN, IPMN should be distinguished between low-grade or high-grade according to their degree of dysplasia[33]. While *KRAS* mutations are frequently found in PanIN, they can only be found in 50% of the cases in IPMN. In contrast, 2/3 of IPMN harbor an activating mutation in *GNAS* which is occasionally found in PanIN[50]. Although both *KRAS* and *GNAS* mutations are often present simultaneously in IPMN, *KRAS* mutations are more common in gastric-type, whereas *GNAS* mutations are more frequently found in the intestinal subtype IPMN[51]. Independent of the differences between low-grade IPMN and PanIN, identical mutations in *CDKN2A*, *TP53* and *SMAD4* are also found in high-grad IPMN[52]. MCN are large cysts, account for 25% of all resected pancreatic cysts and are mostly found in women[53].

Moreover, MCN form an "ovarian-like" stroma as it expresses estrogen and progesterone receptor[53]. Similar to the other two precursor lesions, *KRAS* mutations are frequently found in MCNs, however, they are usually absent of *GNAS* mutations[54,55]. Mutations in *CDKN2A*, *TP53* and *SMAD4* are only present in high-grade MCN but at lower frequency compared to the others[27,37]. Morphological analyses of the different precursor lesions of PDAC display a ductal phenotype, which suggests a ductal cell of origin[56]. However, recent studies have challenged the ductal origin of PDAC as they could show that early progenitor cells, exocrine cells and even acinar and insulin-producing cells can be the origin of PanIN lesions[56]. This has led to the development of an alternative model of pancreatic carcinogenesis, in which PDAC precursors arise in the acinar compartment and develop into PanIN and PDAC through acinar-to-ductal metaplasia[57-59]. Until today, the identification of the cell origin of PDAC remains unclear.

In PDAC, mutations in four driver genes are predominant, being *KRAS*, *CDKN2A*, *TP53* and *SMAD4*[60]. *KRAS* is the most common gene mutated in PDAC and its activation by point mutation leads to the expression of constitutively active RAS which acts through the mitogen-activated protein kinase (MAPK) pathways promoting cell proliferation and survival, among others[60]. In contrast, the tumor suppressor gene *CDKN2A* is genetically inactivated in various ways which leads to a loss of cell cycle control and unrestricted cell growth[60]. Inactivation of *TP53* also induces pancreatic neoplastic progression as it plays a critical role in cell cycle arrest, DNA repair and induction of apoptosis[60]. Loss of *TP53* further enhances the accumulation of genetic alterations[60]. Deletion of *SMAD4* abrogates transforming growth factor beta (TGFβ) signaling which increases cell growth and is generally associated with poor prognosis[61]. In recent years, additional genes were identified that were mutated at a prevalence of 5-10% in PDAC, including *KDM6A*, *RBM10*, *BCORL1*, *MLL3*, *ARID1A* and *TGFBR2*[62-65]. Moreover, a recent copy number analysis in over 100 PDACs provided a more comprehensive description of the genomic alterations of this malignancy[65]. They identified genes related to DNA damage repair and chromatin remodeling being mutated or lost and, on the contrary, they reported other known oncogenes like *MYC*, *GATA6* and *MET* that were found to be amplified in several PDAC samples[65]. Lastly, epigenetic changes that alter gene expression and altered expression in miRNAs have also been reported to influence the genetic landscape of precursor lesions and PDAC[66].

A key characteristic of PDAC is the formation of a dense stroma termed desmoplastic reaction. Approximately 90% of the whole tumor mass is constituted by stroma, which is composed of activated fibroblasts, immune cells, neural cells, blood vessels, and matricellular proteins[26,67,68]. Pancreatic stellate cells (PSCs), which are myofibroblast-like pluripotent cells in the exocrine

region of the pancreas, are responsible for the production of this collagenous stroma[69]. Quiescent PSCs are activated by growth factors such as TGFβ1, fibroblast growth factor (FGF) and platelet-derived growth factor (PDGF), resulting in the secretion of collagen and other components of the extracellular matrix (ECM)[60]. Activated PSCs are featured by increased expression of alpha smooth muscle actin (α*SMA*), desmin, prostaglandin-endoperoxide synthase 2 (*PTGS2*), vascular endothelial growth factor (*VEGF*), *CXCL12*, *PDGF* and *TGFβ1* receptor, secreted protein, acidic, cysteine-rich (*SPARC*), vimentin and intercellular adhesion molecule one (*ICAM-1*)[60,70]. In addition, PSCs have been found to secrete various ECM components, including collagen I, III and IV, laminin, fibronectin and metalloproteinases MMP2, MMP9 and MMP13[70]. In turn, PSCs mediate cancer cell proliferation and migration by TGFB, insulin-like growth factor (IGF), hepatocyte growth factor (HGF), epidermal growth factor (EGF) and other chemokines like CXCL12[71]. By controlling the ECM turnover through secretion of metalloproteinases and metalloproteinase inhibitors, PSCs create a dense stroma which leads to poor vascularization and a hypoxic microenvironment[70]. Moreover, it is composed of immune cells such as lymphocytes, macrophages, mast cells and myeloid derived suppressor cells[72]. In addition to its function as a physical barrier, it became apparent that the stroma is also involved in tumor formation, progression, invasion and metastasis[73]. The stroma's hydrostatic pressure might impede the delivery of chemotherapeutic agents to cancer cells, thus contributing to the therapeutic resistance of PDAC[67]. To date, there is conflicting evidence whether the stroma can also restrain PDAC progression, and studies associated high stromal activity with shorter, but also with longer overall survival[74-76]. Hence a more detailed understanding of the tumor microenvironment remains crucial in PDAC research.

Early-stage PDAC is usually silent and the disease's symptoms become apparent once the tumor starts to invade the surrounding tissue or metastasize to distant organs. In addition, the symptoms of PDAC depend mainly on its location as well as its stage and, thus, PDAC is rarely diagnosed early with the majority of patients being diagnosed at an advanced stage[60,77]. Although the clinical manifestations of this disease are broad, pancreatic cancer often causes abdominal or back pain, jaundice, unexplained weight-loss and nausea[60,61,78]. With advanced tumor stage symptoms manifest systemically with asthenia, anorexia, dysglycemia and new-onset diabetes mellitus[60,78,79]. The majority of pancreatic cancer (~ 70 %) develops in the head of the pancreas, whereas only approximately 30 % are located in the body or tail of the pancreas[26,29,60]. Notably, pancreatic cancer originating in the head of the pancreas can cause obstruction of bile and pancreatic ducts, leading to painless jaundice and pancreatitis[13].

So far, multiphase, multidetector computed tomography (MDCT) with intravenous administration of contrast material is the preferred initial diagnostic test, sufficient in providing high resolution images of the pancreas and surrounding vasculature for evaluating the extent of the disease[60,61]. In addition, most patients undergo endoscopic ultrasonography with fine-needle aspiration biopsy which supports diagnostics in patients without clearly visible tumor masses on CT and is the favored biopsy method to acquire tissue material for diagnostic purposes[60,80,81]. Furthermore, tissue diagnosis is required before the start of chemotherapy or radiation therapy and pathology of the sample can be used to define tumor grade and tumor type[60]. Even though the diagnosis of PDAC is in general based on conventional histology, immunohistochemistry can provide important information that can be used by pathologists for a more detailed analysis[26]. Of note, the majority of PDAC express several cytokeratins such as CK7, CK19 and CK18, mucins, including MUC1, MUC4 and MUC5AC, and the carbohydrate antigen 19-9 (CA19-9)[26]. To date, CA19-9 is the sole FDA approved serum biomarker for PDAC[82]. With an estimated sensitivity and specificity of 80%, CA19-9 is a poor screening tool, but is frequently used to monitor patients under therapeutic intervention and to detect recurrent disease after treatment or post-resection[60,82,83]. However, due to mutations, 10% of patients diagnosed with PDAC are incapable to synthesize CA19-9 and have undetectable levels at any stage of the disease[60]. Current screening methods fail to detect pancreatic cancer at an operable stage which is associated with the best 5-year survival of up to 25%[84]. Hence, there is an urgent need for improved methods that convincingly detect precursor and early stage lesions.

PDAC is currently staged according to the 8th edition of the American Joint Committee on Cancer (AJCC) staging system of pancreatic adenocarcinoma[85-87]. The staging system is based on three key components, being local tumor grade (T), dissemination to regional lymph nodes (N), and the metastatic spread to distant sites (M) (TNM staging)[88]. T1-T3 tumors are considered to be potentially resectable, whereas T4 tumors are considered unresectable[88]. Resectable disease classifies tumors with no involvement of the superior mesenteric artery, celiac axis, portal vein or superior mesenteric vein[89]. Borderline resectable definition is based on the degree of involvement of these structures[89]. An unresectable disease is defined by vascular involvement or by distant metastases[89]. This is also the case, once the tumor has spread to more than 3 regional lymph nodes or beyond to distant sites (metastatic) [89]. Complete staging of pancreatic cancer is summarized in **Table 1**.

Table 1: TNM staging system in patients with pancreatic cancer

Stage	Primary Tumor (T)	Regional Lymph Nodes (N)	Distant Metastases (M)	Median Survival [mo]	Characteristics
IA	T1	N0	M0	38	Maximum tumor diameter ≤2 cm
IB	T2	N0	M0	24	Maximum tumor diameter ≤2 cm but ≤4 cm
IIA	T3	N0	M0	18	Maximum tumor diameter ≤4 cm
IIB	T1-T3	N1	M0	17	Metastasis in 1–3 regional lymph nodes
III	Any T T4	N2 Any N	M0	14	Tumor involves the celiac axis or the superior mesenteric artery (unresectable primary tumor)
IV	Any T	Any N	M1	13	Distant metastasis

1.3 Treatment of pancreatic ductal adenocarcinoma

Surgical resection remains the only chance for cure from cancer in patients with PDAC[90]. However, less than 20% of patients can be considered for resection, whereas the majority are diagnosed with locally advanced or, due to vascular involvement or widespread metastasis, with an unresectable tumor[13]. Those patients who are eligible for resection already have microscopically malignant margins at the time of surgery and more than 90% of patients with resected tumors relapse and die of the disease[13,29,90]. Risk factors for a recurrent disease are high differentiation grade, large tumor size and involvement of lymph nodes[60]. Whether the operative procedure involves cephalic pancreatoduodenectomy (Whipple procedure), distal or total pancreatectomy depends on the location of the tumor[60]. Whereas the Whipple procedure is commonly used to remove pancreatic cancers located in the head or neck of the pancreas, tumors located in the body or tail of the pancreas are removed by distal or total pancreatectomy[29]. In addition, at least 12 to 15 lymph nodes are resected for pathological analyses, staging and prognosis[60]. Of note, a more extensive lymphadenectomy and an arterial en bloc resection do not improve outcomes but increase postoperative morbidity[91]. Given that surgery alone is not sufficient, adjuvant therapy is the standard follow-up treatment of resected tumor patients to reduce the risk of resection and distant metastasis[92,93]. In the recent ESPAC-4 trial, a combination therapy of deoxycytidine analogue gemcitabine and to 5-fluorouracil (5-FU) precursor capecitabine enable a 5-year survival of approximately 30% and in 2017 it has been recommended in the American Society of Clinical Oncology (ASCO) over any other adjuvant therapy for potentially curably pancreatic cancer[94,95]. The most recent APACT trial

from 2019 evaluated the combination of adjuvant albumin-bound paclitaxel (nab-paclitaxel)/gemcitabine versus gemcitabine monotherapy and found that interim median survival was significantly increased in combinatorial therapy (40.5 months) compared to monotherapy (36.2 months)[96].

A rising strategy in patients with resectable, borderline resectable, as well as locally advanced unresectable pancreatic cancer is the use of preoperative (neoadjuvant) treatment[97,98]. Neoadjuvant treatment success in other tumor entities, including gastric, rectal and breast cancer have led to the exploration in pancreatic cancer[99]. In theory, neoadjuvant therapy has the advantage to eliminate micro-metastases, induce shrinkage of the primary tumor and reduce the rate of local failures and positive resection margins after surgery[100-102]. An interim analysis of a phase II/III trial in borderline resectable pancreatic cancer comparing neoadjuvant chemoradiation plus gemcitabine with adjuvant chemoradiation plus gemcitabine demonstrated a median survival of 23 months for the neoadjuvant therapy and 11 months for the adjuvant therapy[90]. Since adjuvant chemoradiations is not considered to be effective and more active chemotherapeutic regimens, like FOLFIRINOX (folinic acid, 5-FU, irinotecan, oxaliplatin), are available, clinical strategy shifts away from chemoradiotherapy towards neoadjuvant chemotherapy[103,104]. Several clinics have reported high resection rates in patients with locally advanced or unresectable disease when treated with neoadjuvant FOLFIRINOX therapy[105]. Latest findings suggest that almost one-third of borderline resectable and locally advanced pancreatic tumors become resectable after neoadjuvant therapy, including similar outcomes compared to initially resectable tumors[98,106]. Especially neoadjuvant FOLFIRINOX seems to have the potential to turn borderline resectable and locally advanced pancreatic tumors into resectable tumors[106-108].The latest results give rise to the hope that more patients with borderline resectable or locally advanced unresectable tumors will get the chance to have their tumor resected which would increase the overall number of patients that might be cured.

Approximately 30% of patients are diagnosed with metastatic or local irresectable disease, and an additional 30% of patients will suffer from a recurrent tumor after treatment of early disease[60]. These patients often have multiple symptoms, including severe pain caused by the tumor, jaundice, nausea and vomiting[5,13]. An integrated supportive care is mandatory to assure patients remain well for as long as possible and the application of systemic palliative chemotherapy aims to improve overall survival[90]. Gemcitabine was the first agent approved by FDA for palliative pancreatic cancer treatment a various combination of gemcitabine with a second agent were tested extensively in the past years[90]. Recently, two clinical trials changed the standard treatment of care in metastatic pancreatic cancer patients from gemcitabine

monotherapy to combination chemotherapy[109,110]. In 2011, the gemcitabine-free FOLFIRINOX regimen yielded an almost 5 months improved overall survival in patients with metastatic pancreatic cancer (11.1 months versus 6.8 months median overall survival)[110]. Two years later, the MPACT trial reported the results of a combinatorial treatment with nab-paclitaxel and gemcitabine (nPG) in metastatic pancreatic cancer patients[111]. Paclitaxel is a hydrophobic compound that needs oil-based solvents for infusion, however, paclitaxel bound to albumin turns it into a water-soluble, hydrophilic formulation that achieved a survival benefit of 2 months over the gemcitabine monotherapy (8.7 months versus 6.6 months)[109,112]. On the contrary, FOLFIRINOX or nPG are associated with a severe toxicity compared to single-agent gemcitabine. Approximately 48% of patients treated with FOLFIRINOX suffer of neutropenia, which also occurs in 38% of patients treated with nPG[90]. Hence FOLFIRINOX is mainly given to patients with an ECOG performance status of 0 or 1, while nPG is also considered to be given to selected patients with ECOG2 status, however, it has been recommended to use gemcitabine monotherapy for that group of patients[113]. In a recent phase 2 clinical trial (NEOLAP) the conversion rate of locally advanced pancreatic cancer after FOLFIRINOX or nPG treatment was investigated. The conversion rate was 30.6% in the NPG group and 45% in the FOLFIRINOX group. Researchers found no significant difference in median overall survival (OS) between nPG group (17.2 months) and FOLFIRINOX group (22.5 months). Nevertheless, among all intention-to-treat patients, a conversion was associated with significantly improved OS of 27.4 months vs 14.2 months[114].

Currently, for the majority of patients diagnosed with PDAC, cytotoxic chemotherapy is standard treatment regimen[90]. Still, there are many studies investigating the benefit of novel treatment approaches in patients with metastatic PDAC. Several randomized trials combined gemcitabine as chemotherapeutic backbone with inhibitors against the PI3K pathway, EGFR pathway, IGF1R pathway, tyrosine kinases and angiogenesis[115]. Of all those trials, only the combination of gemcitabine with erlotinib resulted in a significant increase in survival of two weeks compared to gemcitabine monotherapy[116]. Hence, this minor benefit questions the clinical significance of erlotinib as option for PDAC treatment. More than 90% of patients diagnosed with PDAC show activating mutations in *KRAS*, thus, pharmacological inhibition of EGFR upstream of KRAS might only be of minimal effect[117]. Since the direct targeting of KRAS proteins has proved extremely difficult, novel strategies were developed that take advantage of exosomes or small extracellular vesicles to deliver small interfering RNAs targeting $KRAS^{G12D}$ into the cell[118]. A phase I clinical trial has entered clinical testing including patients with metastatic PDAC (NCT03608631).

One of the hallmarks of cancer is the suppression of the immune response by cancer cells or the tumor microenvironment[119]. In many tumor types, immune checkpoint inhibitors targeting programmed cell death protein 1 (PD-1) or cytotoxic T lymphocyte protein 4 (CTLA4) were of great promise, however, early trials investigating the effect of those treatments in pancreatic cancer were disappointing[120-122]. The combination of increased hydrostatic pressure and poor vascularization in pancreatic tumors might create a barrier against drug uptake and the use of modified hyaluronidase PEGPH20 in combination with FOLFIRINOX and nPG is currently tested in clinical trials (NCT01839487 and NCT01959139). Preliminary results showed that patients with high tumoral hyaluronic acid had increased progression-free survival (9.2 months) under combinatorial treatment of PEGPH20 and nPG compared to nPG alone (4.3 months)[123]. Of note, no statistically significant benefit was observed in patients whose tumors had low tumoral hyaluronic acid. Personalized medicine is a rising concept in the treatment of cancer patients and offers individualized therapy in a patient-specific fashion[124]. In the IMPacCT trial, patients with tumors carrying mutations in genes related to homologous recombination and DNA damage repair (*BRCA1*, *BRCA2*, *PALB2* or *ATM*), including either the absence of *KRAS* mutation or amplified *HER2* are qualified for targeted therapy instead of gemcitabine monotherapy. The COMPASS trial (NCT02750657) sequences cancers to detect actionable drug targets, tumor subclasses and especially patients that would benefit from platinum-based chemotherapy due to defects in DNA repair mechanisms.

In conclusion, Cytotoxic chemotherapies using two combination therapies (FOLFIRINOX and nPG) remain the standard treatment of care in patients diagnosed with PDAC. The choice of first-line treatment regime is currently based on ECOG performance score, age and physician preference[125]. New therapies are emerging and the use of precision medicine could help to define subgroups of patients who benefit the most from certain therapies.

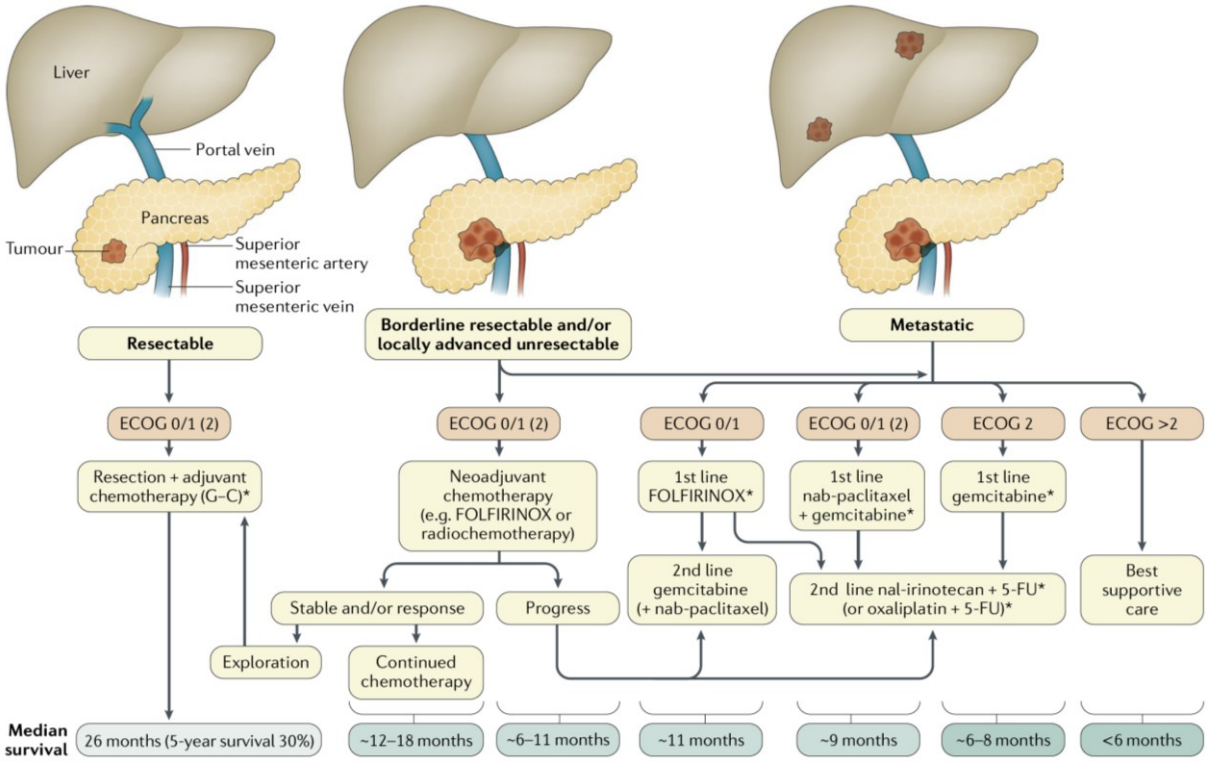

Figure 1 – Chemotherapeutic treatment design for patients with pancreatic cancer
Stratification of patients according to tumor stage (resectable, borderline resectable and locally advanced unresectable, metastatic) and performance status (ECOG score). 5-FU, 5-fluorouracil; FOLFIRINOX, folinic acid, fluorouracil, irinotecan and oxaliplatin; G–C, gemcitabine–capecitabine; nab, nanoparticle albumin-bound; nal, nanoliposomal. *Approaches have been tested in randomized controlled trials (RCTs), whereas the others have not been validated by RCTs. (Figure was taken from Neoptolemos, et al.[90]).

1.4 Subtypes of pancreatic ductal adenocarcinoma

Until 10 years ago, cancer was classified on the basis of tissue of origin, which led to the organization of specialist clinical teams responsible for the management of organ-specific cancers[126]. However, it soon became apparent that histopathologically indistinguishable tumors show substantial variability in their molecular pathology. In order to achieve the optimal clinical management for each patient, subtyping of cancer based on clinical and biological similarities and differences was introduced, which has the potential to improve individual patient management and risk stratification, selection of systemic therapeutic regime, as well as improved therapeutic research and development. In the first attempts cancer subtypes were based on unique molecular markers that have influenced clinical treatment strategies. Such successful therapeutics were found in the anti-ERBB2 treatment of ERBB2+ breast cancers and inhibition of BRAF in $BRAF^{V600E}$ mutated melanoma[127,128]. In pancreatic cancer, studies investigating the utility of aberrant gene expression and mutated genes have not yet been translated into clinical practice[129]. Additionally, with the exception of *KRAS*, *TP53*, *CDKN2A* and *SMAD4*, most mutations occur at a prevalence of <5% which limits the interest in exploring

therapies targeting these mutations in PDAC[126]. Other genomic aberrations such as structural variations of the genome have been used to classify PDAC into four different categories: stable genomes, scattered genomes, locally rearranged genomes and unstable genomes that range from < 50 to > 200 structural variants across the genome[65]. Especially tumors of the unstable subtype imply defects in DNA damage response and could be susceptible to platinum-based therapy[65].

In 2011, transcriptomic subtyping of PDAC was first described by *Collisson* et al. in the analysis of gene expression profile of the microdissected tumor epithelium in untreated, primary resected PDAC[130]. Based on a 62 gene classifier (PDAssigner), *Collisson* et al. defined three subtypes, being Classical, Quasi-mesenchymal (QM-PDA) and Exocrine-like. Of the three subtypes, the QM-PDA correlated with the high tumor grade and the worst prognosis, and together with the Classical subtype, these subtypes were matched with available PDAC cell lines[130].

In 2015, *Moffitt* et al. defined molecular subtypes based on bulk resected, untreated, primary PDAC tumors and metastases in combination with mathematical modeling using gene expression profiling data[131]. In order to correct for the limited tumor cellularity and the presence of desmoplastic stroma, they removed transcripts presumably belonging to normal pancreas and the tumor microenvironment (TME), as well as the organ in which metastasis were found[131,132]. Having removed the corresponding transcription sets, they identified two distinct tumor subtypes termed classical and basal, and also described two stromal subtypes named Normal and Activated. Of note, all four subtypes present prognostic relevance which would hint towards an important interplay between tumor and its stroma that is likely to impact stroma- and immune-modulating therapies[131].

One year later, *Bailey* et al. analyzed bulk transcription data of 266 patients with untreated, primary PDAC covering the entire range of cellularity[133]. PDAC was proposed to be defined by four subtypes termed Squamous, Pancreatic Progenitor, Immunogenic and Aberrantly Differentiated Endocrine exocrine (ADEX)[133]. Application of the PDAssinger to their dataset demonstrated that these subtypes overlapped with subtypes described by Collisson et al., with the exception of the Immunogenic subtype[133]. The QM-PDA, Squamous and Basal-like subtype fairly overlap across all three classifications and are associated with the worse prognosis in the respective cohorts[126]. The Classical subtype overlapped with Pancreatic Progenitor and the Exocrine-like with the ADEX subtype[133]. Although the PDAssigner by Collisson et al. was missing the transcripts that define the Immunogenic subtype, the unsupervised analysis by

Bailey et al. associated the Immunogenic group with the Pancreatic Progenitor or Classical subgroup[133].

In 2018, *Puleo* et al. analyzed 300 PDAC cases from formalin-fixed paraffin-embedded (FFPE) material, excluded transcripts belonging to normal pancreas and identified two subtypes termed Basal-like and Classical which mainly overlapped with the classifications described above[134]. Of note, they also identified two subgroups in the Classical PDAC that differ in immune content and were classified as Immune Classical and Pure Classical.

Taken together, transcriptional subtyping of PDAC discerns tumors into two broad lineages being the Classical and Basal (**Figure 2**). The Classical would incorporate a spectrum of subtypes and can be subdivided into Classical-Progenitor and ADEX subgroups[126]. Molecular subtyping of PDAC has the opportunity to improve patient stratification, selection of the optimal treatment option and therapeutic development.

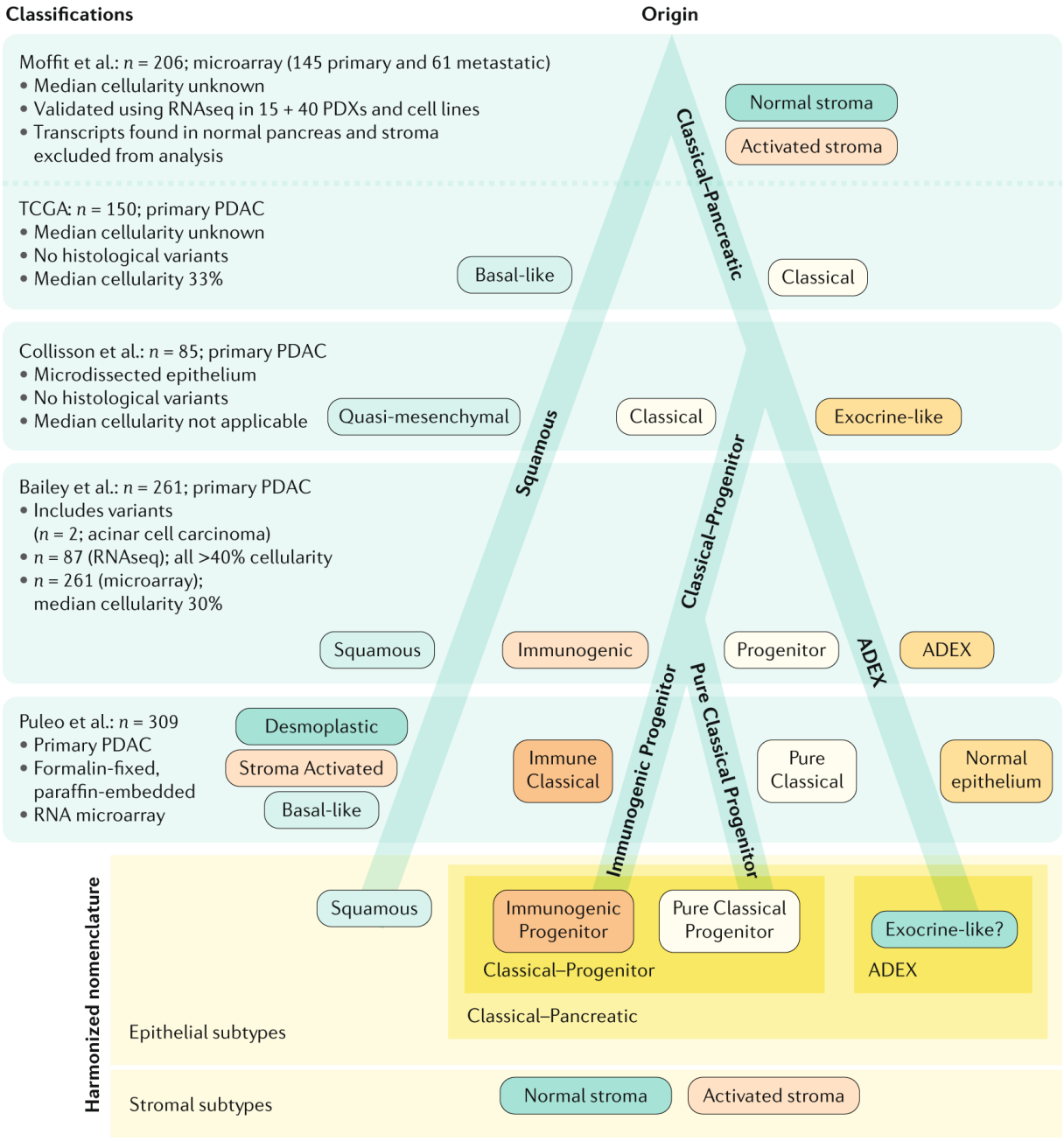

Figure 2 – Phylotranscriptomic tree of PDAC
The experimental design of each of the five studies lets them intersect with the tree at different levels. Two clearly distinct lineages separate PDAC into the Squamous (Basal-like) and Classical subtypes. The Classical subtype might contain a broad spectrum of tumors and can be subdivided into a Classical-Progenitor and an Aberrantly Differentiated Endocrine Exocrine (ADEX) subtype. It remains unclear whether the ADEX arm formed due to contamination by normal epithelium. The Classical-Progenitor can be distinguished between an immunogenic subtype, that is highly infiltrated by immune cells, and a less immunogenic subtype. PDX, patient-derived xenograft; RNA-seq, RNA sequencing; TCGA, The Cancer Genome Atlas (Figure was taken from Collisson, et al.[126]).

1.5 Model systems of pancreatic ductal adenocarcinoma

1.5.1 Conventional cell lines

Establishment of cancer cell lines in fetal calf serum (FCS) enabled the generation of many cancer cell lines and facilitated fundamental cancer research both in vitro and in vivo. Conventional cancer cell lines provided insight into cellular and molecular processes of cancer and served as preclinical screening platform for the identification of novel drug targets and therapy regimens. While conventional cancer cell lines are easy to culture and manipulate in vitro, and efficiently engrafted in vivo, these cell lines clearly simplified cancer biology and failed to mirror the complex architecture of a patient tumor. In addition, long-term culturing of cells with FCS leads to the acquisition of phenotypic and genomics alterations[135,136]. Culture medium supplemented with FCS insufficiently defined and growth factor concentrations vary between batches, which leads to clonal and genetic variability of the same cancer cell line between different labs and studies[137,138]. Moreover, the heterogeneity of the primary patient tumor is lost in the process of establishing FCS-cultured cell lines due to clonal selection[139]. Consequently, this leads to the selection of the most aggressive, high stage and poorly differentiated clones that failed to resemble the histomorphological features of the primary tumor when re-injected into immunodeficient mice[135,140]. Moreover, this selection process causes an underrepresentation of slow growing variants and suggesting that currently available cancer cell lines are unable to represent the heterogeneity of human cancer, e.g. PDAC[141]. In summary, conventional cell lines may be an insufficient for in vivo settings to study response of patient tumors to novel therapies.

1.5.2 Patient-derived tumor xenograft

Similar to cell line xenografts, ectopic or orthotopic transplantation of patient tumor material or cells is used to derive primary xenografts in immunodeficient mice. In order to improve engraftment efficiencies, the non-obese diabetic mouse with severe combined immunodeficiency (NOD/SCID), lacking functional T- and B-cells, has been further modified by a mutation in the interleukin 2y receptor (NOD.Cg-*Prkdc*^{scid} *Il2rg*^{tm1Wjl}, NSG) to also lack functional NK cell cytotoxicity[142]. Patient-derived xenografts (PDX) retain morphological characteristics and heterogeneity of the primary PDAC specimen, showing desmoplastic stroma, keep metastatic potential and maintain genetic hallmarks[143-145]. However, PDXs still undergo clonal selection in immunodeficient mice and it has been shown that more aggressive clones are favored to grow, genetically and phenotypically separating the transplanting tumor from the actual PDAC[146]. Furthermore, although surgical resection specimens contain stroma

surrounding the cancer cells, PDXs still cannot fully recapitulate stromal proliferation of PDAC and completely lack the host immune response[147]. In contrast to conventional cell lines, PDXs maintain their phenotype and biological properties, which would enable a detailed characterization of genomic aberrations and transcriptional profiling that could lead the way to personalized chemotherapeutic treatments[148]. Furthermore, PDXs closely reflect the patient response to chemotherapeutic agents and, hence, are routinely used for biomarker discovery and pre-clinical drug evaluation[149-151]. However, the probability of a successful engraftment of resected tumor material remains low and less than 20% of patients are suitable for surgical removal of the tumor[13]. In addition, it can take up to 6 months for the PDXs to have grown enough to be treated which is untenable for most PDAC patients considering the median survival after diagnosis is 6-11 months under chemotherapeutic treatment[29]. So far, the utility of PDXs is still limited by financial burden, animal welfare regulations, as well as surgical and laborious techniques that need to be improved.

1.5.3 Genetically engineered mouse models

Genetically engineered mouse models (GEMMs) mitigate many of the shortcomings of PDXs and, nowadays, are an important tool to study pancreatic cancer. To create tumors in GEMMs, mouse cells are modified in a tissue- and time-specific manner to overexpress tumor oncogenes, while tumor suppressor genes are removed and targeted mutations are inserted into the genome[152]. The first PDAC in the mouse was accomplished by introducing the activating $KRAS^{G12D}$ mutation, specifically expressed in the pancreas, which led to the development of PanIN lesions that, after several months, could also transform into PDAC[153,154]. However, as a consequence, the $KRAS^{G12D}$ mutant allele is already activated during the embryonic development of the pancreas, which does not mimic the PDAC development in humans[155]. In order to accelerate the formation of PDAC in mice, researchers incorporated mutations in *Kras* and *Tp53*, driven by the pancreas-specific *Pdx1-Cre* transgene, which marked the time of birth of the KPC mouse[156]. These mice recapitulate many features of human PDAC, including symptoms such as pain and cachexia[157,158], as well as poor vascularization and desmoplastic stroma which are hallmarks of PDAC[67,159-161]. These properties made the KPC model an instrumental tool to investigate risk factors, biomarkers of early disease, therapy resistance and discovery of novel therapies[162,163]. For instance, the usage of the KPC model has led to the identification of possible new therapeutic targets, like autophagy, PI3K and Notch pathways[164]. Another property that makes GEMMs advantageous compared to PDXs is the presence of an intact immune system, as ideal characteristic to properly study the immune response in PDAC development and test novel immunological approaches. Over the past decades, many PDAC

GEMMs have been developed addressing specific biological questions concerning the development of human PDAC or the validation of targets whose inhibition could prevent or delay tumor development[165]. On the contrary, generation of new GEMMs is labor and cost intensive, because tumor initiation and progression can take more than 12 months and its monitoring requires specialized imaging equipment[166-168]. Furthermore, mice have different telomere properties than humans which leads to the progression of mutations and alteration of pathways not seen in human PDAC[159,169]. Hence, we need to further intensify the research of GEMMs to identify additional or a combination of targets that could serve to translate novel therapeutic strategies into new clinical approaches.

1.5.4 3D culture of organoids

Growing cells in 2D cultures results in differences in gene expression compared to 3D cultures and fail to recapitulate key features of tumor biology, such as cellular polarity and cell-to-cell contact between layers of tumor cells[170-172]. Organoids are 3D structures derived from embryonic, induced pluripotent or somatic stem cells, as well as tumor cells, in which cells self-organize into structures that mimic structure and function of the corresponding in vivo tissue[173-177]. In addition, monolayer cultures of pancreatic cell lines lack interactions with stromal and immune cells as well as with ECM, as their presence are hallmarks for pancreatic cancer[60]. In 3D cultures, cells are imbedded in ECM-like structures like collagen or Matrigel, or are kept in suspension using ultra-low attachment culture dish, thus preventing the cells from attaching to the bottom of the culture dish[178]. This enables the co-culturing of cancer cells with multiple cell types to closely mimic the structures found in primary pancreatic tumors. Recently, Boj et al. published a protocol that enables a serial culture of murine and human PDAC cells together with normal pancreas under the same conditions[179]. Orthotopically injected tumor cells of these PDAC organoids showed progression from PanIN precursor lesions to invasive adenocarcinoma in vivo[179,180]. The generation of a pancreatic cancer patient-derived organoid (PDO) library presented heterogeneous responses to standard-of-care therapies and enabled a combined genomic, transcriptomic and therapeutic profiling for each PDO[181]. However, the organoid system also bears several disadvantages, one being the enhanced time and resource consumption compared to 2D cultured cancer cell lines. In addition, the use of ECM substitutes like Matrigel, which afford 3D growth of cancer cells, could incorporate undefined factors which may influence drug screening experiments[176]. Lastly, in co-cultures, cancer derived organoids tend to grow slower than organoids derived from normal epithelium which would result in an overgrowth of tumor cells by the normal epithelium[176]. Despite these limitations, individual patient-derived organoid cultures could become highly relevant for the development

of personalized cancer therapy. Nonetheless, it remains essential to improve the generation and expansion of efficient drug screenings in a clinical time frame.

1.5.5 Advanced serum-free cultured cell lines and xenografts

In our group, Dr. Christian Eisen and colleagues established a culturing model for patient-derived PDAC cells that provided an in vitro and in vivo platform for functional studies[182]. In detail, patient-derived PDAC tissue pieces were surgically placed onto the pancreas of immune-deficient NSG mice[182]. Successfully engrafted primary xenografts (PT) revealed similar histopathological features as seen in primary patient tumors[182]. Next, tumors of PTs were used to develop stable, primary PDAC cell cultures in a serum-free, 2D adherent environment. These primary PDAC cell lines (PACO) reflected distinct cellular morphology and, when re-injected orthotopically into NSG mice, the PACO cell line derived tumors (DT) retained tumorigenicity and histomorphological and transcriptional characteristics observed in PTs[182]. In addition, the PACO model maintained genetic stability within a cell line and heterogeneity across different cell lines for at least 20 passages[182]. Hence, the established patient-derived PDAC model serves as new platform to functionally investigate PDAC biology.

Given that the PACO model system retained heterogeneity between PACO cell lines, Eisen et al., sought to identify immunohistochemical markers that could define PDAC subtypes and improve patient stratification[182,183]. A biomarker list was generated, based on differential gene expression between PACO subtypes defined by Collisson et al., which was then further filtered for candidate genes that are heterogeneously expressed across PDAC specimens in the Protein Atlas database[130,184]. In the exocrine-like subtype, GSEA identified an enrichment for transcripts with binding-sites for the hepatocyte nuclear factor 1 alpha (*HNF1A*) which was not found in the other two subtypes (classical and QM-PDA)[183]. This finding was further validated by immunohistochemistry staining in PACO cell lines and respective xenografts and nuclear staining of HNF1A was only specific in the exocrine-like subtype[182,183]. The QM-PDA subtype was exclusively positive for cytokeratin 81 (KRT81), hence, samples that neither stained positive for HNF1A nor KRT81 were classified as double-negative and resembled the classical subtype[182,183]. In summary, protein markers for the three subtypes, classified by Collisson et al., were defined as HNF1A+ KRT81- for the exocrine-like subtype, HNF1A- KRT81+ for the QM-PDA subtype and HNF1A- KRT81- for the classical subtype[130,182,183].

1.6 Therapy resistance in cancer

Resistance to chemotherapy or targeted therapy continues to be the limiting factor which prevents successful treatment of patients with cancer i.e. without relapse (**Figure 3**). In PDAC, one of the biggest challenges include the finding of improved therapeutic options that would overcome resistance of pancreatic cancer to current treatment regimes. Currently, resistance to chemotherapeutics can be categorized into two distinct groups, those being intrinsic and acquired resistances. Intrinsic drug resistance indicates that prior to the start of the treatment administration, resistance mediating factors are already present in the bulk of the tumor which leads to an ineffective treatment regime[185,186]. Acquired drug resistance only develops during treatment in initially drug sensitive tumors through a diverse range of mechanisms and is usually linked to therapy-induced selection of resistant subpopulation that pre-existed in the untreated tumor[185,186]. According to the Goldie-Coldman hypothesis, the probability that a tumor inherits drug resistant subpopulation depends on the mutation rate and the size of the tumor[187]. This is line with the correlation between tumor burden and curability[188].

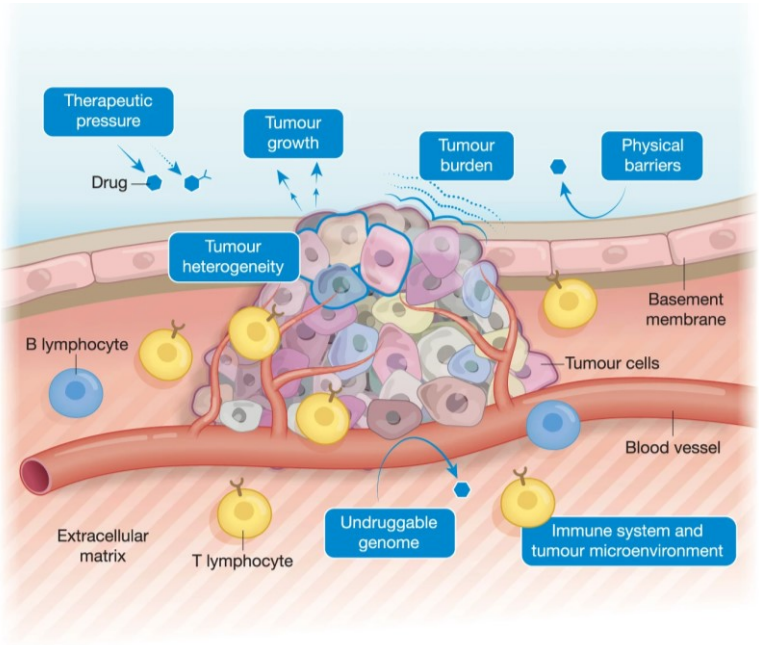

Figure 3 – Biological determinants of drug resistance
Tumors are heterogeneous and are enclosed by basement membrane, vasculature, immune cells and tumor microenvironment. Drivers of drug resistance emerge from changes in the physical parameters, genome and the surrounding environment (Adapted from Vasan, et al.[189]).

Intratumor heterogeneity (ITH) is a multifactorial phenomenon and both genetic and non-genetic mechanisms contribute to the generation of distinct subpopulations of cancer cells within a tumor[190]. A high degree of ITH enhances acquired drug resistance by increasing the probability for a positive selection of drug resistant subpopulations of low prevalence in the

tumor bulk[186,191]. With the acquisition of genomic alterations through various mutational processes, cancer cells gain spatial and temporal diversity[192,193]. Processes inducing these changes vary from age-related mutations to catastrophic events like chromothripsis[194]. Selective therapeutic pressure can lead to loss of targeted clones, acquisition of new resistance mechanisms or adaption to therapy through a variety of mechanisms that result in a new tumor phenotype[195]. Induction of DNA damage by chemotherapeutic drugs is one of various selection pressures which is either repaired by the cell or leads to cell death. Hence, the cancer cells' ability to repair DNA damage dictates the effectiveness of the drug. Once DNA damage is sensed, a cell cycle arrest is induced which allows the cell to repair the damage. In some cancer cells, this response is disrupted by gain-of-function alterations of oncogenes and loss-of-functions of tumor suppressor genes. Loss of functional p53, which is important in the regulation of cell cycle check points, prevents DNA-damage induced cell cycle arrest, hence, loss of p53 is often associated with drug resistance[196].

One of the hallmarks of cancer is resistance to apoptosis that has been linked to drug resistance[119]. Drug resistance can also be acquired through modification of the drug target via mutations or alterations in expression level. Activating *EGFR* mutation in non-small-cell-lung cancers is treated with erlotinib, but cancer cells acquire resistance through gain of gatekeeper mutation ($EGFR^{T790M}$), preventing access to the site where ATP-competitive TKIs bind, making erlotinib ineffective[197]. Activation of oncogenic signaling, like in *KRAS*-mutant tumors do not respond to inhibition of upstream proteins like EGFR[185]. The serine/threonine kinase BRAF downstream of KRAS is frequently activated by mutation in several cancers, especially in melanoma[185]. Inhibitors such as vemurafenib have been developed to target oncogenic $BRAF^{V600E}$; however, secondary resistance inevitably develops despite an initial response rate of approximately 50%, [128]. In PDAC, the stromal compartment induces resistance by protecting cancer cells from cytotoxic compounds[60]. By preventing adequate blood flow, cancer cells can create a hypoxic environment that is pro-tumorigenic and decreases drug exposure. Tumor microenvironment, consisting of immune cells, stroma and vasculature might prevent immune clearance of cancer cells, drug absorption and induce cancer cell growth by stimulating paracrine growth factors[198-200]. Besides, epigenetic alterations could also contribute to drug resistance in cancer[201,202].

Drug activation and inactivation plays an important role for the efficacy of an administered drug. Xenobiotic biotransformation can significantly alter the pharmacokinetics and bioavailability of a drug and is divided into two phases, being phase I (functionalization) and phase II (conjugation)[203]. In phase I, enzymes of the cytochrome P450 (CYP) family oxidize

the substrates by attaching a functional group to it. Next in phase II, the substrates hydrophilicity is increased by addition of a polar group or an endogenous molecule to the functional group by enzymes of the uridine 5' diphospho-glucuronosyltransferase (UGT) family. The increased hydrophilicity enhances the final elimination through the kidney[204]. Currently, half of therapeutic drugs used in clinics are metabolized by the enzymes of the CYP3A family, including several drugs currently used in PDAC treatment (paclitaxel, irinotecan)[90]. In humans, the most prominent members of the CYP3A family are located on chromosome 7, being *CYP3A4*, *CYP3A5* and *CYP3A7* and share up to 71% of their amino acid sequence[205]. Previously, Noll and Eisen, et al have found a subset of PACO cell lines to be resistant to tyrosine kinase inhibitors like erlotinib and dasatinib that have been tested for PDAC therapy in the past[183]. This subset of cell lines also expressed levels of CYP3A5 to the same degree as found in normal liver of pancreas[183]. In addition, PACO cell lines resistant to tyrosine kinase inhibitors, were more resistant to paclitaxel which directly correlated with expression of CYP3A5[183]. Intrinsic resistance to small molecule inhibitors mediated by CYP3A5 was only present in a subset of PACO cell lines; however, when treated with paclitaxel over a longer period of time in vitro, several PACO cell lines became resistant to paclitaxel and expressed increased levels of CYP3A5 compared to the parental cell lines[183]. Of note, other paclitaxel-resistant PACO cell lines remained negative for CYP3A5 which would point towards additional resistance mechanisms that remain to be elucidated[206].

In the past, several transporter proteins in the cell membrane have been linked to drug resistance by promoting drug efflux. Most prominently, membrane transporters belonging to the ATP-binding cassette (ABC) transporter family that regulate flux of many different compounds across the plasma membrane against their concentration gradients[207,208]. ABC transporter are transmembrane proteins that utilize ATP binding and hydrolysis at the two cytoplasmic nucleotide-binding domains (NBDs) localized in the cytosol, which drives conformational changes in their domains[209,210]. Each NBD is linked to a transmembrane domain (TBD) and together, both TMDs form a pore that can be accessed either from the cytoplasm or from outside the cell depending on the conformation status during the catalytic cycle[211]. Although this superfamily is composed of 48 genes and 3 pseudogenes, only three of them have been studied extensively and are related to multi-drug resistance (MDR). Breast cancer resistance protein (*BCRP* or *ABCG2*) has been linked to drug resistance in breast cancer and leukemia, whereas overexpression of MDR-associated protein 1 (*MRP1* or *ABCC1*) has been correlated with drug resistance in breast, prostate and lung cancer[212-217]. Of note, both transporters were found to be expressed in pancreatic cancer samples, as well as in healthy pancreas which was correlated

with resistance to chemotherapy[218-220]. Multi-drug resistance protein 1 (*MDR1*, *P-glycoprotein* or *ABCB1*) is a membrane-bound glycoprotein that is found to be prominently expressed in excretory tissue like colon, small intestine, bile ductules, kidney intestine, adrenal gland and pancreatic ductules[207,210], as well as in testis (blood-testis barrier) and brain capillaries (blood-brain barrier)[221]. ABCB1 plays a crucial role in two physiological processes, being the extrusion of xenobiotics into gut, bile and urine, reducing their bioavailability, and the transport of endogenous molecules (e.g. phospholipids, cytokines) and hormones (e.g. aldosterone, progesterone)[222-224]. More than 30 years ago, expression of ABCB1 was found to be increased in various cancer cell lines after several rounds to treatment with different chemotherapeutic drugs[225-228]. In addition, enhanced expression of ABCB1 was found in several tumor entities and a direct association between expression levels of ABCB1, drug resistance and poor prognosis has been reported in acute myeloid leukemia (AML), osteosarcoma, breast cancer, ovarian cancer and other tumor entities[229-237]. Of note, the FDA recommends that all investigational drugs should first examined with regard to their ability to interact with ABC transporters like ABCB1 or ABCG2.

So far, over 1000 compounds were found to be extruded by ABCB1 which can be explained by the highly flexible and complex structure of the drug binding sites of ABCB1[238,239]. The majority of substrates are hydrophobic, aromatic and their binding to ABCB1 occurs with Kd values ranging between 10µM and 1mM[240]. Its polyspecificity allows ABCB1 to further exploit its role as xenobiotic efflux pump and, sharing substrate bindings with ABCC1, ABCG2 and CYP3A4, protects cells from a high number of cytotoxic drugs[241].

Exposure to cancer chemotherapeutics often causes ABCB1-dependent MDR, hence, inhibition of ABCB1 transporter activity is one of the most studied clinical strategies against development of MDR. Inference of chemotherapeutic drug efflux would lead to an increased accumulation of the drug inside the cancer cell and, subsequently, increase its cytotoxic potential. Verapamil, a calcium channel blocker, was the first ABCB1 inhibitor identified that competed for efflux with chemotherapeutic drugs and increased their intracellular concentration[242]. These first-generation inhibitors were ABCB1 substrates themselves and act by competing for efflux with other ABCB1 substrates. However, due to their low affinity, high systemic concentrations were needed to inhibit ABCB1 transport activity which leads to intrinsic toxicity, unpredictable pharmacokinetic interactions and no significant clinical benefit[210]. Many of the second-generation ABCB1 inhibitors were modified to exhibit enhanced ABCB1 inhibitory activity while decreasing their original therapeutic activity. Even though these compounds successfully inhibit ABCB1, many of them also inhibit enzymes of the CYP family which, again, resulted

in unpredictable pharmacokinetic interactions[243,244]. The development of the third-generation ABCB1 inhibitors was based on quantitative structure-activity relationships (QSAR) and combinatorial chemistry to achieve high specificity and potency at nanomolar concentrations without affecting CYP enzyme activity[224,245]. Hence, most of these compounds were designed to non-competitively inhibit ABCB1 specifically, with elacridar (F12091)[246] and zosuquidar (LY335979)[247] being the most prominent candidates[248,249]. Although third-generation ABCB1 inhibitors did not interact with other drug efflux pumps or CYP enzymes, clinical trials were confronted with unexpected toxicity and only modest results[250-252]. In conclusion, direct inhibition of ABCB1 remains to be problematic and, thus, is not included in routine clinical cancer treatment.

Over the years, various different compounds were found to induce ABCB1 overexpression through multiple mechanisms, including transcriptional upregulation, mRNA splicing, transport and stability, and genomic amplification[224]. Constitutive ABCB1 overexpression mainly depends on several elements, being two GC-boxes located from -56 to -45 bases and from -110 to -103 bases upstream of the major +1 start site in the human *ABCB1* promoter, the Y-box (GCAAT box), the p53 element and the AP-1 and T-cell factor (TCF) elements[190,224]. Induction of *ABCB1* expression has been described to be activated through a variety of stressors, like ROS, heat shock elements and transcription factors, inflammation, chemotherapy and ionizing radiation[224,253-258]. Due to the harsh tumor microenvironment, cancer cells are exposed to endogenous stresses like anaerobic metabolism, glucose deprivation, hypoxia and acidosis which leads to a breakdown in the oxidant-antioxidant balance[253]. Several signaling pathways were proposed to be involved in increased ABCB1 expression through elevated ROS levels, including protein kinase C (PKC), c-Jun NH2-terminal protein kinase (JNK), mitogen-activated protein kinases (MAPKs), phosphoinositide 3-kinase (PI3K)/Akt, extracellular signal-regulated kinases (ERKs), pathways and nuclear factor- B (NF- kB)[259]. A number of putative heat shock element (HSE) sequences are located in the *ABCB1* promoter and some MDR cells lines expressed high levels of heat shock transcription factor (HSF)-DNA binding activity which is supported by the detection of HSF-1 bound to HSEs in the *ABCB1* promoter region[255,260]. Upregulation of ABCB1 is also caused by cellular damage through chemotherapeutic treatment or radiotherapy[253]. Of note, the damage induced by chemotherapeutics has been reported to also induce the generation of ROS and the activation of the pathways described above[261]. In addition, chemotherapeutic compounds can activate pregnane X receptor (PXR) and a direct PXR binding site has been found in the upstream enhancer of *ABCB1*[262]. Furthermore, it was shown that treatment with paclitaxel activates PXR

and enhances ABCB1 mediated drug clearance[262]. The promoter region of *ABCB1* presents several overlapping binding sites for transcription factors which would hint towards a competitive or cooperative interaction. Indeed, a region described as "MDR1 enhancesome" inherits binding sites for the trimeric transcription factor NF-Y and for the specificity protein (SP) family[256,263]. Furthermore, the *ABCB1* gene consists of a proximal and distal promoter region and methylation/demethylation of CpG islands in promoters and gene body determine the activation or repression of ABCB1 expression which was associated with response to treatment and patient survival[264-267]. In both AML and bladder cancer, de-methylation of the *ABCB1* promoter region was proposed to be mandatory for enhanced *ABCB1* transcription and the emergence of an MDR phenotype[268,269].

The human *ABCB1* gene resides in chromosome 7q21.1 region and amplifications in the region of chromosome 7q21 in neuroblastoma, leukemia and lung cancer cell lines correspond to drug resistance and development of MDR phenotype[270-272]. Cancer cells are often affected by genomic instability and chromosomal rearrangements which has been reported to result in genomic amplification and increased expression of ABCB1[273,274]. Usually, these genomic amplifications also affect the genes surrounding *ABCB1* and were found to be co-overexpressed together with ABCB1 in lung cancer cells resistant to paclitaxel[275]. Furthermore, taxane-induced MDR ovarian cancer cell lines showed a regional amplification of 8Mb including 22 genes that surrounded the *ABCB1* gene[276]. These findings were further supported by a study on taxane-resistant breast cancer cell lines that acquired copy number gains of ABCB1 and genes in the close proximity[277]. Moreover, many studies describe a genomic amplification in the region of chromosome 7q21.12 in MDR tumors, where *ABCB1* and related genes are located and that their amplification and overexpression contribute to MDR phenotype[270,271,275,277-283]. In detail, the core genes of the amplified region are Sorci (*SRI*), *ADAM22*, *DBF4*, *SLC25A40*, *RUNDC3B* (*RPIP9*), *ABCB1*, *ABCB4*, *CROT*, *TP53TG1 lncRNA*, *TMEM243* and *DMTF1*[190]. MDR remains a major obstacle in the development of curative chemotherapy in human cancer. Furthermore, ABCB1 plays a significant role in the establishment of MDR in cancer while its inhibition continues to be ineffective in the clinic. Amplification of *ABCB1* and its surrounding genes might contribute to tumor growth and MDR and deciphering their functions could pave the way towards the development of novel biomarkers and therapies.

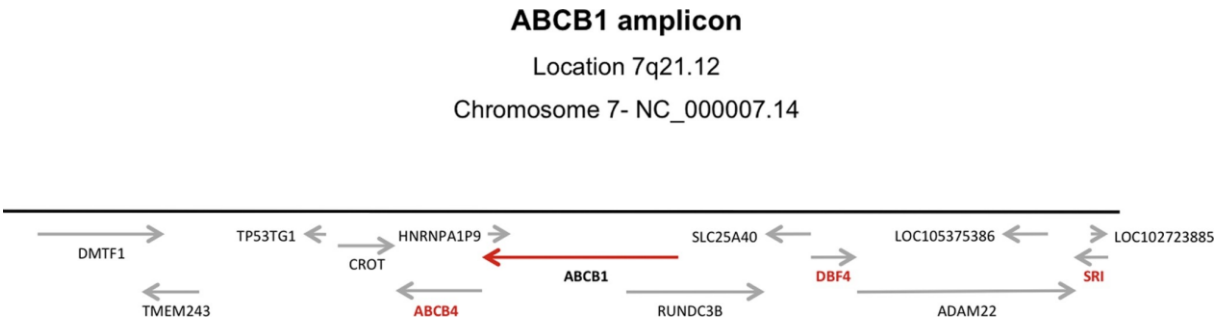

Figure 4 – The ABCB1 amplicon
Genes located in the region 7q21.12 are shown. (Figure from Genovese, et al.[190]).

1.7 Extrachromosomal circular DNA

Extrachromosomal circular DNA (ecDNA) was first reported by Alix Bassel and Yasuo Hoota while investigating the organization of DNA in higher organisms[284]. In electron microscopy images of a part of the DNA was identified in a circular structure[284,285]. Subsequent studies in multiple cancer entities confirm their existence in mammalian cells, but interestingly, these structures are rarely detected in normal human cells[286-288]. Circular DNAs were found in a wide range of sizes from a few hundred base pairs to several megabases and can also be characterized based on their origin from repetitive or unique DNA[289-291]. Of note, only 30% of ecDNA found in a tumor cell are double minutes and the majority of ecDNA belong to the telomeric circles or microDNAs[290]. Additional studies found that methotrexate resistant cancer cells acquired an amplification of the DHFR gene which was either located double minutes of ecDNA or homogeneously staining regions (HSRs) on the chromosome[292,293]. In the 1980s, the first reports described that oncogenes may be located on ecDNA in neuroblastoma and colorectal cancer cell lines[294,295]. Furthermore, studies confirmed that frequency and amplitude of oncogene amplification could be modulated by stimuli, like treatment with hydroxyurea, and it was proposed that ecDNA would underlie the same replication mechanisms as chromosomes[296-298]. Recently, scientist discovered that resistance to EGFR tyrosine kinase inhibitors (TKIs) in glioblastoma was mediated by a reversible loss of a gain of function mutation in *EGFRvIII* that was located on ecDNA[299]. Treatment with EGFR TKIs eliminated ecDNA carrying mutant EGFR, however, after drug withdrawal, ecDNA carrying mutant EGFR quickly reemerged which highlights the dynamics of an ecDNA-based resistance mechanism to applied therapies[299]. Combination of whole genomes sequencing (WGS), cytogenic image and computational analyses enabled an in-depth approach to detect and characterize ecDNA which revealed that oncogene amplification on ecDNA is frequently found in cancer[288,290]. Moreover, combined analysis of corresponding cell culture and orthotopic xenograft models in

glioblastoma showed that the majority of oncogenic gene amplifications on ecDNA were propagated from the tumor to the model systems[300]. Of note, ecDNA was found to be unevenly inherited by offspring cells which is different to chromosomes and directly affects the oncogenic potential of each cell, rapidly increasing intratumoral heterogeneity and enabling cancer cells to quickly adapt to selective pressures like drug therapy[300] (**Figure 5**).

To date, the biogenesis of ecDNA remains to be only poorly understood. Generation of ecDNA could be initiated by a DNA damage or chromothriptic events that induce double-strand breaks or chromosomal rearrangements which result in circularization of DNA segments into ecDNA[301]. Loss of tumor suppressor genes could prevent the apoptotic response to DNA damage and enable replication of ecDNA. However, it remains controversial whether DNA replication alone contributes to ecDNA generation, since studies exist that find ecDNA levels to increase under blockage or absence of DNA replication[302,303]. Most ecDNA lack centromeres and, thus, are randomly distributed to the daughter cells during mitosis, which results in heterogeneous ecDNA counts between cancer cells within a tumor[304]. The localization of oncogenes or resistance mechanisms could provide a selective advantage that would increase the overall number of ecDNA and the copy number of the respective gene within the tumor. Although maintaining the ecDNA might come with a fitness cost, cancer cells that contain ecDNA may be able to respond quicker to changes in the environment, including cancer therapy[299,305,306].

Recently, a study created a theoretical model about the evolutionary dynamics of ecDNA that reports a 300% increased fitness for cells carrying ecDNA[307]. Furthermore, a recent study described ecDNA as a major source of somatic rearrangements that would contribute to oncogenic remodeling through circularization and reintegration into the genome[308]. The rearrangements caused by reintegration of ecDNA could represent a mutagenic process and an additional driver of cancer genome remodeling[308]. Detailed analysis of the ecDNA structure revealed that ecDNA is indeed circular and packed into chromatin with an intact domain structure[309]. However, ecDNA lacks higher-order compaction, that is typically found in chromosomes, which leads to enhanced chromatin accessibility[309]. Hence, oncogenes encoded on ecDNA are found to be the most transcribed genes, correlating increased copy number with enhanced expression levels. Moreover, ecDNA-based amplification of oncogenes yields higher expression levels compared to copy-number-matched chromosomal DNA which was linked to enhanced chromatin accessibility[288]. Interestingly, circular structure of ecDNA enables ultra-long-range chromatin contacts, which allows interaction with distant regulatory elements that could enhance oncogene expression[309]. Indeed, it has been observed, that the topology of

ecDNA enables enhancer rewiring which leads to the contribution of endogenous and new enhancers to cell proliferation and cellular fitness[310]. Patients carrying ecDNA had significant shorter overall survival compared to patients without ecDNA-based oncogene amplification, across many cancer types[288,308]. Thus, understanding the role of ecDNA in tumor development will ultimately lead to improved treatment strategies.

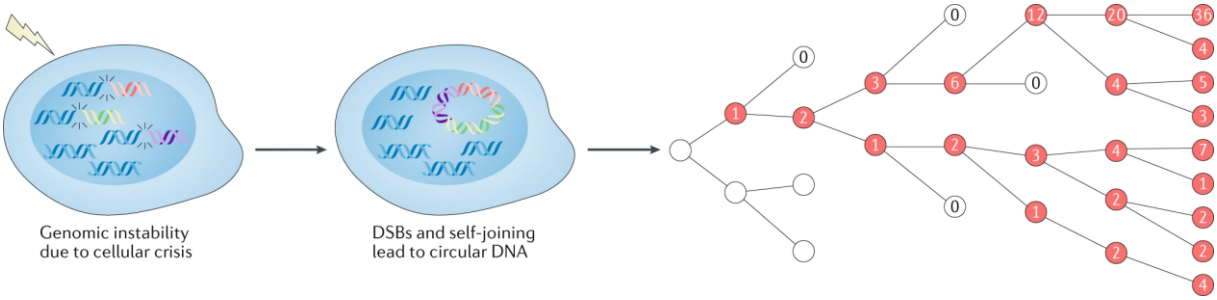

Figure 5 – Proposed model for ecDNA formation and amplification in tumors
Induction of genomic instability or DNA damage cause double-strand breaks and even chromosomal breakage. The resulting DNA segments could form circular extrachromosomal DNA (ecDNA) through non-homologous recombination. Viable tumor cells harboring ecDNA elements would replicate and segregate them to daughter cells. Due to the lack of centromeres, ecDNA would be segregated unevenly to the daughter cells which could rapidly increase heterogeneity of ecDNA counts in each tumor cell. In case of an improved fitness through ecDNA elements, the number of tumor cells carrying ecDNA is rising rapidly. DSB, double-strand break. (Figure from Verhaak, et al.[311])

2 Aim of Dissertation

Pancreatic cancer is an aggressive and lethal disease with a miserable prognosis[1]. Chemotherapeutic regimens, like FOLFIRINOX[110] or gemcitabine plus nab-paclitaxel[111] remain the standard treatment of care in patients diagnosed with PDAC while only achieving a modest increase in overall survival. Transcriptional subtyping of PDAC discerns tumors into two broad lineages which provides the opportunity to improve patient stratification and treatment, but has not been translated into clinical practice yet[90,126]. Meanwhile, resistance to chemotherapy continues to be the limiting factor that prevents a patient's cure from cancer and finding improved therapeutic options could overcome resistance of PDAC to current treatment regimens[125]. Previously, Noll and Eisen *et al.*, identified a subset of patient-derived PDAC (PACO) cell lines with intrinsic resistant to erlotinib, dasatinib and paclitaxel[183]. Moreover, this subset of PACO cell lines expressed similar levels of CYP3A5 as found in the normal liver of patients[183]. Pharmaceutical inhibition of CYP3A5 sensitized this subset of PACO cell lines to tyrosine kinase inhibitors and paclitaxel[183]. In addition, CYP3A5 was identified as mediator of acquired drug resistance in several PACO cell lines, however, some cases of acquired drug resistant PACO cell lines developed a CYP3A5-independent resistance mechanism[206]. These findings point towards additional resistance mechanism in acquired drug resistant PDAC cells that remain to be elucidated by generating additional drug resistant PACO cell lines. Intratumor heterogeneity (ITH) is multifactorial phenomenon based on genetic and non-genetic mechanisms that enhance acquired drug resistance by increasing the probability for the generation of drug resistant subpopulations[186,191]. Investigation of clonal heterogeneity during the generation of drug resistant PACO cell lines could identify the key subclones that mediate acquired drug resistance.

Therefore, the objective of this study is to generate a reliable long-term treatment regimen to identify novel drug resistant mechanisms in PDAC. The investigation of newly identified drug resistant mechanisms on various transcriptional, genetic and epigenetic levels provides the opportunity to identify new vulnerabilities that could be translated into clinical use. In addition, a detailed analysis of pathways involved in drug resistant phenotype has the potential to identify new targets whose inhibition could prevent the development of the drug resistant phenotype.

3 Results

3.1 Gene expression-based stratification of patient derived xenografts

Our lab has previously shown that a subset of PACO cell lines (HNF1A+ cell lines) expressed CYP3A5 on the basal level and this confers them resistance to paclitaxel[183]. CYP3A5 also contributed to acquired resistance in several PACO cell lines after long-term treatment with paclitaxel or other small-drug inhibitors[183]. However, some PACO cell lines acquired paclitaxel-resistance independent of CYP3A5, revealing additional CYP-independent mechanisms that mediate resistance in PDAC[206]. In order to identify patient samples that lack basal expression of CYP3A5, we first analyzed the gene expression profile of the corresponding patient derived xenografts (PDX) using human-specific microarrays. Hierarchical clustering separated xenografts into two groups, independent of the patient tumor or xenograft stratification based on immunohistochemistry staining of HNF1A and KRT81 (**Figure 6A**). Interestingly, almost 75% of PDX with high and medium expression of *CYP3A5* were grouped in cluster 1 (C1), whereas the majority (more than 60%) of low *CYP3A5* expressing PDXs were found in cluster 2 (C2). CYP3A5 positively stained tumors grouped exclusively in C1. Differential gene expression analysis between these two clusters revealed enhanced expression of *CYP3A5* and genes responsible for induction of CYP3A5 expression (*HNF4A*, *NR1I2*) in C1, which correlated with the immunohistochemistry staining for CYP3A5 (**Figure 6B**). In addition, we identified several markers in C1 that have been previously reported to be enriched in the exocrine-like and classical subtypes of PDAC, including *GATA6*, *REG4*, *TSPAN8*, *TOX3*, *CLDN18* and others[130,131]. In C2, we found increased expression of genes that serve as markers for the quasi-mesenchymal and basal-like subtypes, naming *S100A2*, *S100A8*, *CST6* and *CAV1* among others[130,131]. Gene Set Enrichment Analysis (GSEA) of the two clusters, revealed enrichment of genes related Epithelial to Mesenchymal Transition and TNFα signaling via NFKB in xenografts in C2. Both gene sets are linked to invasion and metastasis in cancer cells and support the aggressive phenotype of the basal subtype in PDAC[131,312]. For PDXs that cluster in C1, genes being HNF1 transcription factor targets, as well as genes linked to general digestion were significantly enriched. Both gene sets would suggest that C1 inherited PDX of the classical phenotype as well as tumors of the pancreatic/exocrine-like subtype which could be summarized as classical-pancreatic subtype[126]. In order to confirm our findings, we tested the signatures of previously published subtypes on both clusters (C1 and C2). Applying the gene sets of previously published subtypes, we confirmed that the PDXs belonging to the

classical (C1) subtype were enriched for the Classical signature by Collisson et al., Classical signature by Moffitt et al. and the Progenitor-PDA signature by Bailey et al.[130,131,133] (**Figure 6C**). Furthermore, PDXs classified as basal (C2) were enriched for the QM-Like, Basal and Squamous-PDA signatures, described by the authors above. Based on these findings, the PDXs found in cluster C1 were classified as classical subtype, whereas PDXs grouped in cluster C2 were classified as basal subtype.

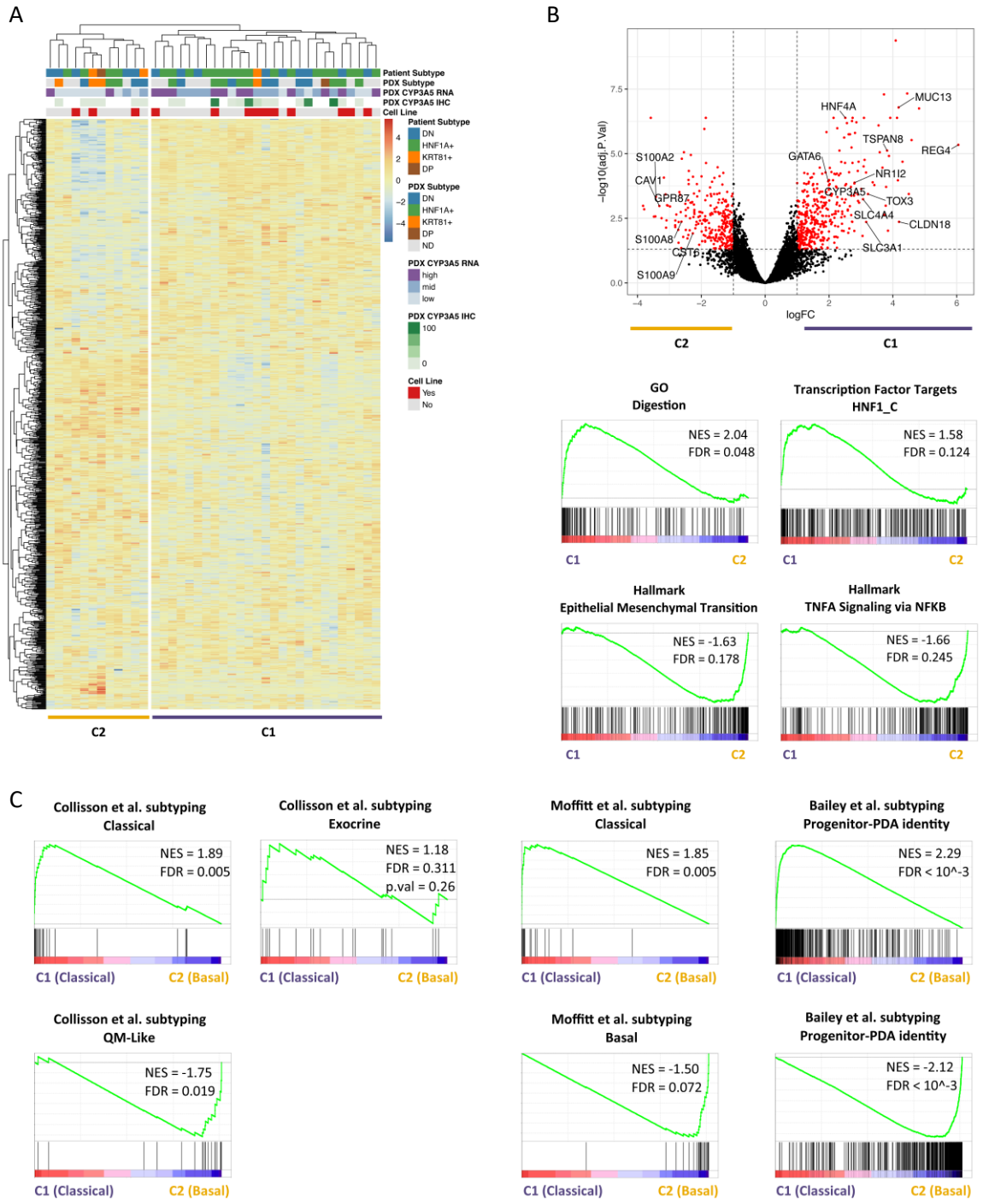

Figure 6 – Gene expression-based stratification of patient derived xenografts
(A) Hierarchical clustering analysis of gene expression microarray data generated from patient derived xenografts (PDXs) of the H015 cohort. Complete Pearson correlation-based distance. Intensities are centered in gene direction and correspond to log2 scale. Colors of patient and PDX subtype correspond to marker-defined subtypes. Colors of PDX CYP3A5 RNA expression corresponds to mean fluorescent intensity (MFI)-based categories of high, mid and low intensity levels. Continuous color scaling for immunohistochemistry (IHC)-based CYP3A5 expression in PDX tumor samples.
(B) Volcano plot of all differentially expressed genes between the two groups identified by hierarchical clustering analysis (C1 and C2). Highlighted in red are all genes that are at least one log2-fold differentially expressed with an adjusted p-value of less than 0.05 according to the Benjamini-Hochberg calculation. Labeled genes have been previously defined to be surrogate markers for molecular subtypes[130,131,133,183].
(C) Gene set enrichment analysis (GSEA) of the previously defined groups of PDXs of the H015 cohort. Statistical significance was assessed using 10,000 permutations on the phenotype. NES, normalized enrichment analysis; FDR, false discovery rate.
(D) GSEA of published PDAC-subtype signatures in C1 and C2[130,131,133]. NES, normalized enrichment analysis; FDR, false discovery rate.

3.2 Genomic characterization of selected PACO cell lines

Next, we aimed to validate the previous findings in vitro and selected a PACO cell line of each group (basal and classical) together with PACO17 that has been previously reported to be independent of CYP3A5 after paclitaxel long-term treatment[183]. Also, we were looking for appropriate cell lines that were not likely to express CYP3A5 as a primary resistance mechanism. For all further studies presented in this dissertation, we have chosen to use the following cell lines which were established in our lab as previously described[182,206]: PACO17, PACO22 (classical) and PACO43 (basal). For each cell line, the characteristics of patient and tumor (including stratification of subtype based on gene expression analysis and definition of CYP3A5 expression levels by IHC), as well as its marker-defined subtype are summarized in **Table 2**. To further characterize these PACO cell lines and to identify important genomic aberrations that could influence the outcome of the long-term drug treatment, we performed whole genome sequencing (WGS) for each cell line, paired with respective blood control of the corresponding patient. First, we analyzed the mutational status of the key genes associated to PDAC[41]. We identified the same hallmark mutation in *KRAS* in all three cell lines (**Table 3**). *TP53* was mutated in PACO17; PACO22 had a frameshift insertion and PACO43 showed loss of heterozygosity (LOH). *CDKN2A* was only mutated in PACO17, whereas the other two lines had deleted *CDKN2A* entirely. In addition, we analyzed the status of *SMAD4* and found LOH in PACO17 and PACO43, and a homologous deletion in PACO22. Of interest, PACO22 was the only cell line that had a *MYC* amplification (>60 copies).

Table 2: Characteristics of patients and tumors used to derive PACO lines.

Cell Line	Age	Sex	Stage	Grade	Tumor	PDX Subtype	PDX IHC CYP3A5	Cell Line Subtype
PACO17	65	M	T3 N1 Mx	G3	PDAC	-	-	DN
PACO22	53	F	T3 N1 M0	G3	PDAC	Classical	Negative	DN
PACO43	56	M	T3 N1 M1	G3	PDAC	Basal	Negative	KRT81+

Table 3: Analysis of KRAS, TP53, CDKN2A, SMAD4 mutations and MCY amplification from selected PACO lines, identified by Whole Genome Sequencing (WGS).

Cell Line	KRAS (NM_004985.5)	TP53 (NM_000546)	CDKN2A (NM_000077)	SMAD4 (NM_005359)	MYC (NM_001354870)
PACO17	c.G35A:p.Gly12 Asp	c.G785T:p.Gly262 Val	c.C247T:p.His83 Tyr	LOH	wt
PACO22	c.G35A:p.Gly12 Asp	c.600_601insGGA AATT:p.L201fs	Homo-Del	Homo-Del	DUP
PACO43	c.G35A:p.Gly12 Asp	LOH	Homo-Del	LOH	wt

Next, we used WGS data to analyze the copy number profile of all chromosomes for each cell line. PACO17 was the only cell with a ploidy of 2, whereas PACO22 and PACO43 were triploid. For PACO17, first part of Chr. 5 was amplified in one allele. Several chromosomes (Chr. 3, 11, 12, 15) experienced complete loss of heterogeneity (LOH), whereas some chromosomes (Chr. 7, 17, 18, 21) had only partial LOH. In PACO22, parts of Chr. 5 and 17 were amplified and Chr. 4, 9 and 15 were affected by LOH. PACO43 showed amplification of parts of Chr. 2, 3, 7, 8 and 19 and had LOH of Chr. 6, 9, 12, 17 and 18. Taken together these data confirm the inter-patient diversity at the genomic and expression level existing in PDAC[65,90,313]. We conclude that all three cell lines differ from each other on the genomic and transcriptional level.

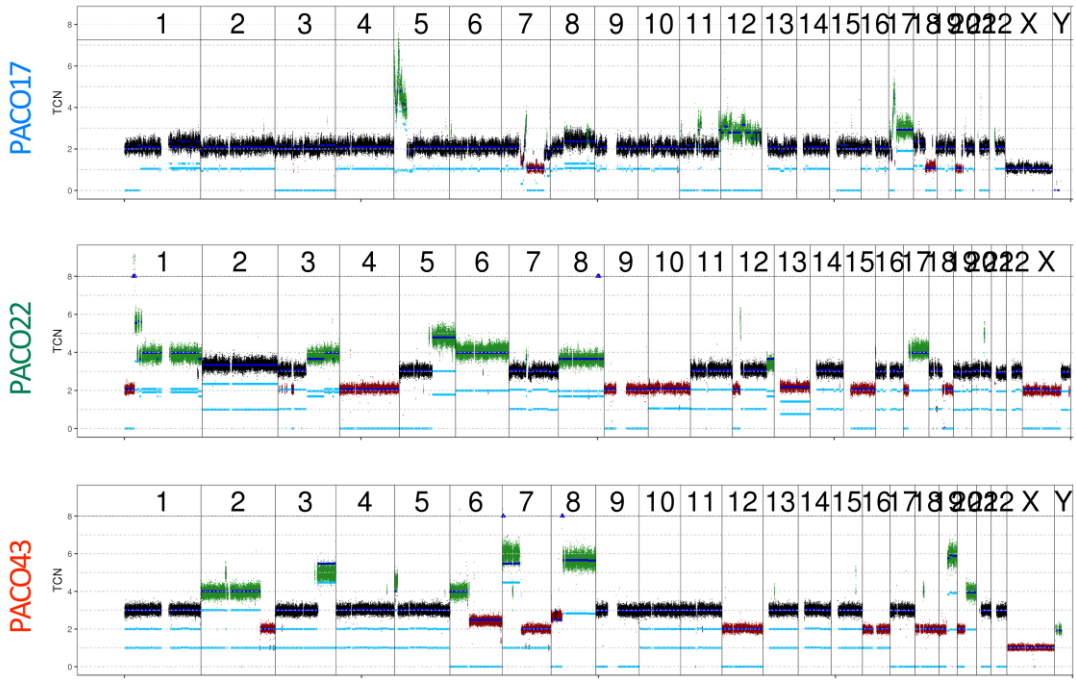

Figure 7 – Copy number profile of the whole genome of each parental PACO cell line
Total copy number (TCN) profile of the genome of the parental cell lines of PACO17, PACO22 and PACO43. Green highlighted regions have an amplified copy number count, red highlighted regions have a reduced copy number count, compared to the ploidy-based standard copy number. Light blue lines correspond to the two parental chromosomes.
TCN, total copy number.

3.3 Generation of drug resistance PACO cell lines by long-term drug treatment

In order to generate clinically relevant drug resistant cell lines, we first analyzed clinical treatment regimens that are used to treat pancreatic cancer. Currently, the majority of pancreatic cancer patients either receive FOLFIRINOX or nab-paclitaxel and gemcitabine (nPG) as standard treatment of care[90]. Patients treated with nPG, receive this combination of drugs once a week for three weeks. Due to high toxicity, this is followed by a one-week recovery time for the patient[109]. Thus, we decided to design a treatment regime that incorporates a single round of treatment followed by a recovery phase. Furthermore, this treatment regime afforded a strong selection pressure on to the cells, with only a small percentage of cells remaining which would then repopulate the flask during the recovery phase. In order to confidentially identify resistance mechanisms for either nab-paclitaxel or gemcitabine, we first aimed to generate single-drug resistant cell lines, followed by nPG-resistant cell lines. We established a pulsed drug treatment regime that consisted out of four days of drug treatment, followed by a recovery phase of at least 1 week in drug-free media until cells fully recovered (**Figure 8A**). Starting from a parental cell line, cells were evenly distributed into six flasks. Half of the flasks were treated with paclitaxel and half with the vehicle compound DMSO to generate appropriate control cells. The use of biological replicates for both paclitaxel-treated cells and control cells permit statistical comparison and the possibility to yield different resistance mechanisms. Drug concentration was stepwise increased during several rounds of treatment until 1µM was reached (**Figure 8A, B**). After the last round of treatment, treated cells completely tolerated 1µM paclitaxel and were tested for acquired drug resistance by cell sensitivity assays. For the initial plaque assay, paclitaxel-treated and control cell lines received a single round of the long-term treatment regime, including recovery phase (i.e. 4 days of 1µM paclitaxel treatment followed by 4 days recovery) and analyzed cell viability based on cell confluency. Importantly, all paclitaxel-treated cell lines of PACO17, PACO22 and PACO43 survived treatment with 1µM of paclitaxel, assuring that treated cells reached the endpoint of long-term treatment regime (**Figure 8C**). Next, we tested for acquired resistance at higher concentrations by CellTiter Blue (CTB) and plaque assay. We could not detect a significant shift in IC50 between paclitaxel-treated and control cell lines of PACO17 and PACO43 (**Figure 8D**). Only in PACO22, paclitaxel- treated replicates had a significantly increased IC50 compared to control replicates and analysis by CTB assay estimated a 100-fold increase in IC50 for paclitaxel-treated replicate compared to control replicates. In order to validate the findings of CTB assay, we performed a plaque assay for concentrations rising from 500nM to 10uM. Again, all paclitaxel-treated cell

lines of PACO17, PACO22 and PACO43 survived treatment with 1 µM of paclitaxel (**Figure 8E**). Since paclitaxel-treated cell lines of PACO17, PACO22 and PACO43 acquired a paclitaxel-resistant phenotype, we classified paclitaxel-treated cells as paclitaxel-resistant (PR) cell lines. Similar to CTB assay, generated PR replicates of PACO22 were able to withstand paclitaxel concentrations up to 10 µM, whereas control cells did not survive treatment with 500 nM of paclitaxel (**Figure 8E**). For PACO43, two out of three PR replicates were able to survive the treatment with 5 µM paclitaxel and control cells already died after treatment with 500 nM paclitaxel. Only one out of the three PR replicates of PACO17 was able to survive 5 µM of paclitaxel treatment and control cells were able to withstand treatment with 500 nM paclitaxel, but died at 1 µM paclitaxel treatment. We can conclude that starting from paclitaxel sensitive population, pulsed treatment regime successfully generated PR cells at 1 µM paclitaxel concentration in all three cell lines. Some of the generated PR replicates also showed resistance at higher drug concentrations.

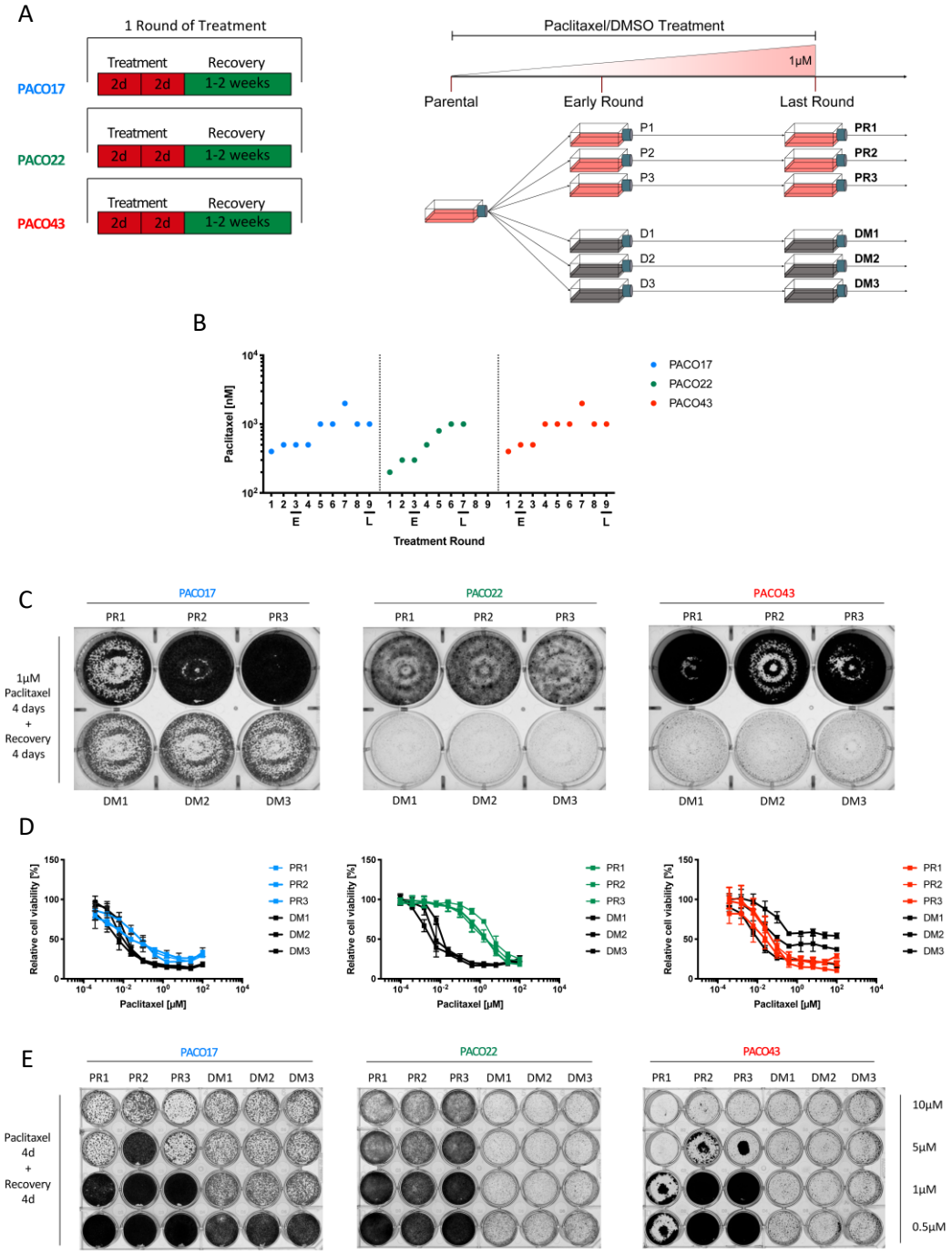

Figure 8 - Generation of paclitaxel resistant PACO lines
(A) Schematic overview of long-term treatment regimen. A single round of treatment is divided in two times two treatment days that are followed by a recovery period. Each parental cell line was divided into two treatment arms with three biological replicates each. Sample collection took place at an early timepoint and after the last round of treatment.
(B) Paclitaxel concentration during each long-term treatment round in the respective cell lines.
(C-E) Sensitivity of PR and DM cell lines of PACO17, PACO22 and PACO43 after the last long-term treatment round to **(C)** treatment with 1 µM paclitaxel for 4 d, followed by 4 d of recovery time. Density of cells is determined by crystal violet staining. **(D)** Treatment with paclitaxel for 72 h determined by Cell Titer Blue metabolism (n = 1 per sample). Error bars depict mean ± 95% confidence interval of technical replicates (n = 4).
(E) Treatment with different paclitaxel concentrations following the experimental setup described in (C).
E, Early round; L, Last Round; P, Paclitaxel-treated; PR, paclitaxel-resistant; D/DM, DMSO-treated.

3.4 Stability of drug resistance mechanism is different between PACO cell lines

After successfully establishing PR cell lines with our long-term treatment regime, we determined the stability of the acquired resistance in the respective cell lines. To this end, PR cell lines were cultured for five passages without further drug treatment (**Figure 9A**). Afterwards, cell lines were tested for drug resistance by CTB and plaque assay. Similar to the results after the last round of treatment, only PR replicates of PACO22 showed a significantly increased IC50 by CTB compared to control cells, whereas PACO17 and PACO43 did not show differences between PR and DMSO-treated (DM) control cell lines (**Figure 9B**). Accordingly, plaque assay analysis confirmed that PR cell lines of PACO17 and PACO43 had lost their resistance to paclitaxel and were similarly sensitive to paclitaxel as the respective control lines (**Figure 9C**). Only PR replicates of PACO22 remained highly resistant against paclitaxel, able to withstand up to 10µM paclitaxel, similar to the results after the last round of treatment (**Figure 8E**). From these findings, we can conclude that PACO17 and PACO43 lose the acquired resistance in PR replicates after five-passage-long drug holiday, whereas PR replicates of PACO22 remained stably resistant against paclitaxel treatment.

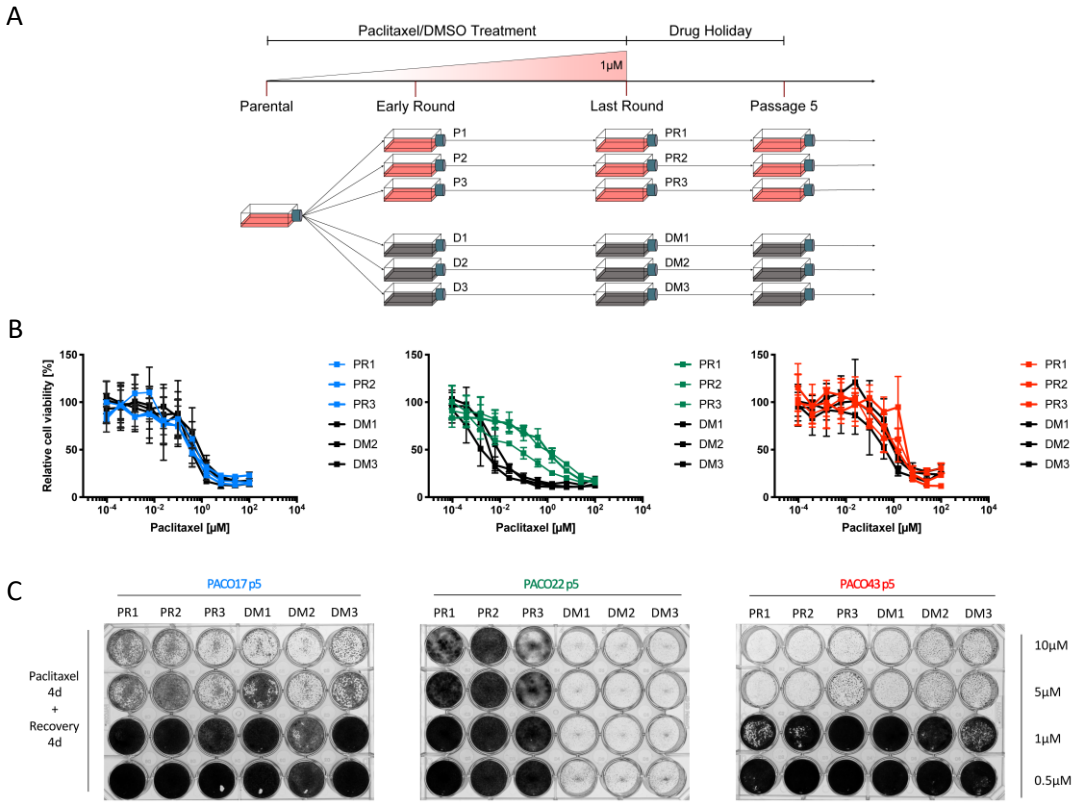

Figure 9 - Stability of drug resistance mechanism is different between PACO cell lines
(A) Schematic overview of long-treatment regimen for paclitaxel including the five passages of drug holiday to test stability of drug resistance phenotype.
(B-C) Sensitivity PR and DM cell lines of PACO17, PACO22 and PACO43 after five passages of drug holiday to paclitaxel treatment for **(B)** 72 h determined by Cell Titer Blue metabolism and for **(C)** 4 d treatment followed by 4 d recovery phase (n = 1 per sample). Error bars depict mean ± 95% confidence interval of technical replicates (n = 4). (C) Density of cells is determined by crystal violet staining.
P, Paclitaxel-treated; PR, paclitaxel-resistant; D/DM, DMSO-treated; p5, Passage 5.

3.5 Identification of ABCB1 as drug resistance mechanism in paclitaxel-resistant cell lines

Next, we aimed to identify the resistance mechanisms the PR cell lines acquired during the long-term treatment. For all three PACO cell lines, we performed human-specific microarray-based gene expression analysis of four different timepoints being: (1) the parental cell lines, (2) an early timepoint after two to three rounds of treatment, (3) the last round of treatment when cells acquired resistance against the highest concentrations of paclitaxel, (4) and five passages after drug holiday (**Figure 9A**) (**Figure 10A**). Hierarchical clustering according to the 100 most variant genes separated cell lines in three distinct groups corresponding to each patient cell line, with PACO22 clustering further apart from PACO43 and PACO17 (**Figure 10B**). To investigate resistance mechanism that could have arisen in all PACO lines, we combined treated samples of all three cell lines for each timepoint and compared them with the respective control

samples by paired analysis. We first performed GSEA on the respective groups after the last round of treatment (3) (**Figure 10A, C**). Paclitaxel-resistant cell lines were enriched for genes involved in interferon alpha response and xenobiotic metabolism and revealed a reduction in genes involved in DNA replication (**Figure 10C**). These gene sets represented the effect of paclitaxel treatment on the cells which resulted in activation of interferon response through DNA damage and xenobiotic metabolism as well as a reduction in cell cycle activity through microtubule stabilization and cell cycle arrest[314,315]. Next, we performed differential gene expression analysis for each of the three timepoints (2) "Early Round", (3) "Last Round" and (4) "Passage 5". In the early round of the long-term treatment, no gene was significantly overexpressed in one of the groups (**Figure 10D)**. After the last round of treatment, *ABCB1* was the only significantly over-expressed gene in PR cell lines compared to control cell lines of all three PACO lines (**Figure 10C**). Next, we investigated whether expression of *ABCB1* remained stable in PR cell lines after five passages of drug holiday. Indeed, *ABCB1* was not significantly over-expressed after drug holiday. Of note, *ABCB1* was found to be overexpressed in the paclitaxel treated group at all three timepoints, however, these findings were not significant in the Early Round and at Passage 5. Hence, the loss of a significant overexpression of *ABCB1* at Passage 5 could correlate with the loss of paclitaxel resistance in two of the three PACO cell lines (PACO17 and PACO43) (**Figure 9C**). Taken together, these findings nominate ABCB1 as a key player in the acquired paclitaxel resistance of PACO cell lines. The differences found on the genetic and transcriptional level between these cell lines could explain the results and a detailed analysis of each cell line should provide further insights into the resistance mechanisms.

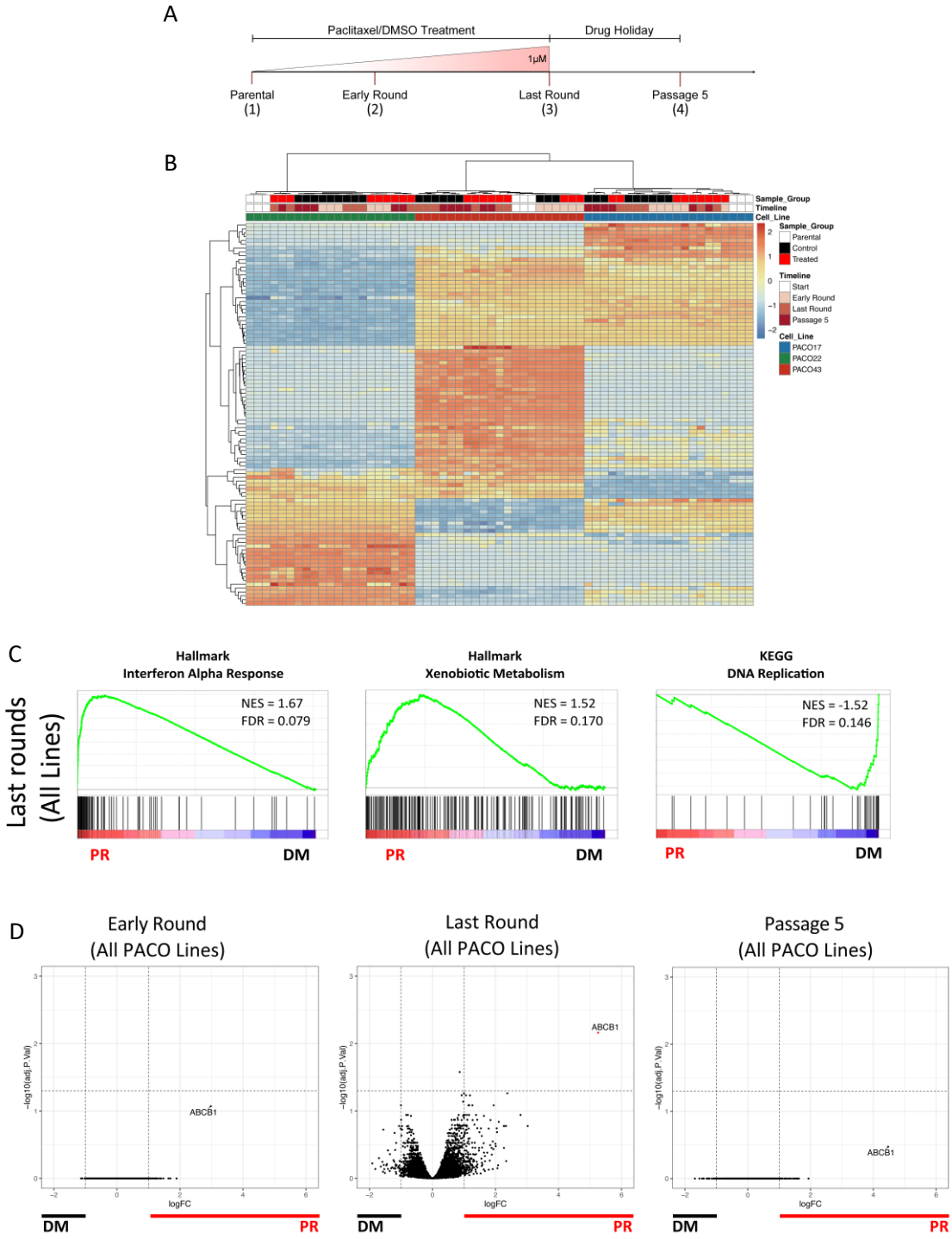

Figure 10 – Identification of *ABCB1* is possible drug resistant mechanism in PR cell lines of PACO17, PACO22 and PACO43

(A) Schematic overview of long-treatment regimen for paclitaxel including the five passages of drug holiday.
(B) Hierarchical clustering analysis of all samples collected at the different timepoints (1-4) of the three PACO cell lines.
(C) Gene set enrichment analysis of combined PR cell lines compared to respective combined DM cell lines out of the three PACO cell lines after the last round of treatment (n = 9 individual cell lines per group). Complete Pearson correlation-based distance. Statistical significance was assessed using 10,000 permutations on the phenotype.
(D) Volcano plot of all differentially expressed genes between combined PR cell lines compared to respective combined DM cell lines of the three PACO cell lines after the last round of treatment (n = 9 individual cell lines per group). Highlighted in red are all genes that are at least one log2-fold differentially expressed with an adjusted p-value of less than 0.05 according to the Benjamini-Hochberg calculation. *ABCB1* is the only gene to be significantly overexpressed in PR group after the last round of treatment.
NES, normalized enrichment analysis; FDR, false discovery rate; PR, paclitaxel-resistant; DM, DMSO-treated.

3.6 PACO cell lines acquire different mechanisms against paclitaxel treatment

Although the PR cell lines of all three PACO lines overexpressed the same gene (*ABCB1*) after the last round of treatment, they remained transcriptionally distinct and kept their cell line identity (**Figure 10B**). Therefore, we aimed to identify differences in the underlying mechanisms that resulted in upregulation of *ABCB1* in PR cell lines. For each PACO cell line, we utilized GSEA to identify differences between PR and DM replicates at the last round of treatment, because at this time point cell viability exhibited the strongest difference upon paclitaxel treatment. GSEA revealed an enrichment of genes related to interferon alpha/beta signaling in PR cell lines of all three PACO cell lines after the last round of treatment (**Figure 11**). Hence, long-term paclitaxel treatment might have activated interferon pathways during the generation of paclitaxel-resistant cells. However, comparison with parental cell line revealed a downregulation of interferon related genes in DMSO cell lines instead (**Supplementary Figure 1**). Furthermore, PACO17 PR cell lines were enriched for genes involved in xenobiotic metabolism and lacked genes related to mismatch repair after long-term paclitaxel treatment (**Figure 11A**). Both gene sets support the development of drug resistant cells that have adapted to paclitaxel treatment[316-319]. DM cell lines of PACO17 were enriched for E2F target genes and genes related to cell cycle, indicating a selection for improved proliferation under these conditions (**Supplementary Figure 1A**). Similar to PACO17, PR cell lines of PACO43 also showed a reduction in mismatch repair genes and, additionally, have downregulated genes involved in activation of ATM- and Rad3-related kinase (ATR) in response to replication stress (**Figure 11C**). This signature of reduced DNA replication stress could have contributed to an improved cell viability of the PR cell lines under paclitaxel treatment[320]. Of interest, DM cell lines were less enriched for genes that are linked to CYP450 mediated metabolism of xenobiotics than the parental cell line (**Supplementary Figure 1C**). Furthermore, DM cell lines of PACO43 were also more enriched for cell proliferation genes than the parental cell line (**Supplementary Figure 1C**). These signatures were not found in PR cell lines of PACO22, however, signatures were enriched for genes related to ABC protein mediated transport including *ABCB1* and genes located on chromosome 7 close to the *ABCB1* locus (**Figure 11B**). This might hint to a grouped induction of expression or a genomic amplification of that region[190]. Similar to PACO17, DM cell lines were less enriched for interferon related genes compared to the parental cell line (**Supplementary Figure 1B**). Also, DM cell lines were less enriched for genes linked to fatty acid metabolism, but more enriched in E2F target genes, which both links to improved proliferation in DM cell lines[321]. From these findings we conclude

that the different PACO cell lines have adapted to paclitaxel treatment in various ways to prevent apoptosis and cell death upon on paclitaxel treatment.

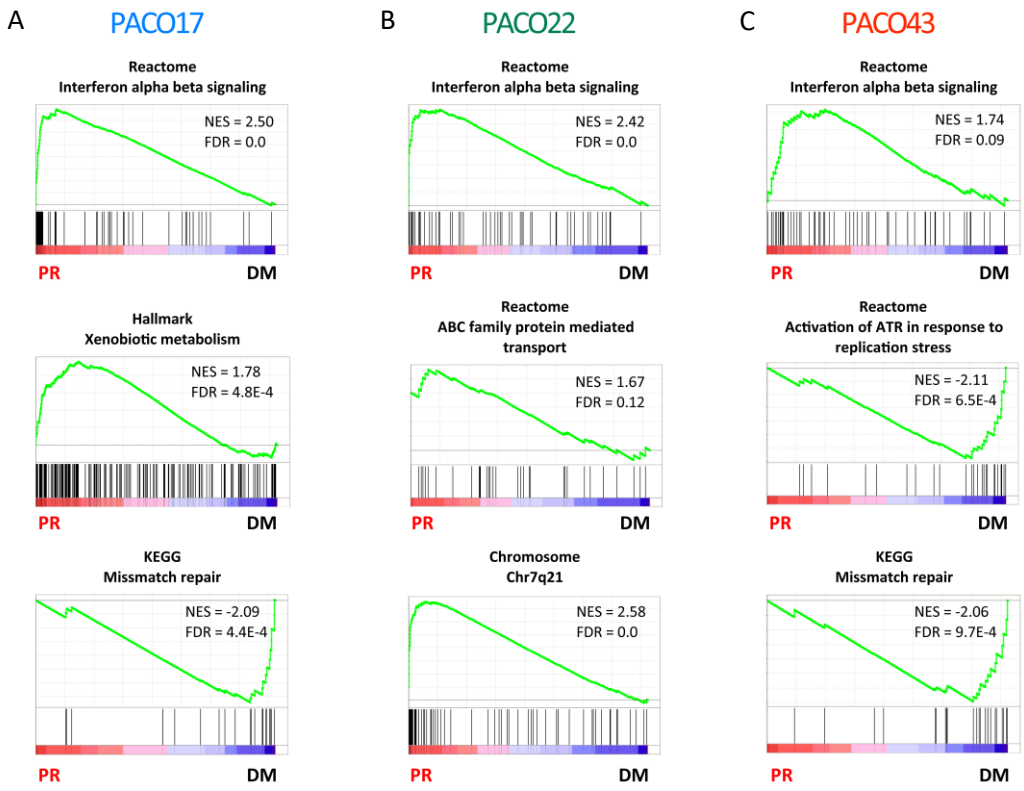

Figure 11 – PACO cell lines acquire different mechanisms against paclitaxel treatment
(A-C) Gene set enrichment analysis (GSEA) plots of PR cell lines compared to DM cell lines after the last round of treatment of **(A)** PACO17, **(B)** PACO22, **(C)** PACO43 (n = 3 individual cell lines per group). Statistical significance was assessed using 1000 permutations on the gene set.
NES, normalized enrichment analysis; FDR, false discovery rate; PR, paclitaxel-resistant; DM, DMSO-treated.

3.7 ABCB1 is significantly enriched during paclitaxel resistance

After the global gene expression analysis of all cell lines and GSEA between PR and DM replicates of each PACO cell line, we continued with the detailed analysis of each single cell line to identify targets responsible for the acquired paclitaxel resistance. Already in the Early round of the long-term treatment, paclitaxel-treated cells of PACO17 had a 3-fold higher expression of *ABCB1* than control cells (**Figure 12A**). *ABCB1* was already the top differentially expressed gene and only few other genes were significantly overexpressed with a fold change (FC) > 2. This changed after the last round of treatment with more than 200 genes detected as significantly overexpressed in PACO17 PR cell lines and PACO17 DM cell lines respectively. *ABCB1* remained over-expressed in PR cell lines and *IFITM1* and other interferon response related genes were also significantly over-expressed in PR cell lines of PACO17. Interestingly, after five passages of drug holiday, *ABCB1* was not significantly overexpressed in paclitaxel-resistant cells anymore. In addition, the number of significantly overexpressed genes was reduced and interferon response related genes were no longer detectable (**Figure 12A**). Mean fluorescent intensity (MFI) values of the samples from each round indicated that the expression of *ABCB1* was increased in paclitaxel-treated cells in the early and late round and decreased during five passages of drug holiday. Collectively, our results show that PR cell lines of PACO17 lose the resistance to Paclitaxel after a five-passage long drug holiday (**Figure 12D**). This loss of the paclitaxel-resistant phenotype is accompanied by the decrease of *ABCB1* expression levels suggesting a possible link between ABCB1 expression and paclitaxel resistance in these cells. Importantly, we validated the gene expression of *ABCB1* by qRT-PCR for these different time points (**Figure 13A**). In PACO17, we focused on the interferon response related gene like *IFITM1* and xenobiotic response genes like *ABCB1* and *CYP3A5* that were found to be upregulated in PR cell lines compared to DM cell lines after the last round of long-term treatment. *ABCB1* was already significantly overexpressed (54x) in paclitaxel-treated replicates (P) compared to DMSO-treated replicates (D) in the early round of the long-term treatment. Expression of *ABCB1* was further increased (347x) in PR replicates of PACO17 after the last round of treatment. Differential gene expression analysis of *ABCB1* showed that PR cell lines lost significant overexpression of ABCB1 after the five-passage-long drug holiday, which was also verified by qRT-PCR. *IFITM1* was one of the interferon response genes that was found to be differentially expressed in PR cell lines compared to DM cell lines after the last round of treatment. The findings by qRT-PCR revealed that DMSO treatment inhibited expression of *IFITM1* in DM cell lines while paclitaxel had only minor effects on its expression levels in PR cell lines. Although there was a nominal difference of 140-fold, the expression

values of PR and DM replicates varied too much to support significance. Of note, after the 5-passage long drug holiday the transcription levels of *IFITM1* were similar between PR and DM cell lines. PACO17 has been previously described to acquire a paclitaxel resistance independent of *CYP3A5* expression[206]. Similarly, *CYP3A5* levels were not significantly increased in PR cell lines at any timepoint. Furthermore, we could not detect CYP3A5 protein in either of the two treatment groups. We validated the membrane expression of ABCB1 at protein level for the last round of long-term drug treatment in PR and DM cell lines of each PACO cell lines by Western blot (**Figure 13D**). ABCB1 is heterogeneously expressed in PR replicates of PACO17, with PR2 expressing more ABCB1 protein than the other two replicates (PR1 and PR3). Similar to transcriptional levels, western blot confirmed that protein levels of ABCB1 were much lower in PR cell lines of PACO17 compared to levels found in the adrenal gland. Furthermore, ABCB1 was not detected in DM cell lines of PACO17 and CYP3A5 was absent in both PR and DM cell lines. We had previously examined that, in contrast to PACO 17-PR, PACO22-PR cells remained resistant even after long term drug holiday (**Figure 9C**). Interestingly, in PR replicates of PACO22, *ABCB1* was the most differentially expressed gene in paclitaxel-treated cell lines of the Early Round ($log_2FC = 5.20$) and the Last Round ($log_2FC = 8.58$) and it remained highly upregulated after a five-passage long drug holiday ($log_2FC = 7.66$). This was in contrast to the number of genes deregulated at the early and last round, which were not maintained during the five-passage-long drug holiday (**Figure 12B**). MFI analysis of *ABCB1* in PACO22 revealed that values remained unchanged for parental and DM cell lines throughout the long-term treatment and that *ABCB1* intensity increased from the early until the last round of treatment in paclitaxel-treated cell lines of PACO22 (**Figure 12D**). After five passages of drug holiday, the intensity of the MFI signal was reduced compared to the last round of treatment but remained significantly higher than in the DM cell lines. Of note, the variation in signal intensity for *ABCB1* between the PR replicates increased after the five-passage long drug holiday. Verification of microarray results by RT-PCR showed strong expression of *ABCB1* already after an early round of treatment (**Figure 13B**). *ABCB4* was only marginally overexpressed which changed after the last round of treatment. After the last round of treatment, both ABCB1 and ABCB4 were highly expressed in PR cell lines compared to DM and parental cell lines. Of interest, transcriptional levels of *ABCB1* and *ABCB4* in PACO22 PR cell lines reached the same levels as found in the adrenal gland after the last round of treatment (**Figure 13B**). Both, *ABCB1* and *ABCB4*, were reduced after five passages of drug holiday and, due to increased variance in both PR and DM, levels of expression were not significantly increased in PR cell lines compared to DM cell lines. Although, differences in *CYP3A5* levels were

significant between PR and DM cell lines in all three timepoints, they only reached a maximum difference of 2.7 after the last round of treatment. ABCB1 protein expression not detectable in DM cell lines, while the high transcriptional levels found by qRT-PCR were verified by Western blot (**Figure 13D**). PACO22 were the only cell line with detectable CYP3A5 protein expression after the last round of treatment. It has been previously shown that CYP3A5 can induce resistance to paclitaxel in PACO cell lines, however, protein levels of these cell lines were significantly higher compared to levels found in PACO22 PR cell lines[183]. Overall, these findings are in line with the phenotype of a significant and stable paclitaxel resistance found in PR cell lines of PACO22 after the last round of treatment and after the five passages of drug holiday. In contrast to the other two cell lines, *ABCB1* was not overexpressed in paclitaxel-treated cell lines of PACO43 in the early round of the long-term treatment and only few genes were found to be differentially expressed between PR and DM cell lines (**Figure 12C**). This changed after the last round of treatment with *ABCB1* being among the most differentially expressed genes (logFC = 3.2) in PR cell lines compared to DM cell lines. Similar to PACO22, the expression of *ABCB1* remained high (logFC = 3.74) in PR cell lines, although without being the most differentially expressed gene. Of note, during long-term treatment, MFI of *ABCB1* continuously decreased in all DM cell lines and reached its lowest value after the drug holiday (**Figure 12D)**. Similar to the other two PACO cell lines, the MFI of *ABCB1* increased in PR cells from the early round to the last round of treatment and reduced, including increasing variance between replicates, after five passages of drug holiday. Of interest, PACO43 PR cell lines lost resistance against paclitaxel after drug holiday, although *ABCB1* remained overexpressed (**Figure 9C)**. This could hint towards a secondary drug resistance mechanism, independent of ABCB1, that was lost during drug holiday and re-sensitized PR cell lines to paclitaxel. By verifying these findings using qRT-PCR, we found *ABCB1* being only 1.6-times overexpressed in PR cell lines compared to DM cell lines after the early round of treatment (**Figure 13C**). After the last round of treatment *ABCB1* was 10-times overexpressed in PR cell lines compared to DM cell lines and remained on the same level of expression after five passages of drug holiday. *S100A2* was one of genes that was found to be downregulated in all treated cell lines and remained low after drug holiday. RT-PCR results didn't verify these findings and but showed a trend in which DM cell lines expressed higher levels of *S100A2* compared to parental lines and PR cell lines further decreased expression of *S100A2* until the five passages of drug holiday. Furthermore, *CYP3A5* was neither found to be significantly overexpressed after the last round of treatment nor after five passages of drug holiday. Protein levels of ABCB1 in PR cell lines of PACO43 were similar to that of PACO17 PR cell line. DM

cell lines also expressed low amounts of ABCB1 which was unique for all control cell lines. Western blot also verified the absent of CYP3A5 expression in both PR and DM cell lines of PACO43 (**Figure 13D**). Comparing all three cell lines, the MFI of *ABCB1* was consistently elevated after the early round of the long-term treatment and was further increased after the last round of treatment (**Supplementary Figure 2A**). With the removal of paclitaxel for five passages, PR cell lines showed an increased variance in overall gene expression including *ABCB1*. When normalized to *ABCB1* expression in adrenal gland, it became apparent that parental cell lines of PACO17 and PACO22 had similar low expression levels whereas the parental cell line of PACO43 already expressed two log fold higher levels (**Supplementary Figure 2B**). Whereas the levels of *ABCB1* did not change by more than a log_2fold in PR cell lines of PACO17 and PACO43, PR cell lines of PACO22 expressed same levels as found in the adrenal gland after the last round of treatment (**Supplementary Figure 2B**). Based on differential gene expression analysis of single PACO cell lines, we identified enhanced expression of ABCB1 in treated samples of all three cell lines independent of co-expressed genes. Although CYP3A5 was detected in PR cell lines by Western blot, both mRNA and protein levels have only marginally increased during the long-term treatment which would hint towards a CYP3A5-independent paclitaxel resistance mechanism. With ABCB1 being known to induce resistance against paclitaxel and being the only gene that has been significantly enriched in in PR cell lines of all three PACO lines, we decided to further analyze its role in the acquired paclitaxel-resistance phenotype in our PACO cell lines.

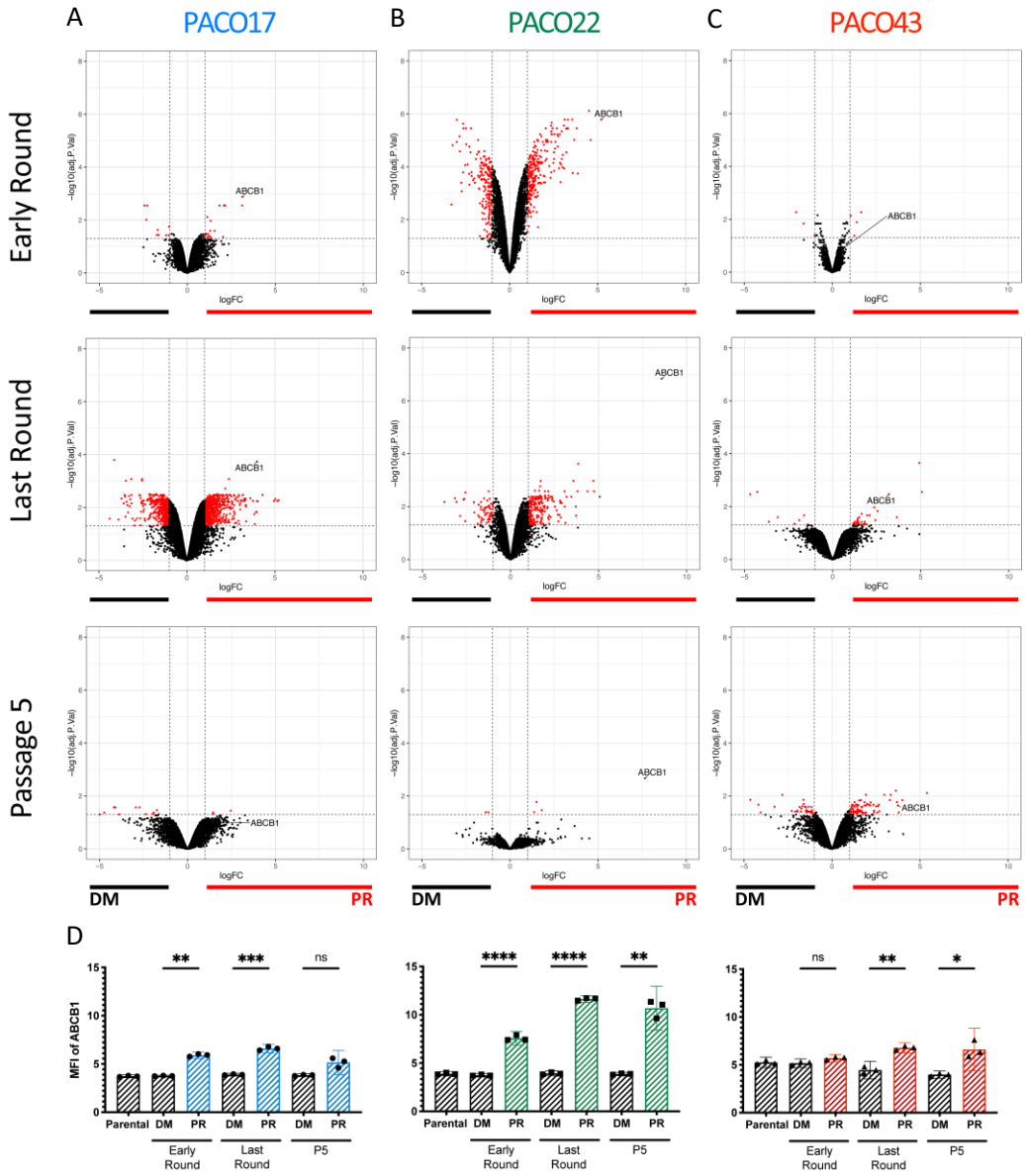

Figure 12 – Paclitaxel-treated cell lines uniformly overexpress *ABCB1* throughout the long-term treatment
(A-C) Volcano plot of all differentially expressed genes between PR cell lines compared to respective DM cell lines at the Early Round, Last Round and after five passages of drug holiday in **(A)** PACO17, **(B)** PACO22 and **(C)** PACO43 (n = 3 individual cell lines per group). Highlighted in red are all genes that are at least one log2-fold differentially expressed with an adjusted p-value of less than 0.05 according to the Benjamini-Hochberg calculation.
(D) Mean fluorescent intensity (MFI) of normalized probes for *ABCB1* at different timepoints for PACO17, PACO22 and PACO43 (n = 3 individual cell lines per group). Error bars depict mean ± s.e.m. * adj.P.val. < 0.05; ** adj.P.val. < 0.01; *** adj.P.val. < 0.001; **** adj.P.val. < 0.0001; determined by linear model fit (limma).
PR, paclitaxel-resistant; DM, DMSO-treated; P5, Passage 5; ns, not significant.

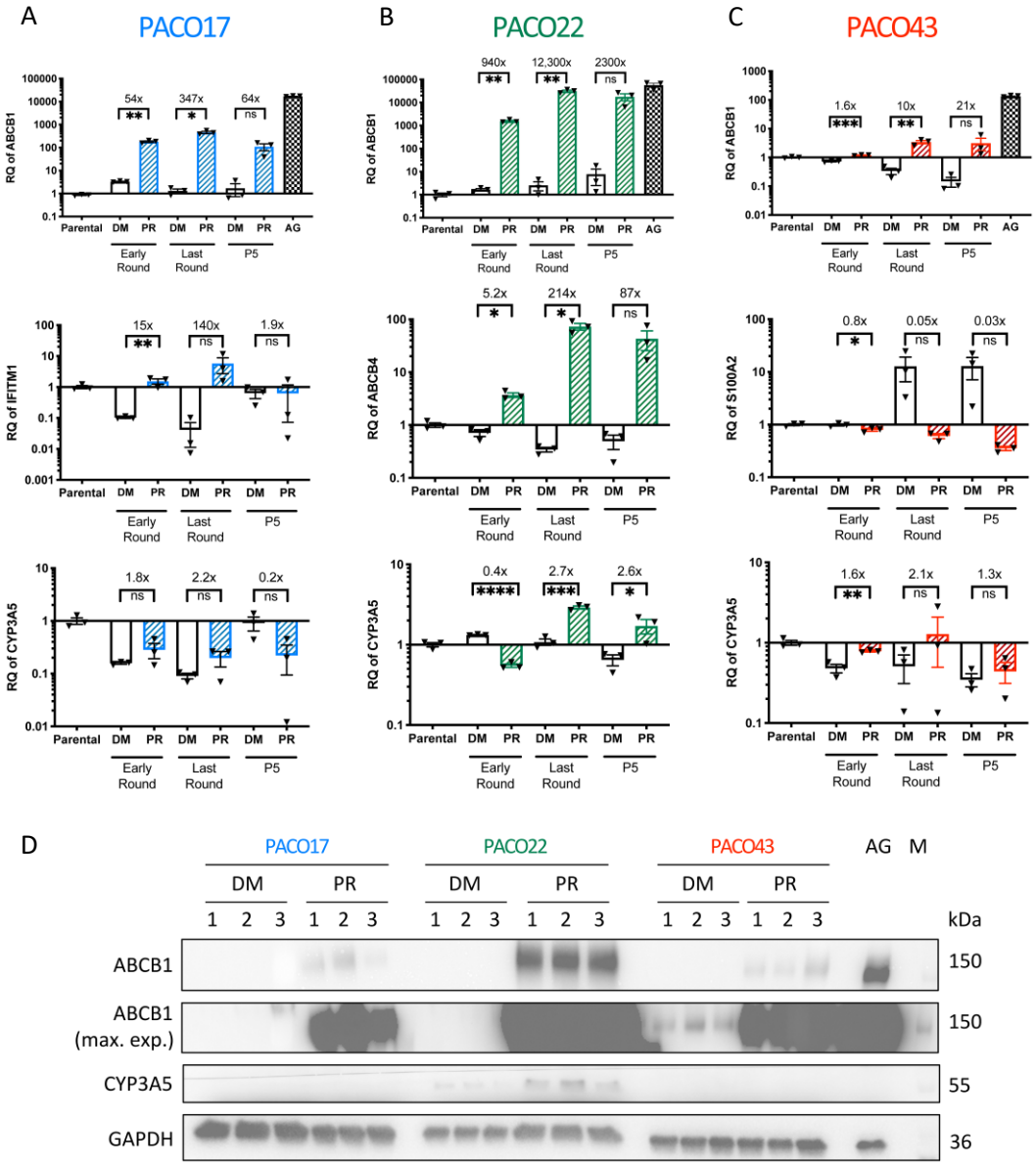

Figure 13 – Validation of gene expression microarray findings by qRT-PCR and Western Blot
(A-C) qRT-PCR analysis of genes, overexpressed in PR cell lines according to differential gene expression analysis, and *CYP3A5* between PR and DM cell lines after the early round, last round and after five passages of drug holiday in **(A)** PACO17, **(B)** PACO22 and **(C)** PACO43 (n = 3 individual cell lines per group)**.** Values are relative to parental cell line. Error bars depict mean ± s.e.m. * adj.P.val. < 0.05; ** adj.P.val. < 0.01; *** adj.P.val. < 0.001; **** adj.P.val. < 0.0001; by Student's t-test.
(D) Western blot analysis of ABCB1 and CYP3A5 in PR and DM cell lines after the last round of treatment in PACO17, PACO22, PACO43. Adrenal gland as positive control for ABCB1[210]. GAPDH as loading control. PR, paclitaxel-resistant; DM, DMSO-treated; P5, Passage 5; ns, not significant; AG, adrenal gland; kDa, kilo Dalton.

3.8 Epigenetic analysis of PACO cell lines

It has been theorized that epigenetic changes could drive development of drug resistance mechanisms[201,322,323]. Hence, we analyzed the methylation pattern of DM and PR cell lines after the last round of treatment. Globally, PACO22 were the most demethylated cell line with the highest density of for demethylated (beta value (ß) ~ 0) sites and the lowest density for methylated (ß ~ 1) sites (**Figure 14A**). For PACO17, the proportion of demethylated sites was higher compared to the methylated sites, however, the difference was smaller compared to PACO22. The distribution of demethylated and methylated sites in PACO43 cell lines was similar to PACO17, having the lowest proportion of demethylated sites of the three cell lines. PCA of PACO17 cell lines revealed that, in contrast to DM cell lines, PR cell lines acquired heterogeneous changes in their global methylation pattern and thus were separated from each other in PC1 and PC2 (**Figure 14B**). In PACO22, one of the three PR cell lines (PR3) was separated from the others by PC2, however, DM and PR cell lines were separated entirely by differences based on PC1 (**Figure 14C**). We identified a similar pattern for PACO43 as observed for PACO17 with PR cell lines that acquired different global methylation pattern which were revealed by PC2 (**Figure 14D**). Pooled gene expression analyses of PACO cell lines identified *ABCB1* as the only gene overexpressed in all PR cell lines after the last round of the long-term treatment (**Figure 10D)**. Hence, we checked both promoter and gene region for change in the methylation pattern (**Supplementary Figure 3**). In all DM cell lines, we found the promoter of *ABCB1* to be highly demethylated. This was also the case for the PR cell lines, except for PACO17, as the PR cell lines increased in the beta value compared to DM cell lines. For the gene body, PR cell lines in all PACO cell lines were more methylated than respective DM cell lines. Overall, the biggest change in methylation pattern was found in the promoter region of *ABCB1* in PACO17 (**Supplementary Figure 3**). Previously, we have identified genes surrounding *ABCB1* on the genome to also be enriched or overexpressed in PACO22 PR cell lines (**Figure 12B**, **Figure 13B**). Hence, we asked whether genomic aberrations that supported expression of *ABCB1* in PR cell lines of the three PACO lines could have developed during long-term treatment. Applying DNA methylation data to the conumee package[324], we performed genomic copy number variations (CNV) analysis and compared CNV profiles of each single PR replicate with the three DM replicates. In one of the PR replicates of PACO17 (PR2), we detected a gain in copy numbers of genes including *ABCB1* (**Figure 14E**). For PR1 of PACO17, we detected genomic amplifications upstream of *ABCB1* that were also found in PR2, however, the area around *ABCB1* remained unchanged. In PR3, a chromosome section upstream of *ABCB1* was completely lost which was unique compared to the other two PR

replicates. Moreover, we identified a broad range in levels of amplification for *ABCB1* and downstream genes which prevented a conclusive analysis. All three PR replicates of PACO22 exhibited strong amplification of *ABCB1* and genes in close proximity, which is line with the findings from GSEA and qRT-PCR (**Figure 11, Figure 14F**). In PACO43, none of the PR replicates displayed an amplification on chromosome 7 (**Figure 14G**). From these findings we can conclude that treatment with paclitaxel induces changes in methylation pattern that differ from changes induced by culturing and treatment with DMSO. However, these changes don't seem to be related to the overexpression of ABCB1. CNV analysis using methylation data revealed genomic aberrations in two of the three PACO cell lines which could play a role in upregulation of ABCB1.

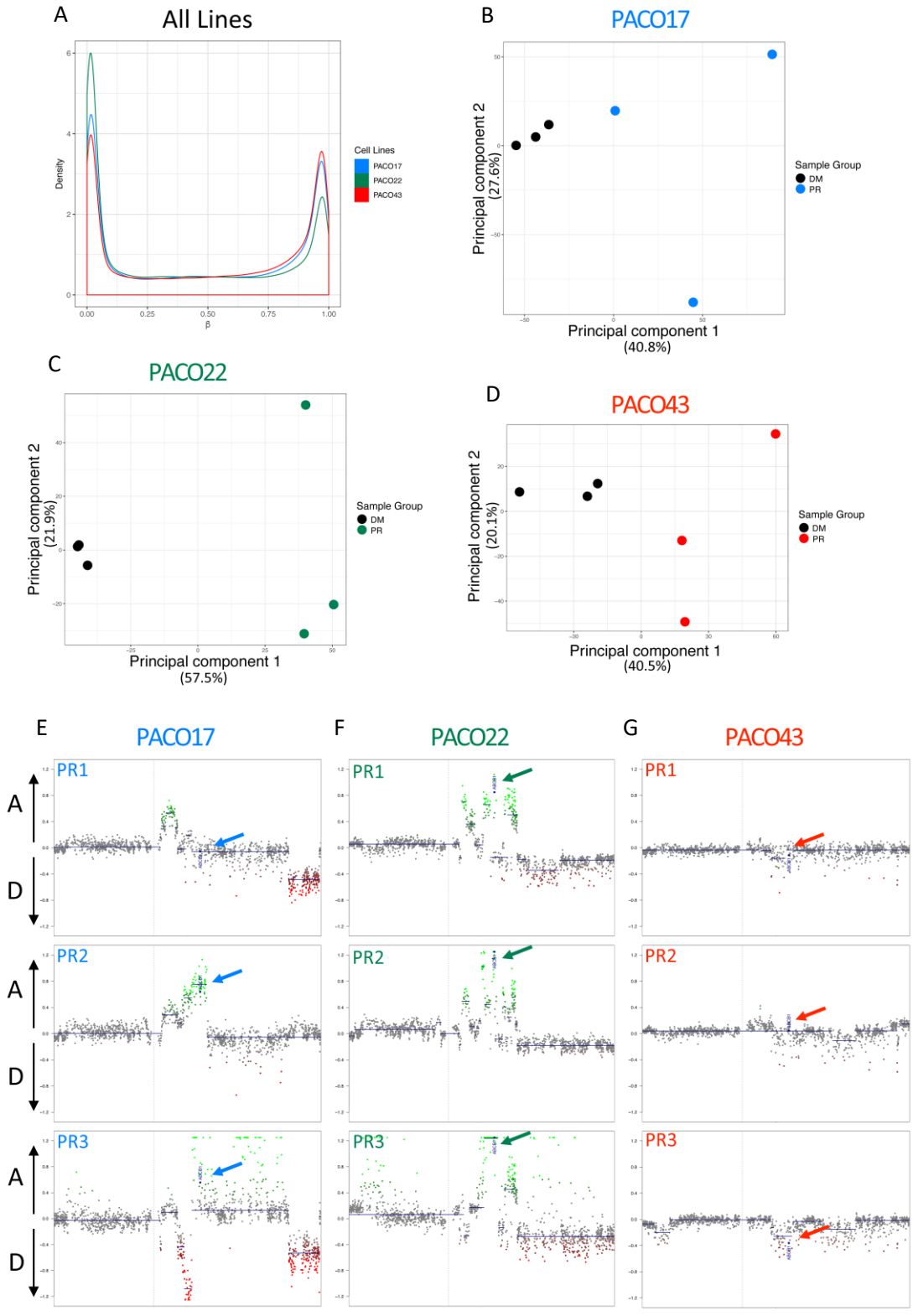

Figure 14 – DNA methylation analysis of PACO cell lines identifies ABCB1 amplification in PR cell lines of PACO22
(A) Methylation value distribution of all probes in PACO17, PACO22 and PACO43 (n = 9 individual cell lines per group, parental, PR and DM cell lines after the last round of treatment).
(B-D) Principal component analysis (PCA) between PR and DM cell lines after the last round of treatment in **(B)** PACO17, **(C)** PACO22 and **(D)** PACO43. Percentage indicates proportion of variance explained by each component.
(E-G) Copy number variation (CNV) plot of chromosome 7 based on methylation intensities of CpGs for single PR replicates after the last round of treatment in **(E)** PACO17, **(F)** PACO22, **(G)** PACO43. Control genome based on DM cell lines (n = 3 individual cell lines). Intensity values of genomic bins are plotted in colored dots. Segments are shown as blue lines. Colored arrows mark position of labeled *ABCB1* gene on chromosome 7.
PR, paclitaxel-resistant; DM, DMSO-treated; A, Amplification; D, Deletion.

3.9 Whole Exome Sequencing analysis revealed genetic amplification of *ABCB1* in PACO22

In order to validate the findings of methylation-based CNV analysis, we performed whole exome sequencing (WES) on DM and PR cell lines of each of the PACO cell lines after the last round of treatment. In addition, to identify possible changes due to the long-term culturing, we analyzed the whole exomes of each parental cell line to compare them with DM cell lines. Surprisingly, when compared to parental cells, control cell lines of either of the PACO cell lines only acquired minor genomic changes, like mutations or copy number variations, throughout the long-term treatment period. These results indicated that DM cell lines remained genetically stable throughout the long-term treatment process and that DMSO treatment didn't induce genomic aberrations. We then compared the CNV profiles of control cell lines with PR cell lines in each PACO cell line by using the WES data. Based on genomic methylation profile, we expected the PR cell lines of PACO17 to vary in regard to their CNV profile and indeed, we identified uniquely amplified areas for each of the PR cell lines that were not present in the DM or parental cell lines (**Figure 15A**). In PR1, a region of 25 megabases (MB) was amplified by 2 to a total copy number (TCN) count of 4, doubling the genomic information in that region. WES analysis verified the previous findings by methylation-based CNV analysis that PR2 carried an amplification around the *ABCB1* locus. For PR3, we found an area of 30 MB on chromosome 4, which DNA content was doubled from 2 to 4 (**Figure 15B**). In PACO22, the major changes took place on chromosome 7 around *ABCB1* (**Figure 16A, B**). We identified massive aberrations in a region of 40 MB size with many small fragments of DNA being highly amplified while others remained unchanged. Although we noticed a strong heterogeneity between the PR cell lines for that region, they all carried an amplification around *ABCB1*, which is in line with previous findings based on GSEA and methylation-based CNV analysis (**Figure 11B, Figure 14F**). In contrast to the other two PACO cell lines, we could not find any major genomic aberration in one of the PACO43 PR cell lines compared to control cell lines (**Figure 17A, B**). This finding verifies the results obtained from the methylation based CNV analysis and underlines the heterogeneous response of the cell lines to paclitaxel treatment.

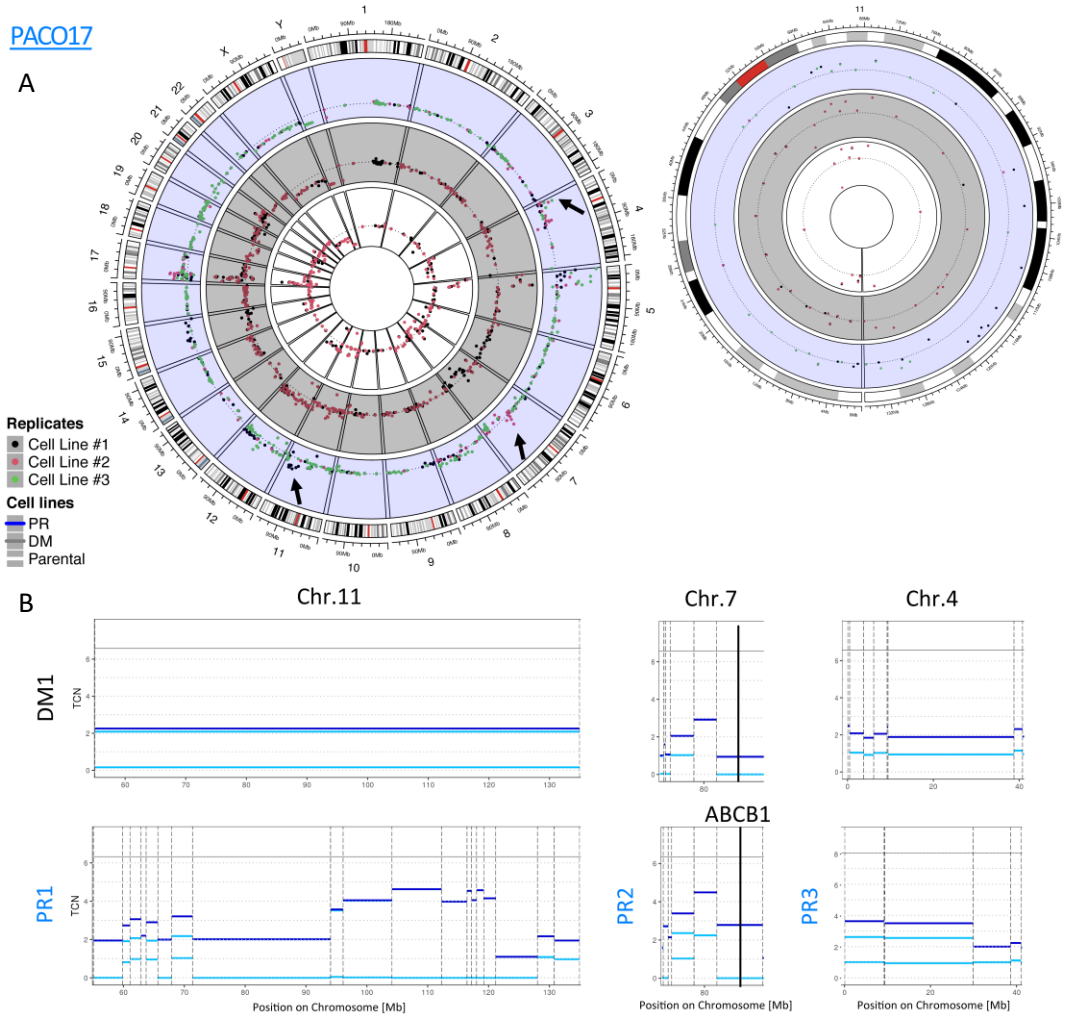

Figure 15 – Copy number variation (CNV) analysis of PACO17 identifies distinct genomic alterations between PR cell lines

(A) Circular visualization of CNV analysis based on whole exome sequencing (WES) in PR and DM cell lines after the last round of treatment and parental cell lines (n = up to 3 individual cell lines). Single Chromosome 11 shows unique amplification in PR1. Dotted line represents ploidy (2) of cell line. Replicates are colored according to their number. The inner circle displays parental cell lines with white background, mid circle displays DM cell lines with grey background and outer circle displays PR cell lines with blue background. Arrows depict unique genomic alterations of PR replicates.

(B) Cut total copy number (TCN) plots of unique genomic alterations of PR replicates compared to a representative DM cell line (DM1).

PR, paclitaxel-resistant; DM, DMSO-treated; Chr., chromosome; Mb, million bases.

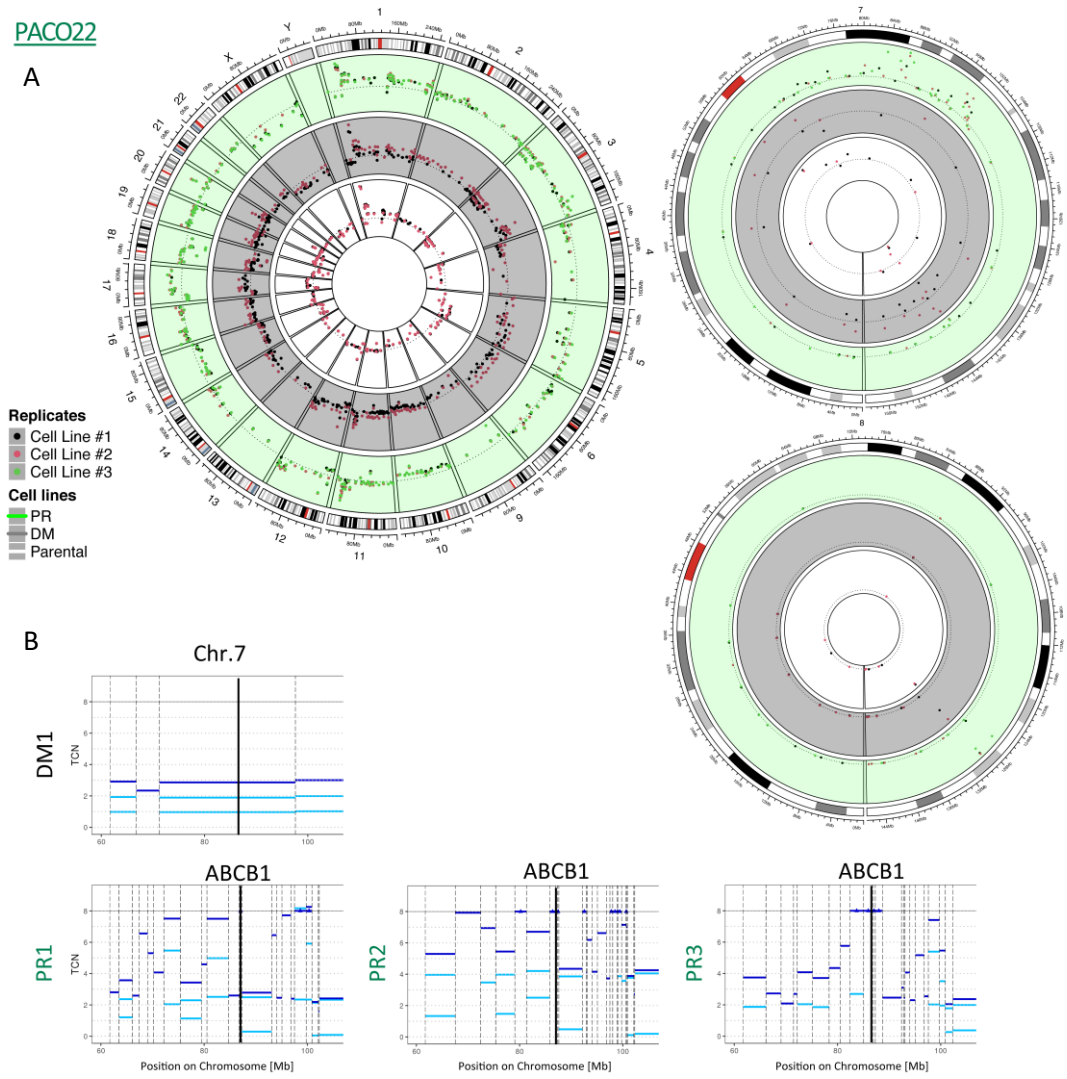

Figure 16 – Copy number variation (CNV) analysis of PACO22 identifies ABCB1 genomic amplification in all PR cell lines

(A) Circular visualization of CNV analysis based on whole exome sequencing (WES) in PR and DM cell lines after the last round of treatment and parental cell lines (n = up to 3 individual cell lines). Single Chromosome 7 shows similar amplification in PR cell lines and single chromosome 8 shows MYC amplification present in all PACO22 cell lines. Dotted line represents ploidy (3) of cell line. Replicates are colored according to their number. The inner circle displays parental cell lines with white background, mid circle displays DM cell lines with grey background and outer circle displays PR cell lines with green background.

(B) Cut total copy number (TCN) plots of genomic alterations in chromosome 7 of PR replicates compared to a representative DM cell line (DM1).

PR, paclitaxel-resistant; DM, DMSO-treated; Chr., chromosome; Mb, million bases.

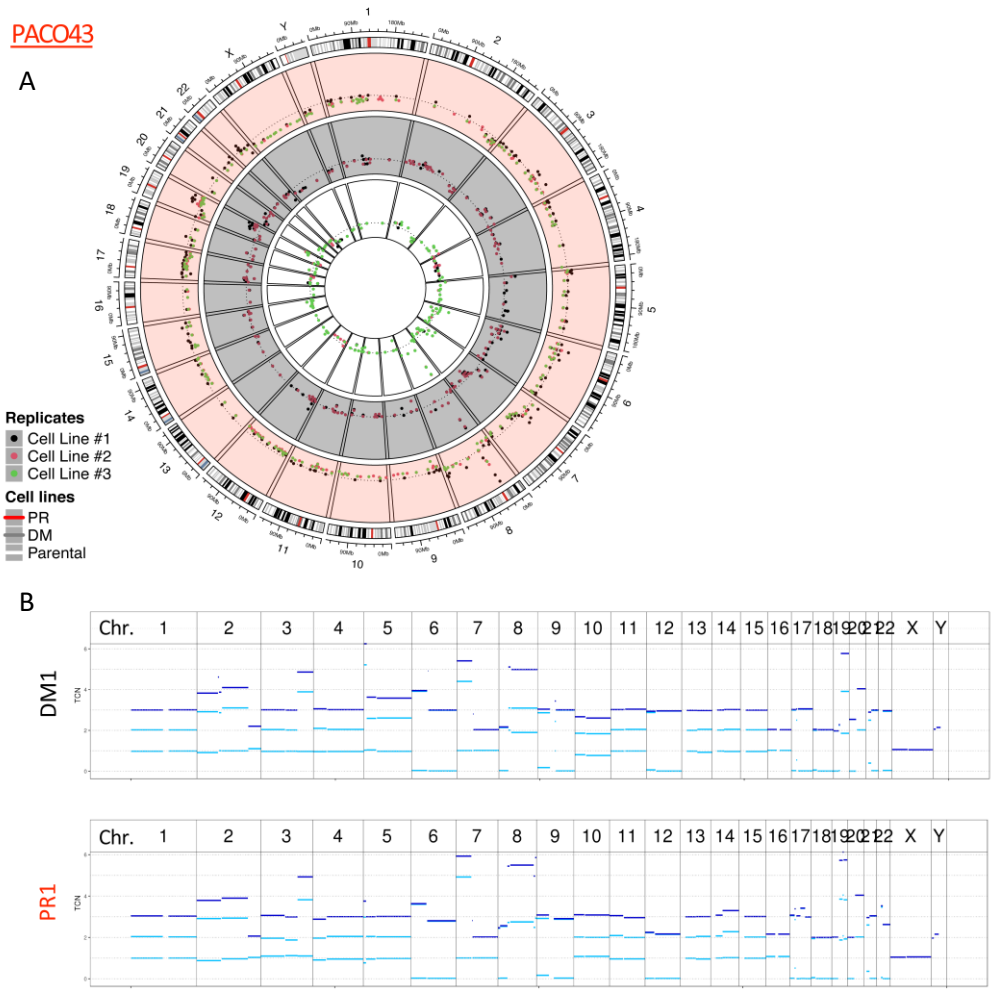

Figure 17 – Copy number variation (CNV) analysis of PACO43 reveals no gain in genomic alterations
(A) Circular visualization of CNV analysis based on whole exome sequencing (WES) in PR and DM cell lines after the last round of treatment and parental cell lines (n = up to 3 individual cell lines). Single Chromosome 11 shows unique amplification in PR1. Dotted line represents ploidy (3) of cell line. Replicates are colored according to their number. The inner circle displays parental cell lines with white background, mid circle displays DM cell lines with grey background and outer circle displays PR cell lines with red background.
(B) Total copy number (TCN) plots of all chromosomes of a representative PR and DM cell line (PR1 and DM1).
PR, paclitaxel-resistant; DM, DMSO-treated; Chr., chromosome; Mb, million bases.

3.10 ABCB1 mediates resistance to paclitaxel in PACO22

ABCB1 has been reported to be responsible for drug resistance to various compounds, including taxanes like paclitaxel or docetaxel[325]. Gene expression analyses indicated that *ABCB1* could play an important role in paclitaxel resistance of the described PACO cell lines. Since PACO22 PR cell lines showed the strongest phenotype, we utilized PACO22 cell lines for the validation of an ABCB1-dependent paclitaxel resistance. PCA analysis of PACO22 cell lines at the different time points separated PR cell lines from DM and parental cell lines (**Figure 18A**). DM samples of the Early Round clustered the closest to the parental samples and DM samples moved further away from basal cell lines with increasing culture time. Instead, PR samples of the Early Round already clustered the furthest away from parental samples, which can be mostly explained due to the differences in PC1. Similar to DM replicates, PR replicates revealed little variance between each other in the early round. This, however, changed after the last round of treatment, with replicate separating from each other while moving away from the Early Round samples. DM replicates after the last round of treatment also moved further away from the parental and Early Round DM replicates, however, they remained closer together. After five passages of drug holiday, PR replicates moved back closer to PR cell lines of the Early Round, which could hint towards a reversion of gene expression pattern upon absence of paclitaxel treatment. This was only the case in one of the DM replicates after the drug holiday, whereas the other two clustered even further away from the other DM samples. Hierarchical clustering confirmed the separation between control cell lines, including parental cell lines, and PR cell lines. *ABCB1* is among the genes that are solely expressed in PR cell lines and absent in DM and parental cell lines (**Figure 13B, Figure 18B)**. In addition, we evaluated whether long-term treatment affected cell proliferation differently in PR and DM cell lines (**Figure 18C)**. Analysis of proliferation by comparing CTB values of PR and DM replicates after seeding over five consecutive days did not result in significant differences, indicating that long-term culturing of PACO cell lines did not affect speed of growth. Furthermore, we counted the cell number in 4 wells per PR and DM replicate 4 days after seeding and could not find a significant difference between the two groups (**Figure 18D)**. In order to identify whether ABCB1 is indeed the key mediator of paclitaxel-resistance in PACO22 PR cell lines, we performed co-treatment of control and PR cell lines with paclitaxel and the third generation ABCB1-inhibitor (Elacridar)[246,326]. In control cell lines, which lack expression of ABCB1 (**Figure 13B, D)**, co-treatment with Elacridar had no adverse effects compared to mono-paclitaxel treatment (**Figure 18E, F**). On the contrary, inhibition of ABCB1 re-sensitized PR cell lines to paclitaxel treatment and reduced the IC50 to the level of control cell lines. Plaque

assay verified the loss of paclitaxel-resistance in PR cells under co-treatment with Elacridar (**Figure 18E, F)**. Although we have previously detected induced expression of CYP3A5 on the RNA and protein level in PR cell lines of PACO22, we couldn't see a rescuing effect of CYP3A5 under ABCB1 inhibition. To further verify that ABCB1 alone is responsible for drug resistance in paclitaxel-treated cells, we performed Clustered Regularly Interspaced Short Palindromic Repeats (CRISPR)/Cas9-mediated knockout (KO) of *ABCB1* in PR cell lines. In order to maintain the population heterogeneity, we implemented ABCB1-KO on the bulk of PR cells (**Figure 19A**). After electroporation, ABCB1-KO efficiency was first determined by FACS analysis comparing ABCB1 protein levels of PR ABCB1-KO cell lines with the control PR cell line (**Figure 19B**). We identified more than 95% of cells have lost ABCB1 expression, however, control PR cell line had also lost the majority (80%) of ABCB1+ cells. Cells that were homologous for ABCB1-KO would be unable to express ABCB1 protein whereas heterologous cells would still be able to express reduced amounts compared to wildtype cells. We have previously shown that long-term paclitaxel treatment lead to the acquisition of paclitaxel resistance and increased expression of ABCB1 in PR cell lines. Hence, we determined the proportion of PR ABCB1-KO cells that was still able to adapt to paclitaxel treatment. Single round of treatment with low paclitaxel concentration (1 nM) increased the proportion of ABCB1 expressing cells by more than 6-fold in PR ABCB1-KO cell lines (**Figure 19B**). In the control cell line this increase was only 2.5-fold resulting in an almost 45% of ABCB1 expressing cells. From this we concluded that the ABCB1 protein expression is suboptimal to assess the degree of KO in PR cell lines. Next, we determined ABCB1-KO efficiency by sanger sequencing of region targeted by RNP complex (**Figure 19C**). Using TIDE software, we identified that at least 80 % of DNA sequences were already altered after the first round of ABCB1-KO, resulting in a single nucleotide frameshift and loss of ABCB1 protein. Loss of a single nucleotide at gRNA binding site marked the major genomic change. With increasing rounds of ABCB1-KO, the proportion of sequences harboring deletion of a single nucleotide in the ABCB1 locus reached over 90% which made them suitable for cell viability tests (**Figure 19C**). While we already noticed a reduced paclitaxel resistance after the first round of ABCB1-KO, plaque assay revealed cells that remained viable and were proliferating after 100 nM paclitaxel treatment (**Figure 19D**). However, after three consecutive rounds of ABCB1-KO, PR cell lines lost ability to withstand 100 nM of paclitaxel treatment (**Figure 19D**). Knockout of *ABCB1* significantly re-sensitized PR cell lines to paclitaxel and after three consecutive rounds of ABCB1-KO, PR cell lines depicted similar sensitivity to paclitaxel as control cell lines (**Figure 19E**). Loss of ABCB1 protein after three rounds of CRISPR/Cas9 mediated KO

was validated by Western Blot (**Figure 19F**). ABCB1 protein was almost completely absent in PR1 and PR3 cell lines while PR2 remained to expressed detectable levels of ABCB1 after maximum exposure. However, these levels were not sufficient to induce resistance against paclitaxel as depicted by cell viability assays (**Figure 19D, E)**. As observed for ABCB1 inhibition, ABCB1-KO completely sensitized PR cell lines to paclitaxel. These findings verify that ABCB1 is the only mediator of acquired paclitaxel resistance in PACO22 PR cell lines.

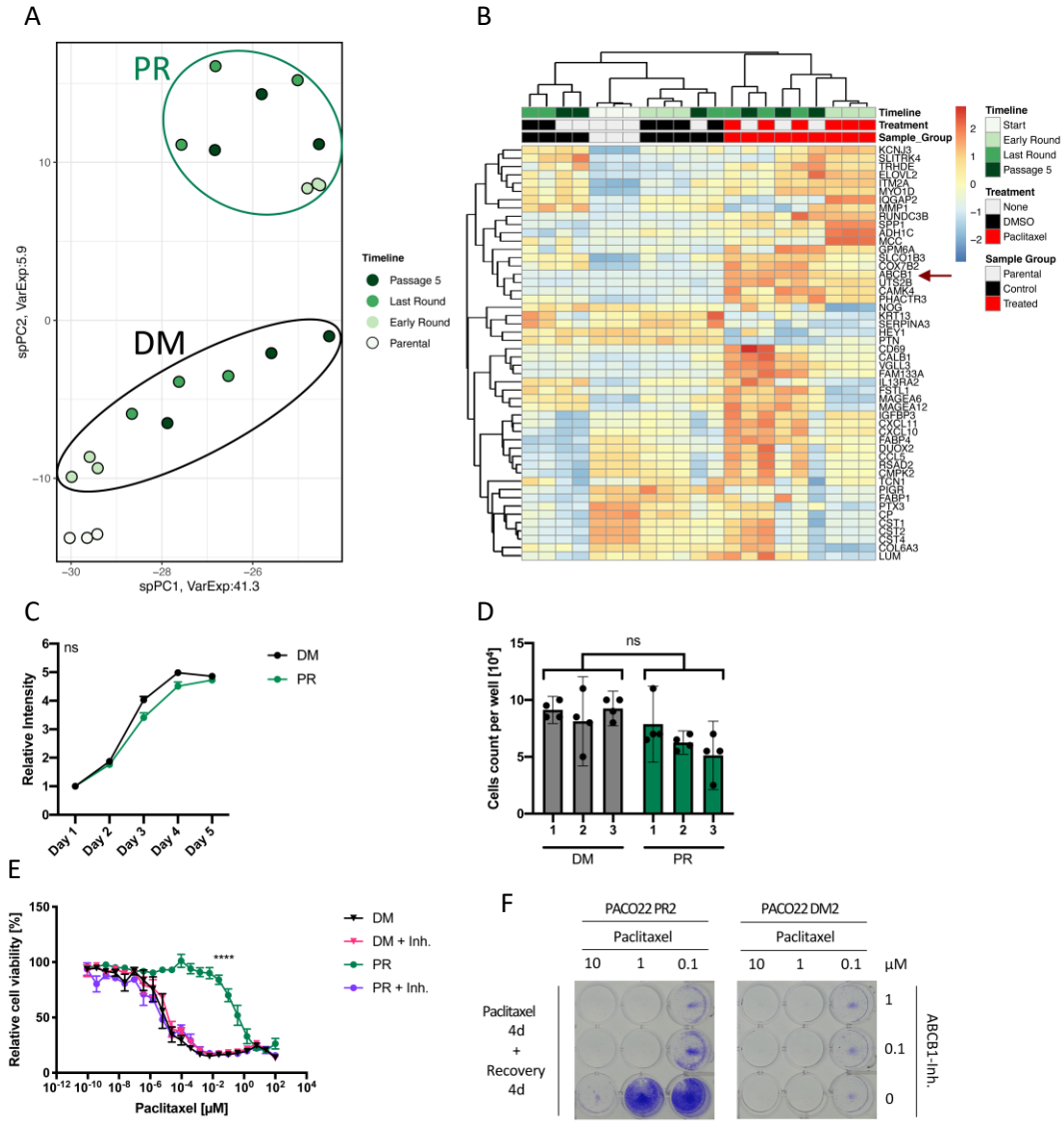

Figure 18 – Gene expression analysis of PACO22 cell lines and pharmacological inhibition of ABCB1
(A) Sparse principal component analysis (spPCA) based on gene expression microarray data of PACO22 cell lines. Each dot represents an individual cell line and the color code indicates the timepoint of sample collection. PR cell lines are enclosed by green circle, DM cell lines are enclosed by black circle. Percentage indicates proportion of variance explained by each component**.**
(B) Hierarchical clustering analysis of PACO22 cell lines at the different timepoints based on the top 50 variant genes. Red arrow highlights *ABCB1*. Complete Pearson correlation-based distance. Intensities are centered in gene direction and correspond to log2 scale.
(C-D) Cell proliferation comparison between PR and DM cell lines by **(C)** CellTiter Blue metabolism and **(D)** cell count (n = 3 individual cell lines per group). (C) 8 technical replicates per timepoint. Data relative to Day 1 of each group. Each dot represents the mean of the three biological replicates. Error bars depict mean ± s.e.m. by multiple unpaired t-tests. Two-stage set-up (Benjamini, Krieger, and Yekutieli) method. (D) Cell number counted after 4 days of culture. 4 technical replicates per group. Each dot represents a technical replicate. Error bars depict mean ± 95% confidence interval by Student's t-test.
(E-F) Sensitivity of PR and DM cell lines of PACO22 to treatment with paclitaxel + ABCB1-inhibitor/DMSO for **(E)** 72 h determined by CellTiter Blue metabolism (n = 3 individual cell lines per group) and for **(F)** 4 d, followed by 4 d of recovery time. Density of cells is determined by crystal violet staining. One representative PR and DM cell lines. Error bars depict mean ± s.e.m. **** P value < 0.0001 by least squares regression model.
PR, paclitaxel-resistant; DM, DMSO-treated; ns, not significant; Inh., inhibitor.

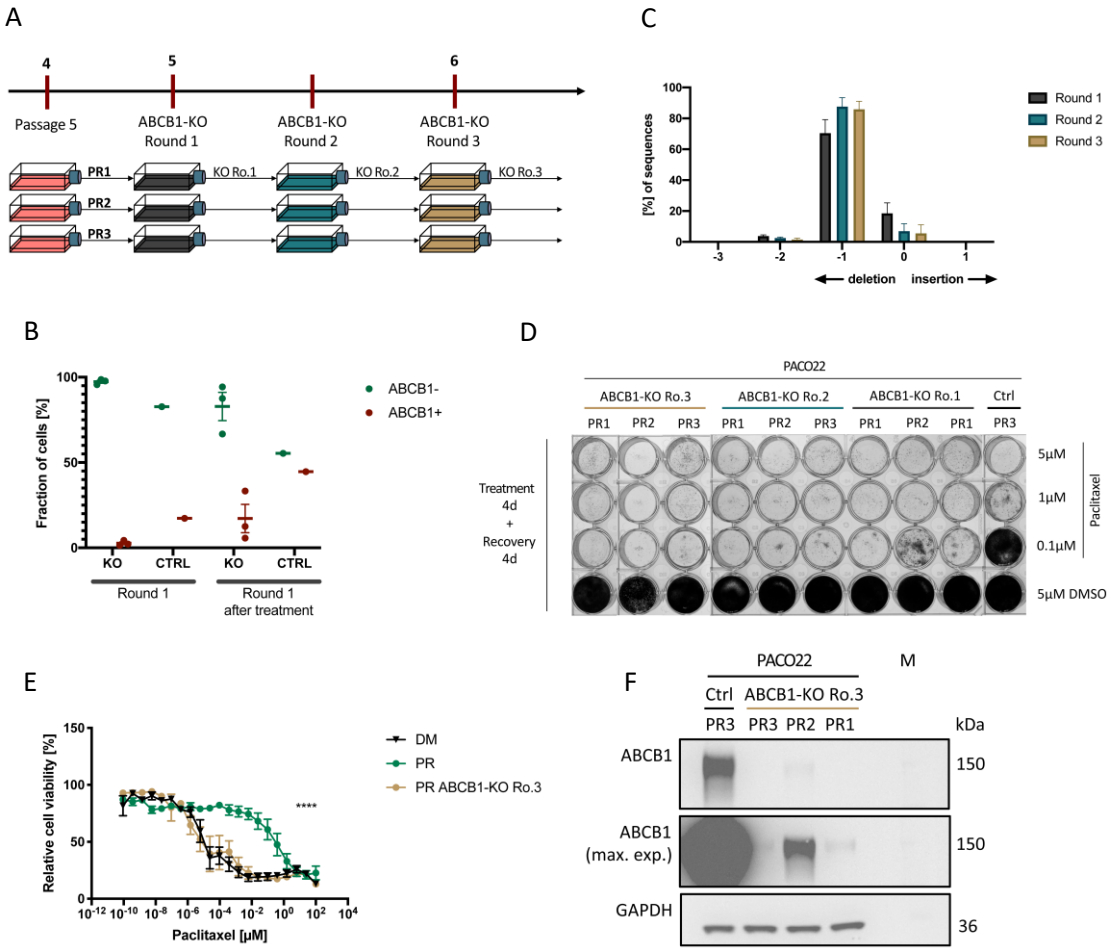

Figure 19 – Serial CRISPR/Cas9-mediated knockout of *ABCB1* re-sensitizes PACO22 PR cell lines to paclitaxel
(A) Schematic overview of serial CRISPR/Cas9-mediated ABCB1-knockout in PR cell lines. Each PR cell line was electroporated with the ribonucleoprotein complex of (CRISPR/Cas9 + ABCB1-gRNA) three times in total. Color of the flasks according to number of ABCB1-knockout rounds.
(B) Flow cytometry analysis of ABCB1 surface expression in PR-ABCB1 KO Round 1 cell lines (n = 3 individual cell lines) and a single control PR cell line (PR3) before and after acute paclitaxel treatment (1 nM). Separation between ABCB1- and ABCB1+ according to isotype.
(C) Evaluation of *ABCB1* genomic sequence alteration after each round of ABCB1-knockout by TIDE software[327] (n = 3 individual cell lines per group). Error bars depict mean ± s.e.m.
(D) Sensitivity of PR ABCB1-KO cell lines and a single control PR cell line (PR3) treated with paclitaxel or DMSO for 4 d, followed by 4 d recovery time. Density of cells is determined by crystal violet staining.
(E) Sensitivity of PR ABCB1-KO Ro.3, PR and DM cell lines treated with paclitaxel for 72 h determined by CellTiter Blue metabolism (n = 3 individual cell lines per group). Errors bars depict mean ± s.e.m. **** P value < 0.0001 by least squares regression model.
(F) Western blot analysis of PR ABCB1-KO Ro.3 and a single control PR cell line (PR3) for ABCB1 expression. GAPDH as loading control.
PR, paclitaxel-resistant; DM, DMSO-treated; KO Ro., knockout round; Ctrl, control; kDa, kilo Dalton.

3.11 Expression of ABCB1 does not mediate cross-resistance in PACO22 PR lines

Some PDAC patients are treated with a combination of nab-paclitaxel and gemcitabine. We were curious whether ABCB1 could mediate co-resistance against gemcitabine in PACO22 PR cell lines[109]. Cell viability assays revealed that PR cell lines remained sensitive to gemcitabine to the same degree as DM cell lines (**Figure 20A, E, F**). In addition, we tested PACO22 cell lines on single compounds of the FOLFIRINOX scheme which is currently the standard treatment of care in patients with an optimal performance status[90]. Neither 5-FU, the active product of irinotecan SN38 nor oxaliplatin were less toxic to PR cell lines of PACO22 compared to DM cell lines (**Figure 20B-D**). Thus, we can conclude that expression of ABCB1 only mediates resistance to paclitaxel treatment without contribution to cross-resistance against common compounds used in treatment of PDAC in patients.

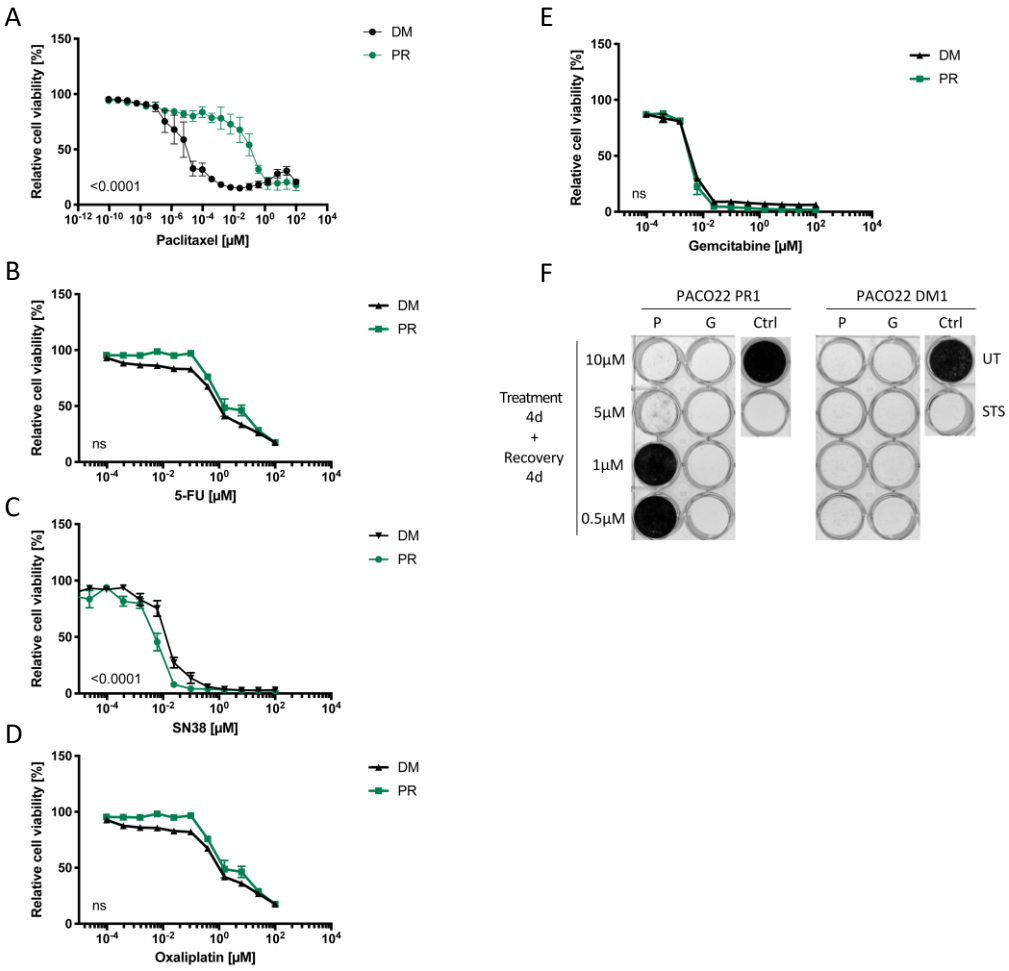

Figure 20 – ABCB1 does not mediate cross-resistance in PACO22 PR cell lines
(A-E) Sensitivity of PR and DM cell lines treated with **(A)** paclitaxel, **(B)** 5-FU, **(C)** SN38, **(D)** oxaliplatin and **(E)** gemcitabine for 72 h determined by CellTiter Blue metabolism (n = 3 individual cell lines per group). Errors bars depict mean ± s.e.m. P value as indicated by least squares regression model.
(F) Sensitivity of representative PR and DM cell line treated with paclitaxel and gemcitabine for 4 d, followed by 4 d recovery time. Density of cells is determined by crystal violet staining. Untreated well as negative control and staurosporine treatment as positive control.
PR, paclitaxel-resistant; DM, DMSO-treated; Ctrl, control; UT, untreated; STS, staurosporine.

3.12 ABCB1-mediated paclitaxel resistance is regulated by paclitaxel-induced gene expression

Previously, we have demonstrated that PR cell lines of PACO22 acquired resistant against paclitaxel treatment after the last round of long-term treatment and remained resistant after a five-passage long drug holiday (**Figure 9B, C**). Therefore, we extended the drug holiday for additional five passages and re-tested PR cell lines for paclitaxel resistance. Interestingly, two out of three replicates (PR1 and PR3) became sensitive to paclitaxel treatment, whereas PR2 remained paclitaxel resistant (**Figure 21A**). In addition, plaque assay revealed a varying degree in loss of paclitaxel resistance in PR cell lines (**Figure 21B**). The acquisition of paclitaxel resistance took several months and the following loss of paclitaxel-resistance developed over ten passages (~ 2 months). Since the dynamics of the paclitaxel-resistant phenotype are of particular importance, we examined in the next step whether PR cell lines were able to re-acquire paclitaxel resistance. A single round of paclitaxel treatment, resembling the long-term treatment regime (i.e. four days of treatment, followed by recovery), led to the re-acquisition of paclitaxel-resistance in previously paclitaxel-sensitive PR1 and PR3 cell lines, whereas PR2 remained resistant (**Figure 21A**, **B**). Paclitaxel resistance correlated with expressions levels of ABCB1 (**Figure 21B**, **C**) as PR1 and PR3 depicted reduced protein levels of ABCB1 after the loss of paclitaxel resistance. Of note, after the re-acquisition of paclitaxel resistance, PR1 and PR3 expressed similar or even higher levels of ABCB1 than the stable resistant PR2 cell (**Figure 21B-D**). Transcription levels of *CYP3A5* were significantly induced in PR cell lines after long-term treatment regimen (**Figure 13B**, **D**). Of note, CYP3A5 protein was only detected in PR2 and protein expression was induced after paclitaxel treatment, however, CYP3A5 expression was not significantly induced by paclitaxel treatment in neither PR nor control cell lines of PACO22 (**Figure 21C**). Gene expression levels of ABCB1 before treatment were highly heterogeneous in PR cell lines but increased significantly after the treatment. The loss of paclitaxel resistance after ten passages of drug holiday in PR cell lines, accompanied by a reduction of ABCB1 expression, and the induction of ABCB1 after paclitaxel treatment were confirmed on the protein level (**Figure 21D**). Hence, we conclude that ABCB1-dependent paclitaxel resistance correlates with ABCB1 expression and that paclitaxel-resistant phenotype is reversible under prolonged drug holiday. Although PR cell lines loose paclitaxel resistance and ABCB1 expression is reduced, the paclitaxel-resistant phenotype can be quickly restored by a single round of paclitaxel long-term treatment.

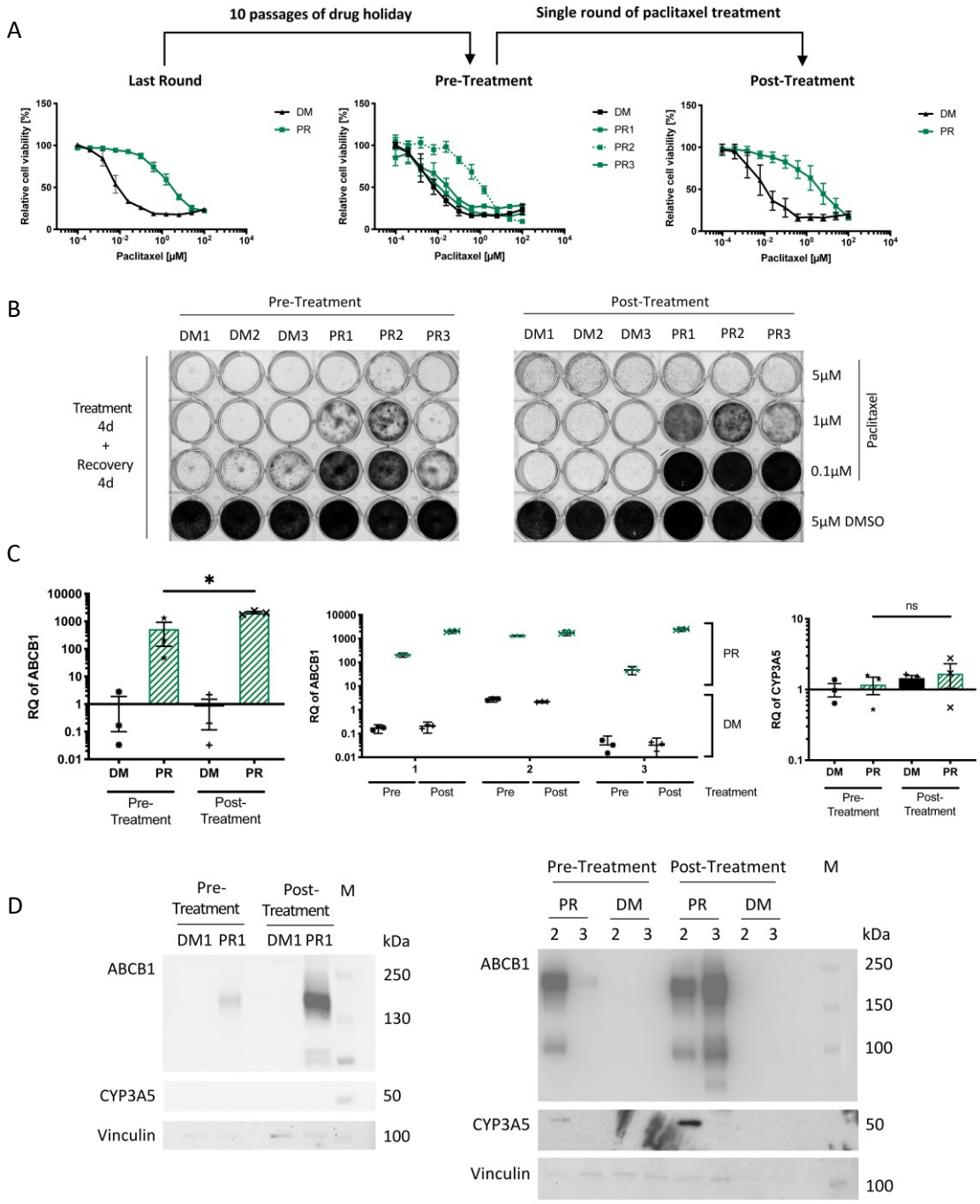

Figure 21 – Paclitaxel-dependent induction of ABCB1 mediates paclitaxel-resistance in PACO22 PR cell lines
(A) Sensitivity of PR and DM cell lines after the last round of treatment, before and after a single round of paclitaxel/DMSO treatment (0.5µM) treated with paclitaxel for 72 h determined by CellTiter Clue metabolism (n = 3 individual cell lines per group). Errors bars depict mean ± s.e.m.
(B) Sensitivity of PR and DM cell lines after ten passages of drug holiday before and after a single round of paclitaxel/DMSO treatment (0.5µM) treated with paclitaxel or DMSO for 4 d, followed by 4 d recovery time. Density of cells is determined by crystal violet staining.
(C) qRT-PCR analysis for *ABCB1* and *CYP3A5* in PR cell lines compared to DM cell after ten passages of drug holiday before and after a single round of paclitaxel/DMSO treatment (0.5µM) (n = 3 individual cell lines per group). Values are relative to DM cell line before single round of treatment. Error bars depict mean ± s.e.m. * adj.P.val. < 0.05; by Student's t-test. Graph in the middle is a showing the same values from the grouped graph on the left with biological replicates separated from each other. Error bards depict mean ± 95% confidence interval. Each dot represents a technical replicate.
(D) Western blot analysis of PR and DM cell lines after ten passages of drug holiday before and after a single round of paclitaxel/DMSO treatment for ABCB1 and CYP3A5 expression. Vinculin as loading control.
PR, paclitaxel-resistant; DM, DMSO-treated; Pre, pre-treatment; Post, post-treatment; kDa, kilo Dalton.

3.13 ABCB1 is heterogeneously expressed in PR cell lines

Intratumor heterogeneity (ITH) plays a key role in the treatment of cancer and has been directly associated with poor outcome and reduced response to cancer therapy in various cancer entities[328]. Due to the relevance of ITH in acquired drug resistance, we examined to which degree ITH is present in our PR and DM cell lines of PACO22 and whether ITH played a role during the long-term treatment regimen. We applied single-cell RNA sequencing on two replicates of PR and DM cell lines at the same timepoints of the long-term treatment regime which we chose for RNA and DNA analyses (Parental, Early Round, Last Round and Passage 5) (**Figure 22A)**. Uniform Manifold Approximation and Projection (UMAP) of all samples of PR1/2 and DM1/2 clustered them according to the treatment regime and treatment round (**Figure 22B**). We identified a heterogeneous expression of *ABCB1* in all treated samples with the highest proportion of ABCB1+ cells found after the last round of treatment. Furthermore, only few cells were found to be ABCB1+ in DM cell lines during the different timepoints. IHC analysis of ABCB1 protein expression validated the findings of single-cell RNA sequencing in PR1 cell lines, however, *ABCB1* was not detected in DM1 cell line (**Figure 22C**). FACS-based analysis of ABCB1 in PR cell lines and DM1 of PACO22 identified a heterogeneous expression in PR cell lines with cells negative for ABCB1 and cells highly positive for ABCB1 (**Figure 22D**). DM1 cell line did not inherit ABCB1-positive cells. Samples of the same treatment regime and timepoint overlapped, except the two samples of PR1 and PR2 after five passages of drug holiday. By conducting differential gene expression between PR and DM cell lines we identified several genes that were found to be exclusively expressed in PR cell lines (**Figure 22E**). Genes that gained expression until the last round of treatment and decreased after drug holiday can be linked to paclitaxel-induced selection pressure. Among them were *ABCB1*, Paternally Expressed 10 (*PEG10*), DNA Methyltransferase 1 (*DNMT1*), Y-Box Binding Protein 1 (*YBX1*) and CCAAT Enhancer Binding Protein Zeta (*CEBPZ*). We have previously shown that paclitaxel treatment induced expression of ABCB1 which correlated with the level of paclitaxel resistance in PR cell lines of PACO22 (**Figure 21B-D**). Single-cell RNA sequencing revealed that PR1 treated with paclitaxel had a higher proportion of ABCB1+ cells compared to cells of PR1 treated with DMSO (**Figure 22F**). We can conclude that ABCB1 is heterogeneously expressed in PR cell lines and the proportion of ABCB1- and ABCB1+ cells in a PR cell line's population can be modulated by paclitaxel treatment. Furthermore, we confirmed that ITH plays an important role in PR cell lines of PACO22 and has resulted in emergence of different subclones in PR1 and PR2 that are transcriptionally similar under paclitaxel treatment, but start to diverge from each other during drug holiday

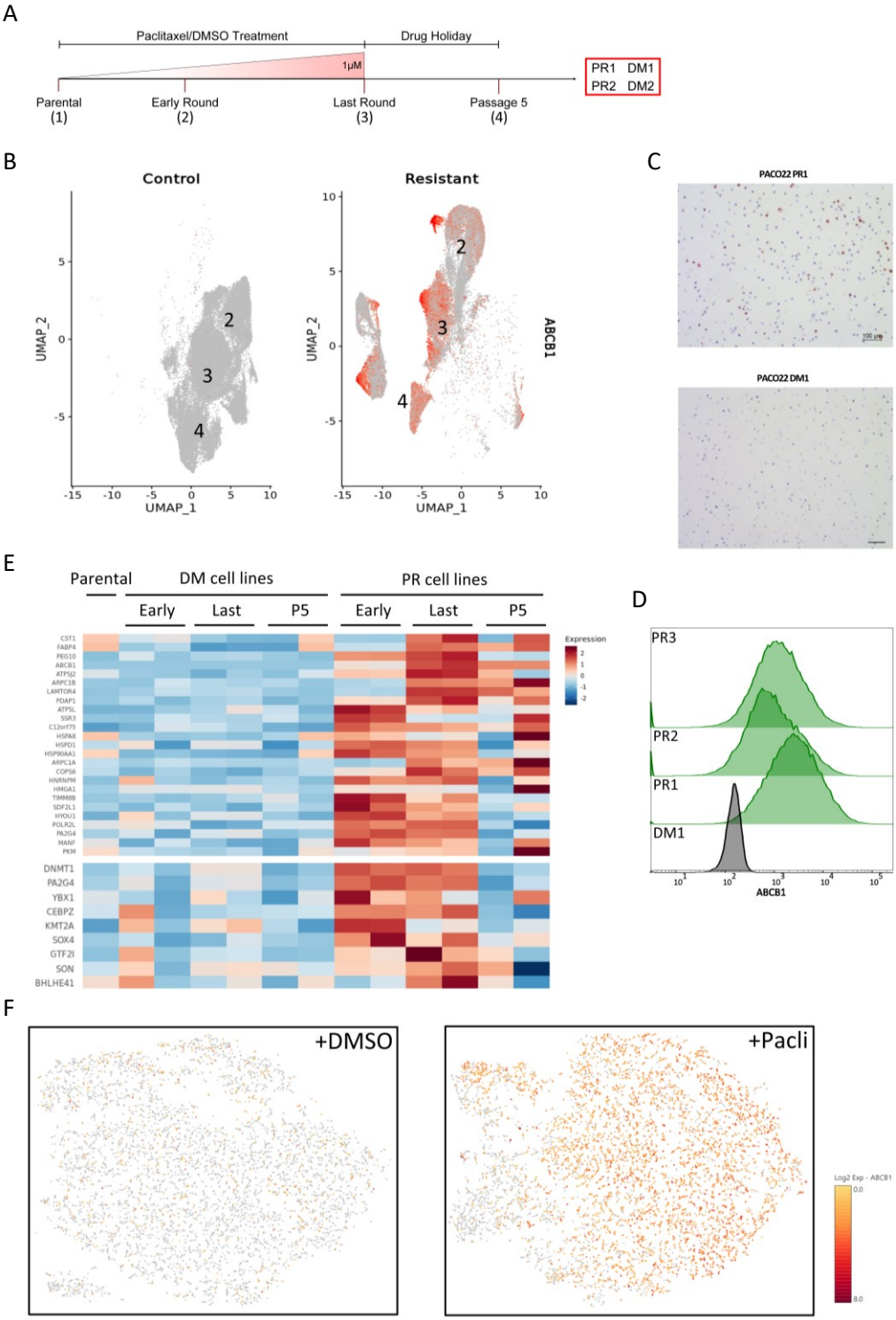

Figure 22 – Single-cell RNA sequencing analysis identified ABCB1+ and ABCB1- clones in PACO22 PR cell lines
(A) Schematic overview of long-treatment regimen for paclitaxel including the five passages of drug holiday with respective cell lines (PR1, PR2, DM1 and DM2) at indicated timepoints that were applied to single-cell RNA sequencing.
(B) Uniform Manifold Approximation and Projection (UMAP) of all samples described in (A). PR and DM cell lines separated in two graphs. Numbers correspond to timepoints labeled in (A). Each dot represents a single cell and intensity of red color corresponds to level of *ABCB1* expression.
(C) Immunohistochemistry staining of ABCB1 in a representative PR and DM cell line after long-term treatment round.
(D) Flow cytometry analysis of ABCB1 expression in PR cell lines and representative DM cell line after long-term treatment round. Half-offset histogram to display ABCB1-intesity (X) to modal cell count (Y).
(E) Differential gene expression analysis based on single-cell RNA sequencing data between group of PR samples and group of DM samples and single parental sample. Upper half displays top 25 overexpressed genes in PR cell lines. Bottom half displays overexpressed transcription factors in PR cell lines. Expression values are log2 scaled.

(legend continued on next page)

3.14 Paclitaxel-resistant cell lines can be distinguished between ABCB1+ and ABCB1- cells

To further investigate ITH related to ABCB1 expression in PR cell lines of PACO22, we used fluorescence-activated cell sorting (FACS) to sort PR cells based on their ABCB1 surface protein expression into two population, being either completely negative for ABCB1 (PR ABCB1-) or expressing high levels of ABCB1 (PR ABCB1+) (**Figure 23A**). All three PR replicates were split in an ABCB1- and ABCB1+ population (PR1 ABCB1+ and ABCB1-, PR2 ABCB1+/-, PR3 ABCB1+/-) (**Figure 23B**). In order to investigate the differences between these two populations we analyzed their cell cycle activity under paclitaxel or DMSO treatment. Paclitaxel has been reported to bind microtubules, stabilizing them and thus preventing their depolymerization leading to cell cycle arrest[314]. We stained the cells with BrdU staining to visualize the effect of paclitaxel to arrest cells in G2M phase. PR ABCB1- cells had a significantly higher proportion of cells in the G2M phase under paclitaxel treatment compared to DMSO treatment. Furthermore, PR ABCB1+ cells were not affected by paclitaxel treatment and the proportion of G2M-phase cells remained similar to the DMSO treatment (**Figure 23C**). Of note, we have previously shown that control and PR cell lines proliferate at similar speed and long-term treatment had no effect on cell cycle activity (**Figure 18C, D**). When analyzing these cell lines in the context of paclitaxel sensitivity, we first compared paclitaxel sensitivity between the two sorted populations by plaque assay. PR ABCB1- cells were more sensitive to high concentrations of paclitaxel than PR ABCB1+ cells (**Figure 23D**). Next, we compared paclitaxel sensitivity of sorted populations with DM cell lines by CTB assay. PR ABCB1- cells became similarly sensitive to paclitaxel treatment as DM cell lines verifying the importance of ABCB1 transporter expression on the cell membrane for paclitaxel resistance (**Figure 23E**). PR ABCB1+ cells were highly resistance against paclitaxel and the difference in sensitivity was further validated by plaque assay. To identify possible differences in cell viability between PR ABCB1- cells and DM cell lines, we extended the drug dilution into femtomolar concentration. Indeed, PR ABCB1- cells were significantly more resistant than DM cell lines. PR ABCB1- cells were sensitive to paclitaxel treatment, which is in line with the findings that ABCB1 mediates paclitaxel resistance and loss of ABCB1 through pharmaceutical inhibition or knockout experiments re-sensitizes the PR cells to paclitaxel (**Figure 18E**, **Figure 19E**, **Figure 23F).** This indicates that the surface protein expression of ABCB1 correlates with level

(F) Spatial clustering of cells according to global gene expression of PR1 after acute DMSO or paclitaxel treatment (0.1µM) for 4 d. Color corresponds to level of log2 expression values of ABCB1.
PR, paclitaxel-resistant; DM, DMSO-treated; Early, early round; Last, last round, P5, passage 5.
Analysis for (B) and (E) conducted by Abdelrahman Mahmoud. IHC staining in (C) was conducted by Vanessa Vogel.

of resistance against paclitaxel treatment. We re-evaluated ABCB1 surface protein expression of sorted ABCB1+ and – cells as well as DM cell lines after paclitaxel or DMSO treatment (**Figure 23G**). DM cell lines continued to be negative for ABCB1 under paclitaxel or DMSO treatment. PR ABCB1- cell lines treated with DMSO were also unchanged and the entire population remained negative for ABCB1. However, treatment with paclitaxel generated ABCB1+ cells from a population that beforehand was completely negative for ABCB1, which was consistent in all three PR replicates. Furthermore, all three replicates of PR ABCB1+ showed a mixture of ABCB1+ and ABCB1- cells under DMSO treatment, whereas paclitaxel treatment increased the proportion of ABCB1+ cells compared to ABCB1- cells without completely removing the ABCB1- negative fraction (**Figure 23G**). Mean fluorescent intensity (MFI) based on FACS of paclitaxel-treated DM cell lines was not significantly different to that of DMSO-treated DM cell lines and also not significantly different to that of DMSO-treated PR ABCB1- cells (**Figure 23H**). However, treatment with paclitaxel significantly increased MFI of ABCB1 in PR ABCB1- cells to the same level as DMSO treated PR ABCB1+ cells. This is in line with a similar proportion of ABCB1+/ABCB1- cells in the populations of paclitaxel-treated PR ABCB1- cells and DMSO-treated PR ABCB1+ cells (**Figure 23G**). In addition, paclitaxel treatment significantly increased MFI of ABCB1 in PR ABCB1+ cells compared to same cell lines under control treatment. ABCB1 protein expression was validated by Western Blot showing the absence of detectable ABCB1 protein in DMSO treated PR ABCB1- replicates, except for PR2, which is line with the levels of drug sensitivity in PR cell lines (**Figure 23I**). Paclitaxel treatment induced expression of ABCB1 in all replicates which further strengthens the hypothesis of a paclitaxel-dependent induction of ABCB1. We have shown that the proportion of ABCB1+ cells in a population is decreasing over time which might hint towards a negative selection of ABCB1+ cells based on reduced cell cycle activity. However, the proportion of cells in G2M, S or G1 phase did not differ between ABCB1- and ABCB1+ PR cell lines under DMSO treatment, meaning without external selection pressures (**Figure 23F**). Based on these findings we can conclude that PR cell lines consists of ABCB1+ and ABCB1- cells which can be sorted into two distinct cell populations with distinct paclitaxel sensitivity. Furthermore, we identified the ABCB1+ population to give rise to ABCB1- cells whereas this is not the case for ABCB1- cells under DMSO treatment. However, paclitaxel treatment induces the formation of ABCB1+ cells in the ABCB1- population which is unique for PR cell lines and was not observed in DM cell lines. Hence, paclitaxel treatment is able to tune ratio between ABCB1+ and ABCB1- cells in a PR cell line.

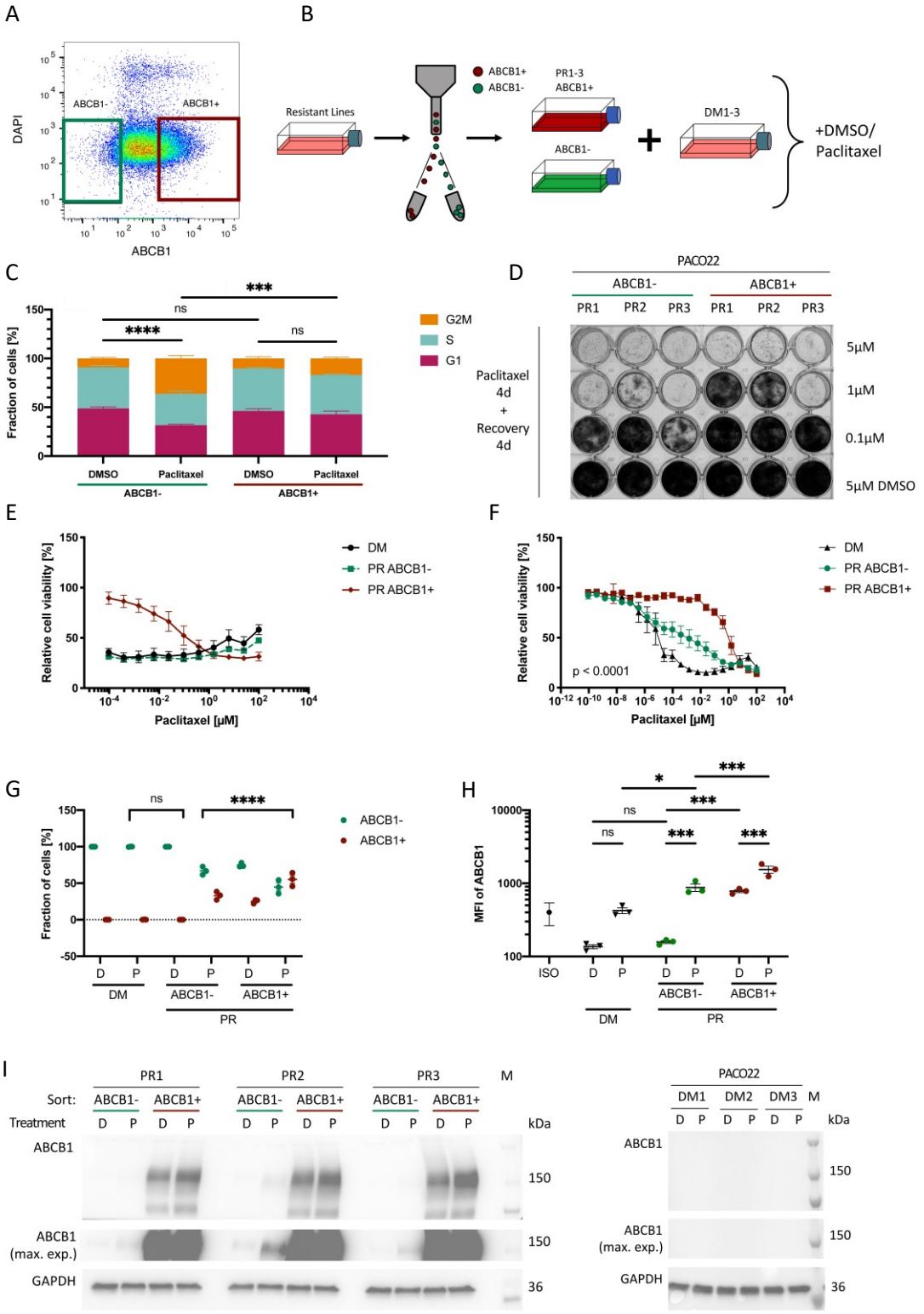

Figure 23 – ABCB1 surface expression correlates with paclitaxel resistance
(A) Flow cytometry plot of PR cell line with gates for ABCB1- and ABCB1+ cell population.
(B) Flow-assisted cell sorting (FACS) scheme for PR cell lines of PACO22. according to gating strategy displayed in (A). Cell sorting followed by treatment with paclitaxel or DMSO (50nM) for 4 d.
(C) Flow cytometry-based cell cycle analysis of PR ABCB1+ and ABCB1- cell lines after treatment with DMSO or paclitaxel as described in (B) (n = 3 individual cell lines per group). Color corresponds to cell cycle phase. Error bars depict mean ± s.e.m. *** P value < 0.001; **** P value < 0.0001; P value corresponds to each cell cycle phase by ordinary two-way ANOVA.
(D) Sensitivity of PR ABCB1- and ABCB1+ cell lines after cell sorting treated with paclitaxel and DMSO for 4 d, followed by 4 d of recovery time. Cell density was determined by crystal violet staining.

(legend continued on next page)

3.15 ABCB1+ cells display distinct gene expression profile

Long-term treatment regime generated PR cell lines that overexpressed ABCB1 in order to sustain paclitaxel treatment. Loss of ABCB1 protein or inhibition of its function sensitized PR cell lines to paclitaxel. Although we have sorted PR cells negative for ABCB1 transporter present on the membrane, PR ABCB1- replicates still displayed an improved survival compared to DM cell lines. We have shown that paclitaxel treatment induced ABCB1 protein expression in PR ABCB1- cells and did increase the proportion of the ABCB1+ cells in PR ABCB1+ cells (**Figure 23G**). Hence, we wanted to elucidate the changes that occurred through the paclitaxel treatment on the transcriptional level in PR and DM cell lines and also identify central differences between PR ABCB1- and ABCB1+ cells. Hierarchical clustering grouped cell lines based on treatment regime (paclitaxel or DMSO) with the exception of paclitaxel treated PR ABCB1+ replicates (**Figure 24A)**. We found paclitaxel-treated PR ABCB1+ replicates clustered closely together with the respective DMSO treated counterpart. Based on cell cycle analysis of paclitaxel and DMSO treated PR ABCB1+ replicates, we hypothesized that they remained unaffected by the paclitaxel treatment which would be in line with the results of gene expression analysis (**Figure 23C**, **Figure 24A**). Of interest, PR ABCB1- replicates closely clustered with PR ABCB1+ replicates under DMSO treatment, however, when treated with paclitaxel, PR ABCB1- grouped together with DM replicates (**Figure 24A, Supplementary Figure 4A, B**). In order to identify the transcriptional changes mediated by paclitaxel treatment, we compared gene expression levels between the two treatment groups, excluding PR ABCB1+ cells (**Figure 24B)**. Paclitaxel treatment induced expression of cellular stress response genes like *MMP1/10*, *DHRS2*, *SERPINB2*, *IL37* and *CDC6*. Both, DM and PR ABCB1- cells, when treated with paclitaxel, showed a similar gene expression pattern and upregulated genes that were linked to cell stress, inflammation, apoptosis and DNA damage repair[329-332] (**Figure 24C)**. We have previously described paclitaxel to induce the expression of ABCB1 protein in PR ABCB1- cells, but not in DM cell lines. In a separate analysis of PR ABCB1- and DM replicates under paclitaxel or DMSO treatment, we identified *ABCB1* only to be significantly

(E-F) Sensitivity of PR ABCB1- and ABCB1+ and DM cell lines after cell sorting treated with paclitaxel for 72 h determined by CellTiter Blue metabolism in a drug titration assay with **(E)** one 96-well plate and **(F)** two 96-well plates (n = 3 individual cell lines per group). P value as indicated by least squares regression model.
(G-H) Flow cytometry analysis of ABCB1 expression after cell sort and treatment described in (B) to determine **(G)** the proportion of ABCB1+ and ABCB1- cells, and **(H)** the mean fluorescent intensity (MFI) of ABCB1 in each cell line (n = 3 individual cell lines per group). Error bars depict mean ± s.e.m. * P value < 0.05; *** P value < 0.001; **** P value < 0.0001. (G) Ordinary two-way ANOVA and Dunnett's multiple comparisons test to ABCB1- and ABCB1+ fraction of DM cell line after DMSO treatment; (H) ordinary one-way ANOVA.
(I) Western blot analysis for ABCB1 expression after cell sort and treatment described in (B). GAPDH as loading control.
PR, paclitaxel-resistant; DM, DMSO-treated; P, paclitaxel treatment; D, DMSO treatment; kDa, kilo Dalton; ns, not significant.
FACS for (B) was conducted by Flow Cytometry core facility.

overexpressed in paclitaxel treated PR ABCB1- replicates (**Supplementary Figure 5A, B**). Detailed comparison between PR ABCB1- and DM cell lines revealed that only few genes, including *ABCB1* ($log_2FC = 3.67$), were differentially expressed under DMSO treatment, indicating that PR ABCB1- and DM cell lines were very similar on the transcriptional level (**Supplementary Figure 4C**). However, paclitaxel treatment increased the number of differentially expressed genes and enhanced the expression of *ABCB1* ($log_2FC = 5.85$) in PR ABCB1- replicates (**Supplementary Figure 4D**). In contrast to DM cell lines, paclitaxel treatment not only enhanced the expression of *ABCB1* in PR ABCB1- cells, but also induced the expression of these neighboring genes except *ABCB4* (**Supplementary Figure 5A, B**). Next, we compared PR ABCB1+ cells with DM cell lines under DMSO treatment and attained a 10-times higher number of differentially expressed genes compared to the comparison between PR ABCB1- cells and DM cell lines. In this comparison (PR ABCB1+ vs DM), *ABCB1* was the most upregulated gene in PR ABCB1+ replicates (**Supplementary Figure 4E**). Of interest, only neighboring genes of *ABCB1* on chromosome 7 were also highly overexpressed in PR ABCB1+ replicates. Moreover, paclitaxel treatment increased the number of differentially expressed genes which is caused by DM cell lines that were affected by paclitaxel treatment. In response, DM cell lines changed their gene expression profile upregulating cell stress response genes, whereas because PR ABCB1+ cells were unaffected by paclitaxel treatment and no genes were found to be differentially expressed between the two regimens (**Supplementary Figure 4F**, **Supplementary Figure 5C**). Next, we examined the central differences between PR ABCB1- and ABCB1+ cells on the transcriptional level under control conditions. Similar to the previous comparisons, both groups only differed in few genes when treated with DMSO instead of paclitaxel (**Figure 24D**). Among them, *ABCB1* was the top differentially expressed gene in PR ABCB1+ cell lines. Interestingly, most of the remaining genes (*ABCB4*, *TP53TG1*, *CROT*, *DMTF1*, *TMEM243*, *KIAA1324L*, *DBF4*) being overexpressed were closely located around *ABCB1* locus on the genome. We have previously reported that all PR cell lines acquired a genomic amplification of *ABCB1* and surrounding genes (*TP53TG1*, *CROT*, *ABCB4*, *RUNDC3B*) (**Figure 16A, B**). GSEA verified that PR ABCB1+ cells were enriched for genes located around *ABCB1* on Chr.7, which has also been shown before for the bulk PR vs DM analysis (**Figure 11B**, **Figure 24E**). In addition, we found enrichment of genes corresponding to enhanced antidrug metabolism, nuclear receptors pathway and interferon alpha response (**Figure 24E)**. Based on the MFI value, *ABCB1* was only significantly induced in PR ABCB1- cells after paclitaxel treatment (**Figure 24F)**. Although paclitaxel treatment could not increase the expression of *ABCB1* in PR ABCB1+

cells, it was already significantly higher expressed compared to PR ABCB1- cells, independent of the treatment regimen (**Figure 24F**). Verification by qRT-PCR for the different cell lines revealed the same stepwise increased expression for *ABCB1* in PR cell lines, however, the difference in *ABCB1* expression between DMSO and paclitaxel treated PR ABCB1- replicates was not significant (**Figure 24G**). DM cell lines presented the lowest expression levels of *ABCB1*, and paclitaxel treatment did not induce expression of *ABCB1* (**Figure 24G**). Although ABCB1 protein expression was lost in ABCB1- PR cell lines, *ABCB1* mRNA levels were significantly increased by 31-fold compared to DM cell lines under DMSO treatment (**Figure 24G**). Although protein expression of ABCB1 was significantly increased in PR ABCB1- after paclitaxel treatment, we did not detect increased mRNA levels compared to DMSO treatment (**Figure 23H**, **Figure 24G**). Similar to PR ABCB1-, paclitaxel treatment did not induce expression of ABCB1 in PR ABCB1+ cells although a gain of ABCB1 protein was confirmed by both FACS and Western Blot (**Figure 23H, I, Figure 24G**). *ABCB4*, a member of the ABC transporter superfamily, is located in close genomic proximity to *ABCB1* (~ 500 kb) and shares 80% of nucleotide sequence identity with *ABCB1*[190]. We have previously shown by exome sequencing that the region around *ABCB1* locus was amplified in PR cell lines of PACO22, which presumably further enhanced elevated expression levels of *ABCB4* compared to DM cell lines (**Figure 13B, Figure 18B**). Similar to ABCB1, single round of paclitaxel treatment did not induce expression of *ABCB4* in DM cell lines of PACO22 (**Figure 24H**). Of note, the levels of *ABCB4* were not significantly increased in DMSO-treated PR ABCB1- replicates compared to the respective DM replicates. In contrast to *ABCB1*, expression of *ABCB4* was not significantly induced by paclitaxel treatment in PR ABCB1- cell lines, which was confirmed by qRT-PCR (**Figure 24F-H, Supplementary Figure 6A**). PR ABCB1+ cells displayed increased expression of *ABCB4* by more than 100-fold compared to DM and PR ABCB1- cell lines under DMSO treatment and remained unchanged when treated with paclitaxel (**Figure 24H**). From this we would hypothesize that PR ABCB1+ cells were co-expressing neighboring genes, independent of short-tern paclitaxel treatment. In order to validate that, we analyzed the expression levels of the remaining neighboring genes, being *CROT*, *RUNDC3B* and *TP53TG1* (**Supplementary Figure 7A-C**). For all three genes, MFI values remained unchanged between DMSO and paclitaxel treatment in DM and PR ABCB1- and PR ABCB1+ cell lines. When comparing the relative MFI values of PR ABCB1- and PR ABCB1+ cells to DM cell lines, only the levels of *ABCB1* and *RUNDC3B* were significantly higher in PR ABCB1- cells compared to DM cell lines, whereas all genes were elevated in PR ABCB1+ cell lines (**Supplementary Figure 6B-E**). However, validation of these findings by qRT-PCR showed that *CROT*,

RUNDC3B and *TP53TG1* were significantly increased in PR ABCB1- cells treated with paclitaxel treatment compared to DMSO treatment (**Supplementary Figure 7A-C**). All three genes were expressed the most in PR ABCB1+ replicates of both treatment regimens compared to the other two groups (DM and PR ABCB1-) which is in line with the microarray data. Additionally, the acute treatment of paclitaxel did not yield in an induction of CYP3A5 as compensatory drug resistant mechanism in drug-sensitive PR ABCB1- cells (**Supplementary Figure 7D**). Still, we found one PR ABCB1+ replicate (PR3) to have increased *CYP3A5* expression. However, PR3 remained the cell line with the lowest paclitaxel resistance of all three PR cell lines (**Figure 23D**) suggesting that the increased levels of CYP3A5 are not sufficient to further improve drug resistance levels in that cell line. Gene expression analysis revealed that DM and PR ABCB1- cell lines shared a similar gene expression profile, with the exception of a few genes including *ABCB1* (**Supplementary Figure 4C-D**). Similarly, PR ABCB1- and ABCB1+ cells differed only in expression of *ABCB1* and its neighboring genes (**Figure 24D**). Acute paclitaxel treatment induced the same transcriptional response in both paclitaxel-sensitive DM and PR ABCB1- cell lines which indicates that long-term treatment maintained the transcriptional profile of PACO22 in both DM and PR cell lines (**Supplementary Figure 5A-B**). We can conclude that PR cells are highly heterogeneous at the single cell level and can be distinguished by ABCB1 cell surface expression. Separation of PR cells based on their ABCB1 surface protein levels divides the population in a drug resistant and drug sensitive subgroup that differ only in the expression levels of *ABCB1* and its neighboring genes.

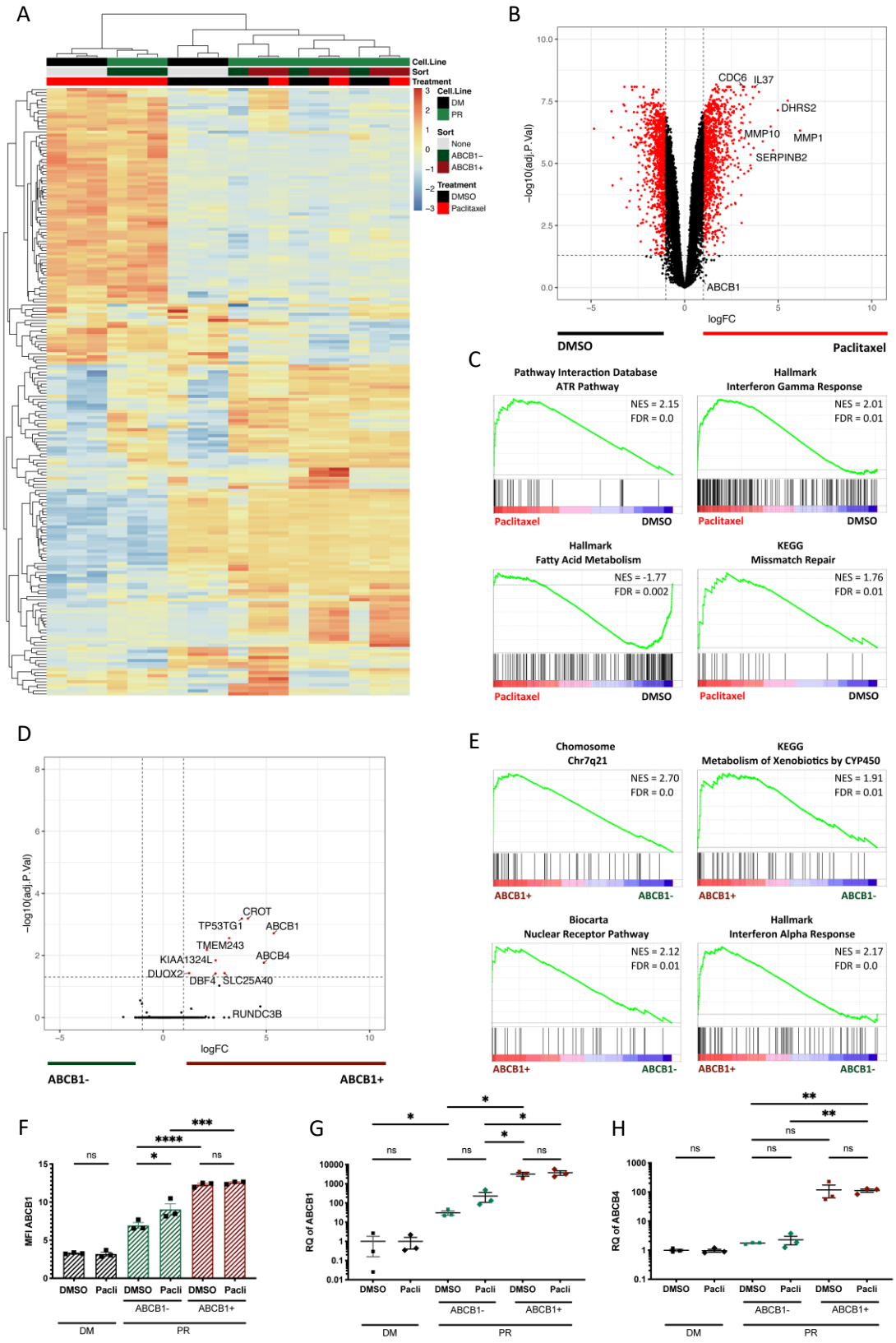

Figure 24 – ABCB1+ population displays distinct gene expression profile

(A) Hierarchical clustering analysis based on gene expression microarray of cell lines described in Figure 23B at the different timepoints based on the top 200 variant genes. Complete Pearson correlation-based distance for samples. Intensities are centered in gene direction and correspond to log2 scale.

(legend continued on next page)

3.16 ABCB1 expression is activated by microtubule targeting agents

The strong upregulation of *ABCB1* in response to paclitaxel treatment in PR cell lines of PACO22 suggests a combination of active transcription and genomic amplification of *ABCB1* that lead to acquired paclitaxel resistance **(Figure 12B, Figure 16A, B**, **Figure 18E**). Based on our findings in the ABCB1+/- sorted populations, translation of ABCB1 appears to be induced by acute paclitaxel treatment, leading to an increase in protein levels without a significant increase in *ABCB1* mRNA levels. However, in PR cell lines, that lost resistance after 10 passages of drug holiday, we found both mRNA and protein levels of *ABCB1* to be significantly increased after a single round of paclitaxel treatment (**Figure 21C**). Moreover, single-cell RNA Sequencing of PR cell lines identified a significant gain in PR ABCB1+ cells after acute paclitaxel treatment compared to DMSO treatment (**Figure 22F**). We thus sought to further examine the mechanism leading to *ABCB1* induction in PR cell lines in more detail. To this aim, we treated the paclitaxel sensitive PR ABCB1- cells of PACO22 for up to 96 h with paclitaxel and compared the expression levels of *ABCB1* and *ABCB4* with the untreated control. Expression of *ABCB1* was significantly increased after 72 h and 96 h of paclitaxel treatment compared to the untreated samples (**Figure 25A**). Expression of *ABCB4* was not induced by paclitaxel treatment even after 96 h, which is in line with previous findings (**Figure 24H**, **Figure 25B)**. Of interest, we could not observe a change in *ABCB1* transcription levels after 24 h and only a positive trend after 48 h of paclitaxel treatment. We compared the expression levels of *ABCB1* in PR ABCB1- cells to DM cell lines and detected a more than 100-fold decreased expression of *ABCB1* with cycle threshold (Ct) values ranging between 33 and 37, whereas they ranged between 23 and 25 for PR ABCB1- cell lines (**Supplementary Figure 8A, C**).

(B) Volcano plot of all differentially expressed genes in DM + PR ABCB1- cell lines between DMSO and paclitaxel (n = 6 individual cell lines per group). Highlighted in red are all genes that are at least one log2-fold differentially expressed with an adjusted p-value of less than 0.05 according to the Benjamini-Hochberg calculation. Labeled genes are related to cell stress, inflammation, apoptosis and DNA damage repair.
(C) Gene set enrichment analysis (GSEA) of the groups described in (B). Statistical significance was assessed using 1000 permutations on the gene set.
(D) Volcano plot of all differentially expressed genes between PR ABCB1- and PR ABCB1+ cells after DMSO treatment (n = 3 individual cell lines per group). Highlighted in red are all genes that are at least one log_2-fold differentially expressed with an adjusted p-value of less than 0.05 according to the Benjamini-Hochberg calculation. Labeled genes included all genes in red and neighboring genes of *ABCB1* on the chromosome.
(E) Gene set enrichment analysis (GSEA) of the groups described in (D). Statistical significance was assessed using 1000 permutations on the gene set.
(F) Mean fluorescent intensity of *ABCB1* probes in cell lines described in Figure 23B (n = 3 individual cell lines per group). Each dot represents a unique cell line. Error bars depict mean ± s.e.m. * P value < 0.05; *** P value < 0.001; **** P value < 0.0001 by ordinary one-way ANOVA.
(G-H) qRT-PCR analysis in cell lines described in Figure 23B of (G) *ABCB1* and (H) *ABCB4* (n = 3 individual cell lines per group). Each dot represents a unique cell line. Values are relative to DMSO-treated DM cell lines. Error bars depict mean ± s.e.m. * P value < 0.05; ** P value < 0.01; Student's t test.
PR, paclitaxel-resistant; DM, DMSO-treated; NES, normalized enrichment analysis; FDR, false discovery rate; Pacli, paclitaxel treatment; ns, not significant.

In addition, expression of *ABCB1* was not induced by paclitaxel, confirming the previous results. Expression of *ABCB4* was lower by more than one log-fold in DM cell lines compared to PR ABCB1- cell lines (**Supplementary Figure 8B, D**). Similar to *ABCB1*, Ct values of *ABCB4* ranged between 33 and 37 in DM cell lines, whereas they ranged between 28 and 30 for PR ABCB1- cells. From these findings we hypothesized that paclitaxel treatment does not lead to an immediate response by induction of *ABCB1* expression in the manner of signaling kinase pathways[333]. It could be possible that the stabilization of microtubules leads to a block of mitosis and taxol-induced cell stress would be the responsible behind the observed induction of *ABCB1* after 72 h of paclitaxel treatment[314,334,335]. Consequently, tests followed to investigate whether additional microtubule targeting compounds would also induce *ABCB1* expression. Vinblastine, vincristine and colchicine are microtubule de-stabilizing agents that induce cell cycle arrest and apoptosis[336]. Of them, only colchicine significantly induced the expression of *ABCB1* after 96 h of treatment to a similar degree as paclitaxel in PR ABCB1- cells compared to the untreated control (**Figure 25C**). In PR ABCB1+ cells, none of the compounds significantly induced expression of *ABCB1* compared to untreated controls (**Figure 25D**). As previously shown for paclitaxel treatment, none of the compounds significantly induced expression of *ABCB4* after up to 96 h of treatment (**Supplementary Figure 8E, F**). Finally, we tested whether these new compounds were also targets of *ABCB1* transporter. For this, we treated bulk DM and PR cell lines with either of these compounds and compared cell viability between the two groups (**Figure 25E**). Strikingly, paclitaxel-resistant PR cell lines (**Figure 18E**) were significantly more resistant than control cell lines for all three microtubule targeting compounds. Indeed, all three compounds have been reported to bind to *ABCB1* with varying degrees of affinity[337,338]. Based on these findings, we conclude that induction of *ABCB1* transcription is not dependent on paclitaxel. Instead, we propose that drug-induced malfunction of microtubules and consecutive cell cycle arrest and cell stress activate transcription of *ABCB1* in PR cell lines.

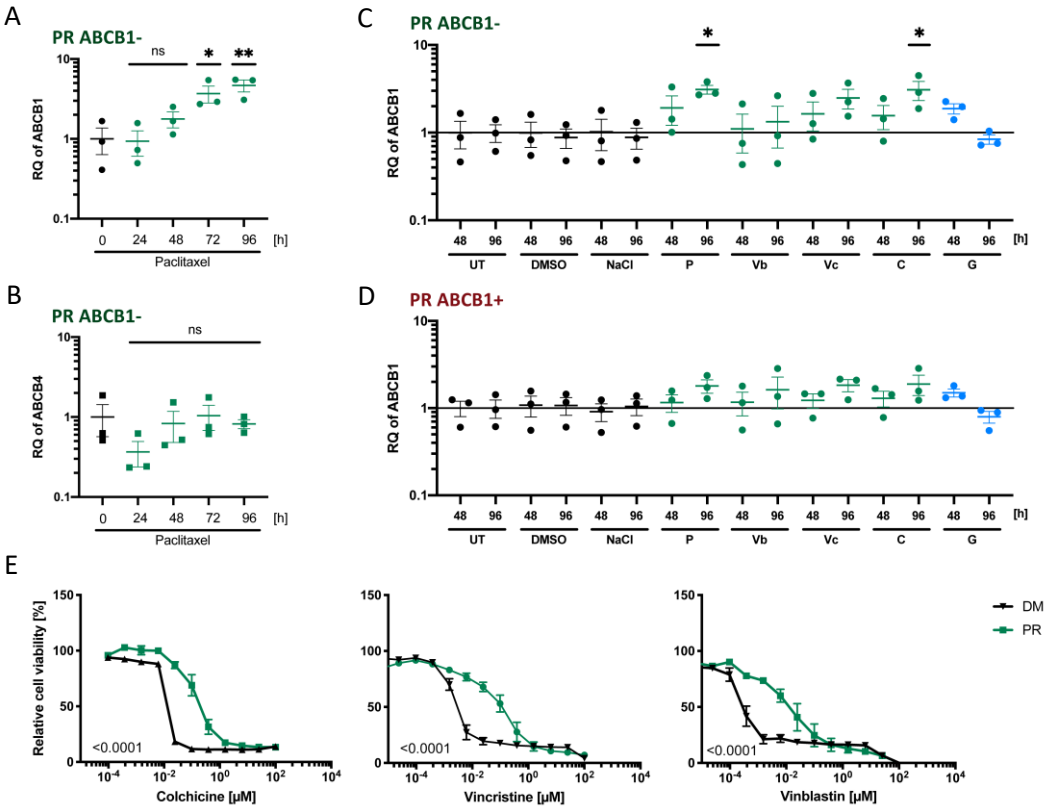

Figure 25- Not only paclitaxel but also other microtubule targeting agents induce expression of ABCB1 in PR cell lines of PACO22

(A-B) qRT-PCR analysis in PR ABCB1- cells treated with paclitaxel (100 nM) for expression of **(A)** *ABCB1* and **(B)** *ABCB4* (n = 3 individual cell lines per group). Each dot represents a unique cell line. Values are relative to untreated control. Error bars depict mean ± s.e.m. * P value < 0.05; ** P value < 0.01; by Student's t test.

(C-D) qRT-PCR analysis of ABCB1 expression after treatment with various compounds for 48 h and 96 h in **(C)** PR ABCB1- cells and **(D)** PR ABCB1+ cells. Each dot represents a unique cell line. Values are relative to untreated control after 48 h. Error bars depict mean ± s.e.m. * P value < 0.05; by Student's t test.

(E) Sensitivity of PR and DM cell lines treated with microtubule de-stabilizer colchicine, vincristine and vinblastine for 72 h determined by CellTiter Blue metabolism (n = 3 individual cell lines per group). Least squares regression model. P values as indicated.

PR, paclitaxel-resistant; DM, DMSO-treated, UT, untreated; P, paclitaxel; Vb, vinblastine; Vc, Vincristine; C, colchicine; G, gemcitabine; ns, not significant.

3.17 Genomic region around *ABCB1* is transcriptionally active in PACO22 PR lines

We have previously shown that PR cell lines acquired the ability to induce expression of *ABCB1* upon acute paclitaxel treatment, whereas DM cell lines were lacking that ability **(Figure 24F**, **Supplementary Figure 8A-D**). To further explore the acquired drug resistance mechanism that is dependent on ABCB1 expression, we performed an Assay for Transposase-Accessible Chromatin (ATAC) using sequencing (ATAC-Seq) on DM and PR ABCB1-/ABCB1+ cell lines to analyze the chromatin status around the *ABCB1* locus. The samples were acquired after a four days drug treatment with paclitaxel or DMSO (**Figure 23B**). In order to investigate genomic changes that were acquired and manifested during long-term drug treatment, we combined DMSO treated PR ABCB1+ and PR ABCB1- cells to a "combined PR" sample and compared them with DM cell lines. ATAC-seq PCA identified major differences between PR cell lines which have been previously described on the DNA and RNA level (**Figure 16**, **Figure 18A, Figure 26A**). Analysis of differentially accessible chromatin region between DM cell lines and combined PR cell lines (PR ABCB1+ and PR ABCB1-) identified a cluster of peaks around *ABCB1* (**Figure 26B**). Of interest, the four genes (*TP53G1*, *ABCB4*, *ABCB1*, *RUNDC3B*) that were massively amplified, as reported by copy number variation analysis (**Figure 16**), were the same genes with the highest fold change with respect to chromatin accessibility (**Figure 26C**). We then compared the identified differential ATAC-seq peaks with the log_2FC values of the differential gene expression analysis of the same samples, comparing DM cell lines with combined PR cell lines (**Figure 26D**). Although the top four candidate genes were higher expressed in combined PR cell lines compared to DM cell lines, only *ABCB1* reached significance. Based on gene expression analysis we knew that DMSO treated PR ABCB1- cells have significantly lower *ABCB1* mRNA levels than corresponding PR ABCB1+ cells (**Figure 24D, G**). PCA based on gene expression showed that PR ABCB1- cell lines clustered between control and PR ABCB1+ cell lines and that only few genes had significantly different expression levels between DM and PR ABCB1- cell lines (**Supplementary Figure 4A**, **C**). Differential gene expression analysis between PR ABCB1+ and DM cell lines correlated with peak fold change values (**Figure 26E**), with results in line with the peak FC values calculated between combined PR cell lines and DM cell lines. Based on these findings one can state that PR cell lines acquired induction of *ABCB1* expression through mechanisms that include an open chromatin state around the *ABCB1* locus. PR cell lines acquired a conformational change of the chromatin specifically around the *ABCB1* locus which enables active transcription of *ABCB1* and its neighboring genes. The ABCB1-dependent drug

resistance mechanism highlights the combination of genomic amplification and gene expression of *ABCB1* that enabled enhanced upregulation and resistance to paclitaxel treatment in PR cell lines (**Figure 12B**, **Figure 16**, **Figure 18E**).

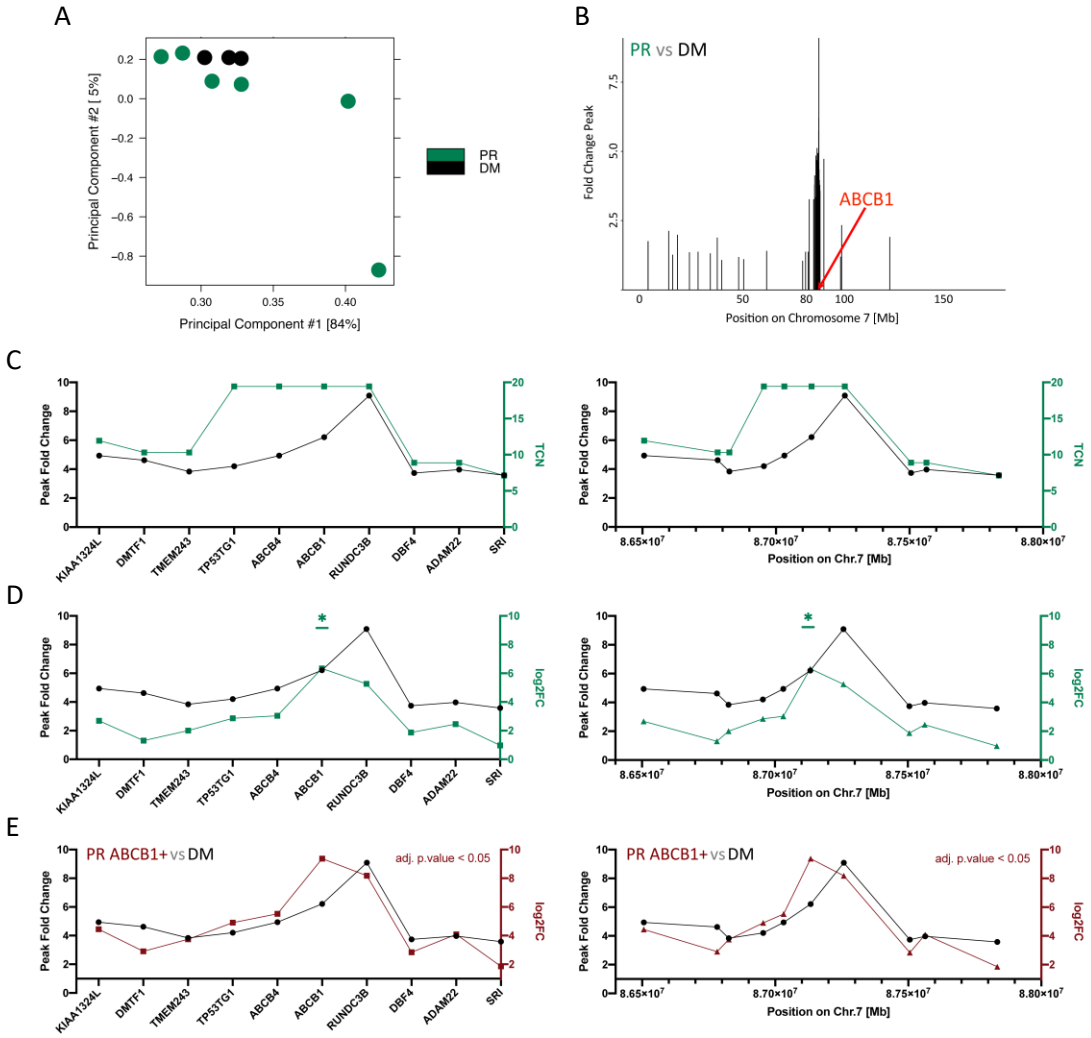

Figure 26 – Genomic region around ABCB1 is transcriptionally active in PR cell lines of PACO22
(A) Principal component analysis (PCA) based on global binding matrix of PR ABCB1- and PR ABCB1+ cells combined as PR group, and DM cell lines after cell sort and DMSO treatment described in Figure 23B (n = 6 individual cell lines for PR group and 3 for DM group).
(B) Plot of significantly differentially peaks of protein-free DNA regions on chromosome 7 in PR group compared to DM cell lines. Red Arrow shows location of *ABCB1* gene on chromosome 7. Peak fold change value is calculated by the difference between the two groups based on number of identified reads.
(C-E) Comparison of peak fold change values with **(C)** total copy number (TCN) count or with **(D-E)** log2-scaled fold change (log2FC) in gene expression for *ABCB1* and neighboring genes. Peak fold change values for each gene derived from analysis performed in (B). TCN values derived from whole exome sequencing (WES) analysis of PR cell lines (mean value of all three values plotted). Log2FC values derived from differential gene expression analysis between **(D)** PR group (PR ABCB1- and ABCB1+ cells) or **(E)** PR ABCB1+ cells and DM cell lines after sort and DMSO treatment as described in Figure 23B. Significantly overexpressed genes were indicated by (D) * (adj.P value < 0.05); (E) all genes were significantly overexpressed (adj.P value < 0.05). Left graph shows order of genes surrounding *ABCB1* on chromosome 7. Right graph shows the starting position of the genes on chromosome 7.
PR, paclitaxel-resistant; DM, DMSO-treated; Mb, million bases, Chr.7, chromosome 7.

3.18 Expression of ABCB1 is enhanced by amplification of ecDNA

WES of PACO22 samples revealed that PR cell lines acquired genomic amplifications on chromosome 7 that included *ABCB1* and its neighboring genes (**Figure 16**). In previous analysis expression levels of *ABCB1* and its genomic neighbors were elevated in PR ABCB1+ cells compared to PR ABCB1- cells but their expression was not induced upon paclitaxel treatment (**Figure 24E, Supplementary Figure 7**). In PR ABCB1- cells, these expression levels were much lower and closer to that of DM cell lines than to PR ABCB1+ cells (**Figure 24E, Supplementary Figure 7**). However, ATAC-Seq analysis showed that the genomic locus around *ABCB1* was transcriptionally active in both PR ABCB1+ and ABCB1- cells compared to DM cell lines (**Figure 26B**). Based on FACS analysis and single-cell RNA-seq, we found *ABCB1* to be heterogeneously expressed in PR cell lines of PACO22 (**Figure 22C**, **E**). Hence, we hypothesized that the genomic amplification, found in bulk PR cell lines, could be heterogeneously distributed between the single cells and could correlate with ABCB1 expression levels. We thus aimed to gain further insight into the formation and structure of the *ABCB1* specific amplicon linked to expression levels of *ABCB1*. PACO22 PR cell lines were FACS sorted based on ABCB1 protein expression and were divided into ABCB1- and ABCB1+ populations as previously described (**Figure 23B**). Next, we determined the number of *ABCB1* genes by Fluorescent in situ hybridization (FISH) in whole cells of the sorted populations. In line with the findings of the WGS analysis, both populations were triploid, carrying three centromeres of chromosome 7 (**Figure 7, Figure 27A**). In PR ABCB1- cells, the majority of cells carried 3 or less copies of the *ABCB1* gene, whereas in PR ABCB1+ cells the mean number of *ABCB1* genes in the cells was almost 100 (**Figure 27A, B**). Of note, a proportion of cells (14%) of the PR ABCB1- cells carried more than three copies of *ABCB1*. Based on previous findings, expression of ABCB1 can be increased by paclitaxel treatment in PR cell lines of PACO22 (**Figure 21C**, **D**, **Figure 22F**, **Figure 23G-I**, **Figure 25A**). Hence, we investigated whether the loss of ABCB1 amplification in PR ABCB1- cells would change upon paclitaxel treatment. To further examined the dynamics and the possible effect of paclitaxel on the generation of these amplifications, we FACS sorted PR cell lines based on ABCB1 protein expression and, similar to the long-term treatment regime, treated paclitaxel-sensitive PR ABCB1- cells with increasing concentrations of paclitaxel while paclitaxel-resistant PR ABCB1+ cells received equal amounts of DMSO (**Figure 27C**). After 13 passages of paclitaxel treatment, FACS analysis revealed that PR ABCB1- cells had a 45-fold higher ΔMFI (16454) for ABCB1 than PR ABCB1+ cells (360) (**Figure 27D)**. FACS analysis revealed that the proportion of PR ABCB1+ cells continuously reduced over the course of this experiment-

(**Figure 27E, Supplementary Figure 9A**). After 13 passages of DMSO treatment more than 99% of previously ABCB1+ cells turned into ABCB1- cells (**Figure 27E**). This confirms our previous findings that paclitaxel is required to induce and maintain ABCB1 protein expression (**Figure 21D**, **Figure 23H**). For PR ABCB1- cells, paclitaxel treatment induced the expression of ABCB1 more rapidly and already after 5 passages more than 85% of the previously ABCB1- population turned ABCB1+ (**Figure 27E, Supplementary Figure 9A)**. Already two passages later, more than 95% of cells were ABCB1+ in PR ABCB1- cells and this proportion remained unchanged until passage 13. While PR ABCB1+ cells had a 2000-fold higher ΔMFI than PR ABCB1- cells at the sort of the cells, this difference disappeared after the first five passages and at passage nine, PR ABCB1- cells had a 20-fold higher ΔMFI than PR ABCB1+ cells (**Figure 27F, Supplementary Figure 9B)**. After 13 passages, PR ABCB1- cells remained to have an almost 20-fold higher ΔMFI than PR ABCB1+ cells (**Figure 27F)**. Gene expression levels of *ABCB1* correlated with loss of ABCB1 protein expression and decreased continuously, reaching its lowest point after passage 13 (**Figure 27G)**. Paclitaxel treatment in PR ABCB1- cells increased expression of *ABCB1* to the same level as in passage 1 of PR ABCB1+ cells after five passages and resulted in a two-fold increased expression after 13 passages of treatment. Although not significant, the levels of *ABCB4* seemed to be also reduced over time in PR ABCB1+ cells, while being increased significantly after nine passages of paclitaxel treatment in PR ABCB1- cells (**Figure 27H)**. Altogether, these data indicate a correlation between ABCB1 protein and mRNA expression in PR cell lines during a long-term treatment experiment. Finally, we asked the question of whether the genomic amplification of *ABCB1* observed in PR ABCB1+ cells is mediated by paclitaxel treatment, i.e. if paclitaxel is needed to maintain the number of amplifications seen in PR ABCB1+ cells. Strikingly, counting of the number of *ABCB1* genes by FISH revealed that PR ABCB1+ cells that were treatment with DMSO, lost the amplification over time, down to the point that the number of *ABCB1* genes counted was equal to the number of chromosome 7 centromeres (**Figure 27I, Supplementary Figure 10)**. In contrast, in PR ABCB1- cells under paclitaxel treatment, *ABCB1* genes counts increased during the passages until the cells had by average more than 20 copies of *ABCB1* gene inside the nucleus (**Figure 27I, Supplementary Figure 11)**. These data indicate that long-term paclitaxel treatment increased the number of *ABCB1* genes in PR ABCB1- cells which correlated with mRNA and protein levels of ABCB1. Furthermore, the absence of paclitaxel treatment leads to a steady reduction in *ABCB1* genes count and to a complete loss of additional *ABCB1* genes in the majority of PR ABCB1+ cells after passage 13 (**Figure 27J**). From these findings we can conclude that paclitaxel treatment does not only induce the expression of

ABCB1 but also induces the amplification of ABCB1 genomic loci. Of interest, we found *ABCB1* genes to be located outside of chromosomes in metaphase cells (**Supplementary Figure 12**). Hence, we hypothesized that the amplifications found inside the nucleus are located on extrachromosomal DNA (ecDNA) that might be generated de novo from the genome and, under persistent paclitaxel treatment, could be further amplified to increase mRNA and, subsequently, protein levels of ABCB1.

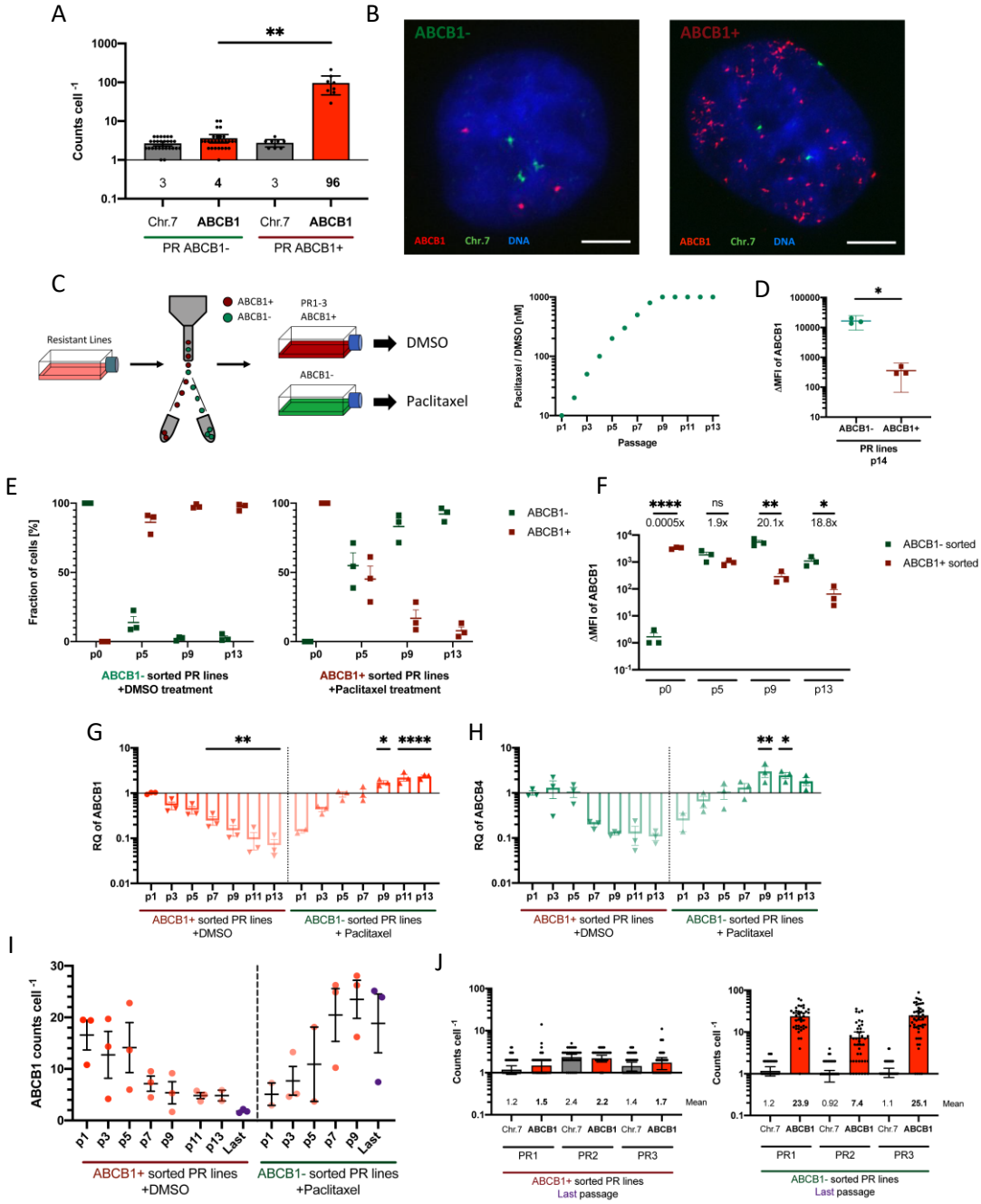

Figure 27 – Expression of ABCB1 is enhanced by generation and amplification of ecDNA carrying ABCB1 gene
(A) Fluorescent in situ hybridization (FISH)-based counting of *ABCB1* in PR ABCB1- and PR ABCB1+ cells after cell sort (n = 27 cells for PR ABCB1- and n = 8 for PR ABCB1+). Centromere of chromosome 7 as reference. Each dot represents a single cell. Error bars depict mean ± s.e.m. ** P value < 0.01 by Students t-test.
(B) Representative image of FISH staining in a PR ABCB1- and PR ABCB1+ cell. *ABCB1* genes are labeled red, centromere of chromosome 7 is labeled green, DNA is labeled blue. Scale bar corresponds to 10 µm.
(C) Flow-assisted cell sorting (FACS) scheme for PR cell lines of PACO22 according to gating strategy displayed in Figure 23B followed by treatment regimen with increasing drug concentration until 1 µM. PR ABCB1+ cells are treated with increasing concentrations of DMSO, PR ABCB1- cells are treated with increasing concentrations of paclitaxel.
(D) Flow cytometry analysis of ABCB1 expression after cell sort and treatment regimen described in (C) to determine the expression of ABCB1 based on the delta mean fluorescent intensity (ΔMFI) in each cell line (n = 3 biological replicates per group). Each dot represents a unique cell line. Error bars depict mean ± s.e.m. * P value < 0.05 by Student's t test.
(E-F) Flow cytometry analysis of ABCB1 expression during treatment regimen described in (C) to determine (E) the proportion of ABCB1+ and ABCB1- cells, and (F) the delta mean fluorescent intensity (ΔMFI) in each cell line (n = 3 biological replicates). Each dot represents a unique cell line. Error bars depict mean ± s.e.m. * P value < 0.05, ** P value < 0.01, **** P value < 0.0001, by Student's t test.

(legend continued on next page)

(G-H) qRT-PCR analysis of sorted cell lines during treatment regimen described in (C) for expression of (A) *ABCB1* and (B) *ABCB4* (n = 3 biological replicates per group). Each dot represents a unique cell line. Values are relative to PR ABCB1+ p1. Each dot represents a unique cell line. Error bars depict mean ± s.e.m. * P value < 0.05; ** P value < 0.01; **** P value < 0.0001; by Student's t test.
(I) FISH-based counting of *ABCB1* genes in sorted cell lines during treatment regimen described in (C). Each dot represents a unique cell line. For each cell line at any timepoint at least 30 nuclei were acquired. Error bars depict mean ± s.e.m.
(J) FISH-based counting of *ABCB1* genes in sorted cell lines after treatment regimen, as described in (C), has ended. Centromere of chromosome 7 as reference. Each dot represents a single cell. Error bars depict mean ± s.e.m.
PR, paclitaxel-resistant; DM, DMSO-treated; Chr.7, chromosome 7.
FISH staining in (A) and (B) was conducted by Vanessa Vogel. FACS for (C) was conducted by Flow Cytometry core facility.

4 Discussion

4.1 Gene expression-based stratification of patient derived xenografts

Stratification of cancer based on clinically and biologically relevant molecular differences and similarities has the potential to improve treatment of pancreatic cancers via biologically-informed selection of optimal, more patient-specific therapeutic regimens[126,339]. For PDAC, it has been previously proposed that subtypes exhibit differences in drug sensitivity[130,183]. However, stratification of PDAC patients into groups of therapeutic regimens has been difficult thereby hampering clinical translation[340]. Moreover, predictive biomarkers of therapeutic response that are currently used in other cancer entities, like *ERBB2* amplification, *BRAF* and *BRCA1* mutation are rare events in PDAC and have not yet proven to be beneficial[126,341-343]. In a recent update of the COMPASS trial it became apparent that gene expression-based stratification into the two major transcriptomic groups, Classical-PDAC and Basal-like-PDAC, was only able to predict objective response to therapy with the best progressive-free survival for patients with a classical tumor treated with modified FOLFIRINOX[344]. The expression of *GATA6*, one of the genes expressed by classical-PDACs but not by basal-like ones[133], could improve patient selection for current treatments[344]. Gene expression-based hierarchical clustering of our xenograft samples resolved two groups, C1 and C2. *GATA6* as well as signatures from the classical subtype were enriched in C1 while basal- or QM-like genes were enriched in C2[131,133]. Although immunohistochemistry (IHC) staining of CYP3A5 did not entirely overlap with gene expression levels of microarray analysis, the majority of samples expressing significant levels of *CYP3A5* were found in the classical subtype. Furthermore, we found genes supporting *CYP3A5* expression like *HNF4A* and *NR1I2* that have been described previously[183]. The group corresponding to the classical subtype might contain a wide spectrum of subgroups, like CYP3A5-positive and negative tumors[126,130,183]. The basal group comprised the majority of the IHC-KRT81+ samples, a feature connected with the quasi-mesenchymal subtype[183]. However, the basal group also contained double-negative and IHC-HNF1A+ samples, which we previously described as characteristics of the classical and exocrine-like subtypes[183]. We compared the groups based on gene expression differences with other classifiers. While Collisson *et al.* used human microdissected specimens of cancer patients, we derived RNA from patient-derived xenografts, which mainly differs in the tumor-microenvironment and the global gene expression profile[130]. Although not significant, the exocrine-like subtype gene signature seemed to be more enriched in the C1/classical group. Moffitt et al. applied a bioinformatical separation of bulk primary tumor samples into tumor,

stromal and normal gene expression and identified two tumor subtypes being “basal-like” and “classical” subtype[131]. The subtypes Pancreatic Progenitor and Squamous defined by Bailey et al. directly overlapped with Classical and Basal subtype of the Moffitt et al. which further strengthens the hypothesis that the two groups identified by gene expression analysis represent the two main subtypes of PDAC[126,133]. But how would the tumors of each subtype react to chemotherapeutic treatment? Are there subtype-specific evasion routes that are linked to global gene expression profile or genetic and epigenetic patterns that could offer therapeutic vulnerabilities[126]? Hence, it might be necessary to define a novel stratification that is based on the response to chemotherapeutic treatment. We selected a representative PACO cell for each molecular subtype, being PACO22 for the classical and PACO43 for the basal subtype. PACO17 had been previously described to be CYP3A5 independent for acquired drug resistance and was included as control cell line[183]. All three cell lines carried similar mutational profile, with the exception of PACO22 that additionally carried a MYC amplification.

4.2 Generation of drug resistance PACO cell lines by long-term drug treatment

Resistance to chemotherapy or targeted therapy continues to be the limiting factor that prevents successful treatment of cancer patients at large. In PDAC, it has become increasingly challenging to find improved therapeutic treatments that could overcome acquired resistance to current treatment regimens[90,126]. In borderline resectable, locally advanced unresectable and metastatic PDAC, FOLFIRINOX (fluorouracil, leucovorin, irinotecan, and oxaliplatin) is currently the standard treatment of care for patients with high performance score[90]. While fluorouracil (5-FU). Irinotecan and oxaliplatin have a cytotoxic effect, folinic acid enhances the effects of 5-FU[345]. The combinatorial treatment nab-paclitaxel and gemcitabine (nPG) is usually applied as second-line therapy or is given to patients that are not suitable for FOLFIRINOX[90]. Our lab has previously identified a CYP3A5-dependent drug resistance mechanism upon paclitaxel treatment and also generated drug resistant cell lines that were independent of CYP3A5 expression levels[183]. Thus, we decided to further focus on the nPG treatment regime and aimed to identify additional drug resistant mechanism that could provide a better patient stratification and an improved personalized treatment regimen. We first generated single-drug resistant cell lines which would simplify the identification of the respective drug resistant mechanisms. Paclitaxel induces a cell cycle arrest that results in apoptosis, whereas gemcitabine is a nucleoside analog that gets incorporated into the DNA,

thus activating the cell's base-excision repair system which ultimately leads to cell death[346,347]. Patients treated with nPG, receive the combination of nab-paclitaxel and gemcitabine once a week for three weeks and, which is followed by a one-week recovery time for the patient due to the high toxicity of the treatment[109,348]. To mimic the clinic scenario, we designed a treatment regime that incorporates a single round of treatment that is followed by a recovery phase. This kind of pulsed treatment regimen has become the preferred method to generate drug resistant cell lines[349-351]. A continuous treatment strategy with cells cultured constantly in the presence of drug has been previously tested and failed to generated paclitaxel resistant PACO cell lines (data not shown). Moreover, a continuous treatment strategy is primarily of clinical relevance for orally given drugs like erlotinib or olaparib with an almost constant amount of drug present in the blood circulation[352]. In PDAC, paclitaxel is frequently administered at a dose of 175 mg/m[352] as a single agent with a peak plasma concentration of 10,000 ng/mL (~11.7 µM) which drops to 50 ng/mL (~58 nM) after one day[109]. In order to stay within the clinically relevant window, we set 1 µM as the maximum concentration that would be applied to cells during the long-term treatment regimen.

Today we know that tumors are heterogeneous and our lab and others have previously shown that our PACO cell lines were able to recapitulate the heterogeneous morphology of a patient-derived xenograft after re-injection of cells into the mice[183,328,353,354]. Thus, we assume that our PACO cell lines are also heterogeneous which would affect the clonal selection during long-term treatment[138]. For the long-term treatment regimen, each parental cell line was split into six flasks that were kept separated from each other. The six flasks were treated in parallel and three flask received paclitaxel while the remaining three flasks received the vehicle (DMSO). A parallel selection based on the same parental cell line with the same chemotherapeutic drug and under the same treatment conditions relies on random natural selection and could lead to the development of similar or different drug resistance mechanisms[352,355]. After the last round of treatment, we identified a clear difference in paclitaxel sensitivity between the two groups (paclitaxel-treated and DMSO-treated) in every single PACO cell line. All members of paclitaxel-treated group tolerated 1 µM paclitaxel treatment, whereas none of the members of DMSO-treated group survived the treatment. Hence, we called the paclitaxel-treated group paclitaxel-resistant (PR) and due to acquisition of a paclitaxel-resistant phenotype we handled them as independent cell lines. CellTiter Blue (CTB) assay identified a significant difference in paclitaxel sensitivity between PR and DM cell lines only in PACO22, whereas the sensitivity assay based on long-term treatment regime confirmed initial findings. These conflicting results could be explained by the different treatment regimen between the assay that were applied to

the cells. During pulsed long-term treatment drug tolerant cells were selected based on a treatment and, importantly, a recovery phase and which the CTB assay lacks but which is included in the plaque assay. An additional plaque assay with different paclitaxel concentrations confirmed acquired resistance in PR cell lines of all three PACO cell lines. Once resistance has been successfully established by our long-term treatment regimen in PR cell lines the stability of the resistance has to be determined. If the resistance is not stable enough to be of practical use in the lab, additional treatment rounds with higher concentrations would be necessary[352]. Stable resistance was only maintained in PR cells of PACO22 which might have acquired a more resistant phenotype compared to the other two PACO cell lines.

4.3 Identification of ABCB1 as drug resistance mechanism in paclitaxel-resistant cell lines

The generation of a drug resistant population is facilitated through many selection steps with increasing selection pressure and a loss of clonal heterogeneity[186,356]. We assumed that the bulk gene expression level is the sum of all clonal subpopulations' gene expression values weighted to their respective proportion in the entire cell population. Rising selection pressure increases the proportion of drug resistant clones in the cell population and increases the drug resistant clones' influence on the bulk gene expression levels. Therefore, we acquired samples of crucial timepoints being the parental cell line, the treated cell lines (paclitaxel and DMSO) after a few rounds of treatment and after the last round of treatment. Based on the molecular subtypes, we have selected distinct PACO cell lines that were treated the same way and developed all a drug resistant phenotype. Hence, we were wondering whether the PACO cell lines adapted to the paclitaxel treatment in a similar way or acquired subtype-specific differences[352]? We investigated intertumoral differences in acquired paclitaxel resistance by comparing PR and DM cell lines of all PACO cell lines together for each respective timepoint. By GSEA, we identified common changes that occurred in PR and DM cell lines. Genes related to interferon alpha response and xenobiotic metabolism were enriched in all PR cell lines. Likely, the expression of these gene sets results from the effect of paclitaxel treatment on the cells which resulted in activation of interferon response through DNA damage, the activation of xenobiotic metabolism pregnane X receptor (PXR) and the constitutive androstane receptor (CAR), as well as, a reduction in cell cycle activity through microtubule stabilization and cell cycle arrest[183,314,315,357]. Even though the three PACO cell lines were transcriptionally different and belong to different molecular subtypes, all PR cell lines overexpressed *ABCB1* when acquired

a paclitaxel-resistant phenotype. ABCB1 a membrane-bound glycoprotein that is primarily found in excretory tissue like colon, small intestine, bile ductules, kidney intestine, adrenal gland and pancreatic ductules[207,210]. More than 30 years ago, expression of ABCB1 was found to be increased in various cancer cell lines after several rounds to treatment with different chemotherapeutic drugs and its level of expression was directly associated with drug resistance and poor prognosis in several tumor entities[225-237]. Over 1000 compounds were identified to be extruded by ABCB1 which can be explained by the highly flexible structure of the drug binding sites of ABCB1[238,239]. Our results, identifying ABCB1, thus expand previous observations and suggest a crucial role of ABCB1 in the acquired resistance of pancreatic cancer cells to paclitaxel treatment[325]. Intriguingly, we have chosen three molecular and morphologically distinct cell lines and by the end of the long-term treatment regimen, the selected PACO cell lines all acquired the same resistance mechanism. We found additional mechanism that might support ABCB1-mediated paclitaxel resistance in PACO17 and PACO43[316-320]. In contrast, PACO22 seemed to rely entirely on ABCB1 expression, which was consistently overexpressed at all timepoints, with the highest expression at the point of highest paclitaxel concentration during the long-term treatment regimen.

Based on GSEA, PR cell lines of PACO17 and PACO43 might have acquired additional drug resistance mechanisms to withstand high paclitaxel concentrations. Compared to expression levels of the parental cell line, ABCB1 was only marginally induced in PR cell lines of PACO43, which would indicate that additional drug resistant mechanisms could play a crucial role in acquired paclitaxel resistance. Our lab reported that CYP3A5 is responsible for acquired resistance against paclitaxel in a subset of PACO cell lines, hence, we analyzed gene expression levels in all samples of PR and DM PACO cell lines[183]. In most cases, we found no significance difference in CYP3A5 levels between the respective DM and PR cell lines, with only few exceptions and only a less than 3-fold difference. Western blot analysis showed that CYP3A5 was not detectable in PACO17 and PACO43, indicating that paclitaxel-resistant phenotype is independent of CYP3A5 in these cell lines. In PACO 22 PR cell lines CYP3A5 was increased, however, based on the strong induction of ABCB1 expression, we concluded that expression of CYP3A5 alone did not mediate paclitaxel-resistance in PR cell lines of PACO22.

4.4 Genomic and epigenetic analysis of PACO cell lines

The acquisition of genomic alterations through various mutational processes increases the spatial and temporal diversity of cancer cells, hence, propagating their clonal evolution[192,193]. These processes can range from single nucleotide variants to large catastrophic events like chromothripsis[194,358]. Chromosomal instability (CIN) plays an important role in cancer evolution and is associated with poor clinical outcome and linked to resistance to chemotherapy agents, like taxanes[359-362]. Similar to gene expression patterns, resistance mutations can pre-exist in a small subset of cells which makes them difficult to be detected via bulk sequencing[363]. Recent data suggest that paclitaxel causes cell death due to a multipolar cell division that results in chromosome missegregation[314]. Moreover, it has been suggested that chromosome segregation errors lead to a variety of genomic rearrengments[301]. Hence, we hypothesized that paclitaxel treatment could facilitate chromosomal instability and generation of genomic alterations. The amplification of ABCB1 is common phenomenon in paclitaxel treated cancer cells that results in ABCB1 overexpression and multidrug resistance[190,274]. Paclitaxel presumably binds and stabilizes microtubules thus arresting the cells during mitosis[314]. Indeed, single point mutations in β1-tubulin have previously been identified in cancer patients that caused paclitaxel resistance in cancer cell lines[364]. However, whole exome sequencing (WES) analysis could not detect mutations in β1-tubulin or other genes that could cause or enhance resistance against paclitaxel in our PR cell lines. Copy number variation (CNV) analysis, identified PR replicate-specific genomic alterations in PACO17, with PR2 acquiring amplification of *ABCB1*. In contrast, all PR replicates of PACO22 acquired strong genomic alterations and amplifications around the *ABCB1* locus on chromosome 7. Of note, it has been previously shown that genes surrounding *ABCB1* were also affected by the genomic amplification and were co-overexpressed together with *ABCB1* in paclitaxel treated cancer cells of other tumor entities[275,276]. In PR cell lines of PACO43, we could not detect any significant genomic alteration compared to DM cell lines. Importantly, DMSO long-term treatment did not induce genomic alterations in any DM cell lines or replicates, which highlights the role of paclitaxel in the acquisition of genomic alterations. From these findings we conclude that the genomic amplification of *ABCB1* enhanced its expression in PACO22. However, the lack of such genomic amplification in most PR replicates of PACO17 and PACO43 indicates that the induction of ABCB1 expression is sufficient to generate a paclitaxel-resistant phenotype.

It has been theorized that epigenetic changes can also drive development of drug resistance mechanisms[201,322,323]. Hence, we analyzed the methylation pattern of DM and PR cell lines after

the last round of treatment. Although PR cell lines of all PACO cell lines acquired a different methylation pattern during the long-term treatment regimen, we could not detect significant changes in the methylation of promoters of genes that were upregulated in gene expression microarray. For ABCB1, the only significant difference was a gain in methylation of the promoter region in PR cell lines of PACO17 compared to DM cell lines, which would be linked to a reduced transcriptional activity[365]. While the assessment of epigenetic heterogeneity has been largely focused on DNA methylation, global epigenetic changes in cancer cell epigenomes also include post-translational modifications of histones and chromatin remodeling[201]. Thus, other epigenetic changes might play an important role for the paclitaxel-resistant phenotype.

The conumee package verified findings by WES and identified genomic amplification around the ABCB1 locus in all PR replicates of PACO22 and in a single replicate (PR2) of PACO17[324]. Based on our findings, we concluded that paclitaxel promoted CIN and genomic alterations that enhanced clonal evolution and, in the case of PACO17, resulted in unique genomic amplifications. Although the effect of paclitaxel treatment was more prominent in PACO22, by the end of the long-term treatment regimen, all three replicates carried the same genomic alterations around *ABCB1*. Amplification of *ABCB1* might have caused a selection advantage big enough to prevent outgrowth of different subclones carrying additional genomic alterations[328]. PACO43 was the only cell line that did not acquire genomic alterations during paclitaxel treatment. This might be related to an already existing increased chromosomal stability or that fitness penalty was too high for clones with genomic alterations to outgrow[358].

4.5 ABCB1 drives paclitaxel-resistance in a subset of PACO cell lines

ABCB1 has been reported to be responsible for drug resistance to various compounds, including paclitaxel[325]. PACO22 PR cell lines depicted the strongest drug resistance phenotype. Thus, we chose to use PACO22 PR cell lines to validate ABCB1-dependent paclitaxel resistance. PCA based on gene expression of PACO22 samples identified the clonal drift of DM cell lines away from the parental cell line with increasing culture time which is a common phenomenon and shows the importance of a proper control[352]. All PR cell lines of the early round adapted similarly n to paclitaxel treatment by their global gene expression changes. Since ABCB1 was not detected in parental and DM cell lines, we concluded that early paclitaxel treatment selected for a specific paclitaxel-tolerant subclone that, with increasing paclitaxel treatment, underwent additional genomic and transcriptional changes and evolved into different paclitaxel-resistant subclones in PR replicates[186,328]. Although PR cell lines have been selected based on paclitaxel resistance and DM cell lines based on seeding and proliferation capabilities,

there was no significant difference in proliferation between the two groups. This is of importance since paclitaxel preferentially acts on fast growing cells, which would provide a disadvantage to DM cell lines[314]. Pharmaceutical inhibition or loss of ABCB1 expression by CRISPR/Cas9-mediated knockout completely sensitized PR cell lines to paclitaxel treatment. In addition, pharmaceutical inhibition of ABCB1 in PR cell lines of PACO17 and PACO43 also completely sensitized PR cell lines to paclitaxel treatment (data not shown)[366]. From these findings we concluded that ABCB1 alone mediates paclitaxel resistance in PR cell lines of PACO22 and also in PR cell lines of PACO17 and PACO43.

Moreover, we can confirm that CYP3A5 does not play a role in acquired paclitaxel-resistance in PR cell lines of PACO17, PACO22 and PACO43[183]. It has been proposed that the co-amplified genes surrounding ABCB1 could support the multidrug resistant phenotype (MDR) and may offer novel targets to overcome cancer MDR[190]. In PR cell lines of PACO22, however, the overexpression of these genes does not seem to play a role in ABCB1-mediated paclitaxel resistance, since pharmaceutical inhibition or ABCB1 knockout caused a complete loss of paclitaxel resistance. Since we were interested in the heterogeneity of the cell population and the analysis of distinct clones, we decided against a single cell expansion in PR cell lines and performed ABCB1-KO on the whole cell population which was then maintained as separate culture. Furthermore, we found that ABCB1 expression on the surface gets lost in PR cells over time. Hence, we could not FACS sort for ABCB1- cells in order to enrich for ABCB1-KO cells. In order to increase the proportion of ABCB1-KO sequences, we performed two additional rounds of ABCB1-KO on each of the PR KO replicates. In this way, we acquired more than 90% of sequences with a frameshift mutation and we verified the loss of ABCB1 protein after three rounds of ABCB1-KO by Western blot analysis and loss of paclitaxel resistance by CTB assay.

4.6 ABCB1 mediates resistance exclusively to paclitaxel in PACO22

Today's standard treatment of care for advanced stage pancreatic cancer is the treatment with either FOLFIRINOX or nPG[90]. Upregulation ABCB1 has been reported to induce sensitivity to gemcitabine treatment but pharmacological inhibition of ABCB1 did not alter the intracellular gemcitabine levels in cancer cells[367,368]. In fact, PR cell lines of PACO22 were similarly sensitive to gemcitabine as DM cell lines, hence overexpression of ABCB1 does not enhance sensitivity to gemcitabine but also does ABCB1 not contribute to gemcitabine resistance. Single treatments with the components of FOLFIRINOX indicated that neither 5-FU, the active product of irinotecan SN38 nor oxaliplatin were less toxic to PR cell lines compared to DM cell

lines. Based on that we conclude that ABCB1 is a paclitaxel-specific resistance mechanism that has neither adverse nor beneficial effects on sensitivity to other chemotherapeutic drugs used in current treatment regimens for pancreatic cancer.

4.7 Paclitaxel regulates expression of ABCB1 which mediates paclitaxel resistance

We have generated PR cell lines by a pulsed treatment regimen and these resistant models are often less stable than their continuously treated counterparts[352]. Two out of three PACO cell lines lost resistant phenotype in PR cell lines after five passages of drug holiday, while the PR cell lines of PACO22 lost resistant against paclitaxel treatment after a prolonged drug holiday (10 passages). Single repeat of pulse treatment with paclitaxel re-established drug resistant phenotype and resulted in elevated ABCB1 mRNA and protein levels for all PR replicates, which is a common tool to maintain drug resistance in an unstable population[369-371]. PR2 remained resistant after 10 passages of drug holiday and expressed higher mRNA and protein levels of ABCB1 compared to the other two replicates (PR1 and PR3). Due to the randomness of natural selection, paclitaxel resistance mechanisms could have evolved differently between the three biological replicates, resulting in different versions of the same mechanism[355]. ABCB1 has been reported to be induced by its substrates, including paclitaxel, which would point towards the development of an ABCB1-specific pathway that is activated by paclitaxel treatment[352,372]. According to the Goldie-Coldman hypothesis, the probability that a tumor inherits drug resistant subpopulations depends on the mutation rate and the size of the tumor[187]. Intratumor heterogeneity (ITH) plays a key role in the treatment of cancer and has been directly associated with poor outcome and reduced response to cancer therapy in various cancer entities[328,373,374]. Heterogeneous primary tumors and their respective cell lines are very much likely to inherit subpopulations of cancer cells with pre-existing partial or complete resistance to therapy through gene expression, genetic or epigenetic mechanisms[328,358]. Furthermore, these subpopulations are likely to interact with each other and evolve under external selection pressures[192,375,376]. Gene expression profiling on the single cell level enables direct analysis of transcriptional differences between cells of a population[328]. Single-cell RNA sequencing for two of the three PR and DM replicates of the previously mentioned timepoints, found *ABCB1* to be heterogeneously expressed in PR cell lines, with the highest proportion of ABCB1+ cells after the last round of treatment. UMAP also separated DM and PR cell lines into two different groups which resembles the findings from bulk expression analysis. Bulk analysis of DM cells

revealed that ABCB1 is not expressed in these cell lines, however, single-cell RNA sequencing identified few cells that were ABCB1+. These cells might be paclitaxel tolerant and withstand low drug concentrations and through our long-term treatment regimen, these cells acquired additional genetic/epigenetic changes that result in resistance phenotype by rewiring of gene regulatory networks[328,356,377]. The selection of ABCB1 expressing cells could have been the initial step towards paclitaxel resistant cell line and additional changes that lead to the development of a highly resistant phenotype[378]. Moreover, we identified increased variance in gene expression patterns between PR cell lines after drug holiday in previous analyses which was also confirmed by single-cell RNA sequencing. Although cells of both replicates expressed ABCB1 they acquired distinct changes which became apparent once the selection pressure through paclitaxel treatment had been removed.

4.8 PR cell lines of PACO22 can be distinguished between ABCB1+ and ABCB1- cells

We selected for paclitaxel-resistant clones during the long-term treatment regimen and ABCB1 was the only mediator of paclitaxel resistance in PR cell lines of PACO22. Furthermore, PR cell lines are composed of a heterogeneous population with ABCB1+ and ABCB1- cells and the proportion of ABCB1+ and ABCB1- cells can be regulated with the addition of paclitaxel. Within the ABCB1+ cell population we detected a broad range in ABCB1 expression levels on both mRNA and protein level. Hence, we were wondering whether PR cell lines evolved into a drug resistant population with new subpopulations that could be distinguished by expression of ABCB1. As expected, PR ABCB1- cells were highly sensitive to paclitaxel treatment, however, still more resistant than DM cell lines. Based on ABCB1 protein levels, PR ABCB1- cells were similar to DM cell lines, but as soon as treated with paclitaxel, they quickly started to re-express ABCB1 which was not found in ABCB1- DM cell lines. Based on WES analysis, we assume that all PR cells acquired a genomic *ABCB1* amplification, PR ABCB1- cells might have shut down expression of *ABCB1* through epigenetic mechanisms, like chromatin remodeling[328]. Under acute DMSO treatment, only PR ABCB1- cells remained negative for ABCB1, while PR ABCB1+ cells quickly evolved into a mixed population of ABCB1+/- cells. Our long-term treatment regimen was aiming for a Darwinian selection of highly drug-resistant clones that would generate a new population[379]. However, these findings indicate that PR cells dynamically change their drug resistant phenotype according to external pressures which would argue for a dynamic fluctuation model[379]. PR cell lines' plasticity allows them to reversibly convert

between a paclitaxel-sensitive and paclitaxel-resistant cell identity and adapt to their environment[380]. Thus, the resistance phenotype in PACO22 PR cell lines does not necessarily need to be stable as cells can gradually loose expression of ABCB1 during continuous drug holiday and re-gain expression of ABCB1 protein under paclitaxel treatment. Gene expression analysis confirmed that PR ABCB1- cells became phenotypically highly similar to DM cell lines, independent of treatment option. The only difference was the ability of PR ABCB1- cells to induce expression of ABCB1, which was further enhanced by *ABCB1* amplification. Although PR ABCB1- cells and DM cell lines acquired distinct on the genomic and epigenetic profiles during long-term treatment, they displayed similarities on the transcriptional level. Under acute paclitaxel treatment, both groups expressed the same genes that have been previously linked to cell stress, inflammation, apoptosis and DNA damage repair[329-332]. In contrast to PR ABCB1- cells, *ABCB1* and its neighboring genes were highly upregulated in PR ABCB1+ cells. In line with previous findings, this phenotype clearly depicts the dynamic character of the PR cell lines and the interplay of genetic and epigenetic alterations that enabled the massive upregulation of ABCB1[201,328,379]. Acute paclitaxel treated increased ABCB1 protein levels and the proportion of ABCB1+ cells in PR ABCB1- populations. Although not verified by qRT-PCR, expression of *ABCB1* was significantly overexpressed in PR ABCB1- cells by paclitaxel treatment compared to DMSO treatment, whereas neighboring genes of *ABCB1* remained unchanged. Moreover, expression levels of *ABCB1* were still 30-fold higher in PR ABCB1- cells compared to DM cell lines. However, based on FACS and Western blot analysis, ABCB1 protein expression was almost entirely lost in PR ABCB1- cells. Presumably, the absence of protein would be linked to the absence of mRNA, however, translation can be regulated on single mRNA level, slowing down or even inhibiting the initiation of translation into protein[381,382]. Hence, paclitaxel treatment could have activated the translation of present ABCB1 mRNA into protein which would increase protein levels independent of newly transcribed mRNA. It has been shown that genomic amplification and increased copy numbers of the ABCB1 gene result in ABCB1 overexpression[273,274]. Many studies reported that the co-overexpression of ABCB1-surrounding genes would contribute to a multi-drug resistant phenotype[270,271,275,277-283]. Indeed, PR ABCB1+ cells expressed 3000-fold higher levels of *ABCB1* than DM cell lines and the expression of the surrounding genes (*ABCB4*, *CROT*, *RUNDC3B*, *TP53TG1*) was between 100- and 1000-fold increased. However, genomic alterations and high copy number are insufficient to explain the high levels of ABCB1 and its neighboring genes which would suggest that additional mechanisms like mRNA stabilization and epigenetic modifications contribute to increased expression. We assume that these

mechanisms might play a crucial role in the reduction in the expression of *ABCB1* and its surrounding genes in PR ABCB1- cells.

4.9 Expression of ABCB1 is activated by microtubule targeting agents

The strong upregulation of ABCB1 in response to paclitaxel treatment in PACO22 PR cell lines results from the combination of active transcription and genomic amplification of *ABCB1* that lead to acquired paclitaxel resistance. Based on our findings in the ABCB1+/- sorted populations, translation of ABCB1 appears to be induced by acute paclitaxel treatment, leading to an increased protein levels without a significant increase in mRNA levels. However, we have previously shown that in PR cell lines, which lost resistance after 10 passages of drug holiday, both mRNA and protein were significantly increased after a single round of paclitaxel treatment. Moreover, single-cell RNA sequencing of PR cell lines revealed a significant gain of ABCB1+ cells after acute paclitaxel treatment compared to DMSO treatment. Hence, we investigate the dynamics of the direct induction of ABCB1 expression by paclitaxel in detail. Expression of ABCB1 was significantly increased after 72 h of paclitaxel treatment in paclitaxel-sensitive PR ABCB1- cells. Interestingly, ABCB4, a neighboring gene, was not induced by paclitaxel treatment, which would correlate with the hypothesis that ABCB1 neighboring genes are co-overexpressed in a passive manner by the amplification and epigenetic changes around the *ABCB1* locus[275,276]. We hypothesized that induction of *ABCB1* could not act in the manner of signaling kinase pathways but rather through a sequence of specific waypoints that result in the elevated expression of ABCB1[333]. Based on the mode of action of paclitaxel we assumed that the stabilization of microtubules leads to a cell cycle arrest and taxol-induced cell stress that ultimately results in the observed induction of ABCB1 after 72h of paclitaxel treatment[314,334,335]. When treated with microtubule de-stabilizing alkaloids (vincristine, vinblastine and colchicine), *ABCB1* was significantly induced after 4 days of colchicine treatment which suggests that the mechanism of *ABCB1* induction is not entirely dependent on paclitaxel treatment but rather on the cell to be arrested in the G2M phase to activate downstream pathways. Of note, all three alkaloids are also direct targets of ABCB1 transporter and PR cell lines showed improved survival compared to DM cell lines[337,338]. Of note, we have treated both PR ABCB1+ and ABCB1- cells with the same drug concentration and drug-resistant phenotype of ABCB1+ cells could have prevented microtubule inhibition and the subsequent induction of ABCB1.

4.10 Genomic region around *ABCB1* is transcriptionally active in PACO22 PR lines

Epigenetic alterations that increase the local accessibility of chromatin are indications for transcriptional activity[383]. The combination of the assay for transposase-accessible chromatin using sequencing (ATAC-Seq) with gene expression microarray data offered the possibility to identify alterations in the chromatin state that manifest themselves by changes in the gene expression levels. In order to compare ATAC-seq results with the WES results of the PR cell lines, PR ABCB1- and ABCB1+ cells were grouped together as "combined PR" group and compared with DM cell lines. Although, PR cell lines acquired the ability to induce ABCB1, which was accompanied with phenotypical, genomic and epigenetic changes, both groups remained to be highly similar based on chromatin accessibility. One of the few differentially accessible regions of the chromatin were the genomic region around *ABCB1*. This region turned into an open-chromatin landscape in PR cell lines compared to DM cell lines, which would indicate that the area around *ABCB1* is transcriptionally active. The accessible region surrounding *ABCB1* might have been developed during the long-term treatment regimen or a cell subpopulation that carried this epigenetic alteration had a survival advantage and became the major cell population during paclitaxel treatment[383]. In Melanoma, it has been shown that in a population consists of cells with distinct abilities to acquire drug resistance[349]. Furthermore, the authors presented that drug treatment induced large changes in a number of accessible sites that points towards a large cellular reprogramming[349]. In PACO22, the genes with high ATAC-seq peak fold change were also highly amplified in PR cell lines, which indicates that the combination of genomic amplification and accessible chromatin structure enhanced the transcriptional activation which resulted in a massive upregulation of *ABCB1* and its neighboring genes[190]. Gene expression analysis identified only *ABCB1* to be differentially overexpressed in combined PR cell lines compared to DM cell lines. However, we have also found that gene expression levels of *ABCB1* neighboring genes were at a similar level in PR ABCB1- cells and DM cell lines. Hence, we excluded PR ABCB1- cells from the gene expression analysis and found that differential gene expression levels and peak fold change values well correlated for *ABCB1* and its neighboring genes.

4.11 Expression of ABCB1 is enhanced by amplification of ecDNA

ATAC-Seq analysis identified an area of open chromatin around *ABCB1* which makes the DNA more accessible, thus, facilitating the transcription processes. Intriguingly, the conformational state of the chromatin was independent of the cells ABCB1 protein expression and might have developed during the long-term treatment regimen. The dynamics of chromatin structure are tightly regulated by several mechanisms, like histone modifications or chromatin remodeling[384]. Binding of activators and the recruitment of co-activators results in DNA to be more accessible to general transcription factors, thus initiating gene transcription[384]. Interestingly, the amplification of *ABCB1* and surrounding genes was similar, but gene expression levels differed between the genes in PR cell lines, as well as in PR ABCB1+ cells. Freshly sorted PR ABCB1+ cell populations not only gave rise to ABCB1- cells within few days, but also depicted a broad variety in ABCB1 protein levels. Counting *ABCB1* copies in PR ABCB1+ and ABCB1- cells revealed that the majority of PR ABCB1- cells had only 3 copies of *ABCB1*. In marked contrast, all PR ABCB1+ cells had more than 20 copies. Furthermore, we acquired few cells that were fixed during the mitotic phase with completely condensed chromosomes. Apart from the duplicated gene copies next to the chromosome 7 centromere, which corresponds to the genomic *ABCB1* gene, we identified several ABCB1 copies that were not located on chromosomes. Thus, we concluded that the *ABCB1* copies lie on extrachromosomal DNA (ecDNA), a common phenomenon in cancer cells[286-288]. Patients with oncogene-carrying ecDNA have an increased tumor cell proliferation, increased probability of lymph node spread at diagnosis and have a significantly shorter overall survival compared to patients without oncogene-carrying ecDNA, across many cancer types[288,308]. Interestingly, ecDNA has been recently rediscovered as an important tool for cancers cells to increase intratumoral heterogeneity and to quickly adapt to selective pressures like drug therapy[300]. Chromosome segregation errors might be the source of ecDNA as these errors were shown to drive the formation of simple and complex genomic rearrangements[301]. Paclitaxel treatment could have caused DNA damage which lead to double-strand breaks on chromosome 7 and the resulting DNA segments, of which some contained *ABCB1* and its neighboring genes, could have ligated into circular ecDNA. A recent study proposed that chromothripsis is an essential tool that accelerates genomic DNA rearrangement and the generation of ecDNA which leads to a rapid acquisition of resistance to drug treatment[385]. It is very likely that ecDNA underlies the same replication mechanisms as chromosomes, but, due to the lack of a centromere, is unevenly distributed to daughter cells[296-298]. In fact, uneven segregation of ecDNA rapidly increases intratumoral heterogeneity and provides the source for which tumors

can quickly adapt to external pressures[386]. Furthermore, uneven segregation would explain the detection of cells with high *ABCB1* copy numbers even after 13 passages of drug holiday[296-298]. Although ecDNA is also packed into a chromatin structure by histones, it lacks higher-order compaction and offers enhanced chromatin accessibility[309]. Hence, the ATAC-seq results were greatly affected by ecDNA and the peaks identified around *ABCB1* might mostly originate from ecDNA[309]. On the contrary, ecDNA highlighted the important role of chromatin remodeling for enhanced transcription of drug resistance genes like ABCB1[385]. Still, the paclitaxel resistance is dependent on expression of ABCB1 which is lost under prolonged drug holiday. Single round of paclitaxel treatment followed by recovery time was able to restore the paclitaxel resistance and restored ABCB1 expression. That could indicate that ecDNA follows similar dynamics and gets lost under prolonged drug holiday. Moreover, we investigate how ecDNA is affected by paclitaxel treatment and whether ecDNA is generated *de novo* or further replicated from existing ecDNA[311]. We FACS sorted PR cell lines into ABCB1+ and ABCB1- subsets and treated PR ABCB1- cells with low but rising concentrations of paclitaxel, while PR ABCB1+ cells received the corresponding DMSO treatment for four days followed by recovery time. In both treatment groups, we could not detect increased cell death or colonies of cells with growth advantage (data not shown). PR ABCB1- cells quickly became ABCB1+ and were completely converted by passage 9, while PR ABCB1+ converted slower and were almost entirely ABCB1- after passage13. Based on these findings we assumed that the generation of ecDNA is an active process that is facilitated by paclitaxel treatment and ecDNA replication. On the contrary, for the loss of ecDNA several mechanisms might come into play. The formation of ecDNA-contained micronuclei has been observed before a reduction of ecDNA, however the exact mechanism of micronuclei-based ecDNA elimination is still unclear[387,388]. Due to uneven segregation of ecDNA to daughter cells, it has been calculated that the frequency of cells containing ecDNA continuously reduces under normal conditions[307]. When we sorted PR ABCB1- cell lines, we detected ABCB1- cells carrying a significant amount of ecDNA. Based on the assumption that ecDNA is replicated and uneven segregated to the daughter cells, it is likely that few cells acquire a large number of ecDNA even without positive selection pressure[307,389]. However, we would conclude that the expression of *ABCB1* is dependent on the activation of transcription and that ecDNA-based *ABCB1* amplification does not automatically lead to enhanced expression levels. Presumably, the mechanism that results in the transcription of *ABCB1* is initiated by the inhibition of microtubules and could play a crucial role in the generation of ecDNA-based *ABCB1* amplification.

4.12 Conclusion and outlook

In conclusion, our findings demonstrate that the long-term, pulsed treatment regime is able to generate drug resistant cell lines from previously drug-sensitive cell lines. We identified ABCB1 as mediator of resistance to paclitaxel and other microtubule targeting agents in a subset of PACO cell lines. Furthermore, we found in a paclitaxel resistant PACO cell line that expression of ABCB1 is enhanced by generation of ecDNA carrying *ABCB1*, upon paclitaxel treatment (**Supplementary Figure 13**). Our findings shed light on the importance of personalized treatment and the need for advanced treatment regimens that allow improved treatment of patients carrying ecDNA. Circulating tumor DNA (ctDNA) has been identified as possible liquid biopsy biomarker for several tumor entities and, similarly, ecDNA might be released by tumor cells and could serve as additional detection marker in patient serum[390,391].

Future studies should focus on the analysis of primary tumor and metastases of PDAC patients before and after chemotherapeutic treatment to investigate possible resistance mechanisms and to identify markers that could predict the development of the respective resistance mechanism. Combination of whole-genome sequencing with improved bioinformatic tools could improve the detection of ecDNA and allow patient stratification according to the likeliness of ecDNA formation under chemotherapeutic treatment[392,393]. Recent analysis of a pan-cancer study revealed that more than 14% of all tumor samples carried at least one circular amplicon and patients whose tumor contained ecDNA had a significantly shorter overall survival compared to patients whose tumor was absent of ecDNA[288]. Recent gene expression-based stratifications of PDAC grouped our PDAC cohort into two groups (basal and classical) and could be used to generally describe the phenotype of PDAC[130,131,133]. However, new stratification methods are needed to better understand differences in the genome that favor ecDNA formation and, thus, a quicker response to applied treatment regimen.

It remains unknown how ecDNA is formed. Based on its structural complexity, several processes like chromothripsis and episome formation could result in their generation[394]. Induction of chromosome segregation errors can be sufficient to induce the formation of ecDNA as direct consequence of chromothripsis[301]. Furthermore, the translocation-deletion-amplification model and breakage-fusion-bridge (BFB) cycle have been described as origin of ecDNA[395,396]. Recently, it was shown that cycles of BFB followed by chromothriptic events could drive the generation and evolution of amplified DNA[385]. Although several models have been proposed to explain the generation and proliferation of ecDNA, further research is needed to fully understand the underlying mechanisms, especially the ligation of a linear chromosome

fragment into a circular form. In addition, no direct evidence whether ecDNA could replicate itself has been provided yet.

The formation of ecDNA is linked to DNA damage and subsequent chromosomal rearrangements[301]. Although the events that ultimately lead to the formation of ecDNA become more apparent, the mechanism through which paclitaxel induces the formation of ABCB1-carrying ecDNA is still unknown. A recent study applied methotrexate, an inhibitor for DNA and RNA synthesis, to common cancer cells which induced chromothripsis, genomic rearrangements and amplification of resistance mechanism in ecDNA[385]. Increasing paclitaxel concentration also increased the number of ecDNA found in PR cell lines of PACO22. This could be an active adaption to increased selection pressure[385]. While increased copy number of the resistance gene on ecDNA promotes drug resistance, the elimination of ecDNA amplified genes could induce sensitivity. It has been proposed that reduction of ecDNA was initiated by increased frequency of ecDNA-contained micronuclei[397]. Due to DNA damage and cell cycle arrest, ecDNA could aggregate at S phase and become incorporated into nuclear buds which would be removed from the nucleus in form of micronuclei, and subsequently degraded or extruded from the cell[398,399]. Mathematical modeling of ecDNA dynamics in a tumor cell population calculated that the frequency of cells without ecDNA continuously increases under neutral conditions, which corresponds to drug holiday in our study[307]. Future studies will be needed to better understand dynamics of ecDNA formation, amplification and reduction which enables cancer cells to quickly adapt to environmental changes.

As all findings about ABCB1 were based on three PACO cell lines and the identification of ecDNA only in one of them, additional PACO cell lines should be used and applied to long-term treatment regimen. We aimed to identify new resistance mechanisms and were able to identify ABCB1 as drug resistance mechanism in PDAC. Hence, using additional PACO cell lines could either identify further resistance mechanisms and/or reproduce the ones that were already described by our studies. Currently, our group identified *CYP3A5* and *ABCB1* as primary resistance mechanism against paclitaxel[183]. These findings were based on our 2D-cultured PACO cell line model which is not only lacking the 3D structure of tumor in patients but also the entire microenvironment. We have translated the *in vitro* long-term treatment regimen to the *in vivo* setting, however, we were unable to generate drug resistant cell lines in immunocompromised mice after several rounds of drug treatment (data not shown). Although the PDX model better reflects the patient setting compared to a 2D cell culture model, we were limited in the amount of chemotherapeutics applied to the mice. Hence, we might not have induced a selection pressure strong enough to generate drug resistant clones or to cause a loss

of drug sensitive clones in the tumor cell population. 3D organoid cultures of PACO cell lines with or without co-cultures of cells of the microenvironment could be applied to the long-term treatment regime to provide a more complex in vitro system that would incorporate the advantages of human cell lines and animal models[400-402].

For the treatment of PDAC, the FOLFIRINOX scheme is the primary option, followed by the combinatorial therapy of nab-paclitaxel and gemcitabine for patients who cannot withstand FOLFIRINOX treatment[90]. We could show that ABCB1 mediates resistance solely against paclitaxel which means that for gemcitabine a different resistance mechanism would be developed by the PACO cells. Hence, we have generated gemcitabine resistant cell lines of the same three PACO cell lines used in this study (**Supplementary Figure 14**). Preliminary analyses show that drug resistance mechanisms are not shared between PACO cell lines and that enzymes involved in the gemcitabine metabolisms might be involved in mediating resistance (data not shown). Furthermore, we are currently generating paclitaxel/gemcitabine resistant (PGR) PACO cell lines that would finally answer whether cancer cells develop a single or separate resistance mechanisms (**Supplementary Figure 15A**). Preliminary experiments with PACO17 detected increased protein expression of ABCB1 in PGR cell lines compared to NaCl/DMSO (ND) treated control cell lines (**Supplementary Figure 15B, C**). Further experiments will try to identify the respective resistance mechanisms and whether double-resistant cell lines validate the findings in the single-resistant cell lines.

In this study, we have generated paclitaxel resistant cell lines that acquired the ability to induce the expression of ABCB1 upon paclitaxel treatment, but were also able to downregulate ABCB1 during drug holiday. Cancer cells can become addicted to therapeutic drugs to which they have acquired resistance[403], however, for PR cell lines of the described PACO cell lines the reversible induction of ABCB1 seems to counter this phenomenon. To date, a long list of molecules, including paclitaxel, has been described to induced expression of *ABCB1* in many different cancer cell lines[190,224]. Besides tissue specific expression of ABCB1 in non-cancerous cells, stress-dependent induction of ABCB1 has been intensively investigated[256]. Due to the number of structurally different inducers of ABCB1, various pathways seem to be able to regulate *ABCB1* transcription to react to external stimuli, among them being heat shock elements, inflammation response, hypoxia, cell and DNA damage response and nuclear receptors[224,256]. Several promoter elements have been found at the *ABCB1* gene, including, activator protein 1 (*AP-1*), steroid xenobiotic receptor (*SXR*) element, specificity protein 1 (*SP1*), Y-box binding protein 1 (*YBX1*), early growth response protein 1 (*EGR-1*) and CCAAT/enhancer-binding protein beta (*C/EBPβ*)[190,224]. Preliminary experiments with

CRISPR/Cas9-mediated KO of these candidates in PR ABCB1- cell lines of PACO22 did not significantly reduce induction of *ABCB1* under acute paclitaxel treatment suggesting a complex induction mechanism that might involve a group of different transcription factors (Data not shown). Our data showed that significant expression of *ABCB1* takes up to 72 h which would hint towards a combination of stress-induced pathways that ultimately lead to the induction of *ABCB1*. Thus, several different transcription factors might be involved, forming an "*ABCB1* enhancesome", a region of the *ABCB1* promoter the various stimuli converge on[256]. Hence, experiments addressing the paclitaxel-based induction of *ABCB1* in PR PACO cell lines might help to understand the different mechanisms taking place inside the cell which could offer novel therapeutic targets to finally prevent induction of *ABCB1* in treated cancer patients.

Lastly, genomic and transcriptomic studies revealed that PDAC is highly heterogeneous[65,130,131,133]. Besides intertumoral heterogeneity, PDAC is featured with a high clonal diversity within a single tumor (intratumor heterogeneity)[313,404]. The sources of intratumor heterogeneity in a tumor lie within genetic, epigenetic and environmental inputs[328]. Genetic heterogeneity is vastly linked with chromosomal instability (CIN), which leads to an increased rate of genomic errors, including rearrangements, loss and gain of large fragments and such large-scale genomic events are more likely to infer with cellular phenotype[328]. Although most of the these changes might have negative effects, CIN increases genomic diversification, thus enhancing clonal evolution during tumor development and treatment exposure[405]. The amplification of oncogenes on ecDNA has been shown to rapidly increase intertumoral heterogeneity through uneven segregation, while avoiding fitness penalties that would be associated with large genomic changes on the chromosomes[288,300,309,311]. Thus, it is important to investigate the role of ecDNA on clonal competition, its dynamics during selective pressure and how ecDNA formation is related to global genomic events like whole-genome doubling or aneuploidy[328,389,394]. Specific monitoring of ecDNA formation and loss in our PACO cell line model could improve our understanding of ecDNA dynamics with and without selective pressure. For that, we have already generated a reporter cell line of PR PACO22 with a fluorescent signal that directly correlates with the number of *ABCB1* amplicons inside the cell (data not shown). Moreover, we could make use of our collection of unique cell lines to identify common attributes that facilitate ecDNA formation. Understanding the clonal evolution, identifying the cause of ecDNA formation and forecasting the genetic and transcriptional changes could improve the selection of new treatment options or combinations. Multi-omics analysis on the single cell level could greatly improve our understanding of the complexity of

the tumor and answer key questions about tumor evolution and the acquisition of drug resistance mechanisms.

5 Material and Methods

5.1 Human tissue specimens

The collection of tissue specimens has been already described elsewhere[183]. In detail, tissue samples were obtained from patients admitted to the Department of General, Visceral and Transplantation Surgery at the University Hospital Heidelberg by Prof. Dr. Markus W. Büchler. The study was approved by the ethical committee of the University of Heidelberg (case number 301/2001) and conducted in accordance with the Helsinki Declaration; written informed consent was obtained from all patients. Patient and tumor characteristics are summarized in (**Table 1**).

5.2 Establishment of new PACO cell lines

The generation of PACO cell lines was conducted according to the protocol published by Noll and Eisen et al[183]. In detail, single cells in Matrigel (2 mg/ml, BD) were injected orthotopically into the pancreas of NSG mice. The tumors engraftment and growth were regularly monitored by palpation of the injection site. After surgically removal, orthotopically grown tumors pieces were first minced by sterile scalpels and dissociated into single cells using Miltenyi dissociation kit and a gentleMACS-Octo. The resulting cell suspension was filtered through a series of 100 µM, 70 µM and 50 µM mesh (BD), followed by centrifugation. In order to remove erythrocytes, the cell pellet was resuspended in 5 ml ACK Lysis Buffer (Lonza) and re-centrifuged. Depending on the cell pellet, a sufficient number of cells was chosen to be seeded in a T25 flask (Primaria, BD) together with serum-free Pancreas TumorMACS™ medium (Miltenyi), which has been described before[183]. For the initial establishment, PACO media was supplemented with 10 µM Y-27632 (Sigma) and Pen/strep. Derived PACO cell lines were cultured as monolayers at 37 °C and 5 % CO2. During tumor cell growth, contaminating mouse fibroblasts were removed by short trypsination with Accutase (Thermo Scientific). Once the PACO cell line has been successfully established in vitro, cells were subsequently cultured in Pancreas TumorMACS™ medium without antibiotics and Y-27632.

In order to passage the PACO cell lines in T25 flasks, Pancreas TumorMACS™ medium was removed and cells were first washed with 4 ml CO2-independent medium (Thermo Scientific), supplemented with 1 % BSA and 2 mM glutamine. After removal of CO2-independent medium, 2 ml Accutase was added to the T25 flask and incubated at 37 °C and 5 % CO2 until cells completely detached from the flask. Once the cells were in suspension, T25 flask was washed

with 8 ml CO2-independent medium and cells were collected in a total volume of 10 ml for centrifugation (300 g, 5 min, RT). Cell pellet was resuspended in 1 ml CO2-independent medium and split in a 1:10 ratio for ongoing culturing. For cell counting, the Neubauer chamber (BRAND) or Cytosmart Exact were used.

For cryopreservation, PACO cell lines were detached and collected from flask as described above and resuspended in 1 ml Cryostor CS10 (Sigma) per cryovials used. Cryovials were transferred to pre-cooled isopropanol chambers and stored at -80 °C overnight. On the next day, cryovials were moved to liquid nitrogen tanks for stable long-term storage.

In order to retrieve stored cell lines, frozen cryovials were put in 37 °C water bath until cell suspension is thawed. Cells were added to 9 ml CO2-independent medium containing 10 µM Y-27632 (Sigma) and centrifuged (300 g, 5 min, RT). The cell pellet was resuspended in an appropriate amount of Pancreas TumorMACS™ medium and cells were seeded in flasks for cultivation.

For authentication and mycoplasma contamination, all cell lines were repeatedly tested and analyzed by single-nucleotide polymorphism (Multiplexion).

5.3 Generation of drug-resistant PACO cell lines

For *in vitro* long-term drug treatment, paclitaxel (Selleckchem) was dissolved in water-free DMSO (Sigma) according to manufacturer's instructions and a 100 mM stock was created and stored at -20 °C. Gemcitabine (Selleckchem) was dissolved in 0.9 % NaCl solution according to the manufacturer's instructions and a 100 mM stock was created and stored at RT. To avoid loss of drugs' therapeutic activity, dissolved compounds were stored for a maximum of 2 two months, before replaced with a fresh vial. Cell lines were split in six separate flasks, of which three were treated with the drug and three were treated with the corresponding vehicle control. For double treatment, cell lines were simultaneously treated with both drugs or both vehicle controls. Each cell line was treated separately with increasing concentrations according to the development of drug tolerance. Biological triplicates of each cell line were treated at the same time with the same drug concentrations.

Cells were exposed to step-wise increased concentrations of the drug or vehicle in a pulsed treatment regimen until the final concentration of 1 µM was reached. In detail, for each round of treatment, Pancreas TumorMACS™ medium was supplemented with either drug(s) or vehicle(s) and was applied to the cells two times for 48 h. After 96 h, medium was removed and replaced with fresh drug-free medium to have cells recover from the treatment. At a

confluency of 90 %, cells were passaged, a back-up was frozen down and cells were seeded for RNA/DNA and the next round of treatment. In total, up to 9 rounds of treatment were necessary until cells were able to withstand a round of 1 µM drug treatment.

5.4 Gene expression analysis

Total RNA was isolated from PACO cell lines at 80 % confluency using the miRNeasy kit (Qiagen) according the manufacturer's instructions. For gene expression microarray submissions, RNA extraction was combined with DNAse treatment of the sample to remove residual DNA. RNA concentration and quality were determined by Nanodrop or Qubit 3.0 fluorometer (Thermo Scientific) according to the manufacturer's instructions. Gene expression analysis was performed using the Affymetrix GeneChip® Human Genome U133 Plus 2.0 Array (Affymetrix) at the Genomics and Proteomics Core Facility of the DKFZ. Expression data was further analyzed using R (3.5.1) and Bioconductor[406,407]. Raw data were processed by a combination of the affy[408] (v.1.60.0), affyQCReport (v.1.60.0), affyPLM (v.1.58.0) and simpleaffy (v.2.58.0) and probes were annotated with the affymetrix Human Genome U133 Plus 2.0 Array annotation dataset (hgu133plus2.db- R package (v.3.2.3). The quality of the normalized arrays was determined using the arrayQualityMetrics package[409] (v3.44.0). Outliers were determined by three different detection methods being Distances between arrays, boxplots (Kolmogorov-Smirnov statistic K_a between each array's distribution and the distribution of the pooled data) and MA plots (Hoeffing's *D*-statistic). If one sample was classified as outlier in at least two metrics, it was removed from the analysis. Using genefilter (v.1.68.0), probes with little variation across samples (within 0.5 quantile of the interquartile range (IQR)) and missing annotation can be disadvantageous for the subsequent data analysis and were removed[410]. Additionally, duplicate removal according to the highest-IQR probe for each gene was conducted. Final probe set was plotted using ggplot2 (v.3.2.1) and pheatmap (v.1.0.12).

In order to reduce the multidimensional gene expression profiles, principal component analysis (PCA) was first conducted on the top 500 variant genes[411,412]. Only samples of interest for the respective analysis were included which maximizes the explanation of variance between the samples. In addition, we performed sparse PCA on our data set using the PMA package[413,414].

Differential gene expression analysis was conducted through following the limma pipeline[415,416]. According to the empirical Bayes method, we first applied an unpaired t-test (two-tailed) to determine statistical significance ($P < 0.05$) and performed Benjamini-Hochberg correction to identify differentially expressed genes with an adjusted p. value < 0.05.

Gene set enrichment analysis (GSEA) was performed on quantile-normalized data provided by the GPCF. GSEA Java Desktop Application (v. 4.0, Broad Institute) was used to identify differentially enriched gene sets provided by Molecular Signature Database (MSigDB, release v. 7.0, Broad Institute). 10^3 permutations based on the gene set were performed to compute the statistical significance of the enrichment score per gene set. Each probe set in the expression dataset was collapsed into a single vector for each gene.

5.5 Quantitative real-time PCR

Total RNA was extracted using the miRNeasy kit (Qiagen) and reverse-transcribed using the high capacity cDNA reverse-transcription kit (Applied Biosystems) according to the manufacturers' protocols. For each gene of interest, 60 ng of reverse transcribed RNA was distributed as cDNA in triplicates and analyzed by quantitative real-time polymerase chain reaction (qRT-PCR). TaqMan™ Fast Advanced Master Mix and TaqMan probes (**Table 4**, 6-carbofluorescein (FAM) labeled, Thermo Scientific) were used acquire expression data with VIIA7 Real-Time PCR or QuantStudio 5 Real-Time PCR Systems (Thermo Scientific). The acquired Ct values were normalized using the ΔΔCt method. In detail, the Ct value of each gene target is normalized to the geometric mean of three housekeeping genes (POLR2A, PPIA and TBP), which corrects for different amounts of cDNA loaded per sample. In order to obtain the relative quantification of each gene target, ΔCt values were normalized the respective ΔCt value of a control sample. The QuantStudioTM Design and Analysis Software (v. 1.4.3) was used for data acquisition and Microsoft Excel for data analysis and GraphPad Prism (v. 8.0.2) software for data visualization and statistical analysis. For ABCB1, adrenal gland was used as positive control (Origene, CR561238).

Table 4: TaqMan probes used for qRT-PCR

TaqMan Probe	Assay ID
ABCB1	Hs00184500_m1
ABCB4	Hs00983957_m1
CROT	Hs00221733_m1
CYP3A5	Hs00241417_m1
IFITM1	Hs00705137_s1
PPIA	Hs99999904_m1
POLR2A	Hs00172187_m1
RUNDC3B	Hs00916137_m1
TBP	Hs00427620_m1
TP53TG1	Hs01567095_g1

5.6 Western Blot analysis

Lysis buffer for PACO cells was prepared using 1X RIPA buffer (Cell Signaling Technology), 10 µM AEBSF (Sigma Aldrich), 5 µM EDTA and 1X Halt Protease-Phosphatase Inhibitor Cocktail (Thermo Scientific). Before cell lysis, cells were washed thrice with ice-cold PBS and incubated in 100 µl lysis buffer for 10 min on ice, corresponding to the area of a single 6-well. Next, cells were scraped and cell suspension was transferred into pre-colled eppendorf tubes and incubated for additional 15 min on ice. In order to remove remaining debris, homogenate was centrifuged at 15.000 g for 15 min at 4°C. The supernatant was transferred into a new Eppendorf tube and either used for immediate protein quantification or stored at -20°C until further processing. Protein quantification was determined using the BCA Protein Assay Reagent kit (Thermo Scientific) according to the manufacturer's protocol.

For protein denaturation, 100 µg of protein lysate were mixed with 4X NuPage LDS sample buffer and 10X Reducing Agent (Thermo Scientific) to a final volume of 100 µl and heated to 70°C for 10 min. For each sample, 15 µl of reduced protein lysate was loaded on 4-15% or 4–20% CriterionTM TGXTM Precast gels (BioRad) with Tris-Glycine-SDS Buffer (TGS) 1x running buffer (BioRad) at 120V for 2h and blotted on PVDF membranes (Trans-Blot® TurboTM Transfer Packs, BioRad). Membranes were blocked for 2h at RT or o/n at 4°C in 1X

Tris-buffered saline (TBS) (10x TBS: 48.4 g TRIS-base, 160 g NaCl, 2 l H_2O, pH 7.5 (Sigma)) supplemented with 0.1% (v/v) Tween-20 (Sigma-Aldrich) and 5% (w/v) BSA (Gibco) or with 5% non-fat dry milk-powder (blocking solution, Sigma). Primary antibodies were incubated o/n at 4°C in blocking solution. After repeated washing in 1X TBS-T (1X TBS and 0.1% Tween-20), membrane was incubated with secondary HRP-coupled antibody (Cell Signaling), diluted 1:10.000 in blocking solution, for 1 hour at RT. Membrane was washed again in 1X TBS-T and immunocomplexes were detected using the ClarityTM Western ECL Substrate kit (BioRad) in a ChemiDocTM imaging system (BioRad). For ABCB1, adrenal gland was used as positive control (NOVUS Biologicals, NB820-59171).

Table 5: Antibodies used for Western Blot

Antigen	Manufacturer (Cat. No.)	Dilution
ABCB1	Cell Signaling (13978S)	1:1000
CYP3A5	Abcam (EPR4396)	1:1000
GAPDH	Cell Signaling (2118S)	1:10,000
Vinculin	Cell Signaling (4650S)	1:10,000

5.7 Flow Cytometry

For flow cytometric analysis, cells were detached from the flask as described before. After cells were collected and spun down, they were resuspended in 1 ml FACS buffer (PBS, 0.5% BSA (Gibco) and 2 mM EDTA (Gibco)) and the cell number was determined. Cells were re-centrifuged at 300 g for 3 min and supernatant was aspirated completely. Up 10^7 cells were resuspended in 100 µl FACS buffer and labeled with fluorophore-coupled antibodies (ABCB1, 1:100, Miltenyi), including isotype-matched controls, for 10 min in the dark at 4°C. After labeling, cells were diluted in 3 ml FACS buffer and centrifuged at 300g for 3 min. Supernatant was aspirated and cells were resuspended in FACS buffer supplemented with 0.1 µg/ml DAPI for live/dead discrimination. Analyses were performed at LSR II or Fortessa flow cytometer (BD Biosciences). Data analysis was conducted with FlowJo Software (Tree Star, Ahsland, OR) and GraphPad Prism software.

For fluorescence activated cell sorting (FACS), cells were processed as described above. Cells were labeled with an ABCB1 PE- or APC-conjugated antibody (Miltenyi, 1:100) for 10 min in

the dark at 4°C. Next, cells were diluted in FACS buffer, centrifuged, resuspended in FACS buffer supplemented with DAPI and filtered. All FACS sorting experiments according to ABCB1 expression were performed using a BD FACS Aria I, II or III flow cytometer (BD) at the Imaging and Cytometry DKFZ Core Facility.

Cell cycle activity was measured using the Click-iT™ Plus EdU Flow Cytometry Assay Kit (Thermo Fisher) according to the manufacturers' protocol. Briefly, cells were seeded in an appropriate number in 6-wells. The next day, cells were either treated with 50 nM paclitaxel or DMSO for 2-times 48 h. Afterwards, drug-supplemented medium was replaced with medium supplemented with 10 µM EdU and incubated for 1 h. Afterwards, cells were harvested as described before, washed with 1% BSA-containing PBS and fixed with Click-iT™ fixative for 15 min. After washing the cells with 1% BSA-containing PBS, cells were resuspended in 1X Click-iT™ permeabilization and wash reagent and incubated for 15 min. In order to detect Click-iT™ EdU, the Click-iT™ Plus reaction cocktail (PBS, copper protectant, fluorescent dye picozyl azide, reaction buffer additive) was added to the cells in incubated for 30 min in the dark. Cells were washed with 1X Click-iT™ permeabilization and wash reagent and stained with DAPI (1:1000, Thermo Fisher) before analyzing them at the LSR II or Fortessa flow cytometer (BD Biosciences). DNA content was detected with linear amplification.

5.8 Hematoxylin and Eosin (H&E) and Immunohistochemistry

Hematoxylin and Eosin (H&E) and immunohistochemistry (ICH) staining analyses were performed by Vanessa Vogel, Ornella Kossi (HI-STEM) and subsequent analysis was supported by Prof. Dr. Albrecht Stenzinger in the Department of Pathology of the University Clinic Heidelberg. The evaluation of the marker expression (CYP3A5, HNF1A, KRT81) in patient and xenograft material has been previously described elsewhere[183,206].

Tumor specimens were fixed in 10% formalin (Sigma) for 48 h, dehydrated with increasing concentrations of ethanol (Sigma), followed by xylene (Sigma) and embedded in paraffin. Before staining, slides were deparaffinized with xylol and ethanol, followed by heat-induced epitope retrieval using damp heat in a steam pot with citrate buffer at pH 6.0 (Dako S2369 1:10).

H&E staining was done using an automatic tissue stainer. Briefly, slides were incubated in hematoxylin according to Mayer (Sigma), rinsed in H2O and stained with Eosine Y (Sigma). Staining was fixed with acetic acid and increasing concentrations of ethanol. Next, slides were covered with a xylene-based mounting medium (ThermoFisher) and a cover slip.

Afterwards, slides were rinsed in H2O and PBS-Tween buffer (MiliporeMerck OmniPur 10xPBS 6505-4l, 1l + 5 ml Tween, 1:10). Primary antibody for ABCB1 () was diluted with Dako antibody diluent 1:100 and incubated for 30 min in a moist chamber at room temperature. Next, slides were rinsed three times in PBS Tween buffer, followed by addition of Peroxidase blocking solution (S2023, Dako) for 5 min at room temperature. Afterwards, EnVision+ Dual Link System-HRP (K4061, Dako) was added to the slides and incubated for 30 min at room temperature, followed by three times washing with PBS-Tween. Finally, Liquid DAB+ Substrate Chromogen System (K3468, Dako) was used to visualize the antibody staining. 100-200 µl DAB (Dako Kit S, 1ml buffer+ 20µl of chromogen) was incubated on the slides until signal can be detected. Slides were covered with aqueous based mounting medium (Sigma) and a cover slip.

Cell lines were detached from the flask as described above. Cell suspension was centrifuged and resuspended in 400 µl pre-heated histogel (70°C, Thermo Fisher) and cooled down in a histogel mold. Once the histogel solidified, the block was removed from the mold and fixed in 10% formalin (Sigma) for 48h and embedded in paraffin. Immunohistochemistry staining was performed as described above.

5.9 Immunofluorescence and FISH

For fluorescent in situ hybridization (FISH), paraffin-embedded cells were cut on slides, deparaffinized and air-dried. Next, slides were re-hydrated and proteins were digested in a pepsin solution (0.005%) for 20 min. After incubation with 2X SSC buffer (Zytovision) for 5 min, slides were washed with H2O and air-dried. DNA-binding probe for ABCB1 and centromere of chromosome 7 (5-10 µL, Empire Genomics) were added to the slides and the added coverslide was sealed with fixogum. Using a ThermoBrite, the slides were denatured at 75°C for 10 min and incubated in humidified chamber over night at 37°C. On the next day, fixogum was removed and slides were washed in H2O and covered with DAPI-ProlongGold Antifade (Thermo Fisher). Images of the nuclei were acquired using the Zeiss Cell Observer. Evaluation of staining and image post-processing was performed using ImageJ software.

5.10 Cell viability assays

For CellTiter-BlueTM (CTB) assay, 8000 cells/well for PACO17 and PACO43 and 5000 cells/well for PACO22 were seeded in 96-well plates (Primaria, BD). After 24 h, individual compounds, starting at 100 µM, were screened in quadruplicates in a 1:4 serial dilution. For co-treatment experiments, Pancreas TumorMACS™ medium was supplemented with ABCB1

inhibitor 100nM Elacridar (GF120918, Selleckchem)[417]. After 72 h, cell viability was assessed by addition of 25 µl CellTiter-Blue reagent (Promega) per well and incubation for 3 h. Metabolic activity was measured by fluorescence intensity (555/585 nm) in a SpectraMax iD3 microplate reader (Molecular Devices). Treatment with 10 µM staurosporine (STS, Selleckchem) was used as positive control and to determine fluorescent background. Each drug concentration was screened in quadruplicates and relative cell viability was calculated by normalization to corresponding vehicle control. Relative cell viability values were plotted using GraphPad Prism software.

For crystal violet (CV) assay, 96-well plates from CTB assay were further used for cell confluency measurements. After CTB measurement, plates were washed with PBS (Sigma) and fixed for at least 24 h in 10% Formalin (Sigma). After fixation, plates were washed with H2O and cells were stained for 30 min with CV (100 µl/well, Sigma). Upon dye removal, plates were washed with H2O, dried and CV was dissolved with 10 % Acetic acid (100 µl/well Roth). CV absorbance was measured at 600 nm in a SpectraMax iD3 microplate reader (Molecular Devices). The data were normalized as described for the CTB assay (see above). Relative cell confluency curves were plotted using GraphPad Prism software.

For plaque assay, $2x10^4$ cells/well were seeded in a 24-well plate. After 24 h, cells were treated with compounds at varying concentrations, including DMSO/NaCl control treatment, for 96 h with refreshed treatment after 48 h. Next, drug treatment was removed and media was replaced to enable cells to recover for 96 h under drug-free conditions. After 8 d, cells were washed with PBS and fixed in 10% Formalin for at least 24 h and subsequently stained with 500 µl CV per well as described above. After CV was dry, plates were imaged using a ChemiDoc imaging system (BioRad).

5.11 ABCB1 induction assay

For each cell line $2x10^4$ cells/well were seeded in duplicates per condition in 24-well plates. Next day, cells were treated either with 100 nM paclitaxel or DMSO for the 96 h timepoint., In order to collect all conditions at the same point, shorter treatment periods were started on the respective days (date of collection minus treatment duration [d]). For RNA collection, duplicates were pooled together and extraction was performed according to the manufacturers' protocol (miRNeasy Kit, Quiagen). Gene expression was analyzed as described before.

5.12 CRISPR-Cas9 mediated knockout

PACO cells were detached from the flask as previously described. For a single reaction, 10^5 cells were used. For stable knockout, crRNA for ABCB1 was designed and, together with necessary reagents, was ordered from IDT and electroporation with NEON (Thermo Scientific) was used according the manufacturer's protocol. In detail, gene specific Alt-R CRISPR-Cas9 crRNA (200 µM, IDT) and universal Alt-R CRISPR-Cas9 tracrRNA (200µM, IDT) were mixed in equimolar concentrations and heated for 95°C for 5 min. In order to have both oligos annealed as gRNA, the mix was allowed to cool down at room temperature (15-25°C). For each reaction, Alt-R Cas9 enzyme (62 µM, IDT) was diluted to 36 µM and 0.5 µl of diluted Cas9 was added to 0.5 µl Alt-R guide RNA and incubated for more than 10 min at room temperature. For each electroporation reaction, cells were resuspended in 9 µl resuspension buffer (Thermo Scientific). Before electroporation, 1 µl RNP complex and 2 µl Alt-R Cas9 Electroporation Enhancer (10.8 µM, IDT) were added to the cells. Supplemented cell suspension was acquired by Neon Pipette (Thermo Scientific) and inserted into pipette station. Electroporation was performed with 1600 V for 10 ms and 4 pulses. Next, cells were transferred to 24-well plate with pre-warmed Pancreas TumorMACS™ media and culture in a tissue culture incubator for 48 h. Validation of knockdown was performed by FACS (surface protein) and sanger sequencing (EurofinsGenomics) of target region.

Table 6: Guide RNA for CRISPR-Cas9 mediated ABCB1 knockout

Gene	Exon	Position	Strand	Sequence	PAM
ABCB1	3	87600161	-	GATCTTGAAGGGGACCGCAA	TGG

5.13 Sanger Sequencing

Genomic DNA was extracted PACO cell lines using DNAeasy Blood and Tissue Kit (Qiagen) according to the manufacturer's instructions. DNA quality and quantity were determined using the NanoDrop (Thermo Scientific). In order to determine the knockout efficiency, the region surrounding the knockout was amplified by PCR using Q5 hot start high-fidelity master mix (New England Biolabs Inc.) according to the manufacturer's instructions. PCR and Sanger Sequencing Primer were summarized in **Table 7**. PCR products were purified by PCR Purification Kit (Qiagen) according to the manufacturer's instructions. Sanger sequencing was performed at EurofinsGenomics, analyzed by SnapGene (GraphPad Software) and knockout

efficiency was determined using TIDE webtool, comparing DNA sequences of wild-type and knockout samples[327].

Table 7: PCR and Sanger Sequencing primer list

Gene Target	Task	Direction	Sequence (5' -> 3')
ABCB1	PCR	Fwd	GCTTCTTGAGGCGTGGATA
	PCR	Rev	GCGACCAACACCACTTGAAA
	Sanger Sequencing	Fwd	CTTCGTGGAGATGCTGGAGA
	Sanger Sequencing	Rev	ATTCCAAAGGCTAGCTTGCG

5.14 ATAC sequencing

Cells were harvested as described before and washed two times with ice-cold PBS (Sigma). Next, cells were centrifuged at 600 g for 3 min at 4 °C and $5x10^4$ cells were collected per sample. Cells were resuspended in transposase reaction mix (Per sample: 12.5 µL 2x TD buffer, 2.5 µL Tn5 transposase (Illumina) and 10 µL nuclease-free H2O (Invitrogen)) and incubated for 30 min at 37 °C with mild agitation. Afterwards, reaction was stopped by addition of 4 µl of 50 nM EDTA and samples were placed on ice for 5 min. DNA fragments were amplified by PCR, using 1X NEBnext PCR master mix and Nextera PCR primers (Illumina) for multiplexing. Libraries were purified using AMPure XP beads (Beckman Coulter) at a 1:1.4 library:beads ratio following the manufacturer's instructions. Library quality and concentration was assessed on an Agilent 2100 Bioanalyzer (Agilent Technologies) and a Qubit 3.0 Fluorometer (Thermo Fisher Scientific). Pooled libraries were sequenced with a NextSeq 550 PE 75 HO at the Genomics and Proteomics Core Facility of the German Cancer Research Center (GPCF DKFZ, Heidelberg). Alignment of sequenced fragments to the reference genome was performed in house using Bowtie[418], the adapters were trimmed using Trim Galore (Babraham Bioinformatics) and the peaks called with MACS2[419]. Data was processed using the Diffbind[420] and chipseeker[421] package and was plotted using ggplot2 package in R.

5.15 Whole Exome Sequencing (WES) and Whole Genome Sequencing (WGS)

Genomic DNA was extracted from PACO cells using DNeasy Blood and Tissue Kit (Qiagen) according to manufacturer's instructions. DNA quality and concentration were determined by

Qubit 3.0 Fluorometer (Thermo Scientific). Whole Exome Sequencing (WES) was performed at the Genomics and Proteomics Core Facility of the German Cancer Research Center (GPCF DKFZ). In brief, appropriate amount of genomic DNA was submitted to the GPCF and libraries were prepared using the Agilent Low Input Exom-Seq Human v6 protocol and sequenced with an HiSeq 4000 PE 100. Alignment of sequences to the reference genome was performed by the Omics IT and Data Management - Core Facility (ODCF) using bwa mem aligner[422]. CNV, single nucleotide variants (SNV) and indels were computed with the help of Gregor Warsow and the cnv kit workflow which was based on ACEseq for CNV calling[423]. However, ACEseq and cnvkit workflow have problems with very pure samples (like cell lines), hence, some samples failed to be analyzed for total copy number count and were not listed in our analysis. Circular visualization of CNV data was conducted using the circlize package[424].

Whole Genome Sequencing (WGS) followed the same procedure as described for WES. Genomic DNA was submitted to GPCF, libraries were prepared using the DNA Seq Nano (Illumina) and sequenced on the HiSeq X PE 150. Alignment of sequences to the reference genome was performed by the Omics IT and Data Management - Core Facility (ODCF) using bwa mem aligner[422]. The analysis of CNV, SNV, indels and structural variants (SV) was performed by ODCF using the ACEseq pipeline[423].

5.16 DNA Methylation analysis

Genomic DNA was extracted from PACO cells using DNeasy Blood and Tissue Kit (Qiagen) according to manufacturer's instructions. DNA quality and concentration were determined by Qubit 3.0 Fluorometer (Thermo Scientific). Genomic DNA Methylation analysis was performed using Infinium MethylationEPIC BeadChips at the Genomics and Proteomics Core Facility of the German Cancer Research Center (GPCF DKFZ). Data was processed with the RnBeads R package[425] and all calculations were conducted in R. For copy-number variation (CNV) analysis of the Infinium MethylationEPIC BeadChip data was analyzed by the minfi[426] and conumee package[324]. For the CNV analysis of each single PR cell line, all three respective DM cell lines were combined together as control.

5.17 Single-Cell RNA Sequencing

Single-cell RNA sequencing was performed using the Chromium™ Single Cell 3' v2 protocol (10X Genomics, CG00052) that produced single cell 3' libraries ready for Illumina sequencing. Briefly, frozen back-up stocks of the timepoints described previously (parental, early round, last round, passage 5) were thawed and seeded in T25 as described before. Once cells fully

recovered and were proliferating, cells were collected, centrifuged and washed with PBS. After counting of viable cells using the Countess™ (Thermo Fisher) a cell concentration of 1000 cells/µL was adjusted and in order to encapsulate ~10,000 cells per sample, 17,400 cells were loaded which was according to manufacturers' suggestion. After successful encapsulation, single cells were lysed and mRNA was transcribed into cDNA inside the Gel Bead-In-EMulsions (GEMs). Next, cDNA was recovered and cleaned using Dynabeads™ MyOne™ Silane (Thermo Fisher) and amplified relative to number of cells loaded. After a clean-up cDNA quality was determined using the Agilent 2100 Bioanalyzer (Agilent Technologies) and library preparation followed with A-tailing incubation and adaptor ligation preparation. Finally, samples were index by i7 primer PCR and a double-sided library size selection was performed. For sequencing, libraries were submitted to the GPCF and sequenced on the NextSeq 550 PE 75 Mid-Output (Illumina) with a single lane per library and a read length of 26/98, specifically for 10X genomics libraries. Sequenced libraries were aligned using the CellRanger pipeline (10X Genomics). For subsequent analysis, Loupe Browser software (10X Genomics) and the R package Seurat[427,428] were used. Differential gene expression analysis and heatmap presentation were performed by Abdelrahman Mahmoud (DKFZ).

5.18 Graphics Software

Adobe Illustrator and BioRender were used to design figures.

Supplementary Figures

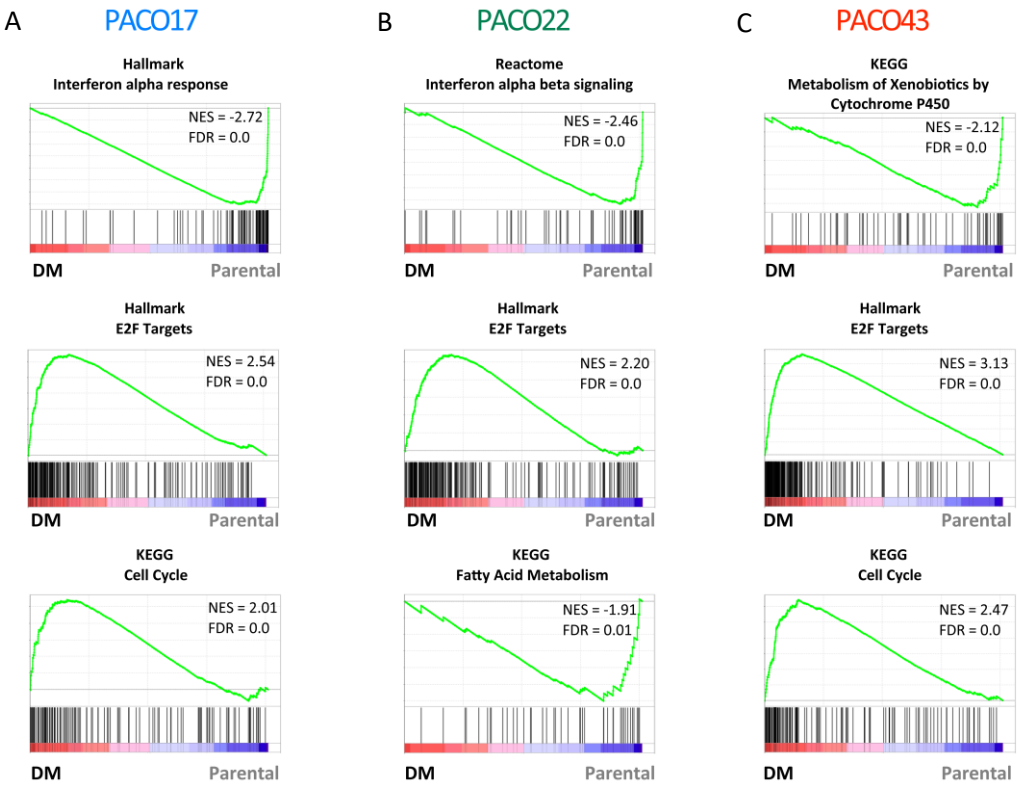

Supplementary Figure 1 – GSEA of PACO cell lines comparing DM cell lines with parental cell line
Gene set enrichment analysis (GSEA) plots of parental cell lines compared to DM cell lines after the last round of treatment of **(A)** PACO17, **(B)** PACO22, **(C)** PACO43 (n = 3 individual cell lines per group). Statistical significance was assessed using 1000 permutations on the gene set.
NES, normalized enrichment analysis; FDR, false discovery rate; DM, DMSO-treated.

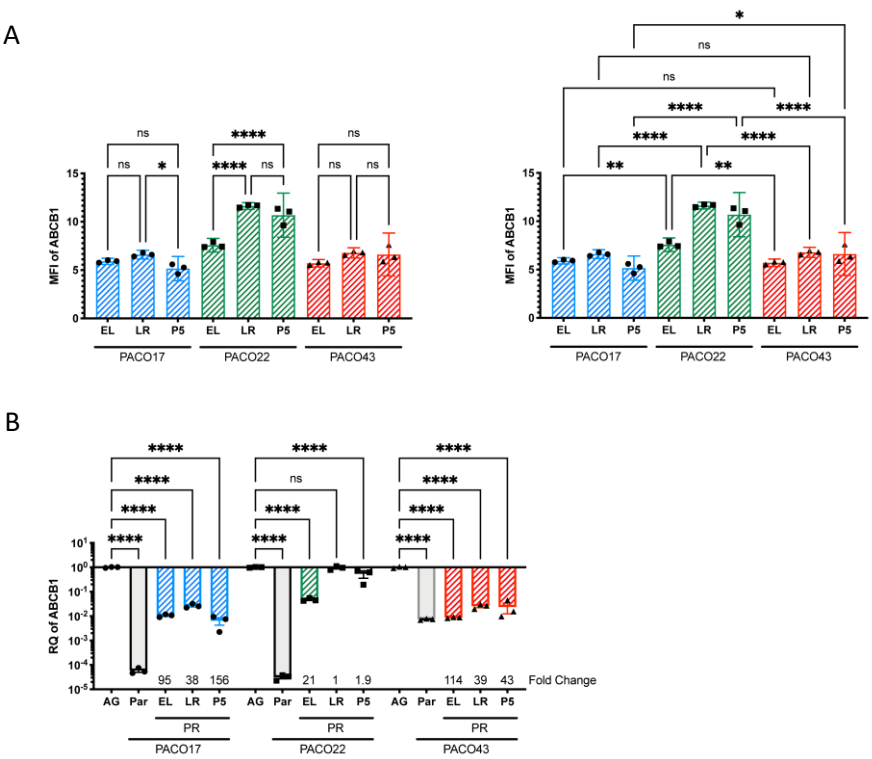

Supplementary Figure 2 – Gene expression analysis of PR cell lines at different timepoints of long-term treatment regimen

(A) Mean fluorescent intensity (MFI) of *ABCB1* probes based on gene expression microarray in PR cell lines of PACO17, PACO22 and PACO43 at indicated timepoints (Early Round, Last Round and Passage 5) (n = 3 individual cell lines per group). Each dot represents a unique cell line. Error bars depict mean ± s.e.m. * P value < 0.05; ** P value < 0.01; **** P value < 0.0001; by ordinary one-way ANOVA.

(B) qRT-PCR analysis of *ABCB1* expression in parental and PR cell lines at indicated timepoints (Early Round, Last Round and Passage 5) of PACO17, PACO22 and PACO43 (n = 3 individual replicates per group). Each dot represents a unique cell line. Values are relative to adrenal gland mRNA. Error bars depict mean ± s.e.m. **** P value < 0.0001, by ordinary one-way ANOVA.

EL, early round; LR, last round; P5, passage 5; AG, adrenal gland, Par; parental; PR, paclitaxel-resistant, RQ, relative quantification ($2^{-\Delta\Delta Ct}$).

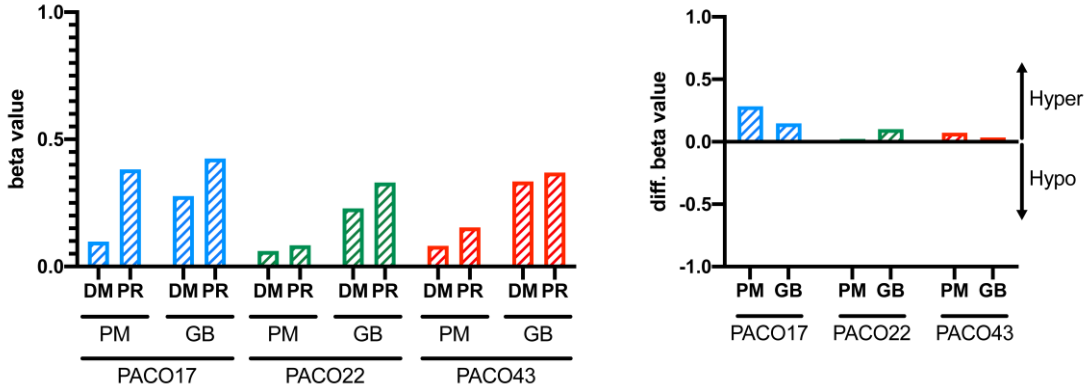

Supplementary Figure 3 – Analysis of beta values of *ABCB1* promoter and gene body region in DM and PR cell lines after last round of treatment

Beta values and differential beta value of *ABCB1* promoter and gene body in PR and DM cell lines after the last round of treatment of PACO17, PACO22 and PACO43. Values derived from differential methylation analysis performed with RnBeads. Differential beta values calculated by the difference between PR and DM cell lines.

PR, paclitaxel-resistant; DM, DMSO-treated; PM, promoter; GB, gene body; Hyper, hypermethylation; Hypo, hypomethylation.

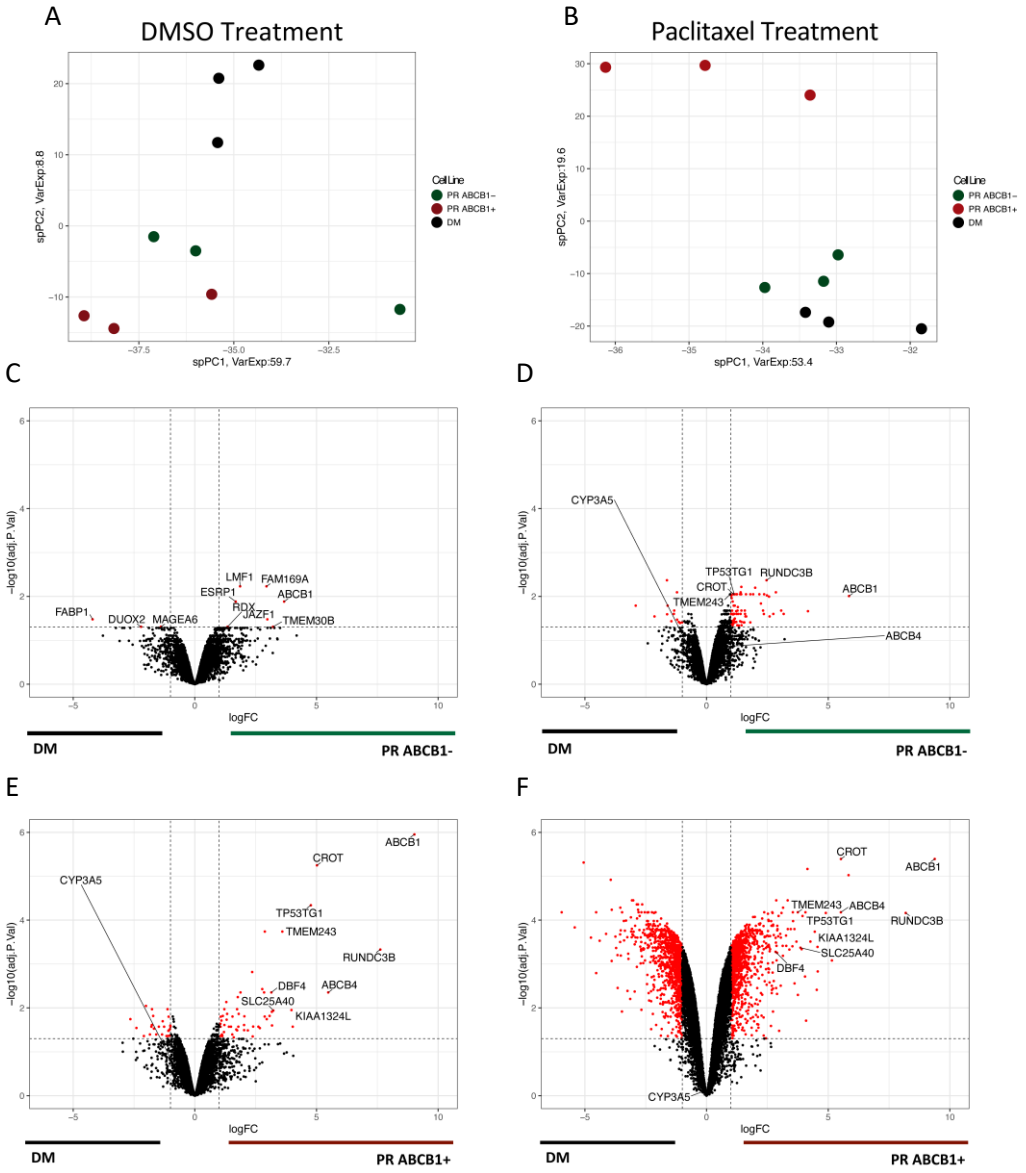

Supplementary Figure 4 – Differential gene expression analysis of DM cell lines and ABCB1 sorted populations
(A-B) Sparse principal component analysis (spPCA) based on gene expression microarray data of PACO22 cell lines after cell sort and 4 d of **(A)** DMSO and **(B)** paclitaxel treatment. Each dot represents an individual cell line and the color code indicates the sample group.
(C-D) Volcano plot of all differentially expressed genes between DM and PR ABCB1- cell lines under **(C)** DMSO or **(D)** paclitaxel treatment (n = 3 individual cell lines per group). Highlighted in red are all genes that are at least one log2-fold differentially expressed with an adjusted p-value of less than 0.05 according to the Benjamini-Hochberg calculation. (C) Labeled genes are all genes significantly differentially expressed. (D) Labeled genes are *ABCB1* and its neighboring genes, and *CYP3A5*.
(E-F) Volcano plot of all differentially expressed genes between DM and PR ABCB1+ cell lines under **(E)** DMSO or **(F)** paclitaxel treatment (n = 3 individual cell lines per group). Highlighted in red are all genes that are at least one log2-fold differentially expressed with an adjusted p-value of less than 0.05 according to the Benjamini-Hochberg calculation. (E-F) Labeled genes are *ABCB1* and its neighboring genes, and *CYP3A5*.
PR, paclitaxel-resistant; DM, DMSO-treated.

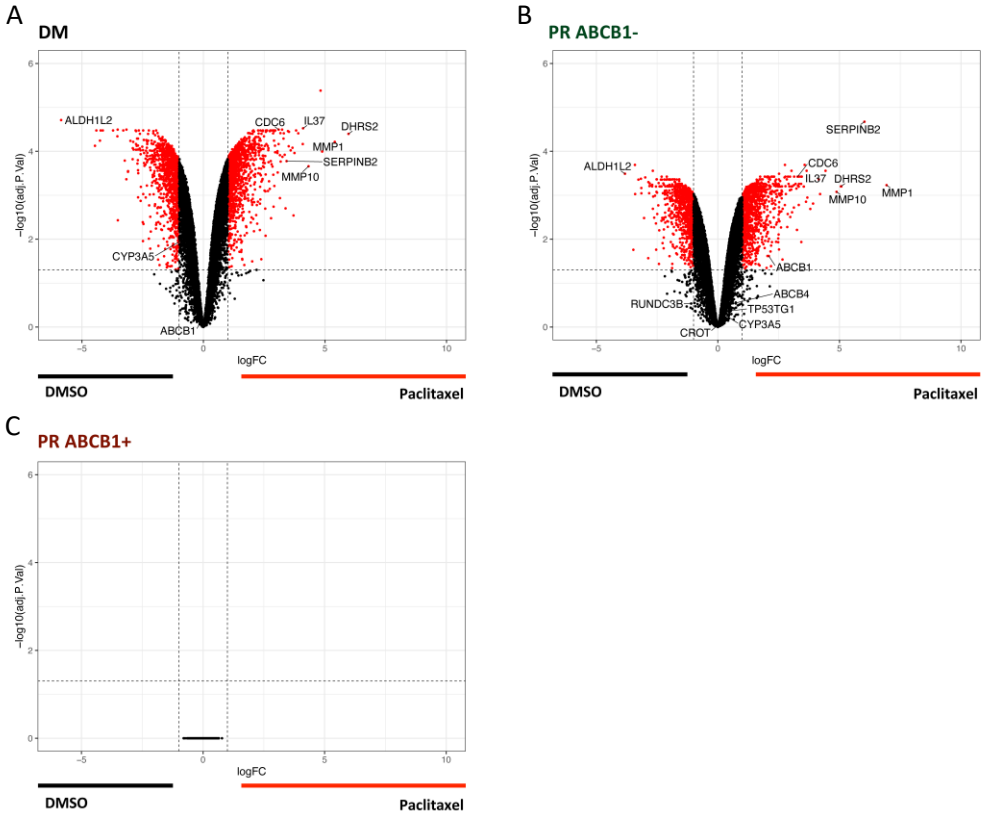

Supplementary Figure 5 – Differential gene expression analysis of DM cell lines and ABCB1 sorted populations
(A-C) Volcano plot of all differentially expressed genes between DMSO and paclitaxel treatment in **(A)** DM, **(B)** PR ABCB1- and **(C)** PR ABCB1+ cell lines. (n = 3 individual cell lines per group). Highlighted in red are all genes that are at least one log2-fold differentially expressed with an adjusted p-value of less than 0.05 according to the Benjamini-Hochberg calculation. (A-B) Labeled genes are related to cell stress, inflammation, apoptosis and DNA damage repair[329-332].
PR, paclitaxel-resistant; DM, DMSO-treated.

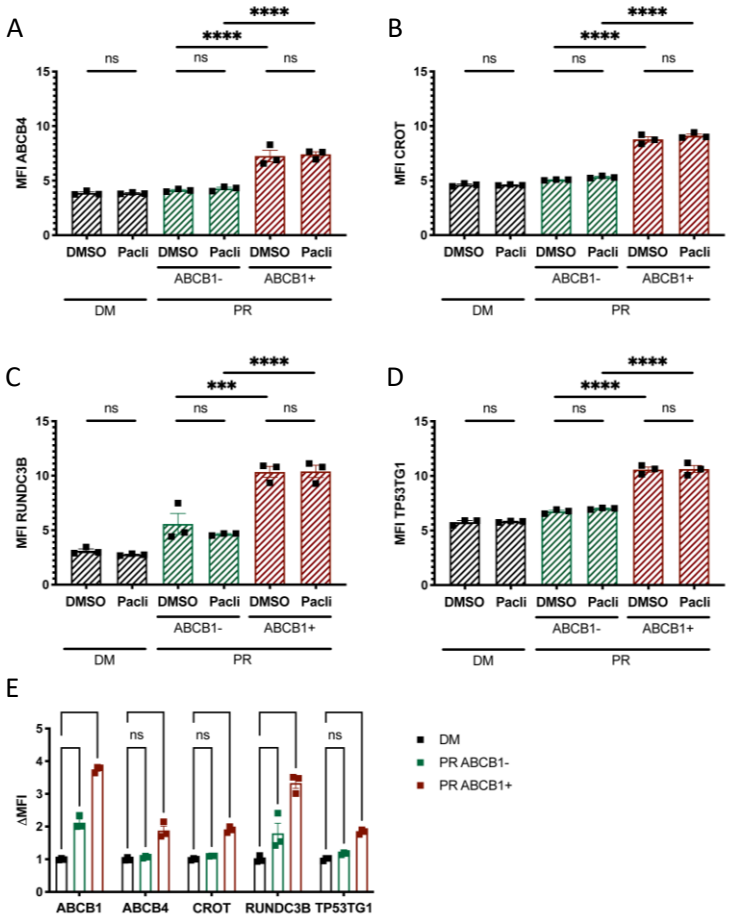

Supplementary Figure 6 – Analysis of MFI values of *ABCB1* neighboring genes PACO22 cell lines
(A-D) Mean fluorescent intensity (MFI) of **(A)** *ABCB4*, **(B)** *CROT*, **(C)** *RUNDC3B*, **(D)** *TP53TG1* probes in cell lines described in Figure 23B (n = 3 individual cell lines per group). Each dot represents a unique cell line. Error bars depict mean ± s.e.m. *** P value < 0.001; **** P value < 0.0001 by ordinary one-way ANOVA.
(E) Relative MFI of genes in cell lines described in Figure 23B (n = 3 individual cell lines per group). Each dot represents a unique cell line. Values are relative to DM cell lines. Error bars depict mean ± s.e.m.
PR, paclitaxel-resistant; DM, DMSO-treated; ns, not significant.

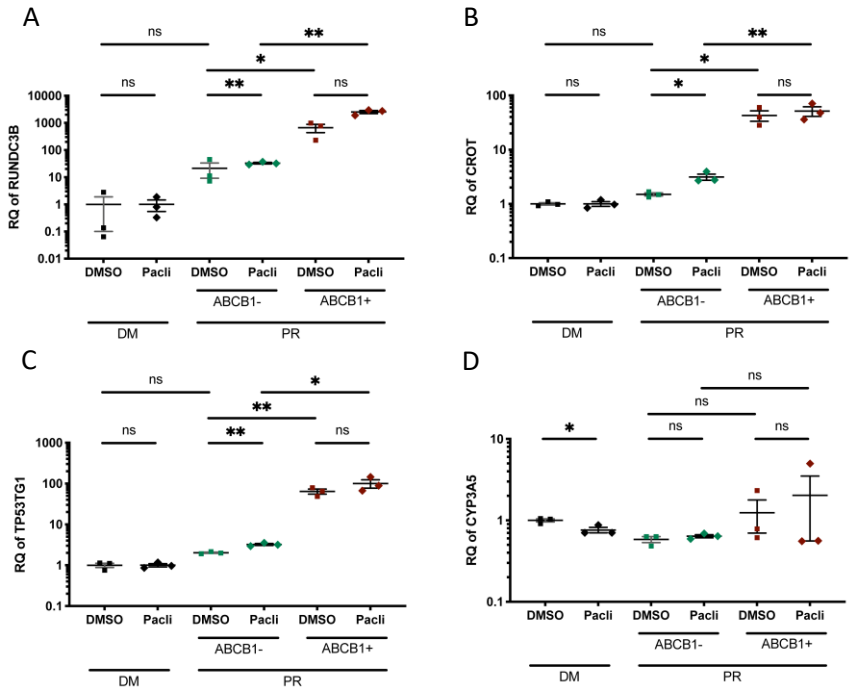

Supplementary Figure 7 – Validation of gene expression microarray findings for ABCB1 neighboring genes and CYP3A5

(A-D) qRT-PCR analysis in cell lines described in Figure 23B of **(A)** *CROT*, **(B)** *RUNDC3B*, **(C)** *TP53TG1*, **(D)** *CYP3A5* (n = 3 individual cell lines per group). Each dot represents a unique cell line. Values are relative to DMSO-treated DM cell lines. Error bars depict mean ± s.e.m. * P value < 0.05; ** P value < 0.01 by Student's t test.

PR, paclitaxel-resistant; DM, DMSO-treated; Pacli, paclitaxel; ns, not significant.

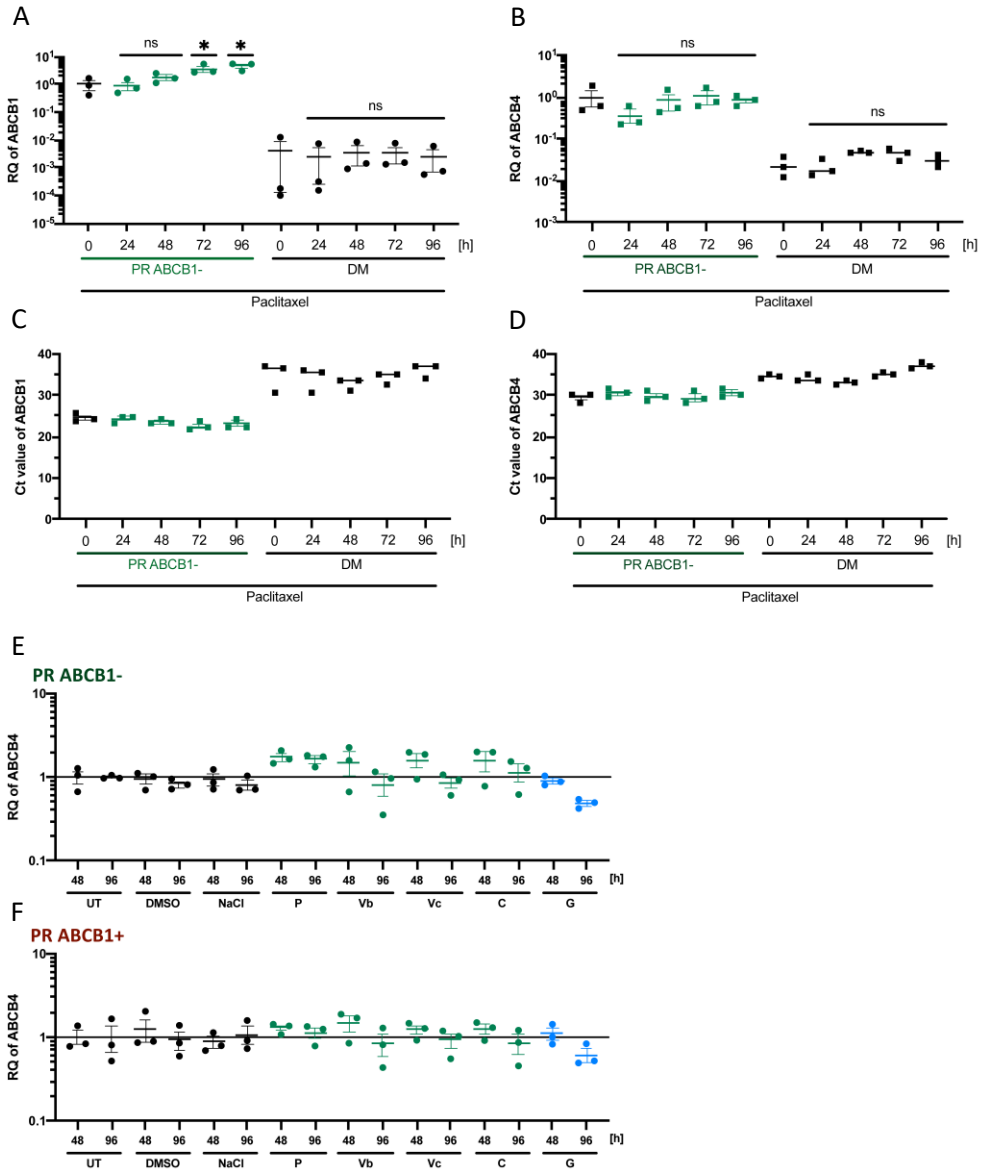

Supplementary Figure 8 – Not only paclitaxel but also other microtubule targeting agents induce expression of *ABCB1* in PR cell lines of PACO22

(A-B) qRT-PCR analysis in PR ABCB1- and DM cell lines treated with paclitaxel (100 nM) for expression of **(A)** *ABCB1* and **(B)** *ABCB4* (n = 3 biological replicates per group). Each dot represents a unique cell line. Values are relative to untreated PR ABCB1-. Error bars depict mean ± s.e.m. * P value < 0.05; ** P value < 0.01; by Student's t test.

(C-D) Ct values of PR ABCB1- and DM cell lines treated with paclitaxel (100 nM) for expression of **(C)** *ABCB1* and **(D)** *ABCB4* (n = 3 individual cell lines per group). Each dot represents a unique cell line. Error bars depict mean ± s.e.m.

(E-F) qRT-PCR analysis of *ABCB4* expression after treatment with various compounds for 48 h and 96 h in **(E)** PR ABCB1- cell lines and **(F)** PR ABCB1+ cell lines. Each dot represents a unique cell line. Values are relative to untreated control after 48 h. Error bars depict mean ± s.e.m. Statistical testing by Student's t test.

PR, paclitaxel-resistant; DM, DMSO-treated, UT, untreated; P, paclitaxel; Vb, vinblastine; Vc, Vincristine; C, colchicine; G, gemcitabine; ns, not significant.

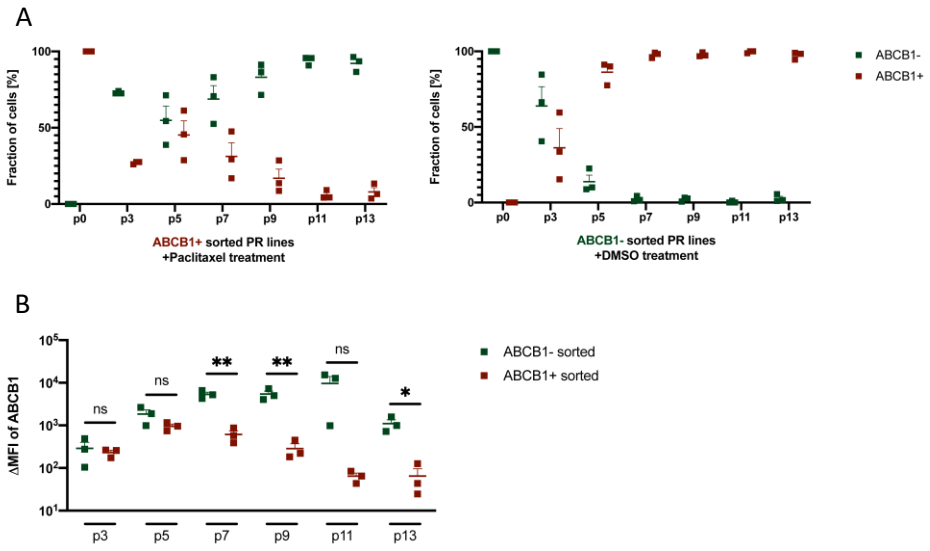

Supplementary Figure 9 – Expression of ABCB1 is enhanced by generation and amplification of *ABCB1*-carrying ecDNA

(A-B) Flow cytometry analysis of ABCB1 expression during treatment regimen described in (**Figure 27C**) to determine **(A)** the proportion of ABCB1+ and ABCB1- cells, and **(B)** the delta mean fluorescent intensity (ΔMFI) in each cell line (n = 3 biological replicates). Each dot represents a unique cell line. Error bars depict mean ± s.e.m. ** P value < 0.01, by Student's t test.

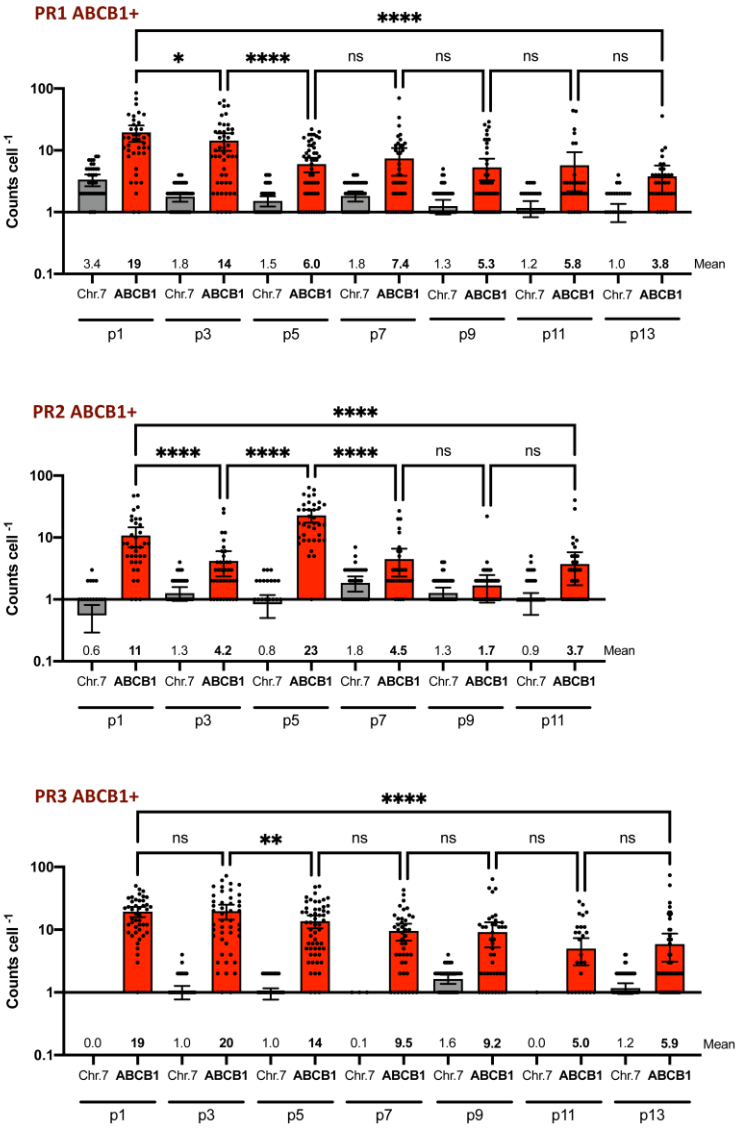

Supplementary Figure 10 – FISH-based count of *ABCB1* loci in PR ABCB1+ cell lines
FISH-based counting of *ABCB1* genes in sorted PR ABCB1+ cell lines during treatment regimen, as described in (Figure 27C). Centromere of chromosome 7 as reference. Each dot represents a single cell. Error bars depict mean ± s.e.m. * P value < 0.05; ** P value < 0.01; **** P value < 0.0001.
PR, paclitaxel-resistant; Chr.7, chromosome 7; ns, not significant.
FISH staining was conducted by Vanessa Vogel.

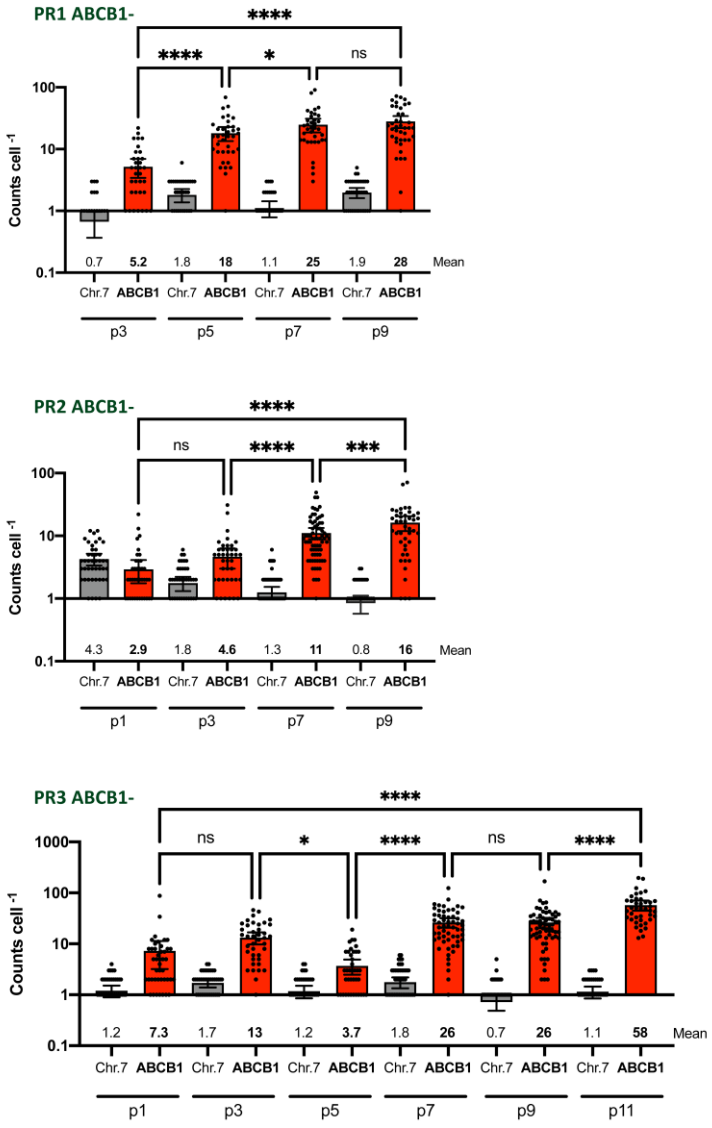

Supplementary Figure 11 – FISH-based count of *ABCB1* loci in PR ABCB1- cell lines
FISH-based counting of *ABCB1* genes in sorted PR ABCB1- cell lines during treatment regimen, as described in (Figure 27C). Centromere of chromosome 7 as reference. Each dot represents a single cell. Error bars depict mean ± s.e.m. * P value < 0.05; *** P value < 0.001; **** P value < 0.0001. PR, paclitaxel-resistant; Chr.7, chromosome 7; ns, not significant.
FISH staining was conducted by Vanessa Vogel.

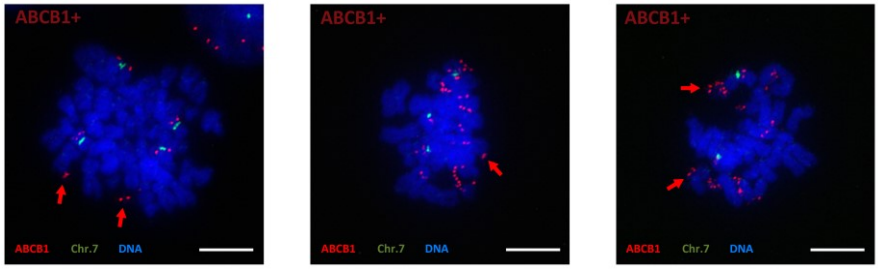

Supplementary Figure 12 – Whole cell image of nuclei with fully condensed chromosomes
Representative image of FISH staining in a PR ABCB1+ cells with fully condensed chromosomes. *ABCB1* genes are labeled red, centromere of chromosome 7 is labeled green, DNA is labeled blue. Scale bar corresponds to 10 µm.
FISH staining was conducted by Vanessa Vogel.

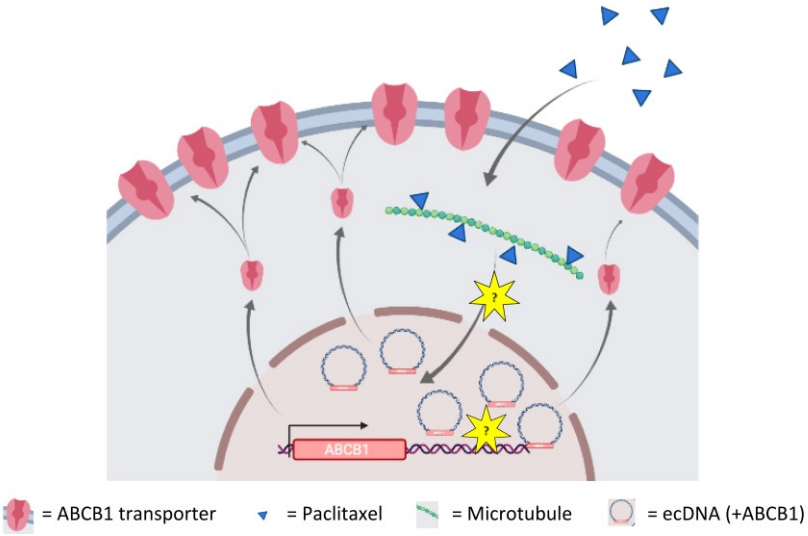

Supplementary Figure 13 – Expression of *ABCB1* is induced by microtubule inhibition and its expression enhanced by ecDNA generation
Pulsed long-term paclitaxel treatment regimen induced expression of *ABCB1* in three individual PACO cell lines which results in acquired drug resistance phenotype. Although the PACO cell lines belonged to different molecular subtypes, they acquired the same paclitaxel-resistance mechanism. Paclitaxel is a microtubule stabilizing agent that induces a cell cycle arrest which results in apoptosis[314]. This triggers a cascade of mechanism which ultimately leads to the induction of ABCB1 and the export of paclitaxel out of the cell. Moreover, we found in PACO22 that prolonged paclitaxel treatment facilitates the formation of *ABCB1*-carrying ecDNA and which enables the cell to dynamically react to drug holiday and paclitaxel treatment with loss or gain of ecDNA-based *ABCB1* amplification. For both observed phenotypes, the mechanistic details remain to be identified Taken together, ABCB1 plays an important role in acquired drug resistance in a subset of PACO cell lines.

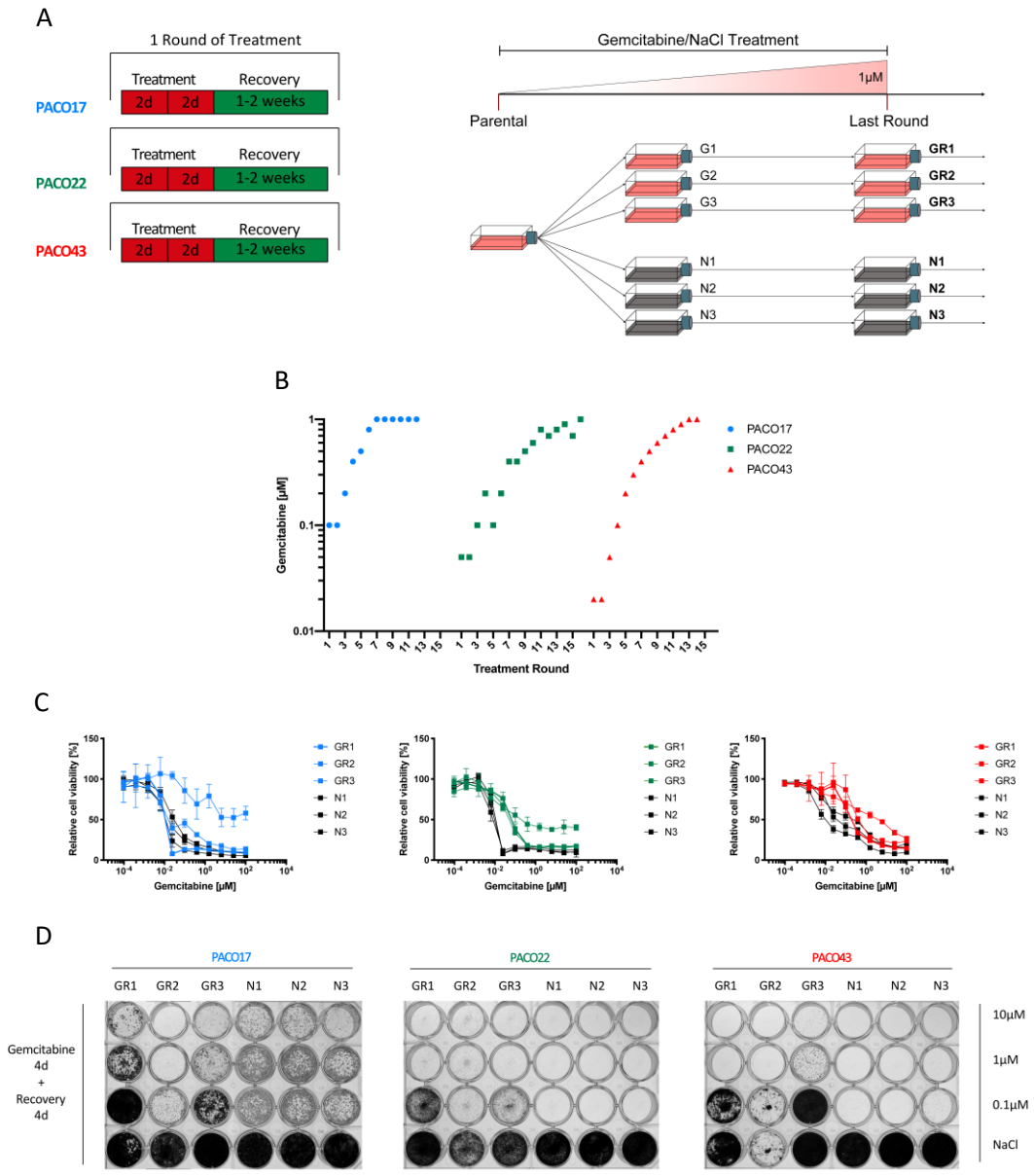

Supplementary Figure 14 – Generation of gemcitabine resistant PACO lines
(A) Schematic overview of long-term treatment regimen. A single round of treatment is divided in two times two treatment days that are followed by a recovery period. Each parental cell line was divided into two treatment arms with three biological replicates each. Sample collection after the last round of treatment.
(B) Gemcitabine concentration during at long-term treatment round in the respective cell line.
(C) Sensitivity of GR and N cell lines of PACO17, PACO22 and PACO43 after the last long-term treatment round to treatment with gemcitabine for 72 h determined by Cell Titer Blue metabolism (n = 1 per sample). Error bars depict mean ± 95% confidence interval of technical replicates (n = 4).
(D) Sensitivity of GR and N cell lines of PACO17, PACO22 and PACO43 after the last long-term treatment round to treatment with gemcitabine or NaCl for 4 d, followed by 4 d of recovery time. Density of cells is determined by crystal violet staining.
G, gemcitabine-treated; GR, gemcitabine -resistant; N, NaCl-treated.

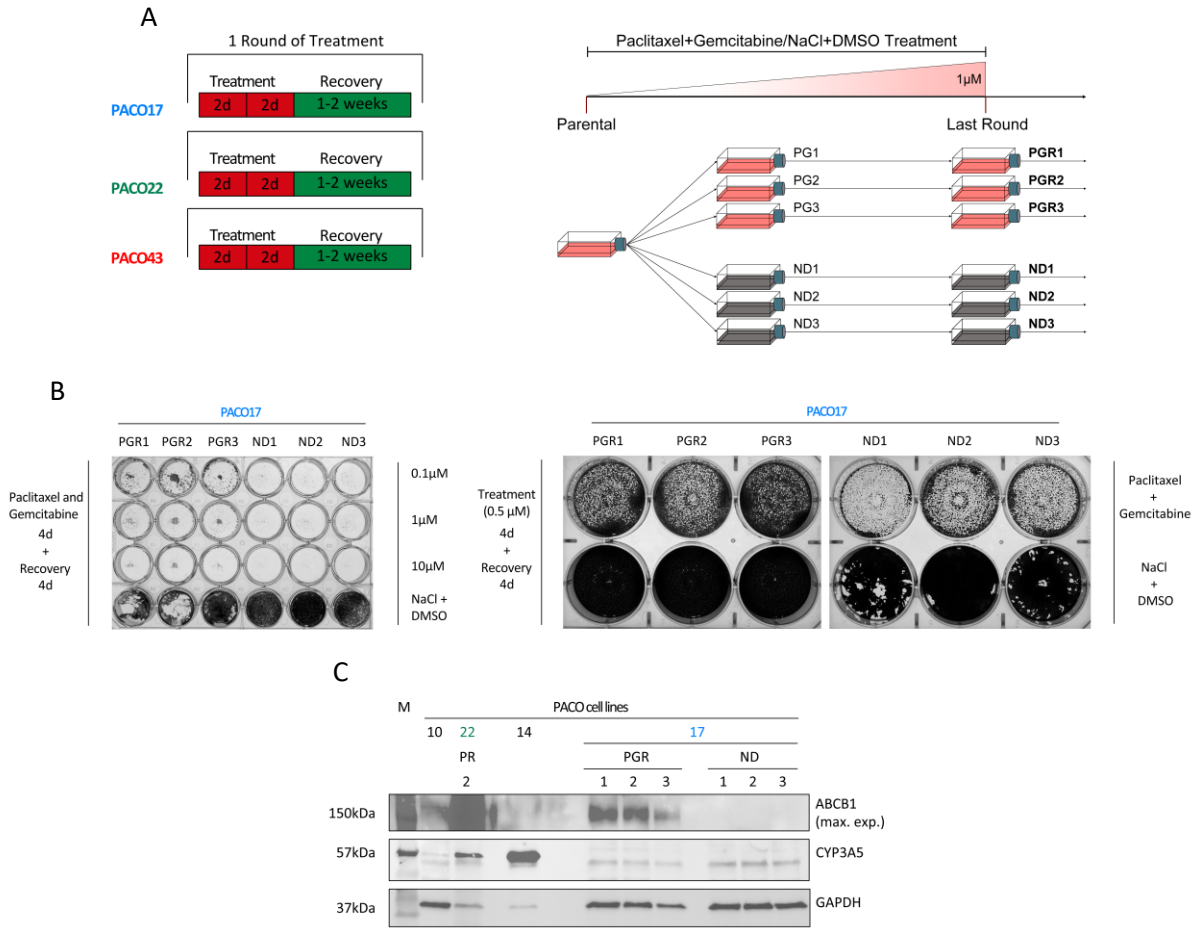

Supplementary Figure 15 – Generation of paclitaxel/gemcitabine resistant PACO lines
(A) Schematic overview of long-term treatment regimen. A single round of treatment is divided in two times two treatment days that are followed by a recovery period. Each parental cell line was divided into two treatment arms with three biological replicates each. Sample collection after the last round of treatment.
(B) Sensitivity of PGR and ND cell lines of PACO17 after the last long-term treatment round to treatment with paclitaxel/gemcitabine or NaCl/DMSO for 4 d, followed by 4 d of recovery time. Density of cells is determined by crystal violet staining.
(C) Western blot analysis of ABCB1 and CYP3A5 in PGR and ND cell lines after the last round of treatment in PACO17. PACO22 PR2 as positive control for ABCB1. PACO10 and PACO14 as positive control for CYP3A5. GAPDH as loading control.
PG, paclitaxel/gemcitabine-treated; PGR, paclitaxel /gemcitabine -resistant; ND, NaCl/DMSO-treated; PR, paclitaxel-resistant; kDa, kilo Dalton.
Long-term treatment of PACO17 (A), sensitivity assays (B) and Western blot (C) were conducted by Ornella Kossi.

Bibliography

1 Siegel, R. L., Miller, K. D. & Jemal, A. Cancer statistics, 2020. *CA Cancer J Clin* **70**, 7-30, doi:10.3322/caac.21590 (2020).

2 Rahib, L. *et al.* Projecting cancer incidence and deaths to 2030: the unexpected burden of thyroid, liver, and pancreas cancers in the United States. *Cancer Res* **74**, 2913-2921, doi:10.1158/0008-5472.CAN-14-0155 (2014).

3 Siegel, R. L., Miller, K. D. & Jemal, A. Cancer statistics, 2016. *CA Cancer J Clin* **66**, 7-30, doi:10.3322/caac.21332 (2016).

4 Ferlay, J. *et al.* Estimating the global cancer incidence and mortality in 2018: GLOBOCAN sources and methods. *Int J Cancer* **144**, 1941-1953, doi:10.1002/ijc.31937 (2019).

5 McGuigan, A. *et al.* Pancreatic cancer: A review of clinical diagnosis, epidemiology, treatment and outcomes. *World J Gastroenterol* **24**, 4846-4861, doi:10.3748/wjg.v24.i43.4846 (2018).

6 Midha, S., Chawla, S. & Garg, P. K. Modifiable and non-modifiable risk factors for pancreatic cancer: A review. *Cancer Lett* **381**, 269-277, doi:10.1016/j.canlet.2016.07.022 (2016).

7 Zhou, Q. & Melton, D. A. Pancreas regeneration. *Nature* **557**, 351-358, doi:10.1038/s41586-018-0088-0 (2018).

8 Daniel Longnecker, M. Anatomy and Histology of the Pancreas. *Pancreapedia*, doi:10.3998/panc.2014.3 (2014).

9 Oberg, K. & Eriksson, B. Endocrine tumours of the pancreas. *Best Pract Res Clin Gastroenterol* **19**, 753-781, doi:10.1016/j.bpg.2005.06.002 (2005).

10 Halfdanarson, T. R., Rabe, K. G., Rubin, J. & Petersen, G. M. Pancreatic neuroendocrine tumors (PNETs): incidence, prognosis and recent trend toward improved survival. *Ann Oncol* **19**, 1727-1733, doi:10.1093/annonc/mdn351 (2008).

11 Orditura, M. *et al.* Pancreatic neuroendocrine tumors: Nosography, management and treatment. *Int J Surg* **28 Suppl 1**, S156-162, doi:10.1016/j.ijsu.2015.12.052 (2016).

12 Salaria, S. N. & Shi, C. Pancreatic Neuroendocrine Tumors. *Surg Pathol Clin* **9**, 595-617, doi:10.1016/j.path.2016.05.006 (2016).

13 Kleeff, J. *et al.* Pancreatic cancer. *Nat Rev Dis Primers* **2**, 16022, doi:10.1038/nrdp.2016.22 (2016).

14 Landi, S. Genetic predisposition and environmental risk factors to pancreatic cancer: A review of the literature. *Mutat Res* **681**, 299-307, doi:10.1016/j.mrrev.2008.12.001 (2009).

15 Wolpin, B. M. *et al.* Variant ABO blood group alleles, secretor status, and risk of pancreatic cancer: results from the pancreatic cancer cohort consortium. *Cancer Epidemiol Biomarkers Prev* **19**, 3140-3149, doi:10.1158/1055-9965.EPI-10-0751 (2010).

16 Stevens, R. J., Roddam, A. W. & Beral, V. Pancreatic cancer in type 1 and young-onset diabetes: systematic review and meta-analysis. *Br J Cancer* **96**, 507-509, doi:10.1038/sj.bjc.6603571 (2007).

17 Huxley, R., Ansary-Moghaddam, A., Berrington de Gonzalez, A., Barzi, F. & Woodward, M. Type-II diabetes and pancreatic cancer: a meta-analysis of 36 studies. *Br J Cancer* **92**, 2076-2083, doi:10.1038/sj.bjc.6602619 (2005).

18 Calle, E. E., Rodriguez, C., Walker-Thurmond, K. & Thun, M. J. Overweight, obesity, and mortality from cancer in a prospectively studied cohort of U.S. adults. *N Engl J Med* **348**, 1625-1638, doi:10.1056/NEJMoa021423 (2003).

19 Lynch, S. M. *et al.* Cigarette smoking and pancreatic cancer: a pooled analysis from the pancreatic cancer cohort consortium. *Am J Epidemiol* **170**, 403-413, doi:10.1093/aje/kwp134 (2009).

20 Bosetti, C. *et al.* Cigarette smoking and pancreatic cancer: an analysis from the International Pancreatic Cancer Case-Control Consortium (Panc4). *Ann Oncol* **23**, 1880-1888, doi:10.1093/annonc/mdr541 (2012).

21 Klein, A. P. *et al.* Linkage analysis of chromosome 4 in families with familial pancreatic cancer. *Cancer Biol Ther* **6**, 320-323, doi:10.4161/cbt.6.3.3721 (2007).

22 Permuth-Wey, J. & Egan, K. M. Family history is a significant risk factor for pancreatic cancer: results from a systematic review and meta-analysis. *Fam Cancer* **8**, 109-117, doi:10.1007/s10689-008-9214-8 (2009).

23 Yeo, T. P. Demographics, epidemiology, and inheritance of pancreatic ductal adenocarcinoma. *Semin Oncol* **42**, 8-18, doi:10.1053/j.seminoncol.2014.12.002 (2015).

24 Bracci, P. M. Obesity and pancreatic cancer: overview of epidemiologic evidence and biologic mechanisms. *Mol Carcinog* **51**, 53-63, doi:10.1002/mc.20778 (2012).

25 Stolzenberg-Solomon, R. Z. *et al.* Dietary and other methyl-group availability factors and pancreatic cancer risk in a cohort of male smokers. *Am J Epidemiol* **153**, 680-687, doi:10.1093/aje/153.7.680 (2001).

26 Haeberle, L. & Esposito, I. Pathology of pancreatic cancer. *Transl Gastroenterol Hepatol* **4**, 50, doi:10.21037/tgh.2019.06.02 (2019).

27 Maitra, A. & Hruban, R. H. Pancreatic cancer. *Annu Rev Pathol* **3**, 157-188, doi:10.1146/annurev.pathmechdis.3.121806.154305 (2008).

28 Vincent, A., Herman, J., Schulick, R., Hruban, R. H. & Goggins, M. Pancreatic cancer. *Lancet* **378**, 607-620, doi:10.1016/S0140-6736(10)62307-0 (2011).

29 Ryan, D. P., Hong, T. S. & Bardeesy, N. Pancreatic adenocarcinoma. *N Engl J Med* **371**, 1039-1049, doi:10.1056/NEJMra1404198 (2014).

30 Mohammed, S., Van Buren, G., 2nd & Fisher, W. E. Pancreatic cancer: advances in treatment. *World J Gastroenterol* **20**, 9354-9360, doi:10.3748/wjg.v20.i28.9354 (2014).

31 Esposito, I., Konukiewitz, B., Schlitter, A. M. & Kloppel, G. Pathology of pancreatic ductal adenocarcinoma: facts, challenges and future developments. *World J Gastroenterol* **20**, 13833-13841, doi:10.3748/wjg.v20.i38.13833 (2014).

32 Aichler, M. *et al.* Origin of pancreatic ductal adenocarcinoma from atypical flat lesions: a comparative study in transgenic mice and human tissues. *J Pathol* **226**, 723-734, doi:10.1002/path.3017 (2012).

33 Basturk, O. *et al.* A Revised Classification System and Recommendations From the Baltimore Consensus Meeting for Neoplastic Precursor Lesions in the Pancreas. *Am J Surg Pathol* **39**, 1730-1741, doi:10.1097/PAS.0000000000000533 (2015).

34 Hruban, R. H. *et al.* An illustrated consensus on the classification of pancreatic intraepithelial neoplasia and intraductal papillary mucinous neoplasms. *Am J Surg Pathol* **28**, 977-987, doi:10.1097/01.pas.0000126675.59108.80 (2004).

35 Hruban, R. H. *et al.* Pancreatic intraepithelial neoplasia: a new nomenclature and classification system for pancreatic duct lesions. *Am J Surg Pathol* **25**, 579-586, doi:10.1097/00000478-200105000-00003 (2001).

36 Maitra, A., Kern, S. E. & Hruban, R. H. Molecular pathogenesis of pancreatic cancer. *Best Pract Res Clin Gastroenterol* **20**, 211-226, doi:10.1016/j.bpg.2005.10.002 (2006).

37 Maitra, A., Fukushima, N., Takaori, K. & Hruban, R. H. Precursors to invasive pancreatic cancer. *Adv Anat Pathol* **12**, 81-91, doi:10.1097/01.pap.0000155055.14238.25 (2005).

38 Hruban, R. H., Goggins, M., Parsons, J. & Kern, S. E. Progression model for pancreatic cancer. *Clin Cancer Res* **6**, 2969-2972 (2000).

39 van Heek, N. T. *et al.* Telomere shortening is nearly universal in pancreatic intraepithelial neoplasia. *Am J Pathol* **161**, 1541-1547, doi:10.1016/S0002-9440(10)64432-X (2002).

40 Hruban, R. H., Maitra, A. & Goggins, M. Update on pancreatic intraepithelial neoplasia. *Int J Clin Exp Pathol* **1**, 306-316 (2008).

41 Feldmann, G., Beaty, R., Hruban, R. H. & Maitra, A. Molecular genetics of pancreatic intraepithelial neoplasia. *J Hepatobiliary Pancreat Surg* **14**, 224-232, doi:10.1007/s00534-006-1166-5 (2007).

42 Hosoda, W. *et al.* Genetic analyses of isolated high-grade pancreatic intraepithelial neoplasia (HG-PanIN) reveal paucity of alterations in TP53 and SMAD4. *J Pathol* **242**, 16-23, doi:10.1002/path.4884 (2017).

43 Lohr, M., Kloppel, G., Maisonneuve, P., Lowenfels, A. B. & Luttges, J. Frequency of K-ras mutations in pancreatic intraductal neoplasias associated with pancreatic ductal adenocarcinoma and chronic pancreatitis: a meta-analysis. *Neoplasia* **7**, 17-23, doi:10.1593/neo.04445 (2005).

44 Lensing, R. J. & Bipat, S. Incidences of Pancreatic Malignancy and Mortality in Patients With Untreated Branch-Duct Intraductal Papillary Mucinous Neoplasms Undergoing Surveillance: A Systematic Review. *Pancreas* **46**, 1098-1110, doi:10.1097/MPA.0000000000000907 (2017).

45 Tanaka, M. *et al.* International consensus guidelines for management of intraductal papillary mucinous neoplasms and mucinous cystic neoplasms of the pancreas. *Pancreatology* **6**, 17-32, doi:10.1159/000090023 (2006).

46 Salvia, R. *et al.* Differences between main-duct and branch-duct intraductal papillary mucinous neoplasms of the pancreas. *World J Gastrointest Surg* **2**, 342-346, doi:10.4240/wjgs.v2.i10.342 (2010).

47 Furukawa, T. *et al.* Classification of types of intraductal papillary-mucinous neoplasm of the pancreas: a consensus study. *Virchows Arch* **447**, 794-799, doi:10.1007/s00428-005-0039-7 (2005).

48 Ban, S. *et al.* Intraductal papillary mucinous neoplasm (IPMN) of the pancreas: its histopathologic difference between 2 major types. *Am J Surg Pathol* **30**, 1561-1569, doi:10.1097/01.pas.0000213305.98187.d4 (2006).

49 Furukawa, T. *et al.* Prognostic relevance of morphological types of intraductal papillary mucinous neoplasms of the pancreas. *Gut* **60**, 509-516, doi:10.1136/gut.2010.210567 (2011).

50 Wu, J. *et al.* Recurrent GNAS mutations define an unexpected pathway for pancreatic cyst development. *Sci Transl Med* **3**, 92ra66, doi:10.1126/scitranslmed.3002543 (2011).

51 Lee, J. H., Kim, Y., Choi, J. W. & Kim, Y. S. KRAS, GNAS, and RNF43 mutations in intraductal papillary mucinous neoplasm of the pancreas: a meta-analysis. *Springerplus* **5**, 1172, doi:10.1186/s40064-016-2847-4 (2016).

52 Kanda, M. *et al.* Presence of somatic mutations in most early-stage pancreatic intraepithelial neoplasia. *Gastroenterology* **142**, 730-733 e739, doi:10.1053/j.gastro.2011.12.042 (2012).

53 Zamboni, G. *et al.* Mucinous cystic tumors of the pancreas: clinicopathological features, prognosis, and relationship to other mucinous cystic tumors. *Am J Surg Pathol* **23**, 410-422, doi:10.1097/00000478-199904000-00005 (1999).

54 Shibata, H. *et al.* Mucinous Cystic Neoplasms Lined by Abundant Mucinous Epithelium Frequently Involve KRAS Mutations and Malignant Progression. *Anticancer Res* **37**, 7063-7068, doi:10.21873/anticanres.12178 (2017).

55 Singhi, A. D. *et al.* Preoperative next-generation sequencing of pancreatic cyst fluid is highly accurate in cyst classification and detection of advanced neoplasia. *Gut* **67**, 2131-2141, doi:10.1136/gutjnl-2016-313586 (2018).

56 Maitra, A. & Leach, S. D. Disputed paternity: the uncertain ancestry of pancreatic ductal neoplasia. *Cancer Cell* **22**, 701-703, doi:10.1016/j.ccr.2012.11.015 (2012).

57 Kopp, J. L. *et al.* Identification of Sox9-dependent acinar-to-ductal reprogramming as the principal mechanism for initiation of pancreatic ductal adenocarcinoma. *Cancer Cell* **22**, 737-750, doi:10.1016/j.ccr.2012.10.025 (2012).

58 Pin, C. L., Ryan, J. F. & Mehmood, R. Acinar cell reprogramming: a clinically important target in pancreatic disease. *Epigenomics* **7**, 267-281, doi:10.2217/epi.14.83 (2015).

59 Chuvin, N. *et al.* Acinar-to-Ductal Metaplasia Induced by Transforming Growth Factor Beta Facilitates KRAS(G12D)-driven Pancreatic Tumorigenesis. *Cell Mol Gastroenterol Hepatol* **4**, 263-282, doi:10.1016/j.jcmgh.2017.05.005 (2017).

60 Hidalgo, M. Pancreatic cancer. *N Engl J Med* **362**, 1605-1617, doi:10.1056/NEJMra0901557 (2010).

61 Wolfgang, C. L. *et al.* Recent progress in pancreatic cancer. *CA Cancer J Clin* **63**, 318-348, doi:10.3322/caac.21190 (2013).

62 Cancer Genome Atlas Research Network. Electronic address, a. a. d. h. e. & Cancer Genome Atlas Research, N. Integrated Genomic Characterization of Pancreatic Ductal Adenocarcinoma. *Cancer Cell* **32**, 185-203 e113, doi:10.1016/j.ccell.2017.07.007 (2017).

63 Humphris, J. L. *et al.* Hypermutation In Pancreatic Cancer. *Gastroenterology* **152**, 68-74 e62, doi:10.1053/j.gastro.2016.09.060 (2017).

64 Witkiewicz, A. K. *et al.* Whole-exome sequencing of pancreatic cancer defines genetic diversity and therapeutic targets. *Nat Commun* **6**, 6744, doi:10.1038/ncomms7744 (2015).

65 Waddell, N. *et al.* Whole genomes redefine the mutational landscape of pancreatic cancer. *Nature* **518**, 495-501, doi:10.1038/nature14169 (2015).

66 Silverman, B. R. & Shi, J. Alterations of Epigenetic Regulators in Pancreatic Cancer and Their Clinical Implications. *Int J Mol Sci* **17**, doi:10.3390/ijms17122138 (2016).

67 Provenzano, P. P. *et al.* Enzymatic targeting of the stroma ablates physical barriers to treatment of pancreatic ductal adenocarcinoma. *Cancer Cell* **21**, 418-429, doi:10.1016/j.ccr.2012.01.007 (2012).

68 Feig, C. *et al.* The pancreas cancer microenvironment. *Clin Cancer Res* **18**, 4266-4276, doi:10.1158/1078-0432.CCR-11-3114 (2012).

69 Apte, M. V. *et al.* Desmoplastic reaction in pancreatic cancer: role of pancreatic stellate cells. *Pancreas* **29**, 179-187, doi:10.1097/00006676-200410000-00002 (2004).

70 Allam, A. *et al.* Pancreatic stellate cells in pancreatic cancer: In focus. *Pancreatology* **17**, 514-522, doi:10.1016/j.pan.2017.05.390 (2017).

71 Pothula, S. P. *et al.* Key role of pancreatic stellate cells in pancreatic cancer. *Cancer Lett* **381**, 194-200, doi:10.1016/j.canlet.2015.10.035 (2016).

72 Waghray, M., Yalamanchili, M., di Magliano, M. P. & Simeone, D. M. Deciphering the role of stroma in pancreatic cancer. *Curr Opin Gastroenterol* **29**, 537-543, doi:10.1097/MOG.0b013e328363affe (2013).

73 Neesse, A., Algul, H., Tuveson, D. A. & Gress, T. M. Stromal biology and therapy in pancreatic cancer: a changing paradigm. *Gut* **64**, 1476-1484, doi:10.1136/gutjnl-2015-309304 (2015).

74 Erkan, M. *et al.* The activated stroma index is a novel and independent prognostic marker in pancreatic ductal adenocarcinoma. *Clin Gastroenterol Hepatol* **6**, 1155-1161, doi:10.1016/j.cgh.2008.05.006 (2008).

75 Bever, K. M. *et al.* The prognostic value of stroma in pancreatic cancer in patients receiving adjuvant therapy. *HPB (Oxford)* **17**, 292-298, doi:10.1111/hpb.12334 (2015).

76 Ozdemir, B. C. *et al.* Depletion of Carcinoma-Associated Fibroblasts and Fibrosis Induces Immunosuppression and Accelerates Pancreas Cancer with Reduced Survival. *Cancer Cell* **28**, 831-833, doi:10.1016/j.ccell.2015.11.002 (2015).

77 Becker, A. E., Hernandez, Y. G., Frucht, H. & Lucas, A. L. Pancreatic ductal adenocarcinoma: risk factors, screening, and early detection. *World J Gastroenterol* **20**, 11182-11198, doi:10.3748/wjg.v20.i32.11182 (2014).

78 Porta, M. *et al.* Exocrine pancreatic cancer: symptoms at presentation and their relation to tumour site and stage. *Clin Transl Oncol* **7**, 189-197, doi:10.1007/BF02712816 (2005).

79 Chari, S. T. *et al.* Probability of pancreatic cancer following diabetes: a population-based study. *Gastroenterology* **129**, 504-511, doi:10.1016/j.gastro.2005.05.007 (2005).

80 Shin, E. J. *et al.* Linear-array EUS improves detection of pancreatic lesions in high-risk individuals: a randomized tandem study. *Gastrointest Endosc* **82**, 812-818, doi:10.1016/j.gie.2015.02.028 (2015).

81 Harinck, F. *et al.* A multicentre comparative prospective blinded analysis of EUS and MRI for screening of pancreatic cancer in high-risk individuals. *Gut* **65**, 1505-1513, doi:10.1136/gutjnl-2014-308008 (2016).

82 Winter, J. M., Yeo, C. J. & Brody, J. R. Diagnostic, prognostic, and predictive biomarkers in pancreatic cancer. *J Surg Oncol* **107**, 15-22, doi:10.1002/jso.23192 (2013).

83 Poruk, K. E. *et al.* The clinical utility of CA 19-9 in pancreatic adenocarcinoma: diagnostic and prognostic updates. *Curr Mol Med* **13**, 340-351, doi:10.2174/1566524011313030003 (2013).

84 Mayo, S. C. *et al.* Management of patients with pancreatic adenocarcinoma: national trends in patient selection, operative management, and use of adjuvant therapy. *J Am Coll Surg* **214**, 33-45, doi:10.1016/j.jamcollsurg.2011.09.022 (2012).

85 Amin, M. B. *et al.* The Eighth Edition AJCC Cancer Staging Manual: Continuing to build a bridge from a population-based to a more "personalized" approach to cancer staging. *CA Cancer J Clin* **67**, 93-99, doi:10.3322/caac.21388 (2017).

86 van Roessel, S. *et al.* International Validation of the Eighth Edition of the American Joint Committee on Cancer (AJCC) TNM Staging System in Patients With Resected Pancreatic Cancer. *JAMA Surg* **153**, e183617, doi:10.1001/jamasurg.2018.3617 (2018).

87 Allen, P. J. *et al.* Multi-institutional Validation Study of the American Joint Commission on Cancer (8th Edition) Changes for T and N Staging in Patients With Pancreatic Adenocarcinoma. *Ann Surg* **265**, 185-191, doi:10.1097/SLA.0000000000001763 (2017).

88 Edge, S. B. & Compton, C. C. The American Joint Committee on Cancer: the 7th edition of the AJCC cancer staging manual and the future of TNM. *Ann Surg Oncol* **17**, 1471-1474, doi:10.1245/s10434-010-0985-4 (2010).

89 Versteijne, E. *et al.* Meta-analysis comparing upfront surgery with neoadjuvant treatment in patients with resectable or borderline resectable pancreatic cancer. *Br J Surg* **105**, 946-958, doi:10.1002/bjs.10870 (2018).

90 Neoptolemos, J. P. *et al.* Therapeutic developments in pancreatic cancer: current and future perspectives. *Nat Rev Gastroenterol Hepatol* **15**, 333-348, doi:10.1038/s41575-018-0005-x (2018).

91 Martin, R. C., 2nd *et al.* Arterial and venous resection for pancreatic adenocarcinoma: operative and long-term outcomes. *Arch Surg* **144**, 154-159, doi:10.1001/archsurg.2008.547 (2009).

92 Neoptolemos, J. P. *et al.* Adjuvant chemotherapy with fluorouracil plus folinic acid vs gemcitabine following pancreatic cancer resection: a randomized controlled trial. *JAMA* **304**, 1073-1081, doi:10.1001/jama.2010.1275 (2010).

93 Oettle, H. *et al.* Adjuvant chemotherapy with gemcitabine and long-term outcomes among patients with resected pancreatic cancer: the CONKO-001 randomized trial. *JAMA* **310**, 1473-1481, doi:10.1001/jama.2013.279201 (2013).

94 Khorana, A. A. *et al.* Potentially Curable Pancreatic Cancer: American Society of Clinical Oncology Clinical Practice Guideline. *J Clin Oncol* **34**, 2541-2556, doi:10.1200/JCO.2016.67.5553 (2016).

95 Neoptolemos, J. P. *et al.* Comparison of adjuvant gemcitabine and capecitabine with gemcitabine monotherapy in patients with resected pancreatic cancer (ESPAC-4): a multicentre, open-label, randomised, phase 3 trial. *Lancet* **389**, 1011-1024, doi:10.1016/S0140-6736(16)32409-6 (2017).

96 Tempero, M. A. *et al.* APACT: phase III, multicenter, international, open-label, randomized trial of adjuvant nab-paclitaxel plus gemcitabine (nab-P/G) vs gemcitabine (G) for surgically resected pancreatic adenocarcinoma. *Journal of Clinical Oncology* **37**, 4000-4000, doi:10.1200/JCO.2019.37.15_suppl.4000 (2019).

97 Bockhorn, M. *et al.* Borderline resectable pancreatic cancer: a consensus statement by the International Study Group of Pancreatic Surgery (ISGPS). *Surgery* **155**, 977-988, doi:10.1016/j.surg.2014.02.001 (2014).

98 Gillen, S., Schuster, T., Meyer Zum Buschenfelde, C., Friess, H. & Kleeff, J. Preoperative/neoadjuvant therapy in pancreatic cancer: a systematic review and meta-analysis of response and resection percentages. *PLoS Med* **7**, e1000267, doi:10.1371/journal.pmed.1000267 (2010).

99 Labori, K. J. *et al.* Neoadjuvant chemotherapy versus surgery first for resectable pancreatic cancer (Norwegian Pancreatic Cancer Trial - 1 (NorPACT-1)) - study protocol for a national multicentre randomized controlled trial. *BMC Surg* **17**, 94, doi:10.1186/s12893-017-0291-1 (2017).

100 Zhan, H. X. *et al.* Neoadjuvant therapy in pancreatic cancer: a systematic review and meta-analysis of prospective studies. *Cancer Med* **6**, 1201-1219, doi:10.1002/cam4.1071 (2017).

101 Evans, D. B. *et al.* Preoperative gemcitabine-based chemoradiation for patients with resectable adenocarcinoma of the pancreatic head. *J Clin Oncol* **26**, 3496-3502, doi:10.1200/JCO.2007.15.8634 (2008).

102 Katz, M. H. *et al.* Borderline resectable pancreatic cancer: the importance of this emerging stage of disease. *J Am Coll Surg* **206**, 833-846; discussion 846-838, doi:10.1016/j.jamcollsurg.2007.12.020 (2008).

103 Neoptolemos, J. P. *et al.* A randomized trial of chemoradiotherapy and chemotherapy after resection of pancreatic cancer. *N Engl J Med* **350**, 1200-1210, doi:10.1056/NEJMoa032295 (2004).

104 Rombouts, S. J. *et al.* Systematic Review of Resection Rates and Clinical Outcomes After FOLFIRINOX-Based Treatment in Patients with Locally Advanced Pancreatic Cancer. *Ann Surg Oncol* **23**, 4352-4360, doi:10.1245/s10434-016-5373-2 (2016).

105 Petrelli, F. *et al.* FOLFIRINOX-based neoadjuvant therapy in borderline resectable or unresectable pancreatic cancer: a meta-analytical review of published studies. *Pancreas* **44**, 515-521, doi:10.1097/mpa.0000000000000314 (2015).

106 Ferrone, C. R. *et al.* Radiological and surgical implications of neoadjuvant treatment with FOLFIRINOX for locally advanced and borderline resectable pancreatic cancer. *Ann Surg* **261**, 12-17, doi:10.1097/SLA.0000000000000867 (2015).

107 Nitsche, U. *et al.* Resectability After First-Line FOLFIRINOX in Initially Unresectable Locally Advanced Pancreatic Cancer: A Single-Center Experience. *Ann Surg Oncol* **22 Suppl 3**, S1212-1220, doi:10.1245/s10434-015-4851-2 (2015).

108 Schorn, S. *et al.* The impact of neoadjuvant therapy on the histopathological features of pancreatic ductal adenocarcinoma - A systematic review and meta-analysis. *Cancer Treat Rev* **55**, 96-106, doi:10.1016/j.ctrv.2017.03.003 (2017).

109 Von Hoff, D. D. *et al.* Increased survival in pancreatic cancer with nab-paclitaxel plus gemcitabine. *N Engl J Med* **369**, 1691-1703, doi:10.1056/NEJMoa1304369 (2013).

110 Conroy, T. *et al.* FOLFIRINOX versus gemcitabine for metastatic pancreatic cancer. *N Engl J Med* **364**, 1817-1825, doi:10.1056/NEJMoa1011923 (2011).

111 Von Hoff, D. D. *et al.* Gemcitabine plus nab-paclitaxel is an active regimen in patients with advanced pancreatic cancer: a phase I/II trial. *J Clin Oncol* **29**, 4548-4554, doi:10.1200/JCO.2011.36.5742 (2011).

112 Goldstein, D. *et al.* nab-Paclitaxel plus gemcitabine for metastatic pancreatic cancer: long-term survival from a phase III trial. *J Natl Cancer Inst* **107**, doi:10.1093/jnci/dju413 (2015).

113 Sohal, D. P., Mangu, P. B. & Laheru, D. Metastatic Pancreatic Cancer: American Society of Clinical Oncology Clinical Practice Guideline Summary. *J Oncol Pract* **13**, 261-264, doi:10.1200/JOP.2016.017368 (2017).

114 Kunzmann, V. *et al.* Conversion rate in locally advanced pancreatic cancer (LAPC) after nab-Paclitaxel/Gemcitabine- or FOLFIRINOX-based induction chemotherapy (NEOLAP) - Final Results of a multicenter randomised Phase 2 AIO trial. *Annals of Oncology* **30**, 253-324, doi:10.1093/annonc/mdz247 (2019).

115 Ottaiano, A. *et al.* Gemcitabine mono-therapy versus gemcitabine plus targeted therapy in advanced pancreatic cancer: a meta-analysis of randomized phase III trials. *Acta Oncol* **56**, 377-383, doi:10.1080/0284186X.2017.1288922 (2017).

116 Moore, M. J. *et al.* Erlotinib plus gemcitabine compared with gemcitabine alone in patients with advanced pancreatic cancer: a phase III trial of the National Cancer Institute of Canada Clinical Trials Group. *J Clin Oncol* **25**, 1960-1966, doi:10.1200/JCO.2006.07.9525 (2007).

117 Michl, P. & Gress, T. M. Current concepts and novel targets in advanced pancreatic cancer. *Gut* **62**, 317-326, doi:10.1136/gutjnl-2012-303588 (2013).

118 Kamerkar, S. *et al.* Exosomes facilitate therapeutic targeting of oncogenic KRAS in pancreatic cancer. *Nature* **546**, 498-503, doi:10.1038/nature22341 (2017).

119 Hanahan, D. & Weinberg, R. A. Hallmarks of cancer: the next generation. *Cell* **144**, 646-674, doi:10.1016/j.cell.2011.02.013 (2011).

120 Silva, I. P. & Long, G. V. Systemic therapy in advanced melanoma: integrating targeted therapy and immunotherapy into clinical practice. *Curr Opin Oncol* **29**, 484-492, doi:10.1097/CCO.0000000000000405 (2017).

121 Brahmer, J. R. *et al.* Safety and activity of anti-PD-L1 antibody in patients with advanced cancer. *N Engl J Med* **366**, 2455-2465, doi:10.1056/NEJMoa1200694 (2012).

122 Royal, R. E. *et al.* Phase 2 trial of single agent Ipilimumab (anti-CTLA-4) for locally advanced or metastatic pancreatic adenocarcinoma. *J Immunother* **33**, 828-833, doi:10.1097/CJI.0b013e3181eec14c (2010).

123 Hingorani, S. R. *et al.* HALO 202: Randomized Phase II Study of PEGPH20 Plus Nab-Paclitaxel/Gemcitabine Versus Nab-Paclitaxel/Gemcitabine in Patients With Untreated, Metastatic Pancreatic Ductal Adenocarcinoma. *J Clin Oncol* **36**, 359-366, doi:10.1200/JCO.2017.74.9564 (2018).

124 Biankin, A. V. & Maitra, A. Subtyping Pancreatic Cancer. *Cancer Cell* **28**, 411-413, doi:10.1016/j.ccell.2015.09.020 (2015).

125 Nevala-Plagemann, C., Hidalgo, M. & Garrido-Laguna, I. From state-of-the-art treatments to novel therapies for advanced-stage pancreatic cancer. *Nat Rev Clin Oncol* **17**, 108-123, doi:10.1038/s41571-019-0281-6 (2020).

126 Collisson, E. A., Bailey, P., Chang, D. K. & Biankin, A. V. Molecular subtypes of pancreatic cancer. *Nat Rev Gastroenterol Hepatol* **16**, 207-220, doi:10.1038/s41575-019-0109-y (2019).

127 Slamon, D. *et al.* Adjuvant trastuzumab in HER2-positive breast cancer. *N Engl J Med* **365**, 1273-1283, doi:10.1056/NEJMoa0910383 (2011).

128 Chapman, P. B. *et al.* Improved survival with vemurafenib in melanoma with BRAF V600E mutation. *N Engl J Med* **364**, 2507-2516, doi:10.1056/NEJMoa1103782 (2011).

129 Garcea, G., Neal, C. P., Pattenden, C. J., Steward, W. P. & Berry, D. P. Molecular prognostic markers in pancreatic cancer: a systematic review. *Eur J Cancer* **41**, 2213-2236, doi:10.1016/j.ejca.2005.04.044 (2005).

130 Collisson, E. A. *et al.* Subtypes of pancreatic ductal adenocarcinoma and their differing responses to therapy. *Nat Med* **17**, 500-503, doi:10.1038/nm.2344 (2011).

131 Moffitt, R. A. *et al.* Virtual microdissection identifies distinct tumor- and stroma-specific subtypes of pancreatic ductal adenocarcinoma. *Nat Genet* **47**, 1168-1178, doi:10.1038/ng.3398 (2015).

132 Biankin, A. V. *et al.* Pancreatic cancer genomes reveal aberrations in axon guidance pathway genes. *Nature* **491**, 399-405, doi:10.1038/nature11547 (2012).

133 Bailey, P. *et al.* Genomic analyses identify molecular subtypes of pancreatic cancer. *Nature* **531**, 47-52, doi:10.1038/nature16965 (2016).

134 Puleo, F. *et al.* Stratification of Pancreatic Ductal Adenocarcinomas Based on Tumor and Microenvironment Features. *Gastroenterology* **155**, 1999-2013 e1993, doi:10.1053/j.gastro.2018.08.033 (2018).

135 Lee, J. *et al.* Tumor stem cells derived from glioblastomas cultured in bFGF and EGF more closely mirror the phenotype and genotype of primary tumors than do serum-cultured cell lines. *Cancer Cell* **9**, 391-403, doi:10.1016/j.ccr.2006.03.030 (2006).

136 Domcke, S., Sinha, R., Levine, D. A., Sander, C. & Schultz, N. Evaluating cell lines as tumour models by comparison of genomic profiles. *Nat Commun* **4**, 2126, doi:10.1038/ncomms3126 (2013).

137 Bjare, U. Serum-free cell culture. *Pharmacol Ther* **53**, 355-374, doi:10.1016/0163-7258(92)90056-6 (1992).

138 Ben-David, U. *et al.* Genetic and transcriptional evolution alters cancer cell line drug response. *Nature* **560**, 325-330, doi:10.1038/s41586-018-0409-3 (2018).

139 Deer, E. L. *et al.* Phenotype and genotype of pancreatic cancer cell lines. *Pancreas* **39**, 425-435, doi:10.1097/MPA.0b013e3181c15963 (2010).

140 Gadaleta, E. *et al.* A global insight into a cancer transcriptional space using pancreatic data: importance, findings and flaws. *Nucleic Acids Res* **39**, 7900-7907, doi:10.1093/nar/gkr533 (2011).

141 Gillet, J. P., Varma, S. & Gottesman, M. M. The clinical relevance of cancer cell lines. *J Natl Cancer Inst* **105**, 452-458, doi:10.1093/jnci/djt007 (2013).

142 Ito, M. *et al.* NOD/SCID/gamma(c)(null) mouse: an excellent recipient mouse model for engraftment of human cells. *Blood* **100**, 3175-3182, doi:10.1182/blood-2001-12-0207 (2002).

143 Fu, X., Guadagni, F. & Hoffman, R. M. A metastatic nude-mouse model of human pancreatic cancer constructed orthotopically with histologically intact patient specimens. *Proc Natl Acad Sci U S A* **89**, 5645-5649, doi:10.1073/pnas.89.12.5645 (1992).

144 Loukopoulos, P. *et al.* Orthotopic transplantation models of pancreatic adenocarcinoma derived from cell lines and primary tumors and displaying varying metastatic activity. *Pancreas* **29**, 193-203, doi:10.1097/00006676-200410000-00004 (2004).

145 Rubio-Viqueira, B. *et al.* An in vivo platform for translational drug development in pancreatic cancer. *Clin Cancer Res* **12**, 4652-4661, doi:10.1158/1078-0432.Ccr-06-0113 (2006).

146 Tentler, J. J. *et al.* Patient-derived tumour xenografts as models for oncology drug development. *Nat Rev Clin Oncol* **9**, 338-350, doi:10.1038/nrclinonc.2012.61 (2012).

147 Yachida, S. *et al.* Distant metastasis occurs late during the genetic evolution of pancreatic cancer. *Nature* **467**, 1114-1117, doi:10.1038/nature09515 (2010).

148 Hidalgo, M. *et al.* A pilot clinical study of treatment guided by personalized tumorgrafts in patients with advanced cancer. *Mol Cancer Ther* **10**, 1311-1316, doi:10.1158/1535-7163.MCT-11-0233 (2011).

149 Garber, K. From human to mouse and back: 'tumorgraft' models surge in popularity. *J Natl Cancer Inst* **101**, 6-8, doi:10.1093/jnci/djn481 (2009).

150 Rajeshkumar, N. V. *et al.* MK-1775, a potent Wee1 inhibitor, synergizes with gemcitabine to achieve tumor regressions, selectively in p53-deficient pancreatic cancer xenografts. *Clin Cancer Res* **17**, 2799-2806, doi:10.1158/1078-0432.CCR-10-2580 (2011).

151 Hidalgo, M. *et al.* Patient-derived xenograft models: an emerging platform for translational cancer research. *Cancer Discov* **4**, 998-1013, doi:10.1158/2159-8290.CD-14-0001 (2014).

152 Huijbers, I. J. Generating Genetically Modified Mice: A Decision Guide. *Methods Mol Biol* **1642**, 1-19, doi:10.1007/978-1-4939-7169-5_1 (2017).

153 Aguirre, A. J. *et al.* Activated Kras and Ink4a/Arf deficiency cooperate to produce metastatic pancreatic ductal adenocarcinoma. *Genes Dev* **17**, 3112-3126, doi:10.1101/gad.1158703 (2003).

154 Hingorani, S. R. *et al.* Preinvasive and invasive ductal pancreatic cancer and its early detection in the mouse. *Cancer Cell* **4**, 437-450, doi:10.1016/s1535-6108(03)00309-x (2003).

155 Garcia, P. L., Miller, A. L. & Yoon, K. J. Patient-Derived Xenograft Models of Pancreatic Cancer: Overview and Comparison with Other Types of Models. *Cancers (Basel)* **12**, doi:10.3390/cancers12051327 (2020).

156 Hingorani, S. R. *et al.* Trp53R172H and KrasG12D cooperate to promote chromosomal instability and widely metastatic pancreatic ductal adenocarcinoma in mice. *Cancer Cell* **7**, 469-483, doi:10.1016/j.ccr.2005.04.023 (2005).

157 Stopczynski, R. E. *et al.* Neuroplastic changes occur early in the development of pancreatic ductal adenocarcinoma. *Cancer Res* **74**, 1718-1727, doi:10.1158/0008-5472.CAN-13-2050 (2014).

158 Gilabert, M. *et al.* Pancreatic cancer-induced cachexia is Jak2-dependent in mice. *J Cell Physiol* **229**, 1437-1443, doi:10.1002/jcp.24580 (2014).

159 Olive, K. P. *et al.* Inhibition of Hedgehog signaling enhances delivery of chemotherapy in a mouse model of pancreatic cancer. *Science* **324**, 1457-1461, doi:10.1126/science.1171362 (2009).

160 Erkan, M. *et al.* Cancer-stellate cell interactions perpetuate the hypoxia-fibrosis cycle in pancreatic ductal adenocarcinoma. *Neoplasia* **11**, 497-508, doi:10.1593/neo.81618 (2009).

161 Jacobetz, M. A. *et al.* Hyaluronan impairs vascular function and drug delivery in a mouse model of pancreatic cancer. *Gut* **62**, 112-120, doi:10.1136/gutjnl-2012-302529 (2013).

162 Menon, R. *et al.* Identification of novel alternative splice isoforms of circulating proteins in a mouse model of human pancreatic cancer. *Cancer Res* **69**, 300-309, doi:10.1158/0008-5472.CAN-08-2145 (2009).

163 Melo, S. A. *et al.* Glypican-1 identifies cancer exosomes and detects early pancreatic cancer. *Nature* **523**, 177-182, doi:10.1038/nature14581 (2015).

164 Alagesan, B. *et al.* Combined MEK and PI3K inhibition in a mouse model of pancreatic cancer. *Clin Cancer Res* **21**, 396-404, doi:10.1158/1078-0432.Ccr-14-1591 (2015).

165 Drosten, M., Guerra, C. & Barbacid, M. Genetically Engineered Mouse Models of K-Ras-Driven Lung and Pancreatic Tumors: Validation of Therapeutic Targets. *Cold Spring Harb Perspect Med* **8**, doi:10.1101/cshperspect.a031542 (2018).

166 Krempley, B. D. & Yu, K. H. Preclinical models of pancreatic ductal adenocarcinoma. *Chin Clin Oncol* **6**, 25, doi:10.21037/cco.2017.06.15 (2017).

167 Wang, Y., Tseng, J. C., Sun, Y., Beck, A. H. & Kung, A. L. Noninvasive imaging of tumor burden and molecular pathways in mouse models of cancer. *Cold Spring Harb Protoc* **2015**, 135-144, doi:10.1101/pdb.top069930 (2015).

168 Becher, O. J. & Holland, E. C. Genetically engineered models have advantages over xenografts for preclinical studies. *Cancer Res* **66**, 3355-3358, discussion 3358-3359, doi:10.1158/0008-5472.CAN-05-3827 (2006).

169 Artandi, S. E. *et al.* Telomere dysfunction promotes non-reciprocal translocations and epithelial cancers in mice. *Nature* **406**, 641-645, doi:10.1038/35020592 (2000).

170 Zschenker, O., Streichert, T., Hehlgans, S. & Cordes, N. Genome-wide gene expression analysis in cancer cells reveals 3D growth to affect ECM and processes associated with cell adhesion but not DNA repair. *PLoS One* **7**, e34279, doi:10.1371/journal.pone.0034279 (2012).

171 Edmondson, R., Broglie, J. J., Adcock, A. F. & Yang, L. Three-dimensional cell culture systems and their applications in drug discovery and cell-based biosensors. *Assay Drug Dev Technol* **12**, 207-218, doi:10.1089/adt.2014.573 (2014).

172 Serebriiskii, I., Castello-Cros, R., Lamb, A., Golemis, E. A. & Cukierman, E. Fibroblast-derived 3D matrix differentially regulates the growth and drug-responsiveness of human cancer cells. *Matrix Biol* **27**, 573-585, doi:10.1016/j.matbio.2008.02.008 (2008).

173 Huch, M. & Koo, B. K. Modeling mouse and human development using organoid cultures. *Development* **142**, 3113-3125, doi:10.1242/dev.118570 (2015).

174 Lei, Y., Jeong, D., Xiao, J. & Schaffer, D. V. Developing Defined and Scalable 3D Culture Systems for Culturing Human Pluripotent Stem Cells at High Densities. *Cell Mol Bioeng* **7**, 172-183, doi:10.1007/s12195-014-0333-z (2014).

175 Sato, T. *et al.* Single Lgr5 stem cells build crypt-villus structures in vitro without a mesenchymal niche. *Nature* **459**, 262-265, doi:10.1038/nature07935 (2009).

176 Drost, J. & Clevers, H. Organoids in cancer research. *Nat Rev Cancer* **18**, 407-418, doi:10.1038/s41568-018-0007-6 (2018).

177 Ware, M. J. *et al.* Generation of an in vitro 3D PDAC stroma rich spheroid model. *Biomaterials* **108**, 129-142, doi:10.1016/j.biomaterials.2016.08.041 (2016).

178 Caliari, S. R. & Burdick, J. A. A practical guide to hydrogels for cell culture. *Nat Methods* **13**, 405-414, doi:10.1038/nmeth.3839 (2016).

179 Boj, S. F. *et al.* Organoid models of human and mouse ductal pancreatic cancer. *Cell* **160**, 324-338, doi:10.1016/j.cell.2014.12.021 (2015).

180 Seino, T. *et al.* Human Pancreatic Tumor Organoids Reveal Loss of Stem Cell Niche Factor Dependence during Disease Progression. *Cell Stem Cell* **22**, 454-467 e456, doi:10.1016/j.stem.2017.12.009 (2018).

181 Tiriac, H. *et al.* Organoid Profiling Identifies Common Responders to Chemotherapy in Pancreatic Cancer. *Cancer Discov* **8**, 1112-1129, doi:10.1158/2159-8290.CD-18-0349 (2018).

182 Eisen, C. Development and investigation of a novel model system representing all three subtypes of pancreatic ductal adenocarcinoma reveals novel biomarkers and distinct drug sensitivities. *Doctor of Natural Sciences thesis, Ruperto-Carola University of Heidelberg* (2012).

183 Noll, E. M. *et al.* CYP3A5 mediates basal and acquired therapy resistance in different subtypes of pancreatic ductal adenocarcinoma. *Nat Med* **22**, 278-287, doi:10.1038/nm.4038 (2016).

184 Uhlen, M. *et al.* Towards a knowledge-based Human Protein Atlas. *Nat Biotechnol* **28**, 1248-1250, doi:10.1038/nbt1210-1248 (2010).

185 Holohan, C., Van Schaeybroeck, S., Longley, D. B. & Johnston, P. G. Cancer drug resistance: an evolving paradigm. *Nat Rev Cancer* **13**, 714-726, doi:10.1038/nrc3599 (2013).

186 Burrell, R. A. & Swanton, C. Tumour heterogeneity and the evolution of polyclonal drug resistance. *Mol Oncol* **8**, 1095-1111, doi:10.1016/j.molonc.2014.06.005 (2014).

187 Goldie, J. H. & Coldman, A. J. A mathematic model for relating the drug sensitivity of tumors to their spontaneous mutation rate. *Cancer Treat Rep* **63**, 1727-1733 (1979).

188 Goldie, J. H. & Coldman, A. J. The genetic origin of drug resistance in neoplasms: implications for systemic therapy. *Cancer Res* **44**, 3643-3653 (1984).

189 Vasan, N., Baselga, J. & Hyman, D. M. A view on drug resistance in cancer. *Nature* **575**, 299-309, doi:10.1038/s41586-019-1730-1 (2019).

190 Genovese, I., Ilari, A., Assaraf, Y. G., Fazi, F. & Colotti, G. Not only P-glycoprotein: Amplification of the ABCB1-containing chromosome region 7q21 confers multidrug resistance upon cancer cells by coordinated overexpression of an assortment of resistance-related proteins. *Drug Resist Updat* **32**, 23-46, doi:10.1016/j.drup.2017.10.003 (2017).

191 Turner, N. C. & Reis-Filho, J. S. Genetic heterogeneity and cancer drug resistance. *Lancet Oncol* **13**, e178-185, doi:10.1016/S1470-2045(11)70335-7 (2012).

192 Nowell, P. C. The clonal evolution of tumor cell populations. *Science* **194**, 23-28, doi:10.1126/science.959840 (1976).

193 Alexandrov, L. B. *et al.* Signatures of mutational processes in human cancer. *Nature* **500**, 415-421, doi:10.1038/nature12477 (2013).

194 Stephens, P. J. *et al.* Massive genomic rearrangement acquired in a single catastrophic event during cancer development. *Cell* **144**, 27-40, doi:10.1016/j.cell.2010.11.055 (2011).

195 McGranahan, N. & Swanton, C. Clonal Heterogeneity and Tumor Evolution: Past, Present, and the Future. *Cell* **168**, 613-628, doi:10.1016/j.cell.2017.01.018 (2017).

196 Fan, S. *et al.* p53 gene mutations are associated with decreased sensitivity of human lymphoma cells to DNA damaging agents. *Cancer Res* **54**, 5824-5830 (1994).

197 Kobayashi, S. *et al.* EGFR mutation and resistance of non-small-cell lung cancer to gefitinib. *N Engl J Med* **352**, 786-792, doi:10.1056/NEJMoa044238 (2005).

198 Bhowmick, N. A., Neilson, E. G. & Moses, H. L. Stromal fibroblasts in cancer initiation and progression. *Nature* **432**, 332-337, doi:10.1038/nature03096 (2004).

199 Shiao, S. L., Ganesan, A. P., Rugo, H. S. & Coussens, L. M. Immune microenvironments in solid tumors: new targets for therapy. *Genes Dev* **25**, 2559-2572, doi:10.1101/gad.169029.111 (2011).

200 Sharma, P., Hu-Lieskovan, S., Wargo, J. A. & Ribas, A. Primary, Adaptive, and Acquired Resistance to Cancer Immunotherapy. *Cell* **168**, 707-723, doi:10.1016/j.cell.2017.01.017 (2017).

201 Mazor, T., Pankov, A., Song, J. S. & Costello, J. F. Intratumoral Heterogeneity of the Epigenome. *Cancer Cell* **29**, 440-451, doi:10.1016/j.ccell.2016.03.009 (2016).

202 Maier, S., Dahlstroem, C., Haefliger, C., Plum, A. & Piepenbrock, C. Identifying DNA methylation biomarkers of cancer drug response. *Am J Pharmacogenomics* **5**, 223-232, doi:10.2165/00129785-200505040-00003 (2005).

203 Nebert, D. W. & Dalton, T. P. The role of cytochrome P450 enzymes in endogenous signalling pathways and environmental carcinogenesis. *Nat Rev Cancer* **6**, 947-960, doi:10.1038/nrc2015 (2006).

204 Sanchez-Dominguez, C. N., Gallardo-Blanco, H. L., Salinas-Santander, M. A. & Ortiz-Lopez, R. Uridine 5'-diphospho-glucronosyltrasferase: Its role in pharmacogenomics and human disease. *Exp Ther Med* **16**, 3-11, doi:10.3892/etm.2018.6184 (2018).

205 van Schaik, R. H. Cancer treatment and pharmacogenetics of cytochrome P450 enzymes. *Invest New Drugs* **23**, 513-522, doi:10.1007/s10637-005-4019-1 (2005).

206 Noll, E. M. CYP3A5 as Mediator of Drug Resistance in Different Subtypes of Pancreatic Ductal Adenocarcinoma. *Doctor of Natural Sciences thesis, Ruperto-Carola University of Heidelberg* (2016).

207 Choi, C. H. ABC transporters as multidrug resistance mechanisms and the development of chemosensitizers for their reversal. *Cancer Cell Int* **5**, 30, doi:10.1186/1475-2867-5-30 (2005).

208 Fletcher, J. I., Williams, R. T., Henderson, M. J., Norris, M. D. & Haber, M. ABC transporters as mediators of drug resistance and contributors to cancer cell biology. *Drug Resistance Updates* **26**, 1-9, doi:https://doi.org/10.1016/j.drup.2016.03.001 (2016).

209 Hyde, S. C. *et al.* Structural model of ATP-binding proteins associated with cystic fibrosis, multidrug resistance and bacterial transport. *Nature* **346**, 362-365, doi:10.1038/346362a0 (1990).

210 Ambudkar, S. V. *et al.* Biochemical, cellular, and pharmacological aspects of the multidrug transporter. *Annu Rev Pharmacol Toxicol* **39**, 361-398, doi:10.1146/annurev.pharmtox.39.1.361 (1999).

211 Ward, A., Reyes, C. L., Yu, J., Roth, C. B. & Chang, G. Flexibility in the ABC transporter MsbA: Alternating access with a twist. *Proc Natl Acad Sci U S A* **104**, 19005-19010, doi:10.1073/pnas.0709388104 (2007).

212 Gottesman, M. M., Fojo, T. & Bates, S. E. Multidrug resistance in cancer: role of ATP-dependent transporters. *Nat Rev Cancer* **2**, 48-58, doi:10.1038/nrc706 (2002).

213 Doyle, L. A. *et al.* A multidrug resistance transporter from human MCF-7 breast cancer cells. *Proc Natl Acad Sci U S A* **95**, 15665-15670, doi:10.1073/pnas.95.26.15665 (1998).

214 Robey, R. W. *et al.* Inhibition of ABCG2-mediated transport by protein kinase inhibitors with a bisindolylmaleimide or indolocarbazole structure. *Mol Cancer Ther* **6**, 1877-1885, doi:10.1158/1535-7163.MCT-06-0811 (2007).

215 Amiri-Kordestani, L., Basseville, A., Kurdziel, K., Fojo, A. T. & Bates, S. E. Targeting MDR in breast and lung cancer: discriminating its potential importance from the failure of drug resistance reversal studies. *Drug Resist Updat* **15**, 50-61, doi:10.1016/j.drup.2012.02.002 (2012).

216 Nooter, K. *et al.* The prognostic significance of expression of the multidrug resistance-associated protein (MRP) in primary breast cancer. *Br J Cancer* **76**, 486-493, doi:10.1038/bjc.1997.414 (1997).

217 Zalcberg, J. *et al.* MRP1 not MDR1 gene expression is the predominant mechanism of acquired multidrug resistance in two prostate carcinoma cell lines. *Prostate Cancer Prostatic Dis* **3**, 66-75, doi:10.1038/sj.pcan.4500394 (2000).

218 Konig, J. *et al.* Expression and localization of human multidrug resistance protein (ABCC) family members in pancreatic carcinoma. *Int J Cancer* **115**, 359-367, doi:10.1002/ijc.20831 (2005).

219 Scheffer, G. L. *et al.* Tissue distribution and induction of human multidrug resistant protein 3. *Lab Invest* **82**, 193-201, doi:10.1038/labinvest.3780411 (2002).

220 Hagmann, W., Jesnowski, R., Faissner, R., Guo, C. & Lohr, J. M. ATP-binding cassette C transporters in human pancreatic carcinoma cell lines. Upregulation in 5-fluorouracil-resistant cells. *Pancreatology* **9**, 136-144, doi:10.1159/000178884 (2009).

221 Schinkel, A. H. P-Glycoprotein, a gatekeeper in the blood-brain barrier. *Adv Drug Deliv Rev* **36**, 179-194, doi:10.1016/s0169-409x(98)00085-4 (1999).

222 Sharom, F. J. ABC multidrug transporters: structure, function and role in chemoresistance. *Pharmacogenomics* **9**, 105-127, doi:10.2217/14622416.9.1.105 (2008).

223 Sharom, F. J. The P-glycoprotein multidrug transporter. *Essays Biochem* **50**, 161-178, doi:10.1042/bse0500161 (2011).

224 Silva, R. *et al.* Modulation of P-glycoprotein efflux pump: induction and activation as a therapeutic strategy. *Pharmacol Ther* **149**, 1-123, doi:10.1016/j.pharmthera.2014.11.013 (2015).

225 Juliano, R. L. & Ling, V. A surface glycoprotein modulating drug permeability in Chinese hamster ovary cell mutants. *Biochim Biophys Acta* **455**, 152-162, doi:10.1016/0005-2736(76)90160-7 (1976).

226 Ueda, K., Cardarelli, C., Gottesman, M. M. & Pastan, I. Expression of a full-length cDNA for the human "MDR1" gene confers resistance to colchicine, doxorubicin, and vinblastine. *Proc Natl Acad Sci U S A* **84**, 3004-3008, doi:10.1073/pnas.84.9.3004 (1987).

227 Assaraf, Y. G., Molina, A. & Schimke, R. T. Cross-resistance to the lipid-soluble antifolate trimetrexate in human carcinoma cells with the multidrug-resistant phenotype. *J Natl Cancer Inst* **81**, 290-294, doi:10.1093/jnci/81.4.290 (1989).

228 Assaraf, Y. G., Molina, A. & Schimke, R. T. Sequential amplification of dihydrofolate reductase and multidrug resistance genes in Chinese hamster ovary cells selected for stepwise resistance to the lipid-soluble antifolate trimetrexate. *J Biol Chem* **264**, 18326-18334 (1989).

229 Goldstein, L. J. *et al.* Expression of a multidrug resistance gene in human cancers. *J Natl Cancer Inst* **81**, 116-124, doi:10.1093/jnci/81.2.116 (1989).

230 Gottesman, M. M., Goldstein, L. J., Fojo, A., Galski, H. & Pastan, I. in *Molecular and Cellular Biology of Multidrug Resistance in Tumor Cells* (ed Igor B. Roninson) 291-301 (Springer US, 1991).

231 Broxterman, H. J. *et al.* Do P-glycoprotein and major vault protein (MVP/LRP) expression correlate with in vitro daunorubicin resistance in acute myeloid leukemia? *Leukemia* **13**, 258-265, doi:10.1038/sj.leu.2401331 (1999).

232 Dorr, R. *et al.* Phase I/II study of the P-glycoprotein modulator PSC 833 in patients with acute myeloid leukemia. *J Clin Oncol* **19**, 1589-1599, doi:10.1200/JCO.2001.19.6.1589 (2001).

233 Chan, H. S., Grogan, T. M., Haddad, G., DeBoer, G. & Ling, V. P-glycoprotein expression: critical determinant in the response to osteosarcoma chemotherapy. *J Natl Cancer Inst* **89**, 1706-1715, doi:10.1093/jnci/89.22.1706 (1997).

234 Burger, H. *et al.* RNA Expression of Breast Cancer Resistance Protein, Lung Resistance-related Protein, Multidrug Resistance-associated Proteins 1 and 2, and Multidrug Resistance Gene 1 in Breast Cancer. *Correlation with Chemotherapeutic Response* **9**, 827-836 (2003).

235 Abe, T. *et al.* Expression of multidrug resistance protein gene in patients with glioma after chemotherapy. *J Neurooncol* **40**, 11-18, doi:10.1023/a:1005954406809 (1998).

236 Tada, Y. *et al.* Increased expression of multidrug resistance-associated proteins in bladder cancer during clinical course and drug resistance to doxorubicin. *Int J Cancer* **98**, 630-635, doi:10.1002/ijc.10246 (2002).

237 Zee, A. G. v. d. *et al.* Value of P-glycoprotein, glutathione S-transferase pi, c-erbB-2, and p53 as prognostic factors in ovarian carcinomas. *Journal of Clinical Oncology* **13**, 70-78, doi:10.1200/jco.1995.13.1.70 (1995).

238 Didziapetris, R., Japertas, P., Avdeef, A. & Petrauskas, A. Classification analysis of P-glycoprotein substrate specificity. *J Drug Target* **11**, 391-406, doi:10.1080/10611860310001648248 (2003).

239 Esser, L. *et al.* Structures of the Multidrug Transporter P-glycoprotein Reveal Asymmetric ATP Binding and the Mechanism of Polyspecificity. *J Biol Chem* **292**, 446-461, doi:10.1074/jbc.M116.755884 (2017).

240 Morrissey, K. M. *et al.* The UCSF-FDA TransPortal: a public drug transporter database. *Clin Pharmacol Ther* **92**, 545-546, doi:10.1038/clpt.2012.44 (2012).

241 Cascorbi, I. Role of pharmacogenetics of ATP-binding cassette transporters in the pharmacokinetics of drugs. *Pharmacol Ther* **112**, 457-473, doi:10.1016/j.pharmthera.2006.04.009 (2006).

242 Miller, T. P. *et al.* P-glycoprotein expression in malignant lymphoma and reversal of clinical drug resistance with chemotherapy plus high-dose verapamil. *J Clin Oncol* **9**, 17-24, doi:10.1200/JCO.1991.9.1.17 (1991).

243 Advani, R. *et al.* A phase I trial of doxorubicin, paclitaxel, and valspodar (PSC 833), a modulator of multidrug resistance. *Clin Cancer Res* **7**, 1221-1229 (2001).

244 Advani, R. *et al.* A phase I trial of liposomal doxorubicin, paclitaxel and valspodar (PSC-833), an inhibitor of multidrug resistance. *Ann Oncol* **16**, 1968-1973, doi:10.1093/annonc/mdi396 (2005).

245 Coley, H. M. Overcoming multidrug resistance in cancer: clinical studies of p-glycoprotein inhibitors. *Methods Mol Biol* **596**, 341-358, doi:10.1007/978-1-60761-416-6_15 (2010).

246 Dorner, B. *et al.* Synthesis and small-animal positron emission tomography evaluation of [11C]-elacridar as a radiotracer to assess the distribution of P-glycoprotein at the blood-brain barrier. *J Med Chem* **52**, 6073-6082, doi:10.1021/jm900940f (2009).

247 Kemper, E. M., Cleypool, C., Boogerd, W., Beijnen, J. H. & van Tellingen, O. The influence of the P-glycoprotein inhibitor zosuquidar trihydrochloride (LY335979) on the brain penetration of paclitaxel in mice. *Cancer Chemother Pharmacol* **53**, 173-178, doi:10.1007/s00280-003-0720-y (2004).

248 Weidner, L. D. *et al.* Tariquidar Is an Inhibitor and Not a Substrate of Human and Mouse P-glycoprotein. *Drug Metab Dispos* **44**, 275-282, doi:10.1124/dmd.115.067785 (2016).

249 Akhtar, N. *et al.* The emerging role of P-glycoprotein inhibitors in drug delivery: a patent review. *Expert Opin Ther Pat* **21**, 561-576, doi:10.1517/13543776.2011.561784 (2011).

250 Pusztai, L. *et al.* Phase II study of tariquidar, a selective P-glycoprotein inhibitor, in patients with chemotherapy-resistant, advanced breast carcinoma. *Cancer* **104**, 682-691, doi:10.1002/cncr.21227 (2005).

251 Ruff, P. *et al.* A randomized, placebo-controlled, double-blind phase 2 study of docetaxel compared to docetaxel plus zosuquidar (LY335979) in women with metastatic or locally recurrent breast cancer who have received one prior chemotherapy regimen. *Cancer Chemother Pharmacol* **64**, 763-768, doi:10.1007/s00280-009-0925-9 (2009).

252 Cripe, L. D. *et al.* Zosuquidar, a novel modulator of P-glycoprotein, does not improve the outcome of older patients with newly diagnosed acute myeloid leukemia: a randomized, placebo-controlled trial of the Eastern Cooperative Oncology Group 3999. *Blood* **116**, 4077-4085, doi:10.1182/blood-2010-04-277269 (2010).

253 Callaghan, R., Crowley, E., Potter, S. & Kerr, I. D. P-glycoprotein: so many ways to turn it on. *J Clin Pharmacol* **48**, 365-378, doi:10.1177/0091270007311568 (2008).

254 Chin, K. V., Tanaka, S., Darlington, G., Pastan, I. & Gottesman, M. M. Heat shock and arsenite increase expression of the multidrug resistance (MDR1) gene in human renal carcinoma cells. *J Biol Chem* **265**, 221-226 (1990).

255 Kim, S. H. *et al.* Involvement of heat shock factor in regulating transcriptional activation of MDR1 gene in multidrug-resistant cells. *Cancer Lett* **115**, 9-14, doi:10.1016/s0304-3835(97)04725-3 (1997).

256 Scotto, K. W. Transcriptional regulation of ABC drug transporters. *Oncogene* **22**, 7496-7511, doi:10.1038/sj.onc.1206950 (2003).

257 Nakatsukasa, H., Silverman, J. A., Gant, T. W., Evarts, R. P. & Thorgeirsson, S. S. Expression of multidrug resistance genes in rat liver during regeneration and after carbon tetrachloride intoxication. *Hepatology* **18**, 1202-1207 (1993).

258 Abolhoda, A. *et al.* Rapid activation of MDR1 gene expression in human metastatic sarcoma after in vivo exposure to doxorubicin. *Clin Cancer Res* **5**, 3352-3356 (1999).

259 Nwaozuzu, O. M., Sellers, L. A. & Barrand, M. A. Signalling pathways influencing basal and H(2)O(2)-induced P-glycoprotein expression in endothelial cells derived from the blood-brain barrier. *J Neurochem* **87**, 1043-1051, doi:10.1046/j.1471-4159.2003.02061.x (2003).

260 Vilaboa, N. E., Galan, A., Troyano, A., de Blas, E. & Aller, P. Regulation of multidrug resistance 1 (MDR1)/P-glycoprotein gene expression and activity by heat-shock transcription factor 1 (HSF1). *J Biol Chem* **275**, 24970-24976, doi:10.1074/jbc.M909136199 (2000).

261 Corna, G., Santambrogio, P., Minotti, G. & Cairo, G. Doxorubicin paradoxically protects cardiomyocytes against iron-mediated toxicity: role of reactive oxygen species and ferritin. *J Biol Chem* **279**, 13738-13745, doi:10.1074/jbc.M310106200 (2004).

262 Synold, T. W., Dussault, I. & Forman, B. M. The orphan nuclear receptor SXR coordinately regulates drug metabolism and efflux. *Nat Med* **7**, 584-590, doi:10.1038/87912 (2001).

263 Jin, W., Scotto, K. W., Hait, W. N. & Yang, J. M. Involvement of CtBP1 in the transcriptional activation of the MDR1 gene in human multidrug resistant cancer cells. *Biochem Pharmacol* **74**, 851-859, doi:10.1016/j.bcp.2007.06.017 (2007).

264 Arrigoni, E., Galimberti, S., Petrini, M., Danesi, R. & Di Paolo, A. ATP-binding cassette transmembrane transporters and their epigenetic control in cancer: an overview. *Expert Opin Drug Metab Toxicol* **12**, 1419-1432, doi:10.1080/17425255.2016.1215423 (2016).

265 Dejeux, E. *et al.* DNA methylation profiling in doxorubicin treated primary locally advanced breast tumours identifies novel genes associated with survival and treatment response. *Mol Cancer* **9**, 68, doi:10.1186/1476-4598-9-68 (2010).

266 Mencalha, A. L., Rodrigues, E. F., Abdelhay, E. & Fernandez, T. S. Accurate monitoring of promoter gene methylation with high-resolution melting polymerase chain reaction using the ABCB1 gene as a model. *Genet Mol Res* **12**, 714-722, doi:10.4238/2013.March.11.20 (2013).

267 Reed, K., Hembruff, S. L., Sprowl, J. A. & Parissenti, A. M. The temporal relationship between ABCB1 promoter hypomethylation, ABCB1 expression and acquisition of drug resistance. *Pharmacogenomics J* **10**, 489-504, doi:10.1038/tpj.2010.1 (2010).

268 Nakayama, M. *et al.* Hypomethylation status of CpG sites at the promoter region and overexpression of the human MDR1 gene in acute myeloid leukemias. *Blood* **92**, 4296-4307 (1998).

269 Tada, Y. *et al.* MDR1 gene overexpression and altered degree of methylation at the promoter region in bladder cancer during chemotherapeutic treatment. *Clin Cancer Res* **6**, 4618-4627 (2000).

270 Flahaut, M. *et al.* Molecular cytogenetic characterization of doxorubicin-resistant neuroblastoma cell lines: evidence that acquired multidrug resistance results from a unique large amplification of the 7q21 region. *Genes Chromosomes Cancer* **45**, 495-508, doi:10.1002/gcc.20312 (2006).

271 Kitada, K. & Yamasaki, T. The MDR1/ABCB1 regional amplification in large inverted repeats with asymmetric sequences and microhomologies at the junction sites. *Cancer Genet Cytogenet* **178**, 120-127, doi:10.1016/j.cancergencyto.2007.06.014 (2007).

272 Kadioglu, O. & Efferth, T. Peptide aptamer identified by molecular docking targeting translationally controlled tumor protein in leukemia cells. *Investigational New Drugs* **34**, 515-521, doi:10.1007/s10637-016-0339-6 (2016).

273 Duesberg, P. *et al.* Cancer drug resistance: the central role of the karyotype. *Drug Resist Updat* **10**, 51-58, doi:10.1016/j.drup.2007.02.003 (2007).

274 Kim, I. W., Han, N., Kim, M. G., Kim, T. & Oh, J. M. Copy number variability analysis of pharmacogenes in patients with lymphoma, leukemia, hepatocellular, and lung carcinoma using The Cancer Genome Atlas data. *Pharmacogenet Genomics* **25**, 1-7, doi:10.1097/FPC.0000000000000097 (2015).

275 Yabuki, N. *et al.* Gene amplification and expression in lung cancer cells with acquired paclitaxel resistance. *Cancer Genet Cytogenet* **173**, 1-9, doi:10.1016/j.cancergencyto.2006.07.020 (2007).

276 Wang, Y. C. *et al.* Regional activation of chromosomal arm 7q with and without gene amplification in taxane-selected human ovarian cancer cell lines. *Genes Chromosomes Cancer* **45**, 365-374, doi:10.1002/gcc.20300 (2006).

277 Hansen, S. N. *et al.* The stepwise evolution of the exome during acquisition of docetaxel resistance in breast cancer cells. *BMC Genomics* **17**, 442, doi:10.1186/s12864-016-2749-4 (2016).

278 Chao, C. C., Ma, C. M. & Lin-Chao, S. Co-amplification and over-expression of two mdr genes in a multidrug-resistant human colon carcinoma cell line. *FEBS Lett* **291**, 214-218, doi:10.1016/0014-5793(91)81287-i (1991).

279 Lee, S. *et al.* Analysis of resistance-associated gene expression in docetaxel-resistant prostate cancer cells. *Oncol Lett* **14**, 3011-3018, doi:10.3892/ol.2017.6541 (2017).

280 Litviakov, N. V. *et al.* Deletions of multidrug resistance gene loci in breast cancer leads to the down-regulation of its expression and predict tumor response to neoadjuvant chemotherapy. *Oncotarget* **7** (2016).

281 Patch, A. M. *et al.* Whole-genome characterization of chemoresistant ovarian cancer. *Nature* **521**, 489-494, doi:10.1038/nature14410 (2015).

282 Torigoe, K. *et al.* A YAC-based contig of 1.5 Mb spanning the human multidrug resistance gene region and delineating the amplification unit in three human multidrug-resistant cell lines. *Genome Res* **5**, 233-244, doi:10.1101/gr.5.3.233 (1995).

283 Van der Bliek, A. M. *et al.* Genes amplified and overexpressed in human multidrug-resistant cell lines. *Cancer Res* **48**, 5927-5932 (1988).

284 Hotta, Y. & Bassel, A. MOLECULAR SIZE AND CIRCULARITY OF DNA IN CELLS OF MAMMALS AND HIGHER PLANTS. *Proceedings of the National Academy of Sciences* **53**, 356-362, doi:10.1073/pnas.53.2.356 (1965).

285 Cox, D., Yuncken, C. & Spriggs, A. I. Minute Chromatin Bodies in Malignant Tumours of Childhood. *Lancet* **1**, 55-58, doi:10.1016/s0140-6736(65)90131-5 (1965).

286 Schimke, R. T. Gene amplification in cultured animal cells. *Cell* **37**, 705-713, doi:10.1016/0092-8674(84)90406-9 (1984).

287 Stark, G. R., Debatisse, M., Giulotto, E. & Wahl, G. M. Recent progress in understanding mechanisms of mammalian DNA amplification. *Cell* **57**, 901-908, doi:10.1016/0092-8674(89)90328-0 (1989).

288 Kim, H. *et al.* Extrachromosomal DNA is associated with oncogene amplification and poor outcome across multiple cancers. *Nat Genet* **52**, 891-897, doi:10.1038/s41588-020-0678-2 (2020).

289 Paulsen, T., Kumar, P., Koseoglu, M. M. & Dutta, A. Discoveries of Extrachromosomal Circles of DNA in Normal and Tumor Cells. *Trends Genet* **34**, 270-278, doi:10.1016/j.tig.2017.12.010 (2018).

290 Turner, K. M. *et al.* Extrachromosomal oncogene amplification drives tumour evolution and genetic heterogeneity. *Nature* **543**, 122-125, doi:10.1038/nature21356 (2017).

291 Shibata, Y. *et al.* Extrachromosomal microDNAs and chromosomal microdeletions in normal tissues. *Science* **336**, 82-86, doi:10.1126/science.1213307 (2012).

292 Haber, D. A. & Schimke, R. T. Unstable amplification of an altered dihydrofolate reductase gene associated with double-minute chromosomes. *Cell* **26**, 355-362, doi:10.1016/0092-8674(81)90204-x (1981).

293 Alt, F. W., Kellems, R. E., Bertino, J. R. & Schimke, R. T. Selective multiplication of dihydrofolate reductase genes in methotrexate-resistant variants of cultured murine cells. *J Biol Chem* **253**, 1357-1370 (1978).

294 Alitalo, K., Schwab, M., Lin, C. C., Varmus, H. E. & Bishop, J. M. Homogeneously staining chromosomal regions contain amplified copies of an abundantly expressed cellular oncogene (c-myc) in malignant neuroendocrine cells from a human colon carcinoma. *Proc Natl Acad Sci U S A* **80**, 1707-1711, doi:10.1073/pnas.80.6.1707 (1983).

295 Kohl, N. E. *et al.* Transposition and amplification of oncogene-related sequences in human neuroblastomas. *Cell* **35**, 359-367, doi:10.1016/0092-8674(83)90169-1 (1983).

296 Ruiz, J. C., Choi, K. H., von Hoff, D. D., Roninson, I. B. & Wahl, G. M. Autonomously replicating episomes contain mdr1 genes in a multidrug-resistant human cell line. *Mol Cell Biol* **9**, 109-115, doi:10.1128/mcb.9.1.109 (1989).

297 Carroll, S. M. *et al.* Double minute chromosomes can be produced from precursors derived from a chromosomal deletion. *Mol Cell Biol* **8**, 1525-1533, doi:10.1128/mcb.8.4.1525 (1988).

298 Von Hoff, D. D. *et al.* Elimination of extrachromosomally amplified MYC genes from human tumor cells reduces their tumorigenicity. *Proc Natl Acad Sci U S A* **89**, 8165-8169, doi:10.1073/pnas.89.17.8165 (1992).

299 Nathanson, D. A. *et al.* Targeted therapy resistance mediated by dynamic regulation of extrachromosomal mutant EGFR DNA. *Science* **343**, 72-76, doi:10.1126/science.1241328 (2014).

300 deCarvalho, A. C. *et al.* Discordant inheritance of chromosomal and extrachromosomal DNA elements contributes to dynamic disease evolution in glioblastoma. *Nat Genet* **50**, 708-717, doi:10.1038/s41588-018-0105-0 (2018).

301 Ly, P. *et al.* Chromosome segregation errors generate a diverse spectrum of simple and complex genomic rearrangements. *Nat Genet* **51**, 705-715, doi:10.1038/s41588-019-0360-8 (2019).

302 Sunnerhagen, P., SjÖberg, R.-M., Karlsson, A.-L., Lundh, L. & Bjursell, G. Molecular cloning and characterization of small polydisperse circular DNA from mouse 3T6 cells. *Nucleic Acids Research* **14**, 7823-7838, doi:10.1093/nar/14.20.7823 (1986).

303 Cohen, S. & Mechali, M. A novel cell-free system reveals a mechanism of circular DNA formation from tandem repeats. *Nucleic Acids Research* **29**, 2542-2548, doi:10.1093/nar/29.12.2542 (2001).

304 Levan, A. & Levan, G. Have double minutes functioning centromeres? *Hereditas* **88**, 81-92, doi:10.1111/j.1601-5223.1978.tb01606.x (1978).

305 Nikolaev, S. *et al.* Extrachromosomal driver mutations in glioblastoma and low-grade glioma. *Nature Communications* **5**, 5690, doi:10.1038/ncomms6690 (2014).

306 Xue, Y. *et al.* An approach to suppress the evolution of resistance in BRAF(V600E)-mutant cancer. *Nat Med* **23**, 929-937, doi:10.1038/nm.4369 (2017).

307 Pichugin, Y., Huang, W. & Werner, B. (bioRxiv, 2019).

308 Koche, R. P. *et al.* Extrachromosomal circular DNA drives oncogenic genome remodeling in neuroblastoma. *Nat Genet* **52**, 29-34, doi:10.1038/s41588-019-0547-z (2020).

309 Wu, S. *et al.* Circular ecDNA promotes accessible chromatin and high oncogene expression. *Nature* **575**, 699-703, doi:10.1038/s41586-019-1763-5 (2019).

310 Morton, A. R. *et al.* Functional Enhancers Shape Extrachromosomal Oncogene Amplifications. *Cell* **179**, 1330-1341 e1313, doi:10.1016/j.cell.2019.10.039 (2019).

311 Verhaak, R. G. W., Bafna, V. & Mischel, P. S. Extrachromosomal oncogene amplification in tumour pathogenesis and evolution. *Nature Reviews Cancer* **19**, 283-288, doi:10.1038/s41568-019-0128-6 (2019).

312 Prabhu, L., Mundade, R., Korc, M., Loehrer, P. J. & Lu, T. Critical role of NF-kappaB in pancreatic cancer. *Oncotarget* **5**, 10969-10975, doi:10.18632/oncotarget.2624 (2014).

313 Hayashi, A. *et al.* A unifying paradigm for transcriptional heterogeneity and squamous features in pancreatic ductal adenocarcinoma. *Nature Cancer* **1**, 59-74, doi:10.1038/s43018-019-0010-1 (2020).

314 Weaver, B. A. How Taxol/paclitaxel kills cancer cells. *Mol Biol Cell* **25**, 2677-2681, doi:10.1091/mbc.E14-04-0916 (2014).

315 Haschka, M., Karbon, G., Fava, L. L. & Villunger, A. Perturbing mitosis for anti-cancer therapy: is cell death the only answer? *EMBO Rep* **19**, doi:10.15252/embr.201745440 (2018).

316 Pors, K. & Patterson, L. H. DNA mismatch repair deficiency, resistance to cancer chemotherapy and the development of hypersensitive agents. *Curr Top Med Chem* **5**, 1133-1149, doi:10.2174/156802605774370883 (2005).

317 Russo, M. *et al.* Adaptive mutability of colorectal cancers in response to targeted therapies. *Science* **366**, 1473-1480, doi:10.1126/science.aav4474 (2019).

318 Lolodi, O., Wang, Y. M., Wright, W. C. & Chen, T. Differential Regulation of CYP3A4 and CYP3A5 and its Implication in Drug Discovery. *Curr Drug Metab* **18**, 1095-1105, doi:10.2174/1389200218666170531112038 (2017).

319 Chen, Y. *et al.* Nuclear receptors in the multidrug resistance through the regulation of drug-metabolizing enzymes and drug transporters. *Biochem Pharmacol* **83**, 1112-1126, doi:10.1016/j.bcp.2012.01.030 (2012).

320 Shiotani, B. & Zou, L. ATR signaling at a glance. *Journal of Cell Science* **122**, 301-304, doi:10.1242/jcs.035105 (2009).

321 Aiderus, A., Black, M. A. & Dunbier, A. K. Fatty acid oxidation is associated with proliferation and prognosis in breast and other cancers. *BMC Cancer* **18**, 805, doi:10.1186/s12885-018-4626-9 (2018).

322 Flavahan, W. A., Gaskell, E. & Bernstein, B. E. Epigenetic plasticity and the hallmarks of cancer. *Science* **357**, doi:10.1126/science.aal2380 (2017).

323 Easwaran, H., Tsai, H. C. & Baylin, S. B. Cancer epigenetics: tumor heterogeneity, plasticity of stem-like states, and drug resistance. *Mol Cell* **54**, 716-727, doi:10.1016/j.molcel.2014.05.015 (2014).

324 Hovestadt V, Z. M. conumee: Enhanced copy-number variation analysis using Illumina DNA methylation arrays. *R package version 1.9.0. <URL: http://bioconductor.org/packages/conumee/>* (2017).

325 Vaidyanathan, A. *et al.* ABCB1 (MDR1) induction defines a common resistance mechanism in paclitaxel- and olaparib-resistant ovarian cancer cells. *Br J Cancer* **115**, 431-441, doi:10.1038/bjc.2016.203 (2016).

326 Aleksandra Adamska, M. F. ATP-binding cassette transporters in progression and clinical outcome of pancreatic cancer: what is the way forward? *World J Gastroenterol* (2018).

327 Brinkman, E. K., Chen, T., Amendola, M. & van Steensel, B. Easy quantitative assessment of genome editing by sequence trace decomposition. *Nucleic Acids Res* **42**, e168, doi:10.1093/nar/gku936 (2014).

328 Marusyk, A., Janiszewska, M. & Polyak, K. Intratumor Heterogeneity: The Rosetta Stone of Therapy Resistance. *Cancer Cell* **37**, 471-484, doi:10.1016/j.ccell.2020.03.007 (2020).

329 Ouyang, P. *et al.* IL-37 promotes cell apoptosis in cervical cancer involving Bim upregulation. *Onco Targets Ther* **12**, 2703-2712, doi:10.2147/OTT.S201664 (2019).

330 Mayle, R. *et al.* Mcm10 has potent strand-annealing activity and limits translocase-mediated fork regression. *Proceedings of the National Academy of Sciences* **116**, 798-803, doi:10.1073/pnas.1819107116 (2019).

331 Murayama, T. *et al.* MCM10 compensates for Myc-induced DNA replication stress in breast cancer stem-like cells. *bioRxiv*, 2020.2007.2020.211961, doi:10.1101/2020.07.20.211961 (2020).

332 Cook-Mills, J. M., Marchese, M. E. & Abdala-Valencia, H. Vascular cell adhesion molecule-1 expression and signaling during disease: regulation by reactive oxygen species and antioxidants. *Antioxid Redox Signal* **15**, 1607-1638, doi:10.1089/ars.2010.3522 (2011).

333 Schonholzer, M. T. *et al.* Real-time sensing of MAPK signaling in medulloblastoma cells reveals cellular evasion mechanism counteracting dasatinib blockade of ERK activation during invasion. *Neoplasia* **22**, 470-483, doi:10.1016/j.neo.2020.07.006 (2020).

334 Parker, A. L., Kavallaris, M. & McCarroll, J. A. Microtubules and their role in cellular stress in cancer. *Front Oncol* **4**, 153, doi:10.3389/fonc.2014.00153 (2014).

335 Notte, A. *et al.* Taxol-induced unfolded protein response activation in breast cancer cells exposed to hypoxia: ATF4 activation regulates autophagy and inhibits apoptosis. *Int J Biochem Cell Biol* **62**, 1-14, doi:10.1016/j.biocel.2015.02.010 (2015).

336 Stanton, R. A., Gernert, K. M., Nettles, J. H. & Aneja, R. Drugs that target dynamic microtubules: a new molecular perspective. *Med Res Rev* **31**, 443-481, doi:10.1002/med.20242 (2011).

337 Safa, A. R. Identification and characterization of the binding sites of P-glycoprotein for multidrug resistance-related drugs and modulators. *Curr Med Chem Anticancer Agents* **4**, 1-17, doi:10.2174/1568011043482142 (2004).

338 de Lannoy, I. A., Mandin, R. S. & Silverman, M. Renal secretion of vinblastine, vincristine and colchicine in vivo. *J Pharmacol Exp Ther* **268**, 388-395 (1994).

339 Mendelsohn, J. Personalizing oncology: perspectives and prospects. *J Clin Oncol* **31**, 1904-1911, doi:10.1200/JCO.2012.45.3605 (2013).

340 Costello, E., Greenhalf, W. & Neoptolemos, J. P. New biomarkers and targets in pancreatic cancer and their application to treatment. *Nat Rev Gastroenterol Hepatol* **9**, 435-444, doi:10.1038/nrgastro.2012.119 (2012).

341 Slamon, D. J. *et al.* Use of chemotherapy plus a monoclonal antibody against HER2 for metastatic breast cancer that overexpresses HER2. *N Engl J Med* **344**, 783-792, doi:10.1056/NEJM200103153441101 (2001).

342 Bollag, G. *et al.* Clinical efficacy of a RAF inhibitor needs broad target blockade in BRAF-mutant melanoma. *Nature* **467**, 596-599, doi:10.1038/nature09454 (2010).

343 Ledermann, J. *et al.* Olaparib Maintenance Therapy in Platinum-Sensitive Relapsed Ovarian Cancer. *New England Journal of Medicine* **366**, 1382-1392, doi:10.1056/NEJMoa1105535 (2012).

344 Aung, K. L. *et al.* Genomics-Driven Precision Medicine for Advanced Pancreatic Cancer: Early Results from the COMPASS Trial. *Clin Cancer Res* **24**, 1344-1354, doi:10.1158/1078-0432.CCR-17-2994 (2018).

345 Moran, R. G. & Keyomarsi, K. Biochemical rationale for the synergism of 5-fluorouracil and folinic acid. *NCI Monogr*, 159-163 (1987).

346 Binenbaum, Y., Na'ara, S. & Gil, Z. Gemcitabine resistance in pancreatic ductal adenocarcinoma. *Drug Resist Updat* **23**, 55-68, doi:10.1016/j.drup.2015.10.002 (2015).

347 Giordano, G. *et al.* Nano albumin bound-paclitaxel in pancreatic cancer: Current evidences and future directions. *World J Gastroenterol* **23**, 5875-5886, doi:10.3748/wjg.v23.i32.5875 (2017).

348 Petrillo, A. *et al.* Nab-paclitaxel plus gemcitabine as first line therapy in metastatic pancreatic cancer patients relapsed after gemcitabine adjuvant treatment. *Med Oncol* **36**, 83, doi:10.1007/s12032-019-1306-9 (2019).

349 Shaffer, S. M. *et al.* Rare cell variability and drug-induced reprogramming as a mode of cancer drug resistance. *Nature* **546**, 431-435, doi:10.1038/nature22794 (2017).

350 Chen, R. *et al.* Disrupting glutamine metabolic pathways to sensitize gemcitabine-resistant pancreatic cancer. *Sci Rep* **7**, 7950, doi:10.1038/s41598-017-08436-6 (2017).

351 Shukla, S. K. *et al.* MUC1 and HIF-1alpha Signaling Crosstalk Induces Anabolic Glucose Metabolism to Impart Gemcitabine Resistance to Pancreatic Cancer. *Cancer Cell* **32**, 71-87 e77, doi:10.1016/j.ccell.2017.06.004 (2017).

352 McDermott, M. *et al.* In vitro Development of Chemotherapy and Targeted Therapy Drug-Resistant Cancer Cell Lines: A Practical Guide with Case Studies. *Front Oncol* **4**, 40, doi:10.3389/fonc.2014.00040 (2014).

353 Marusyk, A. & Polyak, K. Tumor heterogeneity: causes and consequences. *Biochim Biophys Acta* **1805**, 105-117, doi:10.1016/j.bbcan.2009.11.002 (2010).

354 Gerlinger, M. & Swanton, C. How Darwinian models inform therapeutic failure initiated by clonal heterogeneity in cancer medicine. *Br J Cancer* **103**, 1139-1143, doi:10.1038/sj.bjc.6605912 (2010).

355 Tegze, B. *et al.* Parallel Evolution under Chemotherapy Pressure in 29 Breast Cancer Cell Lines Results in Dissimilar Mechanisms of Resistance. *PLOS ONE* **7**, e30804, doi:10.1371/journal.pone.0030804 (2012).

356 Seth, S. *et al.* Pre-existing Functional Heterogeneity of Tumorigenic Compartment as the Origin of Chemoresistance in Pancreatic Tumors. *Cell Rep* **26**, 1518-1532 e1519, doi:10.1016/j.celrep.2019.01.048 (2019).

357 Wang, Y. M., Ong, S. S., Chai, S. C. & Chen, T. Role of CAR and PXR in xenobiotic sensing and metabolism. *Expert Opin Drug Metab Toxicol* **8**, 803-817, doi:10.1517/17425255.2012.685237 (2012).

358 Turajlic, S., Sottoriva, A., Graham, T. & Swanton, C. Resolving genetic heterogeneity in cancer. *Nat Rev Genet* **20**, 404-416, doi:10.1038/s41576-019-0114-6 (2019).

359 Carter, S. L., Eklund, A. C., Kohane, I. S., Harris, L. N. & Szallasi, Z. A signature of chromosomal instability inferred from gene expression profiles predicts clinical outcome in multiple human cancers. *Nat Genet* **38**, 1043-1048, doi:10.1038/ng1861 (2006).

360 Walther, A., Houlston, R. & Tomlinson, I. Association between chromosomal instability and prognosis in colorectal cancer: a meta-analysis. *Gut* **57**, 941-950, doi:10.1136/gut.2007.135004 (2008).

361 Jamal-Hanjani, M. *et al.* Extreme chromosomal instability forecasts improved outcome in ER-negative breast cancer: a prospective validation cohort study from the TACT trial. *Ann Oncol* **26**, 1340-1346, doi:10.1093/annonc/mdv178 (2015).

362 Swanton, C. *et al.* Chromosomal instability determines taxane response. *Proc Natl Acad Sci U S A* **106**, 8671-8676, doi:10.1073/pnas.0811835106 (2009).

363 Misale, S. *et al.* Emergence of KRAS mutations and acquired resistance to anti-EGFR therapy in colorectal cancer. *Nature* **486**, 532-536, doi:10.1038/nature11156 (2012).

364 Yin, S., Bhattacharya, R. & Cabral, F. Human mutations that confer paclitaxel resistance. *Mol Cancer Ther* **9**, 327-335, doi:10.1158/1535-7163.MCT-09-0674 (2010).

365 Greenberg, M. V. C. & Bourc'his, D. The diverse roles of DNA methylation in mammalian development and disease. *Nature Reviews Molecular Cell Biology* **20**, 590-607, doi:10.1038/s41580-019-0159-6 (2019).

366 Fornés, V. C. ABCB1 AS MEDIATOR OF PACLITAXEL RESISTANCE IN PANCREATIC DUCTAL ADENOCARCINOMA. *Masters Thesis* (2020).

367 Seo, H. K., Lee, S. J., Kwon, W. A. & Jeong, K. C. Docetaxel-resistant prostate cancer cells become sensitive to gemcitabine due to the upregulation of ABCB1. *Prostate* **80**, 453-462, doi:10.1002/pros.23946 (2020).

368 Rudin, D. *et al.* Gemcitabine Cytotoxicity: Interaction of Efflux and Deamination. *J Drug Metab Toxicol* **2**, 1-10, doi:10.4172/2157-7609.1000107 (2011).

369 Cullen, K. V., Davey, R. A. & Davey, M. W. Verapamil-stimulated glutathione transport by the multidrug resistance-associated protein (MRP1) in leukaemia cells. *Biochem Pharmacol* **62**, 417-424, doi:10.1016/s0006-2952(01)00681-5 (2001).

370 Davey, R. A. *et al.* Drug resistance mechanisms and MRP expression in response to epirubicin treatment in a human leukaemia cell line. *Leuk Res* **19**, 275-282, doi:10.1016/0145-2126(94)00159-8 (1995).

371 Locke, V. L., Davey, R. A. & Davey, M. W. Altered drug sensitivity in response to idarubicin treatment in K562 human leukaemia cells. *Br J Haematol* **106**, 86-91, doi:10.1046/j.1365-2141.1999.01494.x (1999).

372 Harmsen, S. *et al.* PXR-mediated induction of P-glycoprotein by anticancer drugs in a human colon adenocarcinoma-derived cell line. *Cancer Chemother Pharmacol* **66**, 765-771, doi:10.1007/s00280-009-1221-4 (2010).

373 Morris, L. G. *et al.* Pan-cancer analysis of intratumor heterogeneity as a prognostic determinant of survival. *Oncotarget* **7**, 10051-10063, doi:10.18632/oncotarget.7067 (2016).

374 Almendro, V. *et al.* Inference of tumor evolution during chemotherapy by computational modeling and in situ analysis of genetic and phenotypic cellular diversity. *Cell Rep* **6**, 514-527, doi:10.1016/j.celrep.2013.12.041 (2014).

375 Yates, L. R. & Campbell, P. J. Evolution of the cancer genome. *Nat Rev Genet* **13**, 795-806, doi:10.1038/nrg3317 (2012).

376 Tabassum, D. P. & Polyak, K. Tumorigenesis: it takes a village. *Nature Reviews Cancer* **15**, 473-483, doi:10.1038/nrc3971 (2015).

377 Pisco, A. O. & Huang, S. Non-genetic cancer cell plasticity and therapy-induced stemness in tumour relapse: 'What does not kill me strengthens me'. *Br J Cancer* **112**, 1725-1732, doi:10.1038/bjc.2015.146 (2015).

378 Hong, S. P. *et al.* Single-cell transcriptomics reveals multi-step adaptations to endocrine therapy. *Nature Communications* **10**, 3840, doi:10.1038/s41467-019-11721-9 (2019).

379 Boumahdi, S. & de Sauvage, F. J. The great escape: tumour cell plasticity in resistance to targeted therapy. *Nat Rev Drug Discov* **19**, 39-56, doi:10.1038/s41573-019-0044-1 (2020).

380 Tata, P. R. & Rajagopal, J. Cellular plasticity: 1712 to the present day. *Curr Opin Cell Biol* **43**, 46-54, doi:10.1016/j.ceb.2016.07.005 (2016).

381 Gebauer, F. & Hentze, M. W. Molecular mechanisms of translational control. *Nat Rev Mol Cell Biol* **5**, 827-835, doi:10.1038/nrm1488 (2004).

382 de Sousa Abreu, R., Penalva, L. O., Marcotte, E. M. & Vogel, C. Global signatures of protein and mRNA expression levels. *Mol Biosyst* **5**, 1512-1526, doi:10.1039/b908315d (2009).

383 Buenrostro, J. D., Giresi, P. G., Zaba, L. C., Chang, H. Y. & Greenleaf, W. J. Transposition of native chromatin for fast and sensitive epigenomic profiling of open chromatin, DNA-binding proteins and nucleosome position. *Nat Methods* **10**, 1213-1218, doi:10.1038/nmeth.2688 (2013).

384 Li, B., Carey, M. & Workman, J. L. The role of chromatin during transcription. *Cell* **128**, 707-719, doi:10.1016/j.cell.2007.01.015 (2007).

385 Shoshani, O. *et al.* Chromothripsis drives the evolution of gene amplification in cancer. *Nature*, doi:10.1038/s41586-020-03064-z (2020).

386 Dagogo-Jack, I. & Shaw, A. T. Tumour heterogeneity and resistance to cancer therapies. *Nat Rev Clin Oncol* **15**, 81-94, doi:10.1038/nrclinonc.2017.166 (2018).

387 Valent, A. *et al.* In vivo elimination of acentric double minutes containing amplified MYCN from neuroblastoma tumor cells through the formation of micronuclei. *Am J Pathol* **158**, 1579-1584, doi:10.1016/S0002-9440(10)64112-0 (2001).

388 Shimizu, N. Extrachromosomal double minutes and chromosomal homogeneously staining regions as probes for chromosome research. *Cytogenet Genome Res* **124**, 312-326, doi:10.1159/000218135 (2009).

389 Liao, Z. *et al.* Classification of extrachromosomal circular DNA with a focus on the role of extrachromosomal DNA (ecDNA) in tumor heterogeneity and progression. *Biochim Biophys Acta Rev Cancer* **1874**, 188392, doi:10.1016/j.bbcan.2020.188392 (2020).

390 Phallen, J. *et al.* Direct detection of early-stage cancers using circulating tumor DNA. *Sci Transl Med* **9**, doi:10.1126/scitranslmed.aan2415 (2017).

391 Kumar, P. *et al.* Normal and Cancerous Tissues Release Extrachromosomal Circular DNA (eccDNA) into the Circulation. *Mol Cancer Res* **15**, 1197-1205, doi:10.1158/1541-7786.MCR-17-0095 (2017).

392 Deshpande, V. *et al.* Exploring the landscape of focal amplifications in cancer using AmpliconArchitect. *Nature Communications* **10**, 392, doi:10.1038/s41467-018-08200-y (2019).

393 Rajkumar, U. *et al.* EcSeg: Semantic Segmentation of Metaphase Images Containing Extrachromosomal DNA. *iScience* **21**, 428-435, doi:10.1016/j.isci.2019.10.035 (2019).

394 Bailey, C., Shoura, M. J., Mischel, P. S. & Swanton, C. Extrachromosomal DNA-relieving heredity constraints, accelerating tumour evolution. *Ann Oncol* **31**, 884-893, doi:10.1016/j.annonc.2020.03.303 (2020).

395 Barr, F. G. *et al.* In vivo amplification of the PAX3-FKHR and PAX7-FKHR fusion genes in alveolar rhabdomyosarcoma. *Hum Mol Genet* **5**, 15-21, doi:10.1093/hmg/5.1.15 (1996).

396 Mc, C. B. Chromosome organization and genic expression. *Cold Spring Harb Symp Quant Biol* **16**, 13-47, doi:10.1101/sqb.1951.016.01.004 (1951).

397 Valent, A. *et al.* In Vivo Elimination of Acentric Double Minutes Containing Amplified MYCN from Neuroblastoma Tumor Cells Through the Formation of Micronuclei. *The American Journal of Pathology* **158**, 1579-1584, doi:https://doi.org/10.1016/S0002-9440(10)64112-0 (2001).

398 Shimizu, N., Itoh, N., Utiyama, H. & Wahl, G. M. Selective entrapment of extrachromosomally amplified DNA by nuclear budding and micronucleation during S phase. *J Cell Biol* **140**, 1307-1320, doi:10.1083/jcb.140.6.1307 (1998).

399 Shimizu, N. Extrachromosomal Double Minutes and Chromosomal Homogeneously Staining Regions as Probes for Chromosome Research. *Cytogenetic and Genome Research* **124**, 312-326, doi:10.1159/000218135 (2009).

400 Zhang, H. C. & Kuo, C. J. Personalizing pancreatic cancer organoids with hPSCs. *Nat Med* **21**, 1249-1251, doi:10.1038/nm.3992 (2015).

401 Huang, L. *et al.* Ductal pancreatic cancer modeling and drug screening using human pluripotent stem cell- and patient-derived tumor organoids. *Nat Med* **21**, 1364-1371, doi:10.1038/nm.3973 (2015).

402 Hwang, C. I., Boj, S. F., Clevers, H. & Tuveson, D. A. Preclinical models of pancreatic ductal adenocarcinoma. *J Pathol* **238**, 197-204, doi:10.1002/path.4651 (2016).

403 Kong, X. *et al.* Cancer drug addiction is relayed by an ERK2-dependent phenotype switch. *Nature* **550**, 270-274, doi:10.1038/nature24037 (2017).

404 Peng, J. *et al.* Single-cell RNA-seq highlights intra-tumoral heterogeneity and malignant progression in pancreatic ductal adenocarcinoma. *Cell Res* **29**, 725-738, doi:10.1038/s41422-019-0195-y (2019).

405 Tang, Y. C. & Amon, A. Gene copy-number alterations: a cost-benefit analysis. *Cell* **152**, 394-405, doi:10.1016/j.cell.2012.11.043 (2013).

406 Huber, W. *et al.* Orchestrating high-throughput genomic analysis with Bioconductor. *Nat Methods* **12**, 115-121, doi:10.1038/nmeth.3252 (2015).

407 Ihaka, R. & Gentleman, R. R: A Language for Data Analysis and Graphics. *Journal of Computational and Graphical Statistics* **5**, 299-314, doi:10.2307/1390807 (1996).

408 Gautier, L., Cope, L., Bolstad, B. M. & Irizarry, R. A. affy--analysis of Affymetrix GeneChip data at the probe level. *Bioinformatics* **20**, 307-315, doi:10.1093/bioinformatics/btg405 (2004).

409 Kauffmann, A., Gentleman, R. & Huber, W. Huber W: arrayQualityMetrics–a bioconductor package for quality assessment of microarray data. *Bioinformatics (Oxford, England)* **25**, 415-416, doi:10.1093/bioinformatics/btn647 (2009).

410 Bourgon, R., Gentleman, R. & Huber, W. Independent filtering increases detection power for high-throughput experiments. *Proceedings of the National Academy of Sciences* **107**, 9546-9551, doi:10.1073/pnas.0914005107 (2010).

411 Sánchez, J. MARDIA, K. V., J. T. KENT, J. M. BIBBY: Multivariate Analysis. Academic Press, London-New York-Toronto-Sydney-San Francisco 1979. xv, 518 pp. *Biometrical Journal* **24**, 502-502, doi:https://doi.org/10.1002/bimj.4710240520 (1982).

412 Ripley, W. N. V. D. Modern Applied Statistics with S. *Springer*, doi:https://doi.org/10.1007/978-0-387-21706-2 (2002).

413 Witten, D. M., Tibshirani, R. & Hastie, T. A penalized matrix decomposition, with applications to sparse principal components and canonical correlation analysis. *Biostatistics* **10**, 515-534, doi:10.1093/biostatistics/kxp008 (2009).

414 Zou, H., Hastie, T. & Tibshirani, R. Sparse Principal Component Analysis. *Journal of Computational and Graphical Statistics* **15**, 265-286, doi:10.1198/106186006X113430 (2006).

415 Phipson, B., Lee, S., Majewski, I. J., Alexander, W. S. & Smyth, G. K. Robust Hyperparameter Estimation Protects against Hypervariable Genes and Improves Power to Detect Differential Expression. *Ann Appl Stat* **10**, 946-963, doi:10.1214/16-AOAS920 (2016).

416 Ritchie, M. E. *et al.* limma powers differential expression analyses for RNA-sequencing and microarray studies. *Nucleic Acids Res* **43**, e47, doi:10.1093/nar/gkv007 (2015).

417 Hyafil, F., Vergely, C., Du Vignaud, P. & Grand-Perret, T. In vitro and in vivo reversal of multidrug resistance by GF120918, an acridonecarboxamide derivative. *Cancer Res* **53**, 4595-4602 (1993).

418 Langmead, B., Trapnell, C., Pop, M. & Salzberg, S. L. Ultrafast and memory-efficient alignment of short DNA sequences to the human genome. *Genome Biology* **10**, R25, doi:10.1186/gb-2009-10-3-r25 (2009).

419 Zhang, Y. *et al.* Model-based Analysis of ChIP-Seq (MACS). *Genome Biology* **9**, R137, doi:10.1186/gb-2008-9-9-r137 (2008).

420 Ross-Innes, C. S. *et al.* Differential oestrogen receptor binding is associated with clinical outcome in breast cancer. *Nature* **481**, 389-393, doi:10.1038/nature10730 (2012).

421 Yu, G., Wang, L.-G. & He, Q.-Y. ChIPseeker: an R/Bioconductor package for ChIP peak annotation, comparison and visualization. *Bioinformatics* **31**, 2382-2383, doi:10.1093/bioinformatics/btv145 (2015).

422 Li, H. & Durbin, R. Fast and accurate long-read alignment with Burrows-Wheeler transform. *Bioinformatics* **26**, 589-595, doi:10.1093/bioinformatics/btp698 (2010).

423 Kleinheinz, K. *et al.* ACEseq – allele specific copy number estimation from whole genome sequencing. *bioRxiv*, 210807, doi:10.1101/210807 (2017).

424 Gu, Z., Gu, L., Eils, R., Schlesner, M. & Brors, B. circlize implements and enhances circular visualization in R. *Bioinformatics* **30**, 2811-2812, doi:10.1093/bioinformatics/btu393 (2014).

425 Assenov, Y. *et al.* Comprehensive analysis of DNA methylation data with RnBeads. *Nat Methods* **11**, 1138-1140, doi:10.1038/nmeth.3115 (2014).

426 Fortin, J. P., Triche, T. J., Jr. & Hansen, K. D. Preprocessing, normalization and integration of the Illumina HumanMethylationEPIC array with minfi. *Bioinformatics* **33**, 558-560, doi:10.1093/bioinformatics/btw691 (2017).

427 Stuart, T. *et al.* Comprehensive Integration of Single-Cell Data. *Cell* **177**, 1888-1902 e1821, doi:10.1016/j.cell.2019.05.031 (2019).

428 Butler, A., Hoffman, P., Smibert, P., Papalexi, E. & Satija, R. Integrating single-cell transcriptomic data across different conditions, technologies, and species. *Nature Biotechnology* **36**, 411-420, doi:10.1038/nbt.4096 (2018).

List of Abbreviations

%	Percent
2D	Two Dimensional
3D	Three Dimensional
5-FU	5-Fluorouracil
ABC	ATB-Binding Casette Transporter
ABCB1	ATP Binding Cassette Subfamily B Member 1
ABCB4	ATP Binding Cassette Subfamily B Member 4
ABCC1	ATP Binding Cassette Subfamily C Member 1
ABCG2	ATP Binding Cassette Subfamily G Member 2
ADAM22	A Disintegrin And Metalloproteinase Domain 22
ADEX	Aberrantly Differentiated Endocrine Exocrine
AFL	Atyplical Flat Lesions
AG	Adrenal Gland
AJCC	American Joint Committee On Cancer
AML	Acute Myeloid Leukemia
AP-1	Activator Protein 1
ARID1A	At-Rich Interaction Domain 1a
ASCO	American Society Of Clinical Oncology
aSMA	Alpha Smooth Muscle Actin
ATAC	Assay For Transposase-Accessible Chromatin
ATAC-seq	ATAC Sequencing
ATM	Ataxia Telangiectasia Mutated Serine/ Threonine Kinase
ATP	Adenosine Triphosphate
ATR	ATR Serine/Threonine Kinase
BCA	Bicinchoninic Acid
BCORL1	BCL16 Corepressor Like 1
BCRP	Breast Cancer Resistance Protein
BFB	Breakage-Fusion-Bridge
Bis-Tris	Bis (2-Hydroxyethyl)-Amino-Tris (Hydroxymethyl) Methane
BMI	Body Mass Index
bp	Base Pair
BRAF	B-RAF Proto-Oncogene, Serine/Threonine Kinase
BRCA1	Breast Cancer 1, Early Onset
BRCA2	Breast Cancer 2, Early Onset
BSA	Bovine Serum Albumin
C	Colchicine

CA19-9	Carbohydrate Antigen 19-9
CAR	Constitutive Adrostane Receptor
CAV1	Caveolin 1
CDC6	Cell Division Cycle 6
CDKN2A	Cycline Dependent Kinase Inhibitor 2A
CEBPZ	Ccaat Enhancer Binding Protein Zeta
Chr	Chromosome
CIN	Chromosome Instability
CK	Cytokeratin
CLDN18	Claudin 18
CNV	Copy Number Variation
CRISPR	Clustered Regularly Interspaced Short Palindromic Repeats
CROT	Carnitine O-Octanoyltransferase
CST6	Cystatin E/M
Ct	Cycle Threshold
CT	Computed Tomography
CTB	CellTiter Blue
ctDNA	Circulating Tumor DNA
CTLA4	Cytotoxic T Lymphocyte Protein 4
Ctrl	Control
CXCL12	C-X-C Motif Chemokine Ligand 12
CYP3A4	Cytochrome P450 Family 3 Subfamily A Member 4
CYP3A5	Cytochrome P450 Family 3 Subfamily A Member 5
CYP3A7	Cytochrome P450 Family 3 Subfamily A Member 7
D	DMSO Treated
DBF4	DBF4 Zinc Finger
Del	Deletion
DHRS2	Dehydrogenase/Reductase 2
DM	DMSO Treated
DMSO	Dimethylsulfoxid
DMTF1	Cyclin D Binding MYB Like Transcription Factor 1
DNA	Deoxyribonucleic Acid
DNMT1	DNA Methyltransferase 1
DT	Derived Tumor
DUP	Duplication
E	Early Round
ecDNA	Extrachromosomal Circular DNA
ECM	Extracellular Matrix

EGF	Epidermal Growth Factor
EGR-1	Early Growth Response Protein 1
EL	Early Round
ERBB2 /Her2	ERBB2 Receptor Tyrosine Kinase 2
ERK	Extracellular Signal-Regulated Kinase
FACS	Fluorescence-Activated Cell Sorting
FANCC	Fa Complementation Group C
FANCG	Fa Complementation Group G
FC	Fold Change
FCS	Fetal Calf Serum
FDA	Food And Drug Administration
FDR	False Discoery Rate
FFPE	Formalin-Fixed Praffin-Embeded
FISH	Fluorescent In Situ Hybridization
FOLFIRINOX	Folinic Acid, Fluorouracil, Irinotecan, Oxaliplatin
G	Gemcitabine
G-C	Gemcitabine-Capecitabine
GAPDH	Glyceraldehyde-3-Phosphate Dehydrogenase
GATA6	Gata-Binding Factor 6
GB	Gene Body
GEMM	Genetically Engineered Mouse Models
GNAS Polypeptide 1	Guanine Nucleotide Binding Protein (G Protein), Alpha Stimulating Activity
GR	Gemcitabine Resistant
GSEA	Gene Set Enrichment Analysis
HGF	Hepatocyte Growth Factor
HNF1A	Hepatocyte Nuclear Factor 1 Alpha
HSE	Heat Shock Element
HSF	Heat Shock Transcription Factor
HSR	Homogeneously Staining Regions
ICAM-1	Intercellular Adhesion Molecule One
IFITM1	Interferon Induced Transmembrane Protein 1
IGF	Insulin-Like Growth Factor
IL37	Interleukin 37
Inh	Inhibitor
IPMN	Mucinous Neoplasms
ITH	Intratumor Heterogeneity
JNK	C-Jun NH2-Terminal Protein Kinase

kb	Kilo Bases
kDa	Kilo Dalton
KDM6A	Lysine Demethylase 6A
KIAA1324L	Endosome-Lysosome Associated Apoptosis And Autophagy Regulator Family Member 2
KO	Knockout
KRAS	KRAS Proto-Oncogene, GTPase
L	Last Round
log	Logarithmic
LOH	Loss Of Heterogeneity
LR	Last Round
MAPK	Mitogen-Activated Protein Kinase
MCN	Mucinos Cystic Neoplasm
MDCT	Multiphase, Multidetector Computed Tomography
MDR	Multi-Drug Resistance
MET	MET Proto-Oncogene, Receptor Tyrosine Kinase
MFI	Mean Fluorescent Intensity
MLH1	MUTL Homolog 1
MLL3	Lysine Methyltransferase 2c
MMP	Metalloproteinases
mRNA	Messenger RNA
MRP1	MDR-Associated Protein 1
MUC	Mucin
MYC	MYC Proto-Oncogene, BHLH Transcription Factor
nab	Nanoparticle Albumin-Bound
nal	Nanoliposomal
NBD	Nucleotide-Binding Domains
ND	NaCl/DMSO
NES	Normalized Enrichment Analysis
NF- kB	Pathways And Nuclear Factor- B
No	Number
nPG	Nab-Paclitaxel And Gemcitabine
ns	Not Significant
OS	Overall Survival
P	Paclitaxel Treated
P	Paclitaxel
P5	Passage 5
PACO	Primary PDAC

PALB2	Partner And Localizer Of Brca2
PanIN	Pancreatic Intraepithelial Neoplasia
Par	Parental
PCA	Principal Component Analysis
PD-1	Programmed Cell Death Protein
PDAC	Pancreatic Ductal Adenocarcinoma
PDGF	Platelet-Derived Growth Factor
PDO	Patient-Derived Organoid
PDX	Patient-Derived Xenograft
Pdx1	Pancreatic And Duodenal Homeobox 1
PEG10	Paternally Expressed 10
PEGPH20	Pegylated Recombinant Human Hyaluronidase
PG	Paclitaxel/Gemcitabine Treated
PGR	Paclitaxel/Gemcitabine Resistant
PI3K	Phosphoinositide 3-Kinase
PKC	Protein Kinase C
PM	Promoter
PNET	Pancreatic Neuroendocrine Tumor
PR	Paclitaxel Resistant
PRSS1	Serine Protease 1
PSC	Pancreatic Stellate Cells
PT	Patient-Derived Tumor
PTGS2	Prostaglandin-Endoperoxide Synthase 2
PXR	Pregnane X Receptor
QM-PDA	Quasi-Mesenchymal
qRT-PCR	Quantitatve Real-Time Polymerase Chain Reaction
QSAR	Quantitative Structure-Activity Relationships
RBM10	Rna Binding Motif Protein 10
REG4	Regenerating Family Member 4
RNA	Ribonucleic Acid
RNA-seq	RNA Sequencing
RNP	Ribonucleoprotein
Ro.	Round
ROS	Reactive Oxygen Species
RQ	Relative Quantification
RUNDC3B	Run Domain Containing 3b
s.e.m.	Standard Error Of Mean
S100A2	S100 Calcium Binding Protein A2

SERPINB2	Serpin Family B Member 2
SLC25A40	Solute Carrier Family 25 Member 40
SMAD4	SMAD Family Member 4
SP	Specificity Protein
SPARC	Secreted Protein, Acidic, Cysteine-Rich
spPCA	Sparse Principal Component Analysis
STK11	Serine/Threonine Kinase 11
STS	Staurosporine
SXR	Steroid Xenobiotic Receptor
TBD	Transmembrane Domain
TCF	T-Cell Factor
TCGA	The Cancer Genome Atlas
TGFb	Transforming Growth Factor Beta
TGFBR2	Transforming Growth Factor Beta Receptor 2
TKI	Tyrosine Kinase Inhibitors
TME	Tumor Microenvironment
TMEM243	Transmembrane Protein 243
TOX3	TOX High Mobility Group Box Family Member 3
TP53	Tumor Protein P53
TP53TG1	TP53 Target 1
TSPAN8	Tetraspanin 8
UGT	Uridine 5’ Diphospho-Glucuronosyltransferase
UMAP	Uniform Manifold Approximation And Projection
UT	Untreated
Vb	Vinblastine
Vc	Vincristine
VEGF	Vascular Endothelial Growth Factor
WES	Whole Exome Sequencing
WGS	Whole Genome Sequencing
WT	Wildtype
YBX1	Y-Box Binding Protein
µg	Microgram
µl	Microliter
µM	Micromolar
µm	Micrometer

List of Figures

List of Supplementary Figures

List of Tables

Contributions

The following people significantly contributed to the work presented in this doctoral thesis:

The presented study was supervised by Prof. Dr. A. Trumpp and Dr. M. R. Sprick. The patient-derived PDAC cell culture model was established by Dr. C. Eisen, who also identified HNF1A and KRT81 as immunohistochemistry markers for PDAC subtype stratification. Dr. E. M. Noll identified CYP3A5 as drug resistance mechanism in a subset of our PACO cell lines and generated the first drug resistant PACO cell lines in out lab. Hence, the work presented in this doctoral thesis is based on the previous findings described by *Noll and Eisen* et al.[183]. C. Klein, O. Kossi and V. Vogel provided essential technical and experiment support. Dr. E. Donato was a crucial support for the ATAC sequencing library generation, the subsequent alignment and analysis. A. Mahmoud carried out improved alignment and a detailed single-cell RNA sequencing analysis on PR and DM cell lines of PACO22. Dr. A.-M. Mikecin and Dr. P Sommerkamp provided important initial support for the CRISPR/Cas9-guided ABCB1 knockout experiments. T. Rubner and F. Blum from the DKFZ Flow Cytometry core facility performed fluorescence-activated cell sorting for PACO22 PR ABCB1+ and ABCB1- cells. M Brom and Dr. D. Krunic from the DKFZ Light Microscopy core facility provided support in all aspects of microscopy. Especially Dr. D. Krunic significantly contributed to the ImageJ-based analysis of all FISH images. Dr. B. Meissburger from the DKFZ Sample Processing Laboratory provided and submitted RNA and DNA from all H015 patients presented in this study for subsequent analyses. Whole exome, whole genome, ATAC and single-cell RNA sequencings were conducted and supported by the High Throughput Sequencing unit of the DKFZ Genomics & Proteomics core facility. Whole exome and whole genome sequence alignment was carried out by the DKFZ Omics IT and Data Management core facility. Dr. G. Warsow performed CNV, SNV and Indel analysis of the whole exome sequencing samples. The Microarray unit of the DKFZ Genomics & Proteomics core facility carried out gene expression and DNA methylation microarray service. A. Rathgeb and her team of the Center for Preclinical Research monitored animal welfare.

I would like to thank Dr. Stewart ‘Mac’ Mein, Dr. Elisa Espinet and Dr. Martin Sprick for proofreading this doctoral thesis.

Acknowledgments

First of all, I would like to deeply thank **Dr. Martin Sprick**. Thank you for giving me the opportunity to join the METICS group and to trust in me to successfully continue the project on drug resistance in pancreatic cancer. Especially in the beginning of the PhD your door remained always open and you welcomed me to every question I raised. I very much enjoyed every meeting that usually ended up in long discussions, theory crafting and fascinating hypotheses that were mostly stopped by my need for a timely lunch. I will definitely miss these moments. Moreover, your intellectual and technical input helped me to improve my scientific skills, raised my awareness about critical points and kept me on track. Nevertheless, you gave me the freedom to develop the project into my personal project of which I am proud to be able to write my PhD thesis about. Thank you for your supervision and the exciting time in the METICS group.

I would like to thank my PhD supervisor, **Prof. Dr. Andreas Trumpp**, for giving me the opportunity to perform my PhD thesis in your laboratory. You gave me the space to develop my project and my scientific personality and provided a unique international environment that enabled countless opportunities and enhanced the scientific communication. I very grateful for your never-ending ideas to further push the project to a successful ending. Your drive for science is truly inspiring and I am very thankful for your support.

Thank you, **Dr. Richard Harbottle** for your role as my second examiner of my PhD thesis and being part of my defense committee.

Thank you, **Prof. Dr. Jan Lohmann** and **Prof. Dr. Christoph Plass** for being members of my defense committee.

I would like to thank my TAC committee members **Prof. Dr. Christoph Plass** and **Prof. Dr. Albrecht Stenzinger** for their constant support and important contributions to this PhD thesis.

A special thanks goes to all present and past members of the METICS group. It was an honor and a pleasure to work with you. Thank you for your support and crucial input: **Dr. Lisa Becker, Tasneem Cheytan, Dr. Elisa Espinet, Victor Campos Fornés, Dr. Felix Geist, Dr. Sarah Jauch, Corinna Klein, Ornella Kossi, Sarah-Jane Neuberth, Dr. Elisa Noll, Paul Schwerd-Kleine, Jonas Schwickert, Vera Thiel, Dr. Massimo Saini, Jaime Fernandez Sobaberas, Vanessa Vogel, Tim Vorberg, Dr. Jennifer Wischhusen, Dr. Roberto Würth, Dr. Franziska Zickgraf.**

I especially would like to thank **Dr. Elisa Noll** for your great supervision in the beginning of my PhD life. You were a great support and I very much enjoyed working with you together. Thank you for providing such a smooth perfect start!

I consider myself the luckiest guy that I had the chance to work together with **Corinna Klein**, **Ornella Kossi** and **Vanessa Vogel**! My time as a PhD in the lab would not have been the same without you three wonderful women.
Corinna, from the first moment on, I knew that we were more than just colleagues sharing the same aquarium. You are a terrific mouse surgeon and the confidence you put in your work was astonishing. Besides, being a great colleague and working with was nothing but joy, I am grateful that we have also become friends. I could share all my thoughts, ideas, fears, whishes with you and you never lacked a helpful advice. Thank you for your endless support. **Ornella**, I am deeply thankful that you ended up joining our group. You are a true perfectionist in the lab and I enjoyed your insatiable demand to learn new technologies. You acquired every new technology with ease and by the end of my PhD it was me that learned from you. I am thankful that you took over a part of the project and for your never-ending support helped to get through the hardest times. You have become an important friend and the time we spent together in the lab is everything but boring. I can always count on you. Thank you! **Vanessa**, I am so thankful for your support in immunohistochemistry. Moreover, I can only express my deepest gratitude that you picked up the FISH staining and never stopped believing in the perfect protocol. It was always fun working with you and I very much enjoyed every coffee we shared together. Thank you for all the great laughs and the often interesting and sometimes even educational chats.

Dr. Felix Geist, you were the perfect match as my office neighbor. I could always rely on your support and advice and we raised the bioinformatical level of the METICS to another level. You always had an answer to my questions and it was a joy working with you together. You are a terrific colleague!

Thank you, **Dr. Elisa Espinet** for your constant support and ideas. You were the PDAC expert, I was always looking up to and never managed to reach. Your ability to ask the right questions and by that to improve every project in the lab is inspiring. Thank you for your mentoring, your honesty and expertise.

I would like to thank the whole HI-STEM and A010 team. Special thanks go to **Dr. Natasha Anstee, Dr. Julius Gräsel, Dr. Maren Pein and Dr. Jacob Rodriguez**. Thank you, **Dr. Elisa Donato** for your endless support in ATAC sequencing and I enjoyed every experiment and

analysis we did together. Thank you, **Dr. Mattia Falcone** for your bioinformatical support, your wits and wisdom and thank you, for being such a fantastic friend.

Dr. Megan Druce and **Dr. Stewart 'Mac' Mein**, we me at the selection and started our PhD adventure together. We experienced so many ups and downs, intense moments and beautiful occasions, and although we also grew up and changed throughout that time, you both became one of my closest friends. I am deeply grateful for your immense support and friendship in every moment of my PhD life and beyond.

A special thanks goes to my dearest friends, the Haribros, **Maximilian Hartmann, Steffen Reibold, Steffen Ruland und Torsten Ruland**. Thank you for your support for many years and letting me know that there is also a world outside the lab.

Von ganzem Herzen möchte ich mich bei meinen Eltern, **Barbara** und **Klaus Reitberger**, meinem Stiefvater **Walter Horn**, meiner Schwester **Julia Reitberger**, meiner Schwiegermutter **Renate Holz** und **Erik Steinkampf** für eure immerwährende Unterstützung und Rückhalt bedanken. Ihr habt mich auf dem Weg vom Abitur über das Studium bis zum Ende des PhDs immer begleitet und ohne euch wäre ich nie soweit gekommen. Eure Liebe und euer Verständnis haben mich immer begleitet und mir den Rücken gestärkt. Vielen Dank!

Laura, du bist die Liebe meines Lebens, mein engster Freund und Partner. Vielen Dank für deine nimmer endende Unterstützung und Liebe. Du hast immer an mich geglaubt, bist immer für mich da gewesen, wenn ich dich brauchte, hast mir immer zugehört, mich aufgemuntert und meine Launen ertragen. Danke, dass du immer an meiner Seite warst und mich auf diesem Weg nie alleine gelassen hast. Ohne dich wäre diese Arbeit nicht möglich gewesen und dafür bin ich dir auf ewig dankbar. Ich liebe dich!